Oklahoma Geological Survey
Charles J. Mankin, *Director*

Circular 107
ISSN 0078-4397

Revisiting Old and Assessing New Petroleum Plays in the Southern Midcontinent, 2001 Symposium

BRIAN J. CARDOTT, *Editor*

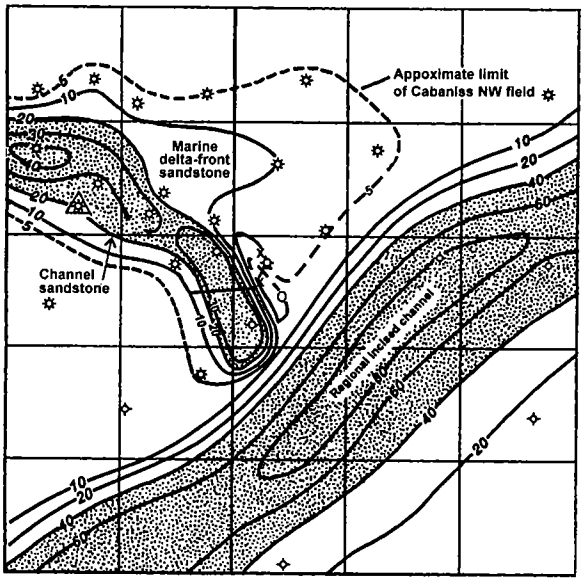

Proceedings of a symposium held May 8–9, 2001, in Oklahoma City, Oklahoma.

Co-sponsored by:

Oklahoma Geological Survey

and

National Petroleum Technology Office,
U.S. Department of Energy

The University of Oklahoma
Norman

2002

OKLAHOMA GEOLOGICAL SURVEY

CHARLES J. MANKIN, *Director*

SURVEY STAFF

JAMES H. ANDERSON, *Manager of Cartography*
RICHARD D. ANDREWS, *Geologist IV*
LARRY T. AUSTIN, *Core and Sample Library Assistant*
BETTY D. BELLIS, *Word-Processing Operator II/Technical Typist*
MITZI G. BLACKMON, *Clerk-Typist I*
DAN T. BOYD, *Geologist III*
JERLENE A. BRIGHT, *Technical Project Specialist*
RAYMON L. BROWN, *Geophysicist III*
RUTH E. BROWN, *Assistant to the Director*
JOCK A. CAMPBELL, *Geologist IV*
BRIAN J. CARDOTT, *Geologist IV*
JAMES R. CHAPLIN, *Geologist IV*
JANISE L. COLEMAN, *Office Assistant IV*
CHRISTIE L. COOPER, *Managing Editor*
TAMMIE K. CREEL-WILLIAMS, *Secretary II*
CHARLES R. DYER III, *Drilling Technician*
WALTER C. ESRY, *Manager, Core and Sample Library*
ROBERT O. FAY, *Geologist IV*
AMIE R. FRIEND, *Research Specialist I*
PRISCILLA A. JOHNSON, *Office Assistant IV*
JAMES W. KING, *Research Specialist II*
STANLEY T. KRUKOWSKI, *Geologist III*
JAMES E. LAWSON, JR., *Chief Geophysicist*
LAURIE A. LOLLIS, *Cartographic Technician II*
KENNETH V. LUZA, *Geologist IV*
MICHAEL J. MERCER, *Manager, Log Library*
GALEN W. MILLER, *Research Associate*
RICHARD G. MURRAY, *Copy Center Operator*
SUE M. PALMER, *Office Assistant II*
DAVID O. PENNINGTON, *Operations Assistant II*
CONNIE G. SMITH, *Promotion and Information Specialist*
PAUL E. SMITH, *Supervisor, Offset Press Copy Center*
G. RUSSELL STANDRIDGE, *Information Tech Analyst I*
THOMAS M. STANLEY, *Geologist III*
LLOYD N. START, *Assistant Drilling Technician*
JOYCE A. STIEHLER, *Chief Clerk*
MICHELLE J. SUMMERS, *Technical Project Coordinator*
NEIL H. SUNESON, *Assistant Director, Geological Programs*
JANE L. WEBER, *Publication and Database Coordinator*

Cover Picture

Gross-sandstone isopach map of the Hartshorne Formation in Cabaniss NW field as an example of applying new interpretations of existing data to finding petroleum deposits (modified from Fig. 5, p. 133, this volume).

This publication, printed by the Oklahoma Geological Survey, is issued by the Oklahoma Geological Survey as authorized by Title 70, Oklahoma Statutes, 1981, Sections 231–238. 1,050 copies have been prepared for distribution at a cost of $9,377 to the taxpayers of the State of Oklahoma. Copies have been deposited with the Publications Clearinghouse of the Oklahoma Department of Libraries.

PREFACE

Petroleum exploration and development decisions are made based on technical information and data. To facilitate this technology transfer, the Oklahoma Geological Survey (OGS) and the U.S. Department of Energy, National Petroleum Technology Office (DOE–NPTO), in Tulsa, cosponsored a symposium dealing with new ideas and approaches to the improved recovery of known accumulations and the discovery of new reservoirs in the southern Midcontinent. The symposium was held on May 8–9, 2001, in Oklahoma City, Oklahoma. This volume contains the proceedings of that symposium.

Research reported upon at the symposium focused on the application of new technologies and new interpretations of existing data to finding new petroleum deposits. The symposium covered a wide range of topics, including seismic and well-log analysis, computer modeling, petroleum engineering, seal formation and timing, surface geochemistry, remote sensing, coalbed methane, and enhanced oil recovery. We hope that the symposium and these proceedings will bring such research to the attention of the geoscience and energy-research community, and will help foster exchange of information and increased research interest by industry, academic, and government workers.

Fifteen talks presented at the symposium are printed here as full papers or extended abstracts. An additional five talks are presented as abstracts in alphabetical order at the end of the volume. About 150 persons attended the symposium. Stratigraphic nomenclature and age determinations used by the various authors in this volume do not necessarily agree with those of the OGS.

This is the fourteenth symposium in as many years dealing with topics of major interest to geologists and others involved in petroleum-resource development in Oklahoma and adjacent states. These symposia are intended to foster the exchange of information that will improve our ability to find and recover our Nation's oil and gas resources. Earlier symposia covered: Anadarko Basin (published as OGS Circular 90); Late Cambrian–Ordovician Geology of the Southern Midcontinent (OGS Circular 92); Source Rocks in the Southern Midcontinent (OGS Circular 93); Petroleum-Reservoir Geology in the Southern Midcontinent (OGS Circular 95); Structural Styles in the Southern Midcontinent (OGS Circular 97); Fluvial-Dominated Deltaic Reservoirs in the Southern Midcontinent (OGS Circular 98); Simpson and Viola Groups in the Southern Midcontinent (OGS Circular 99); Ames Structure in Northwest Oklahoma and Similar Features—Origin and Petroleum Production (OGS Circular 100); Platform Carbonates in the Southern Midcontinent (OGS Circular 101); Marine Clastics in the Southern Midcontinent (OGS Circular 103); Pennsylvanian and Permian Geology and Petroleum in the Southern Midcontinent (OGS Circular 104); Silurian, Devonian, and Mississippian Geology and Petroleum in the Southern Midcontinent (OGS Circular 105); and Petroleum Systems of Sedimentary Basins in the Southern Midcontinent (OGS Circular 106).

Persons involved in the organization and planning of this symposium include: Brian Cardott and Charles Mankin of the OGS; and Bill Lawson and Herb Tiedemann of DOE–NPTO. Other OGS personnel who contributed include Michelle Summers and Tammie Creel, registration co-chairs; LeRoy Hemish, poster-session chair; and Connie Smith, publicity chair. Appreciation is expressed to each of them and to the many authors who worked toward a highly successful symposium. Special thanks are extended to OGS managing editor Christie Cooper, to William D. Rose (Frederick, Maryland) for technical editing of this volume, and to Virginia Rose (Frederick, Maryland) for layout and production.

BRIAN J. CARDOTT
General Chairman

CONTENTS

Petroleum Developments in the Southern Midcontinent—An Overview

Charles J. Mankin
Oklahoma Geological Survey
Norman, Oklahoma

Robert A. Northcutt
Independent Geologist
Oklahoma City, Oklahoma

Dan T. Boyd
Oklahoma Geological Survey
Norman, Oklahoma

ABSTRACT.—The southern Midcontinent is a geologic province that encompasses all or parts of seven states in the central United States. Within the thick sequence of Cambrian through Cretaceous sedimentary rocks that were deposited in this region is an abundance of oil and gas reservoirs. These reservoirs are distributed throughout the southern Midcontinent, but relative to their oil and gas volumes those present in the greater Anadarko, Arkoma, and Ardmore–Marietta basins dominate.

Commercial oil and gas production in the southern Midcontinent began in 1860 on the Cherokee platform in southeastern Kansas. However, it was nearly 30 years before this production eventually spread into northeastern Oklahoma, in 1889. After the turn of the century, petroleum development moved in rapid succession from the Arkoma basin in 1902, to the Ardmore–Marietta basin in 1904, and to the Nemaha uplift by 1910. The discovery of gas between 1918 and 1923, in what became the giant Panhandle-Guymon-Hugoton gas field, completed the expansion of oil and gas production through the western extent of the southern Midcontinent.

Through random drilling, increased geological understanding, and the march of technology, these outposts of production have gradually expanded to include all of the oil and gas areas that are known today. While this expansion has been episodic, with spurts in activity coinciding with the advent of new geologic plays, new technology, political events, and/or fluctuations in price, advances continue to this day.

INTRODUCTION

The southern Midcontinent region encompasses Oklahoma, Kansas, Missouri, northern Arkansas, southeastern Colorado, southern Nebraska, and the Texas Panhandle (Fig. 1). Within this extensive area is a thick column of sedimentary deposits ranging in age from Cambrian to Cretaceous. These rocks are now host to the thousands of oil and gas fields, of virtually all sizes and descriptions, that now blanket vast areas of the geologic basins and adjacent uplifts (Fig. 2).

The highly productive greater Anadarko basin, in western Oklahoma, the Texas Panhandle, southeastern Colorado, and western Kansas, dominates the region. The Ardmore–Marietta basin of southern Oklahoma and the Arkoma basin of eastern Oklahoma and western Arkansas, together with their platforms and adjacent uplifts, complete the list of major petroleum provinces of the southern Midcontinent. The Hollis–Hardeman basin of southwestern Oklahoma and the Forest City basin of northeastern Kansas–northwestern Missouri, though relatively minor, are still productive. The north–south-trending Nemaha uplift/fault zone separates the Anadarko shelf from the Cherokee platform and has been a focus of production in both Kansas and Oklahoma. Other structural highs that have concentrated significant oil and gas production include the central Kansas uplift, the Seminole arch, the northern part of the Amarillo–Wichita Mountain uplift, and the Cimarron arch.

EARLY DISCOVERIES AND DEVELOPMENT

The first commercial oil discovery in the southern Midcontinent was drilled in southeastern Kansas in Miami County. This 1860 discovery postdated by only 1 year the first commercial oil well in the United States, which was drilled by Edwin L. Drake in 1859 in Titusville, Pennsylvania. Coming from an extensive Pennsylvanian sand at a depth of 275 ft, this initial Kansas production opened what was to become the Paola field. The development of this field was delayed by events surrounding the Civil War, but by 1889 it was producing approximately 500 barrels of oil (BO)

Mankin, C. J.; Northcutt, R. A.; and Boyd, D. T., 2002, Petroleum developments in the southern Midcontinent—an overview, *in* Cardott, B. J. (ed.), Revisiting old and assessing new petroleum plays in the southern Midcontinent, 2001 symposium: Oklahoma Geological Survey Circular 107, p. 1–15.

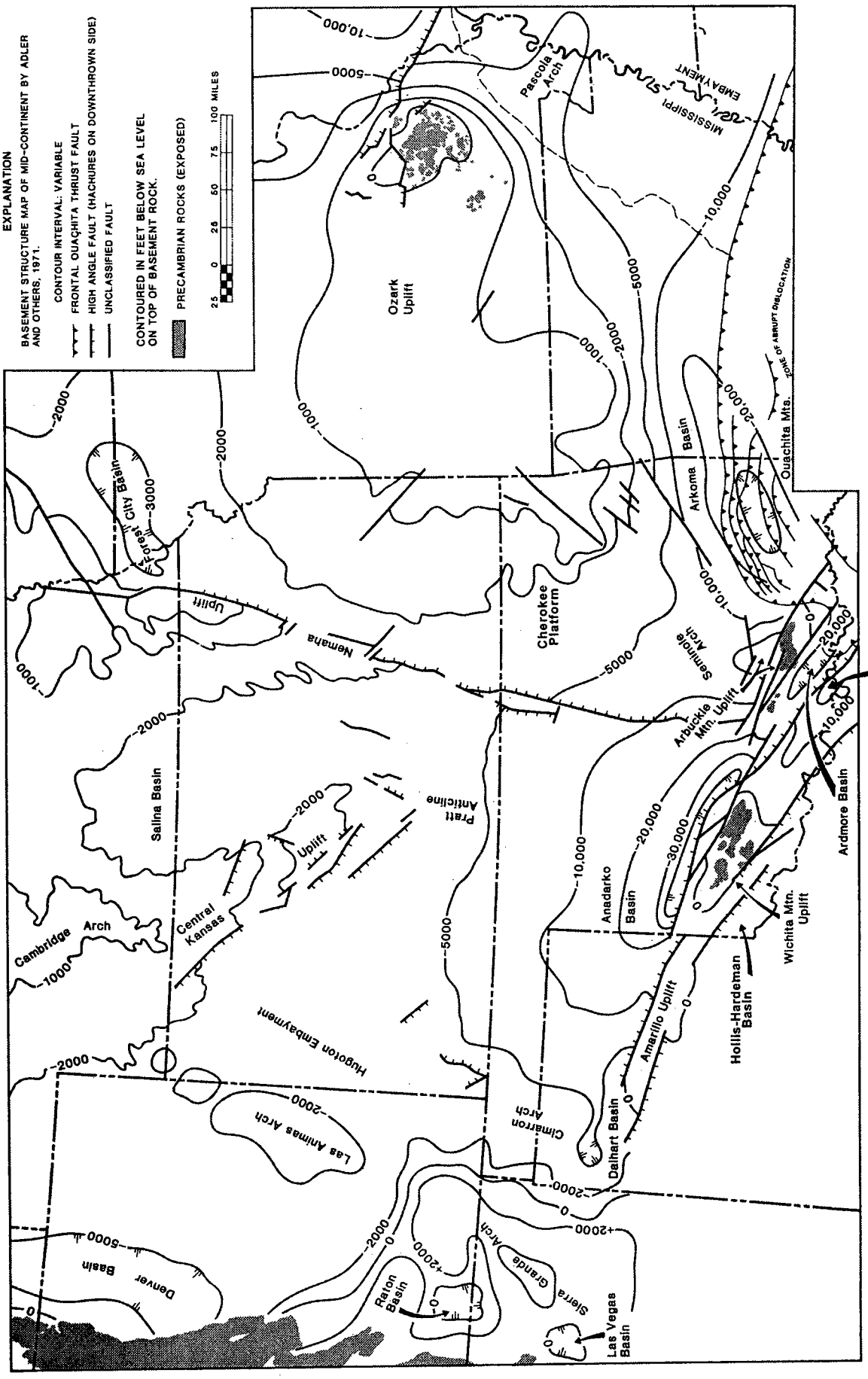

Figure 1. Basement-structure map of the southern Midcontinent, showing major structural features. Contour interval is variable. Modified from Adler and others (1988).

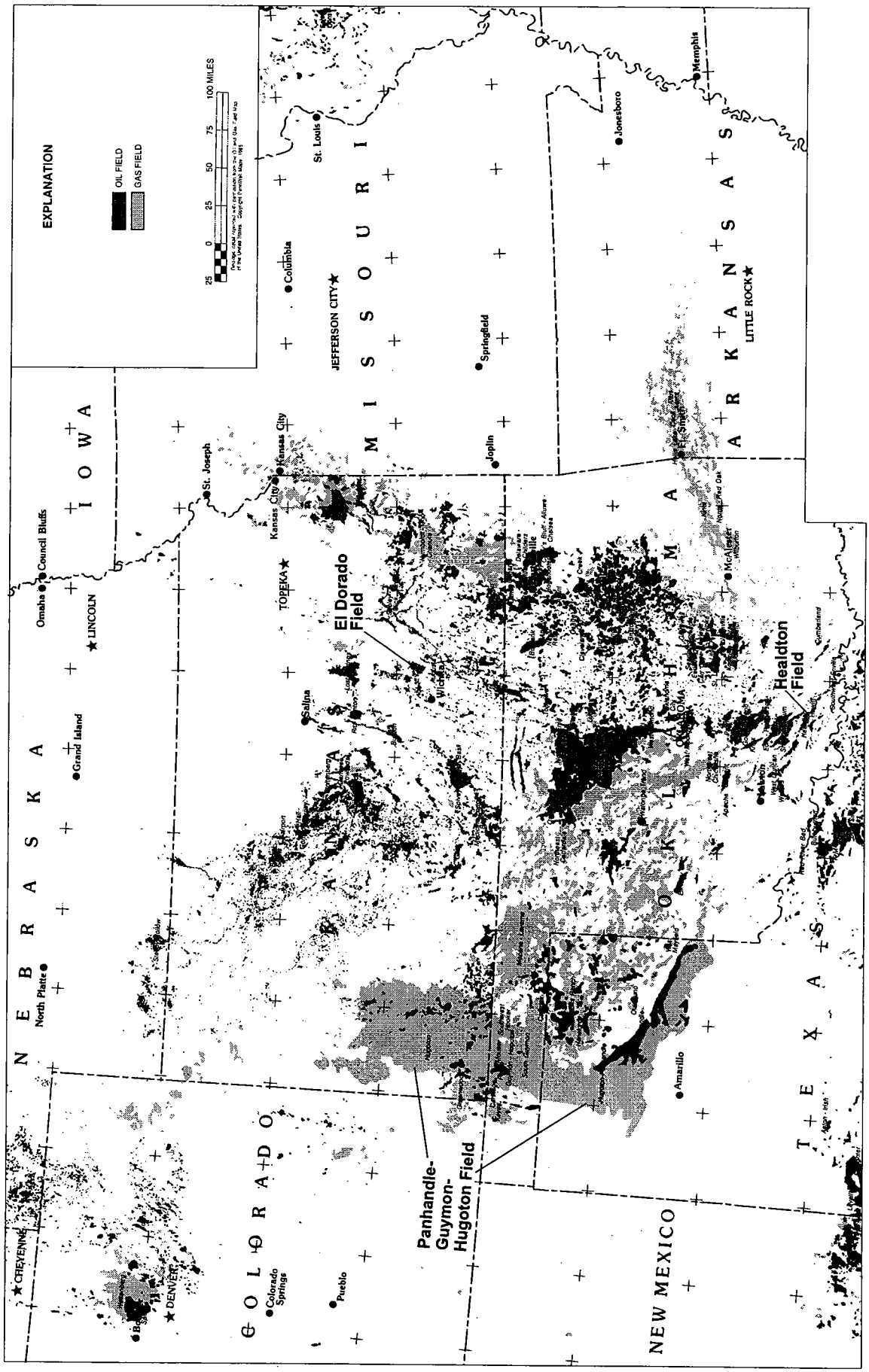

Figure 2. Oil- and gas-field map of the southern Midcontinent area. From PennWell Maps (1985).

per year, which constituted the total production for the State (Jewett, 1954).

Petroleum exploration and development spread from eastern Kansas into northeastern Oklahoma in 1889 when a small, noncommercial Cherokee (Pennsylvanian) sand was encountered in a well drilled near Chelsea in Rogers County (Mills-Bullard, 1928). However, it was not until the 1897 discovery in the prolific Bartlesville sand at Bartlesville-Dewey field in Washington County that petroleum activity in Oklahoma began in earnest.

Natural-gas exploration and development in the southern Midcontinent began in 1902 with the discovery of gas in the Arkoma basin from a shallow Atoka sand in what became Mansfield field in Sebastian County, Arkansas (Croneis, 1930). This production was extended into the Oklahoma portion of the Arkoma basin in 1910 with the discovery of a shallow Atoka gas sand in Red Oak field in Latimer County (Mills-Bullard, 1928). However, mimicking the slow start of oil production in the southern Midcontinent, the full potential of this prolific gas province was not fully recognized until the discovery of the deeper Atoka (Spiro) gas sands in 1930 in Clarksville field in Le Flore County, Oklahoma (Branan, 1968).

In Oklahoma the expansion of oil and gas production spread south into the Ardmore–Marietta basin in 1904 when Wheeler field was discovered in shallow Permian sands in Carter County (Gouin, 1956). This was followed in 1910 by the discovery of gas in shallow Permian "sands" to the north on the Nemaha uplift in Ponca field in Kay County. However, it was not until 1917 that oil production in the Ponca field was discovered in deeper Pennsylvanian reservoirs (Clark and Cooper, 1930).

To the north in Kansas, also on the north-trending Nemaha uplift, the Augusta field in Butler County was opened with the discovery of oil in the Ordovician "Varner sand" in 1914 (Berry and Harper, 1948). In the following year (1915) El Dorado field, also in Butler County, was discovered, with oil production coming from sandstones in the Permian Admire Group. El Dorado quickly became the most productive oil field in Kansas, and in 1918 it was the largest oil field in the United States (Jewett, 1954).

Also in 1918, gas was discovered in the Texas Panhandle in Chase Group carbonates (Permian) in Potter County. This was followed in 1921 with the discovery of oil, also in the Chase Group, in Carson County. Chase Group gas development moved northward into Seward County, Kansas, in 1922 and Texas County, Oklahoma, in 1923. All of these discoveries were eventually recognized as being part of what is now the prolific Panhandle-Guymon-Hugoton field (Mason, 1968). This giant field is one of the world's largest known gas accumulations. Extending >200 mi through southwestern Kansas and the Oklahoma and Texas Panhandles, it dominates gas production for the entire southern Midcontinent (Fig. 2). Its importance is illustrated by the fact that, although only a small portion of the field is in Oklahoma, it is still the largest gas field in the State.

MULTISTAGE DEVELOPMENT IN EARLY FIELDS

After discovery, most large fields undergo an episodic development that often greatly increases initial estimates of recoverable reserves. Usually these reserve additions are a direct result of the application of new geologic/geophysical/engineering ideas and techniques. These bring about the testing of potential reservoirs that are both deeper and shallower than the original discovery zone, as well as exploitation of trapping styles not initially identified. In addition, advances in evaluation technology (e.g., wireline logging) have permitted the identification of overlooked reservoirs; drilling and completion technology, the penetration and production of high-pressure or easily damaged reservoirs; and secondary- or enhanced-recovery technology, the ability to get the most out of the reservoirs that have been found.

To illustrate this, three fields were chosen that were discovered early in the 20th century. Identified by utilizing one of the oldest and most basic techniques—surface geologic mapping—all three are excellent examples of this multistage development. Healdton, El Dorado, and Panhandle-Guymon-Hugoton fields are each >80 years old, and as such have durations that encompass the bulk of the time that mankind has heavily relied on hydrocarbon-based energy. These fields provide many insights into the evolution of petroleum exploration and production, with histories that span the early years of a fledgling oil and gas business through its growth into the industry of today.

Healdton Field, Carter County, Oklahoma

Healdton field is in western Carter County and northeastern Jefferson County, Oklahoma. This structurally trapped field, in the Ardmore–Marietta basin of southern Oklahoma, lies northwest of the Criner uplift and is bounded to the northeast by the Duncan–Criner fault (Fig. 3).

Field-Discovery Wells

The well that is recognized for the discovery of Healdton field is the Red River Oil Co. No. 1 Wirt Franklin (sec. 5, T. 4 S., R. 3 W.). This well was completed in August 1913, producing 100 barrels of oil per day (BOPD) from a depth of 919 ft. The initial production was from four Pennsylvanian sands of the Hoxbar Group (Missourian) that were fully developed by 1919 (Mills-Bullard, 1928; Latham, 1970). The stratigraphic section at Healdton field is shown on the composite electric–lithologic-log curves in Figure 4. The northwest-trending anticline that is depicted on the Healdton sandstone structure map in Figure 5 has structurally trapped these productive sands. The relatively simple folding of the Pennsylvanian Healdton sands, and the contrasting complex folding and fault-

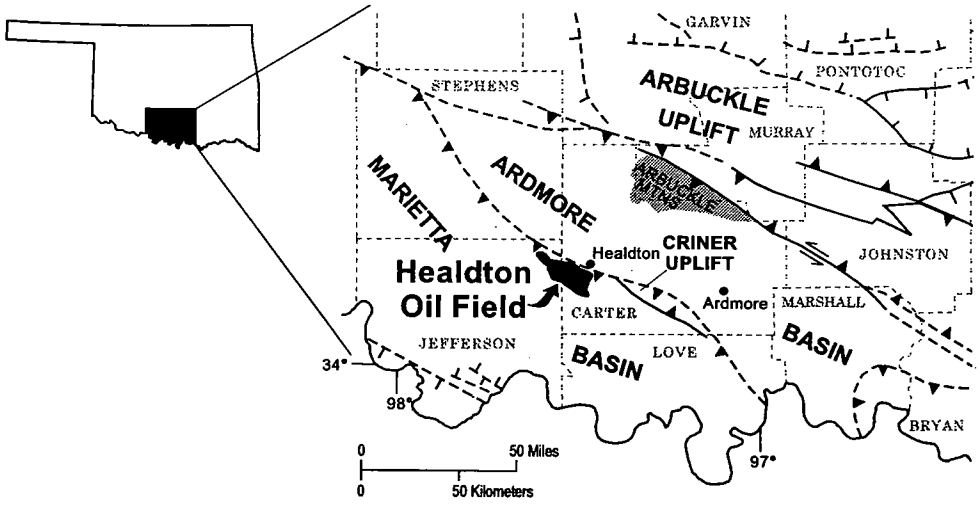

Figure 3. Map of major faults in south-central Oklahoma, showing Healdton field. From Terry (1999).

ing in the underlying Ordovician carbonates, are shown by the cross section in Figure 6. This figure also highlights the magnitude of the uplift and erosion that occurred prior to deposition of the Healdton sands.

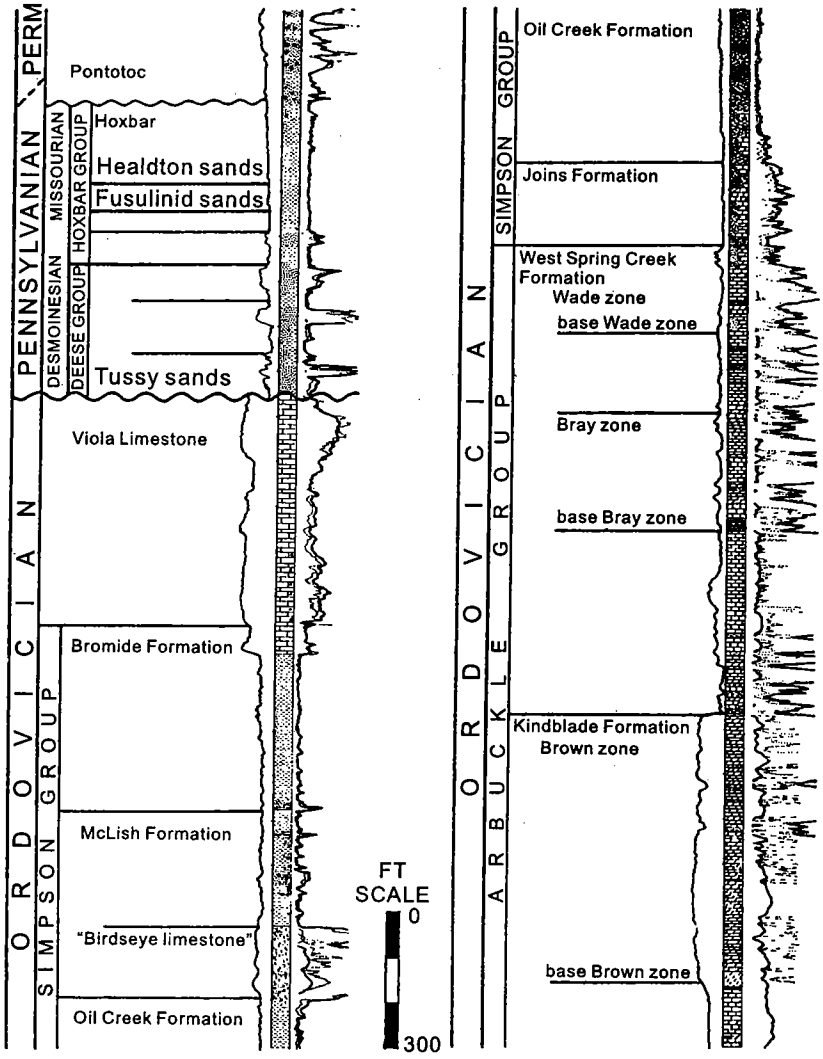

Figure 4 *(left)*. Composite electric–lithologic log of stratigraphic section for Healdton field. From Latham (1970).

Deeper and Shallower Field Development

From the discovery of Healdton field in 1913 until 1960, most development activity was focused on the Healdton (Hoxbar Group) sands. The discovery of production below this interval, in the Tussy and Fusulinid sands (Deese Group), began in the late 1950s and led to additional field development (Terry, 1999). However, though somewhat deeper, all production remained above the pre-Pennsylvanian unconformity that is shown in Figure 6.

Several deep wells were drilled early in the field's history to test Arbuckle (Lower Ordovician) rocks, but without success. In 1960 the Arbuckle was tested in its Brown, Wade, and Bray zones with mixed but mildly encouraging results. However, in 1961 Sinclair Oil and Gas Co. completed the fourth recent Arbuckle test. Drilled in the central part of the field, it flowed 336 BOPD from a depth of 3,999 ft. This deeper pool discovery began a period of significant Arbuckle development (Latham, 1968), which by 1981 had even added production from the Middle Ordovician Oil Creek Formation (Simpson Group) to the eastern part of the field (Terry, 1999).

Other Events

Secondary-recovery (waterflooding) operations in the Healdton sands, which commenced in the late 1960s and the early 1970s, were successful in significantly increasing production (Terry, 1999). The sequence of Healdton field development activities is shown in Table 1.

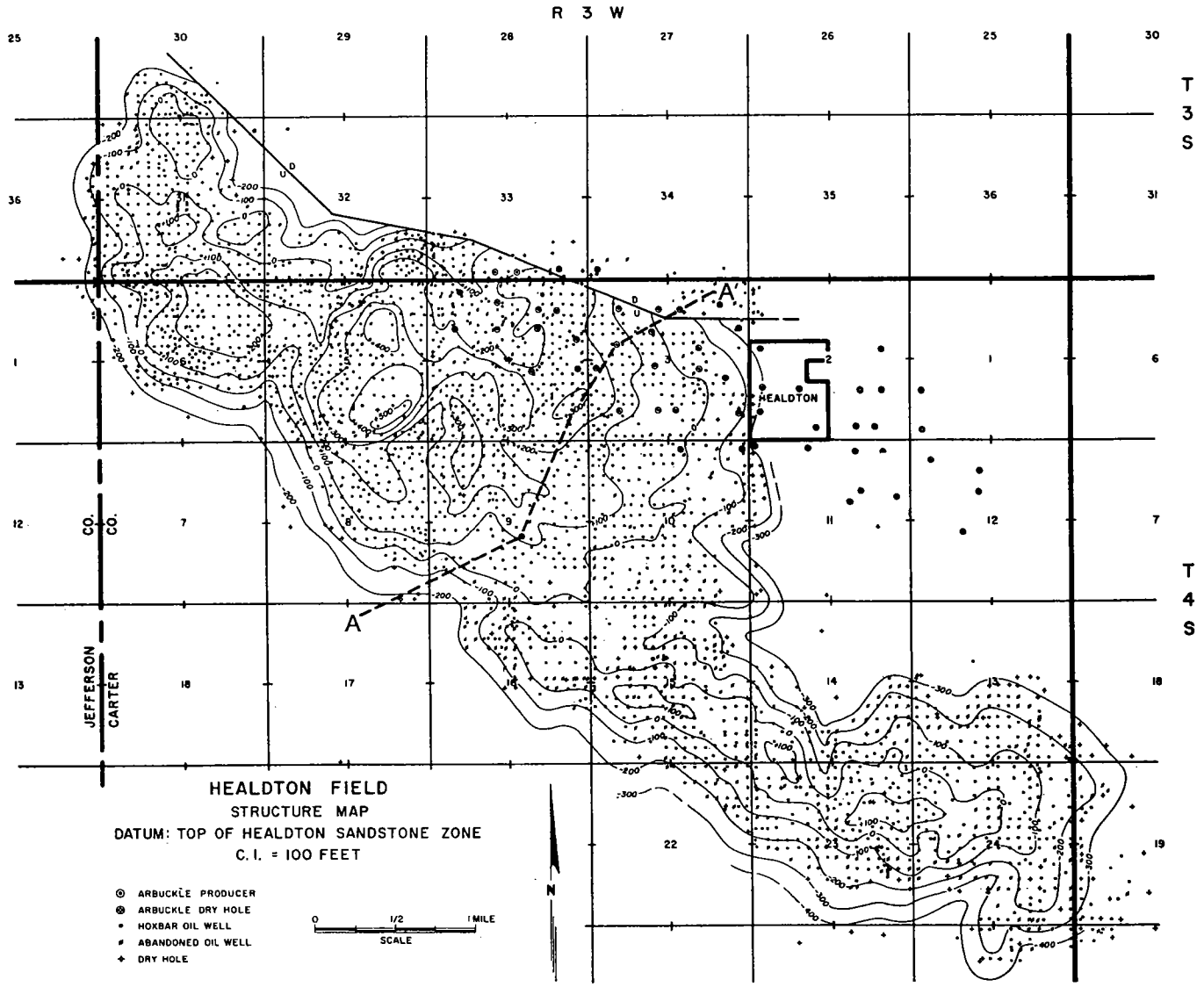

Figure 5. Structure map depicting the top of the Healdton sandstone in Healdton field. Line A–A′ shows location of cross section portrayed in Figure 6. From Latham (1970).

Oil and Gas Production

The geographic distribution of production from both Pennsylvanian and Ordovician reservoirs in Healdton field is shown in Figure 7. Cumulative production from all reservoirs in the field is 353 million barrels of oil (MMBO) and 16 billion cubic ft of gas (BCFG), making it the seventh largest field in Oklahoma.

El Dorado Field, Butler County, Kansas

El Dorado field is a structurally controlled field in southeastern Kansas on the north-trending Nemaha uplift. This uplift, which becomes a fault zone to the south, is a major structural feature in the southern Midcontinent that extends from eastern Nebraska through central Oklahoma (Fig. 8).

Field-Discovery Wells

The discovery well for El Dorado field was the Wichita Natural Gas Co. No. 1 Stapleton (sec. 29, T. 25 S., R. 5 E.), which was completed in 1915. The initial production in this well came from sandstones in the Admire Group (Permian) at a depth of ~600 ft. In late 1915 the well was deepened to 2,465 ft and completed for 175 BOPD in what became known as the "Stapleton zone." In El Dorado field this is the name given to all Ordovician rocks, from the Viola Group down through the Arbuckle Group, which are separated from the overlying Pennsylvanian rocks by a prominent angular unconformity (Fig. 9) (Jewett, 1954). A structural cross section (Fig. 10) shows the relationship between pre- and post-unconformity rocks in El Dorado field.

An Arbuckle structure map of the field (Fig. 11) shows that the trap has been broken into seven structural "highs," or domes. These domes were caused by a series of small faults west of the much larger Nemaha fault, which defines the eastern limit of both the Nemaha uplift and the field. The magnitude of pre-Pennsylvanian uplift and erosion that resulted from this

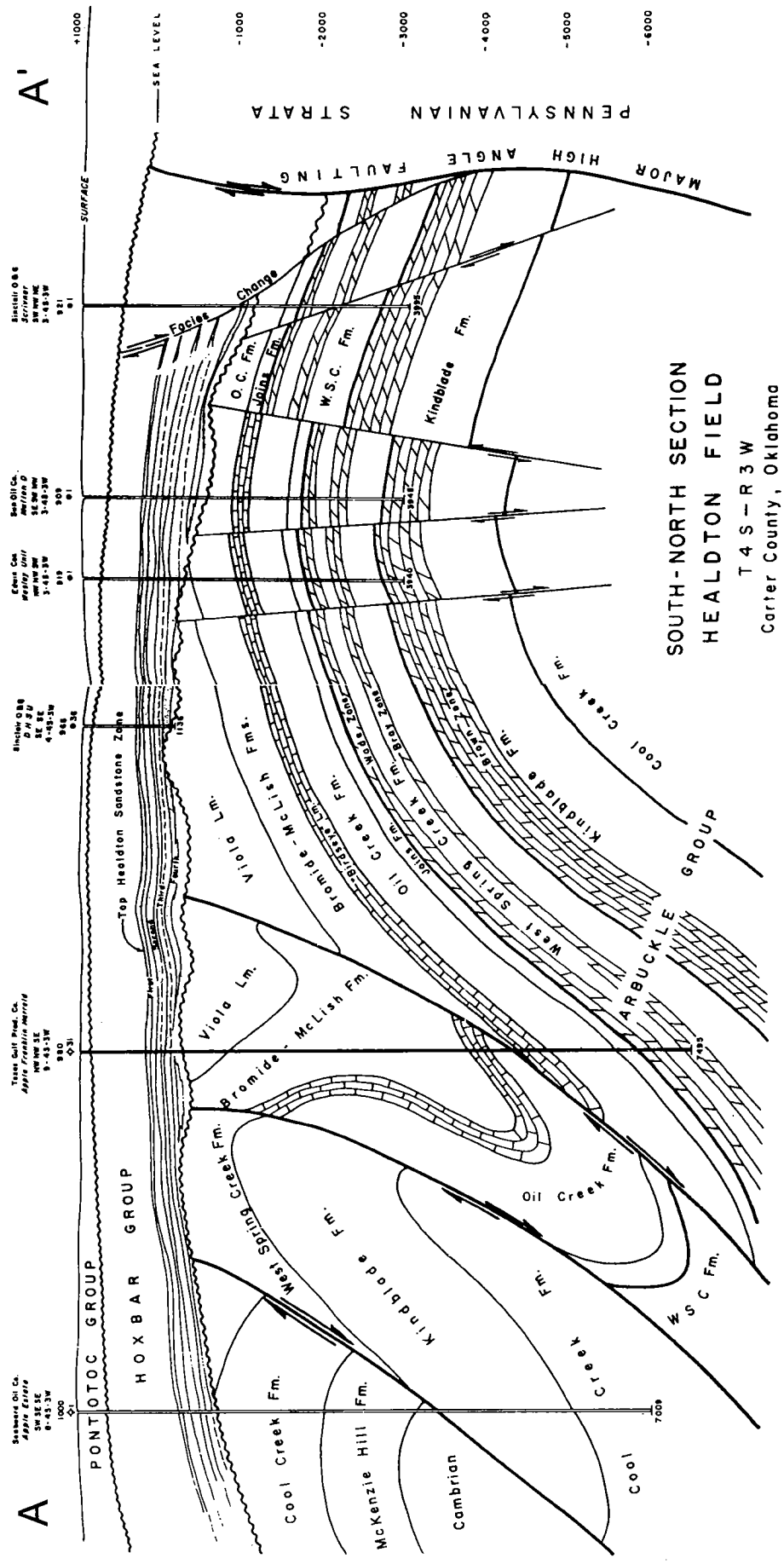

Figure 6. Schematic geologic cross section A–A′ through Healdton field. No vertical exaggeration. Line of section shown in Figure 5. From Latham (1970).

Table 1. — Chronology of Significant Events in Healdton Field, Carter County, Oklahoma

Year(s)	Event
1913	Discovery of oil in Healdton sand zone
1947–60	New wells and workovers in Healdton sand zone
1950s	Discovery and development of Fusulinid and Tussy sand zones
1962	Discovery of Arbuckle Group reservoir (Brown, Wade, Bray zones)
Late 1960s–mid 1970s	Waterflood in Healdton sand zone
1970s	Acid-completion method in carbonate reservoirs
1980s	Workovers and waterflood in Healdton sand zone (south-central part of field)
1981	Discovery and development of Simpson Group reservoir (Oil Creek Formation)

Source: Terry (1999).

tectonic movement can clearly be seen in Figure 10.

The development of El Dorado field was rapid. By 1916, the year after its discovery, 600 wells were producing >12,000 BOPD. Two years later, in 1918, El Dorado was the leading field in the United States, with a cumulative production of ~29 MMBO (Jewett, 1954).

Deeper and Shallower Field Development

By 1920, El Dorado field was essentially fully developed, with a total of 15 productive zones spanning a stratigraphic interval from the Upper Pennsylvanian through the Ordovician.

Other Events

Arbuckle completions began watering out in the 1920s and early 1930s, and many of these wells were plugged. When it was discovered in the late 1930s that acid treatments could be used to stimulate production in carbonate rocks, those remaining Arbuckle wells that had not yet been plugged were treated with

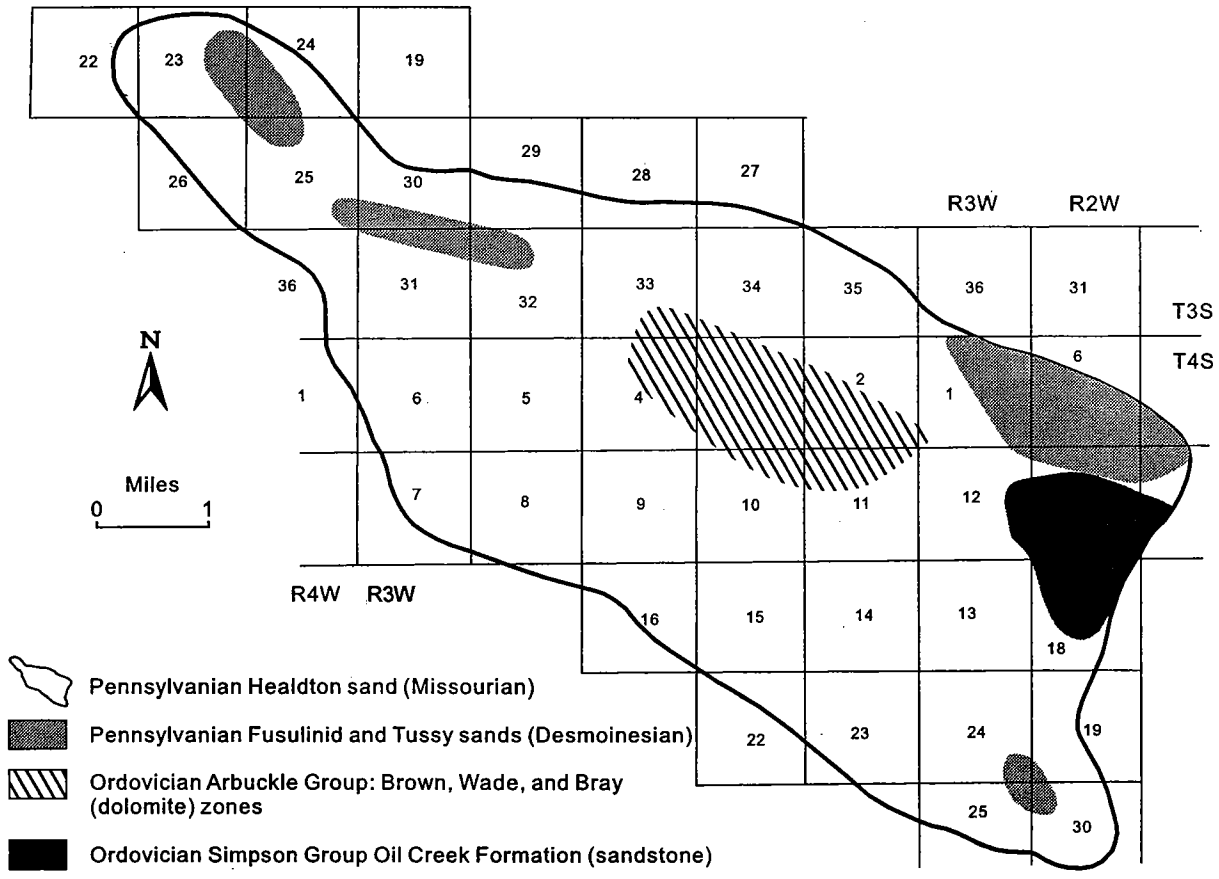

Figure 7. Map of Healdton field showing productive areas by reservoir. From Terry (1999).

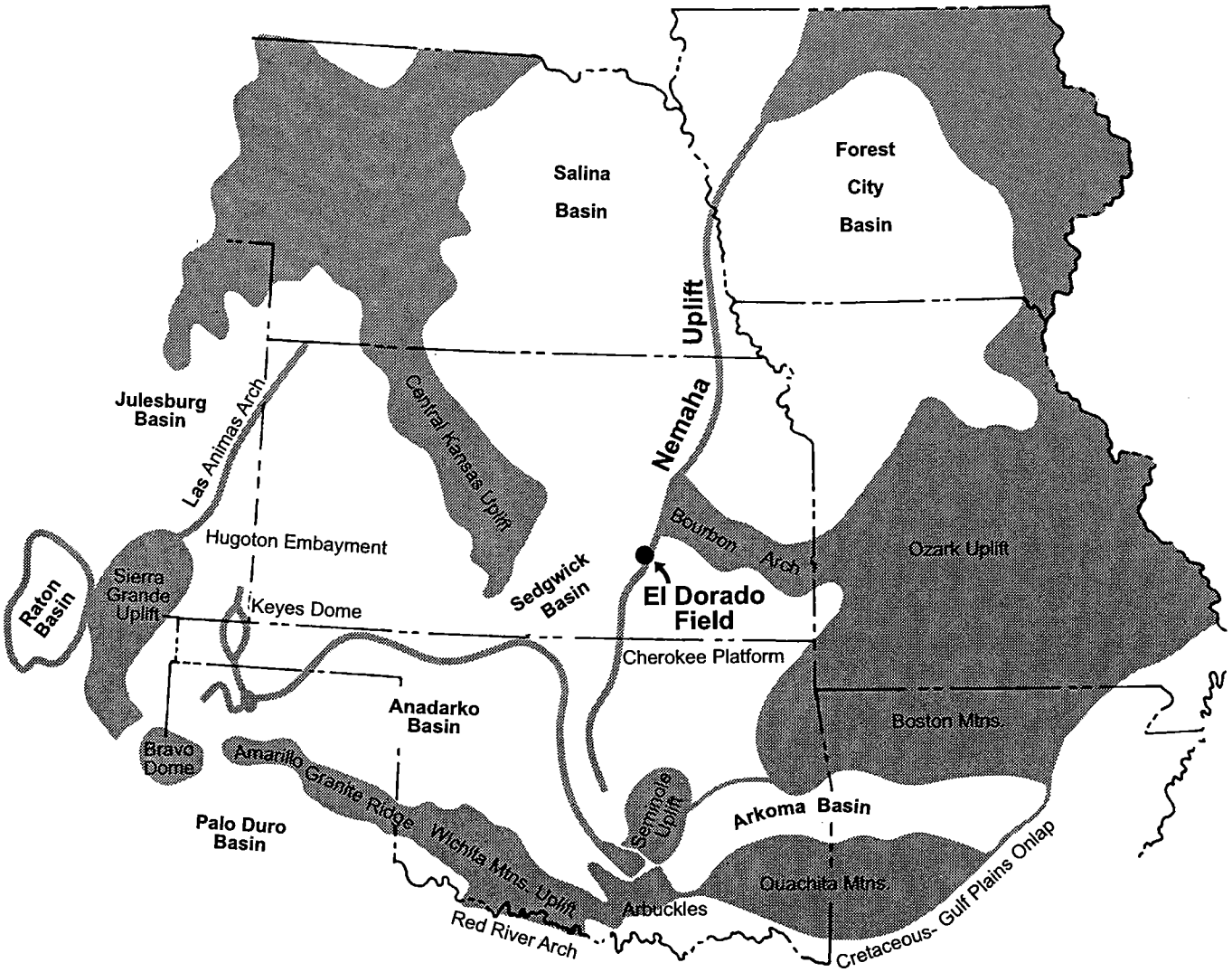

Figure 8. Regional tectonic map of the southern Midcontinent, showing El Dorado field. Modified from Ramondetta (1990).

acid. This yielded a marked improvement in their production and extended the reservoir life significantly.

Many of the Admire Group wells that were completed in the 1920s were fractured by the use of nitroglycerin. This was one of the first times that nitroglycerin was used to stimulate wells. Also in the 1920s, Admire Group wells saw one of the first uses of air injection as a secondary-recovery technique. Later, in the 1940s and 1950s, waterfloods were initiated in both the Admire and Lansing–Kansas City Group reservoirs. In 1974 a chemical-injection pilot project in the Admire Group was tried, but without appreciable success (Ramondetta, 1990). A complete chronology of El Dorado field-discovery and -development events is shown in Table 2.

Oil and Gas Production

At the end of 2000 the Kansas Geological Survey reported cumulative production from El Dorado field to be 302 MMBO. At this time, in spite of the fact that the field was 85 years old, production was still continuing at a rate of approximately 600,000 barrels per year from 532 producing wells.

Panhandle-Guymon-Hugoton Field, Texas and Oklahoma Panhandles, Southwestern Kansas

The giant Panhandle-Guymon-Hugoton field covers an immense area of 8,500 mi^2, including all or parts of 22 counties in Texas, Oklahoma, and Kansas (Fig. 12). This field, the largest gas field in the United States, is structurally trapped on the south by the Amarillo uplift (Fig. 1) and hydrodynamically trapped as it extends northward along the western flank of the Anadarko basin (Mason, 1968).

Field-Discovery Wells

Surface geologic mapping of the "John Ray dome," a part of the larger Amarillo uplift in Potter County, Texas, determined where the discovery well for the field was to be located. Drilled by Amarillo Oil Co., the No. 1 Masterson C (Sec. 65, Block 0-18, D&P Survey) was completed in 1918. The well was drilled to a

Table 2. — Chronology of Significant Events in El Dorado Field, Butler County, Kansas

Year(s)	Event
1915	650-ft Admire and 2,500-ft Stapleton (Ordovician) oil discoveries
1916–18	Admire development drilling completed
1917	1,700-ft Lansing and 2,000-ft Kansas City oil discoveries
1920s	Admire wells fractured with nitroglycerin
1920s	Admire air-injection project started (first secondary-recovery project?)
1930s	Acidization of Arbuckle wells
1940s–1950s	Waterflooding began of Admire and Lansing–Kansas City reservoirs
1974	Admire chemical-injection pilot project
1976–83	650-ft Admire micellar-polymer flood project

Source: Ramondetta (1990).

total depth of 2,395 ft and gauged natural gas at a rate of 5 million cubic feet per day (MMCFPD) from the Lower Permian (Wolfcampian) dolomites of the Chase Group (Pippin, 1970) (Fig. 13). The field-area map (Fig. 12) shows the locations of the four initial "discoveries" and outlines the ultimate extent of the field area after development.

The next significant event in the life of the field

System	Series	Stage	Group	Formation†	Approx. Depth*	
Permian	Lower	Gearyan	Chase	Winfield	Surface	
				Towanda	Surface	
				Fort Riley	Surface	
			Council Grove			
			Admire§		500-700	
Pennsylvanian	Upper	Virgilian	Wabaunsee	Burlingame§	800	
				White Cloud§	900	
			Shawnee	Lecompton		
				Oread		
			Douglas	Douglas sand§	1,500	
		Missourian	Lansing§		1,650	
			Kansas City§		1,950	
			Pleasanton	Checkerboard	2,200	
				Hepler sand§	2,200	
	Middle	Desmoinesian	Marmaton	Altamont	2,200	
				Pawnee		
				Fort Scott		
			Cherokee		2,300	
			Pre-Pennsylvanian Unconformity			
Mississippian	Lower	Osagian§			2,600	
Ordovician	Middle		Viola§		2,500	
			Simpson§	Saint Peter§ sandstone	2,500	
	Lower		Arbuckle§	Cotter§	2,300-2,500	
Cambrian	Upper			Eminence		
				Reagan or Lamotte sandstone	2,500 to 4,000	
Precambrian				Granite		

Stapleton Zone

* Many of the following depths are near the upper limits and indicate the approximate level at which the appropriate formations are productive.
† Not all formations are listed below.
§ Has produced hydrocarbons within El Dorado field.

Figure 9. Stratigraphic chart for El Dorado field, showing ages, names, and approximate depths (in feet) of formations. Productive formations are indicated. From Ramondetta (1990).

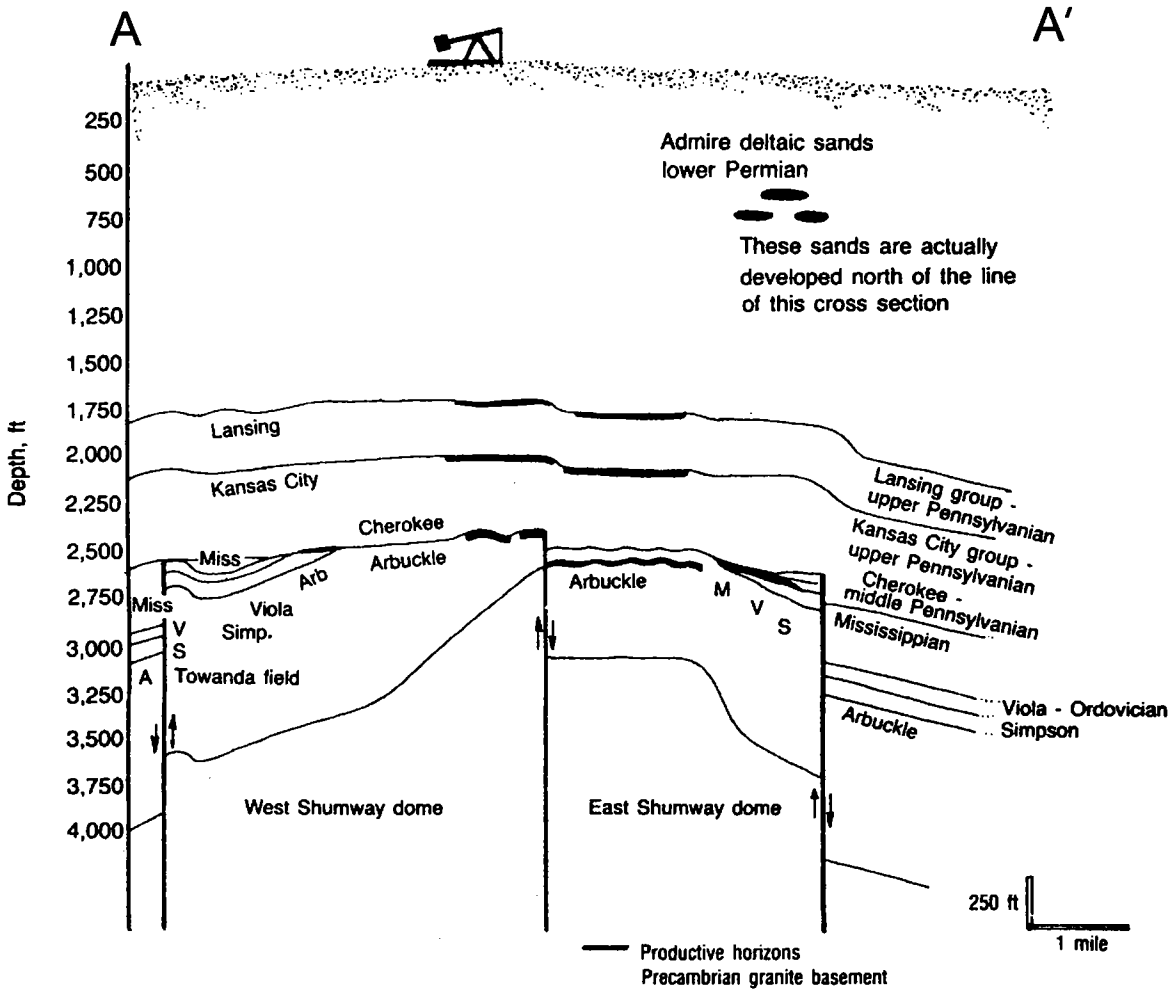

Figure 10. Schematic geologic cross section A–A′ through El Dorado field from west to east. Line of section shown in Figure 11. From Ramondetta (1990).

was the addition of Wolfcampian oil from Carson County, Texas. The discovery well, the Gulf Producing Co. No. 2 Burnett (Sec. 106, Block 5, I&GN Survey), was completed in 1921 with an initial flowing potential of 200 BOPD from an interval called "granite wash." This was the first well drilled into what would become the Texas Panhandle oil field, which is actually the massive oil rim of a southern part of the Panhandle-Guymon-Hugoton gas field. The drilling of a prolific well in 1925 initiated the systematic development of the oil field (Pippin, 1970).

The Hugoton discovery well in Kansas, the Defenders and Traders Gas Co. No. 1 Boles (sec. 3, T. 35 S., R. 34 W.), was drilled in Seward County. Completed in 1922 just north of the Oklahoma border, this well increased drilling activity in the area and led to a similar "discovery" in the Oklahoma Panhandle (Pippin, 1970). This well was the Home Development Co. No. 1 (sec. 4, T. 1 N., R. 12 E.C.M.), in Texas County. It was drilled to a depth of 3,040 ft and produced from what was described as a gas sand in the Permian "Big lime" at a depth of 2,695 ft (Six, 1930).

The recognition that these four "discovery" wells were in fact all parts of one enormous field did not come until 1927, when a gas well drilled in Stevens County, Kansas, near the town of Hugoton, was completed in 1927, flowing from a Permian Chase Group reservoir. This well helped reveal the true nature of the accumulation and initiated a large-scale development program in the Hugoton area that saw 75 gas wells completed by 1930 (Pippin, 1970).

A structure map depicting the top of the productive Hugoton reservoirs (Fig. 14) illustrates the domal character of the Texas portion of Panhandle-Guymon-Hugoton field and the hydrodynamic trapping character of the Oklahoma and Kansas portions. The gas–oil and oil–water contacts in the southern part of the field delineate Panhandle oil field. The updip and downdip gas–water contacts show the upper and lower limits of gas production in the Chase Group carbonates.

Deeper and Shallower Field Development

Prior to the northward expansion of Hugoton field in Kansas, exploration in western Kansas, utilizing seismic surveys, had identified a number of deeper oil and gas pools. Nunn oil field, discovered in 1938 in north-

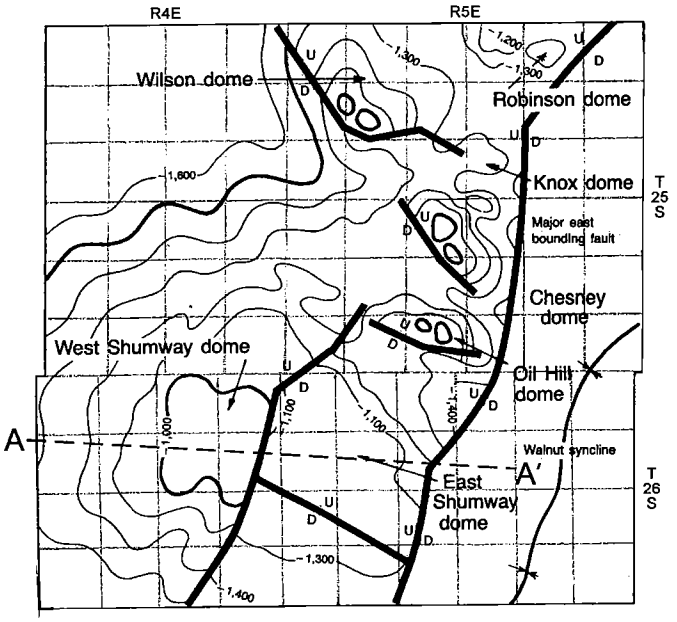

Figure 11. Structure map depicting the top of the Arbuckle Group in El Dorado field, showing the seven named domes. Contour interval is 100 ft. From Ramondetta (1990). Section A–A´ is shown in Figure 10.

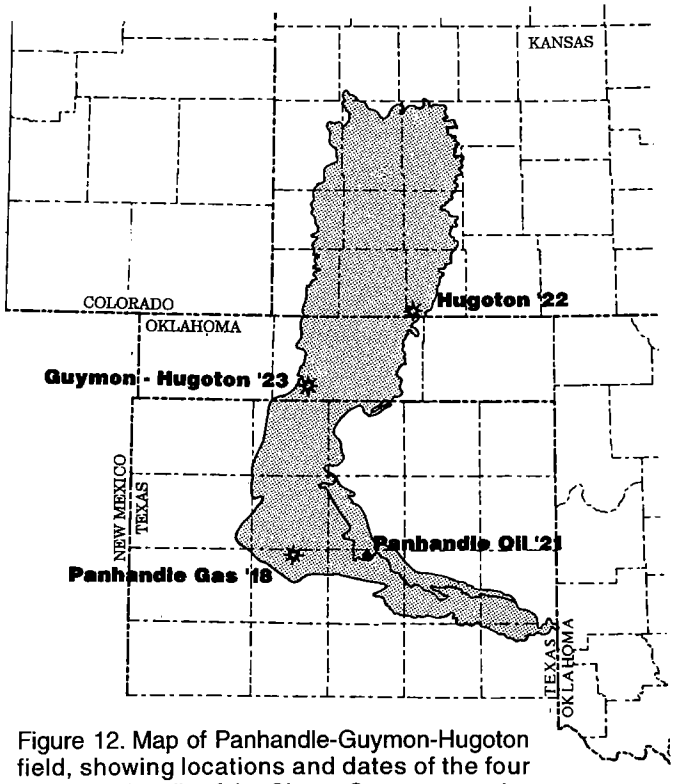

Figure 12. Map of Panhandle-Guymon-Hugoton field, showing locations and dates of the four "discovery" wells of the Chase Group reservoirs. Modified from Davis and Northcutt (1989).

ern Finney County, Kansas, produced from a structural trap in reservoirs ranging from the Mississippian St. Louis through the Pennsylvanian Cherokee (Aukerman, 1959). In addition, 1941 saw the discovery of stratigraphically trapped Morrow oil in southeastern Kearny County's Patterson field (Davis, 1959).

SYSTEM	SERIES	GROUP	LOCAL NOMENCLATURE: PANHANDLE FIELD	LOCAL NOMENCLATURE: HUGOTON FIELD
PERMIAN	LEONARD	SUMNER	RED CAVE	RED CAVE
			WICHITA	WICHITA
	WOLFCAMP	CHASE	BROWN DOLOMITE	HERINGTON
				KRIDER
			WHITE DOLOMITE	WINFIELD
			MOORE Co. LIME	FT. RILEY
			ARK. DOLOMITE	
			ARK. LIME	
				WREFORD
		COUNCIL GROVE	GRANITE WASH	COUNCIL GROVE
		ADMIRE		ADMIRE
PENNSYLVANIAN	VIRGIL	WABAUNSEE	GRANITE Pε	WABAUNSEE
		SHAWNEE		SHAWNEE

Figure 13. Stratigraphic column for Panhandle-Guymon-Hugoton gas field. From Pippin (1970).

The demand for natural gas increased in the mid-1930s in tandem with the construction of a large number of gas pipelines. These events combined to increase the average price of gas, which spurred a more rapid development of Panhandle-Guymon-Hugoton field during the 1940s and early 1950s (Mason, 1968). Following this period, operators began to explore for deeper accumulations. To do this, they utilized the large volume of structural data derived from shallower drilling to high-grade prospective areas for seismic investigation. This effort, combined with ongoing deep field development, resulted in the addition of large oil and gas volumes to the reserves assigned to the field. These additional reserves were primarily in reservoirs of the Council Grove (Lower Permian), Topeka (Pennsylvanian), Lansing–Kansas City (Pennsylvanian), Atoka (Pennsylvanian), Morrow (Pennsylvanian), and St. Louis (Mississippian) stratigraphic units. The shallower Red Cave (Permian) gas potential in the Texas Panhandle was discovered in 1919 but was not developed until 1960–65. Prior to this the Red Cave was bypassed in order to produce the deeper, more economic Chase Group gas reservoirs (Rogers, 1961). Figure 15 is a map showing the deeper and shallower areas of oil and gas development within Panhandle-Guymon-Hugoton field.

Other Events

It was discovered early that the gas produced from Panhandle-Guymon-Hugoton field contained more than simply hydrocarbons. In 1929 the extraction of helium from the natural gas produced from the field began, initiating this field as the primary source of helium for the United States.

A variety of successful secondary or enhanced oil-

recovery techniques began in many of the oil accumulations in 1946. These techniques included gas injection, waterflooding, and thermal applications.

Infill drilling (increased density) for gas in the Kansas portion of the field was authorized by the Kansas Corporation Commission in 1986, resulting in the addition of >600 wells. However, a study and report on this program concluded that no untapped gas was identified as a result of this additional drilling (McCoy and others, 1992). A complete chronology of the discovery and development events for Panhandle-Guymon-Hugoton field is shown in Table 3.

Oil and Gas Production

Cumulative production for greater Panhandle-Guymon-Hugoton field through 2001 was ~72 trillion cubic feet of gas (TCFG) and 1.6 billion barrels of oil. In 1999 the field produced an average of ~1.5 BCFG and 12,000 BO per day. This translates to an annual production rate of ~0.5 TCFG and 4 MMBO.

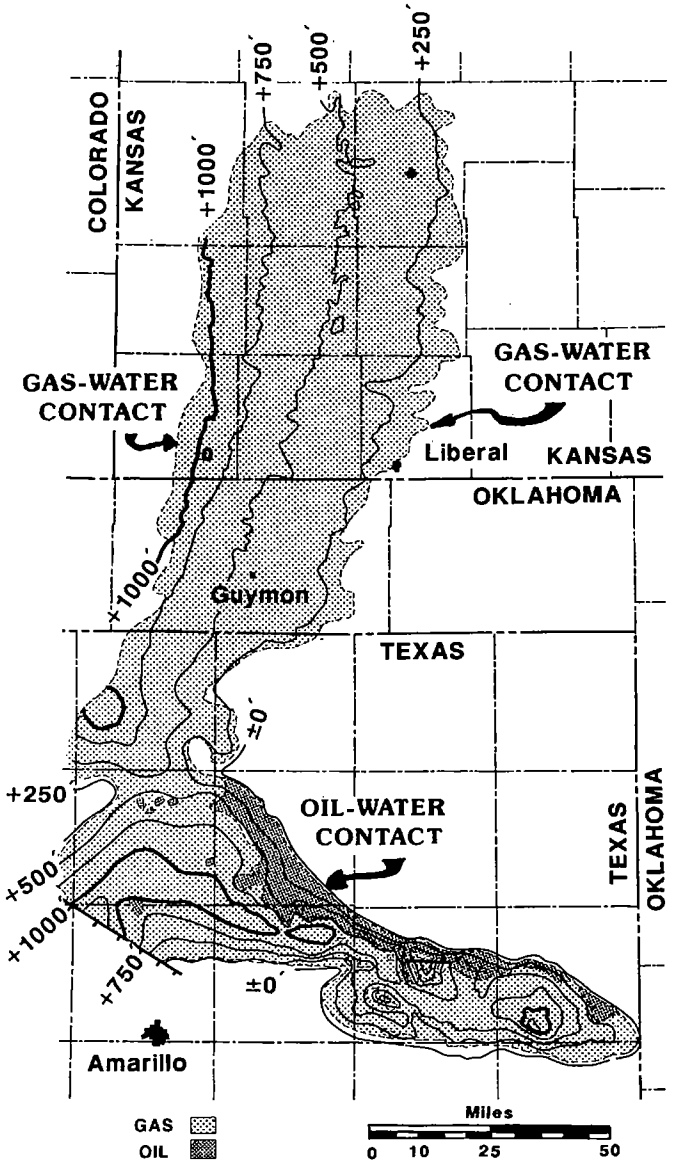

Figure 14. Structure map depicting the top of the Hugoton pay in Panhandle-Guymon-Hugoton gas field, showing fluid contacts. Contour interval is 250 ft. From Davis and Northcutt (1989).

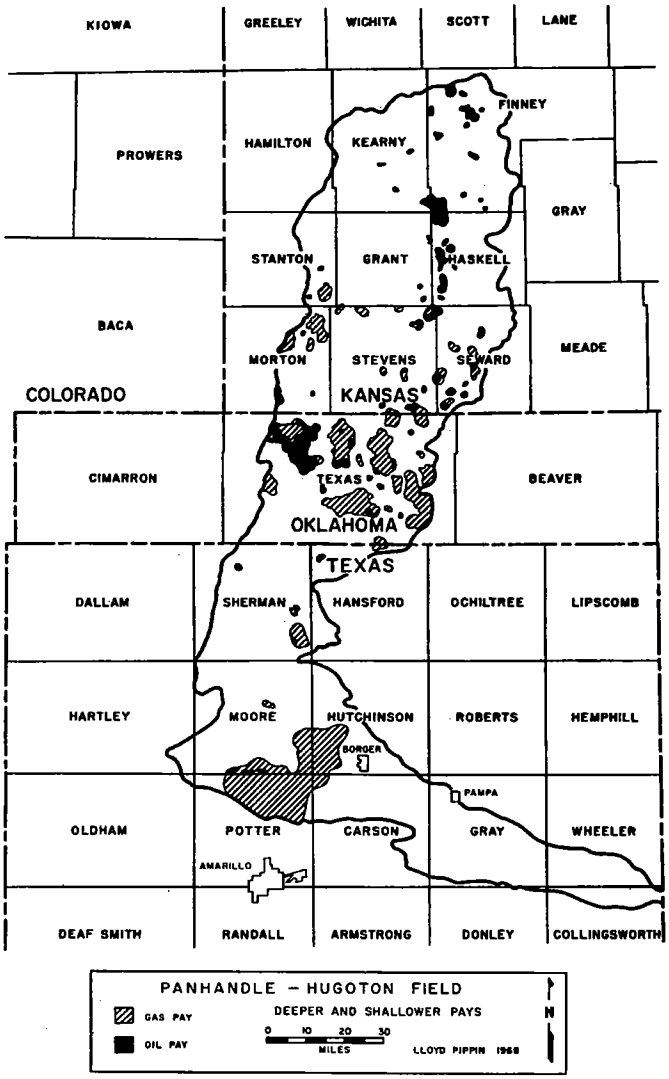

Figure 15. Map of Panhandle-Guymon-Hugoton gas field, showing areas producing from deeper and shallower pays. From Pippin (1970).

CONCLUSIONS

Almost every known trapping mechanism for oil and gas is represented somewhere in the southern Midcontinent. During the earliest development of the petroleum industry this area became the laboratory for the evolving sciences of petroleum geology and geophysics, as well as engineering. The relative abundance of data that was provided by numerous well penetrations permitted the geology of the southern Midcontinent to be comparatively well understood. An understanding of some of the basics of hydrocarbon-source rocks and trapping mechanisms provided the basis for turning the southern Midcontinent into the proving ground for developing and testing theories of

Table 3. — Chronology of Significant Events in Panhandle-Guymon-Hugoton Gas Field, Kansas, Oklahoma, Texas

Year(s)	County, State	Field	Event
1918	Potter Co., TX	Panhandle gas	Chase Group gas discovery [a]
1921	Carson Co., TX	Panhandle oil	Chase Group oil discovery [a]
1922	Seward Co., KS	Hugoton gas	Chase Group gas discovery [a]
1923	Texas Co., OK	Guymon gas	Chase Group gas ciscovery [b]
1929	Potter Co., TX	Panhandle gas	Helium-gas extraction began [a]
1938	Kansas	Hugoton gas	Acid treatment of productive interval [c]
1946	Hutchinson Co., TX	Panhandle oil	Secondary recovery (gas injection, waterflood, and thermal) [c]
1947	Seward Co., KS	Liberal SE field	Morrow gas discovery [d]
1951	Finney Co., KS	Damme field	Mississippian St. Louis oil discovery [e]
1956	Stevens Co., KS	Panoma gas area	Council Grove gas discovery [f]
1956	Texas Co., OK	Guymon S field	Morrow gas discovery
1956–58	Texas Co., OK	Carthage gas area	Topeka and upper Morrow gas discoveries [g]
1958	Haskell Co., KS	Eubank field	Lansing–Kansas City oil discovery [h]
1958	Texas Co., OK	Guymon-Hugoton gas area	Council Grove gas discovery
1958	Texas Co., OK	Postle field	Upper Morrow oil discovery [i]
1959	Morton Co., KS	Kinsler field	Desmoines, Atoka, upper and lower Morrow, and St. Louis gas discoveries [j]
1960s	Kansas	Hugoton gas	Hydraulic fracturing used to stimulate well production
1987	Kansas	Hugoton gas	Infill-drilling program authorized by Kansas Corporation Commission [k]

Sources: (a) Pippin (1970); (b) Six (1930); (c) Rogatz (1961); (d) Strothmeyer (1959); (e) Schmidlapp (1959); (f) Davis and Northcutt (1989); (g) Stratigraphic Committee (1961); (h) Fugitt and Wilkinson (1959); (i) Northcutt (1985); (j) Davis (1964); (k) McCoy and others (1992).

petroleum generation, migration, and accumulation. In so doing, it also provided the opportunity to learn to overcome the myriad problems encountered in the drilling, completion, and production of petroleum reservoirs. The lessons learned here have repeatedly proved their value all over the world.

SELECTED REFERENCES

Adler, F. J.; Caplan, W. M.; Carlson, M. P.; Goebel, E. D.; Henslee, H. T.; Hicks, I. C.; Larson, T. G.; McCracken, M. H.; Parker, M. C.; Rascoe, Bailey, Jr.; Schramm, M. W., Jr.; and Wells, J. S., 1988, Basement structure map, *in* Rascoe, Bailey, Jr.; and Hyne, N. J. (eds.), Petroleum geology of the Mid-Continent: Tulsa Geological Society Special Publication 3, pl. 2, p. 5.

Aukerman, R. A., 1959, Nunn field, *in* Kansas oil and gas fields: Kansas Geological Society, Wichita, v. 2, Western Kansas, p. 118–125.

Berry, G. F., Jr.; and Harper, P. A., 1948, Augusta field, Butler County, Kansas, *in* Howell, J. V. (ed.), Structure of typical American oil fields: American Association of Petroleum Geologists, Tulsa, v. 3, p. 213–224.

Branan, C. B., Jr., 1968, Natural gas in Arkoma basin of Oklahoma and Arkansas, *in* Beebe, B. W. (ed.), Natural gases of North America: American Association of Petroleum Geologists Memoir 9, v. 2, p. 1616–1635.

Clark, G. C.; and Cooper, C. L., 1930, Kay, Grant, Garfield, and Noble Counties, *in* Oil and gas in Oklahoma: Oklahoma Geological Survey Bulletin 40, v. 2, p. 67–104.

Croneis, Carey, 1930, Geology of the Arkansas Paleozoic area: Arkansas Geological Survey Bulletin 3, 457 p.

Davis, H. G., 1964, Kinsler Morrow gas field, Morton County, Kansas: Shale Shaker, v. 14, no. 8, p. 2–20.

Davis, H. G.; and Northcutt, R. A., 1989, The greater Anadarko basin: an overview of petroleum exploration and development, *in* Johnson, K. S. (ed.), Anadarko basin symposium, 1988: Oklahoma Geological Survey Circular 90, p. 13–24.

Davis, R. M., 1959, Patterson field, *in* Kansas oil and gas fields: Kansas Geological Society, Wichita, v. 2, Western Kansas, p. 126–130.

Fugitt, L. B.; and Wilkinson, R. D., 1959, Eubank field, *in* Kansas oil and gas fields: Kansas Geological Society, Wichita, v. 2, Western Kansas, p. 13–20.

Gouin, Frank, 1956, Surface criteria of southern Oklahoma oil fields, *in* Ardmore Geological Society, Petroleum geology of southern Oklahoma: American Association of Petroleum Geologists, Tulsa, v. 1, p. 14–35.

International Oil Scouts Association, 1999, Annual review of oil and gas production by field, v. 70.

Jewett, J. M., 1954, Oil and gas in eastern Kansas: Kansas Geological Survey Bulletin 104, 397 p.

Latham, J. W., 1968, Petroleum geology of the Arbuckle Group (Ordovician), Healdton field, Carter County, Oklahoma: American Association of Petroleum Geologists Bulletin, v. 52, p. 3–20.

_____1970, Petroleum geology of Healdton field, Carter County, Oklahoma, *in* Halbouty, M. T. (ed.), Geology of giant petroleum fields: American Association of Petroleum Geologists Memoir 14, p. 255–276.

Mason, J. W., 1968, Hugoton Panhandle field, Kansas, Oklahoma and Texas, *in* Beebe, B. W. (ed.), Natural gases of North America: American Association of Petroleum Geologists Memoir 9, v. 2, p. 1539–1547.

McCoy, T. F.; Fetkovich, M. J.; Needham, R. B.; and Reese, D. D., 1992, Analysis of the Kansas Hugoton in-fill drilling program (SPE Paper 20779): Journal of Petroleum Technology, June, p. 714–723.

Mills-Bullard, Bess, 1928, Digest of Oklahoma oil and gas fields, *in* Oil and gas in Oklahoma: Oklahoma Geological Survey Bulletin 40, v. 1, p. 102–276.

Northcutt, R. A., 1985, Oil and gas development in Oklahoma, 1891–1984: Shale Shaker, v. 35, no. 6, p. 123–132.

PennWell Maps, 1985, Oil and gas fields of the Mid-Continent, *in* Rascoe, Bailey, Jr.; and Hyne, N. J. (eds.), 1988, Petroleum geology of the Mid-Continent: Tulsa Geological Society Special Publication 3, pl. 1, p. 2.

Pippin, Lloyd, 1970, Panhandle-Hugoton field, Texas–Oklahoma–Kansas—the first fifty years, *in* Halbouty, M. T. (ed.), Geology of giant petroleum fields: American Association of Petroleum Geologists Memoir 14, p. 204–222.

Ramondetta, P. J., 1990, El Dorado: an old field with potential: Oil and Gas Journal, v. 88, no. 13, p. 110–114, 116.

Rogatz, Henry, 1961, Shallow oil and gas fields of the Texas Panhandle and Hugoton, *in* Wagner, C. R. (ed.), Oil and gas fields of the Texas and Oklahoma Panhandles: Panhandle Geological Society, Amarillo, Texas, p. 8–37.

Rogers, R. G., 1961, The Red Cave Formation of the Texas Panhandle, *in* Wagner, C. R. (ed.), Oil and gas fields of the Texas and Oklahoma Panhandles: Panhandle Geological Society, Amarillo, Texas, p. 38–44.

Schmidlapp, R. L., 1959, Damme and Finnup fields, *in* Kansas oil and gas fields: Kansas Geological Society, Wichita, v. 2, Western Kansas, p. 8–12.

Six, R. L., 1930, Beaver, Texas, and Cimarron Counties, *in* Oil and gas in Oklahoma: Oklahoma Geological Survey Bulletin 40, v. 2, p. 461–491.

Stratigraphic Committee, 1961, Carthage field, *in* Wagner, C. R. (ed.), Oil and gas fields of the Texas and Oklahoma Panhandles: Panhandle Geological Society, Amarillo, Texas, p. 248–249.

Strothmeyer, R. C., 1959, Liberal Southeast field, *in* Kansas oil and gas fields: Kansas Geological Society, Wichita, v. 2, Western Kansas, p. 84–91.

Terry, S. P., 1999, The Healdton field, Oklahoma—history of development: Oklahoma Geology Notes, v. 59, p. 4–16.

Texas Bureau of Economic Geology (coordinating group), 1993, Atlas of major Mid-Continent gas reservoirs: University of Texas, Austin, p. 9–12.

Petroleum Charge to the Mill Creek Syncline and Adjacent Areas, Southern Oklahoma

Alton Brown
Consultant
Richardson, Texas

ABSTRACT.—Woodford-generated oil and asphalt accumulations occur in the central and eastern Mill Creek syncline, north of the Arbuckle uplift, yet none of the preserved Woodford source rock in the central and eastern parts of the syncline is thermally mature. The burial history of the Ardmore basin, Mill Creek syncline, and eastern Anadarko basin were modeled to determine the origin of this oil and asphalt as well as the overall generation history of central and western Oklahoma.

Geohistory models of the deep, central Ardmore basin show that Woodford oil generation initiated during the rapid pulse of early Desmoinesian deposition. In deeper parts of the basin, the Woodford Shale entered the gas-generation window before the Virgilian Arbuckle orogeny. Oil generation predates the Virgilian uplift of the Arbuckle anticline and Tishomingo high, so south-to-north oil migration into the eastern and central Mill Creek syncline was unimpeded. Woodford oil generation in the Ardmore basin west of the Caddo anticline is mostly Permian, owing to a much thinner Desmoinesian section and less burial. The Woodford Shale is now in the oil window over much of the western Ardmore basin, but generation and migration have been minor since the Permian owing to the absence of renewed burial.

Despite its relatively deep burial, the Woodford Shale in deeper parts of the western Mill Creek syncline is marginally mature. According to the model, oil generation and migration began during the Permian Period, and most of the oil generated is Triassic and younger. Deep areas in the western Mill Creek syncline are in a position that can charge surrounding traps, but not traps farther to the east. Lower overall transformation and a small generative area limit charge volume. Oil was generated in subthrust Woodford Shale south of the Mill Creek syncline by Virgilian thrust loading, and terminated with erosion of the upper parts of the thrust sheet.

Prolific eastern Anadarko basin Woodford oil generation and migration began with Permian molasse deposition. Petroleum migrated after most deformation took place, so migration is controlled by a structural pattern similar to that of today. Oil migrating toward the eastern and central Mill Creek syncline has been diverted northward by the Pauls Valley uplift or southward to the Eola high, so oil migrating from the Anadarko basin cannot charge traps in the central or eastern Mill Creek syncline. However, Pennsylvanian stratigraphic traps and Virgilian structures at the western end of the Mill Creek syncline can be charged from the eastern Anadarko basin.

Model results indicate that the Woodford oil charge to the central and eastern Mill Creek syncline is mainly from the Ardmore basin, and charge timing is predominantly Desmoinesian and Missourian. Atokan structures along the axis of the present Arbuckle anticline probably spilled oil during Virgilian deformation, resulting in oil remigration to Virgilian structures farther north. Outcrop evidence supports this timing. The Buckhorn asphalt is actually a sea-floor oil seep of Desmoinesian age, demonstrating petroleum migration at this time. Other major asphalt deposits are Virgilian structures charged and breached prior to late Virgilian deposition.

INTRODUCTION

Shallow oil and asphalt accumulations occur in the central part of the Mill Creek syncline, a small basin in southern Oklahoma north of the Arbuckle anticline and the Tishomingo anticline (Fig. 1). Most oils and asphalts have been geochemically typed to the Woodford Shale, a prolific Devonian–Mississippian source rock that generated most of the oils in southern Oklahoma (Wavrek, 1992). However, temperatures of approximately 100°C or greater are required

Brown, Alton, 2002, Petroleum charge to the Mill Creek syncline and adjacent areas, southern Oklahoma, *in* Cardott, B. J. (ed.), Revisiting old and assessing new petroleum plays in the southern Midcontinent, 2001 symposium: Oklahoma Geological Survey Circular 107, p. 17–36.

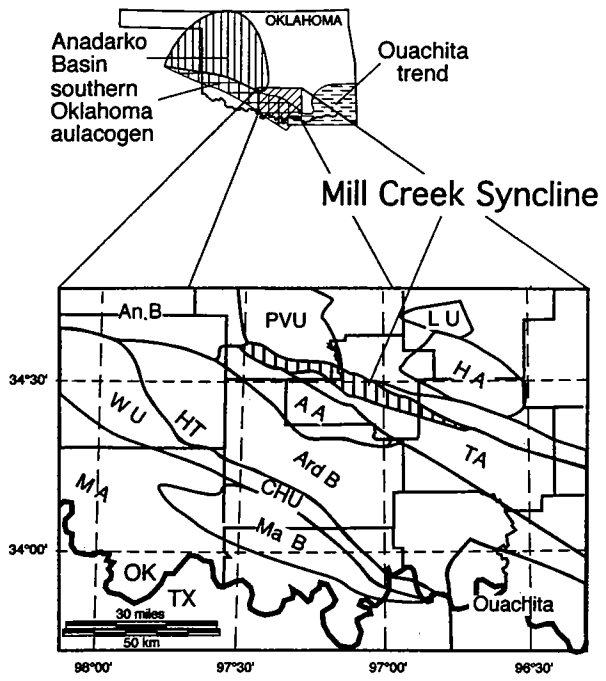

Figure 1. Location map of Mill Creek syncline and other southern Oklahoma tectonic features. Dashed lines are county outlines. Abbreviations: *A A* = Arbuckle anticline; *An B* = Anadarko basin; *Ard B* = Ardmore basin; *CHU* = Criner Hills uplift; *L U* = Lawrence uplift; *H A* = Hunton anticline; *HT* = Harrisburg trough; *M A* = Muenster arch; *Ma B* = Marietta basin; *Ouachita* = Ouachita facies; *PVU* = Pauls Valley uplift; *T A* = Tishomingo anticline; *W U* = Wichita uplift. Compiled from many sources.

to crack kerogen to oil at geologically significant rates (Quigley and Mackenzie, 1988). This usually requires burial to about 3 or more km. The Woodford Shale is buried to a maximum of about 2 km in the eastern Mill Creek syncline (Fig. 2). It therefore appears that oils in the Mill Creek syncline were not generated in the eastern part of the basin, and that oils could not have charged the eastern basin from nearby thermally mature source rocks under present structural configuration. This anomalous petroleum distribution requires further investigation both to expand our understanding of petroleum systems and to lead to new exploration opportunities in this mature petroleum province.

The purpose of this paper is to evaluate how oil charged the eastern Mill Creek syncline. The petroleum charge to the eastern Mill Creek syncline will be investigated by modeling the time of petroleum generation in different potential petroleum "kitchens" and by evaluating petroleum migration controlled by the structural configuration at that time. First, southern Oklahoma structural history and oil-type distribution were reviewed. Then, geohistory models for locations in the eastern Anadarko basin, western Mill Creek syncline, and Ardmore basin were constructed to determine where and when petroleum was generated.

Three possible scenarios might explain Mill Creek syncline oil: (1) Woodford source rock was buried deeply enough to generate oil within the basin sometime in the past, but the overburden was removed after generation. This scenario is improbable, because Woodford strata preserved in the eastern part of the syncline and exposed in the Arbuckle Mountains area are thermally immature for oil generation (Cardott and others, 1990; Glash and Friedman, 1988; Brown and Corrigan, 1997). (2) Oil might have migrated from the Anadarko basin or the deeper western Mill Creek syncline. This also seems unlikely, because present structural configuration does not favor migration from these areas into the eastern Mill Creek syncline. However, to fully evaluate this hypothesis, paleostructure has to be investigated to determine if west-to-east migration was possible in the past. (3) Oil might have migrated north from the Ardmore basin prior to elevation of the Arbuckle anticline and the Tishomingo anticline. This possibility is most likely, but Woodford oil would have to have been generated in the Ardmore basin before its isolation from the Mill Creek syncline. Of course, charge from the Arkoma basin also has to be considered. Structural and paleostructural analysis indicates that migration from the east is almost impossible for oil generated at any time during the late Paleozoic to the Holocene, so this scenario will not be investigated further.

It will be demonstrated that significant volumes of oil were generated from the Woodford Shale in the Ardmore basin prior to uplift of the Arbuckle anticline. This is the probable source for the oil that formed the asphalt deposits as well as some of the conventional oil deposits. In contrast, Woodford oils were generated after the major Virgilian deformation in the western Mill Creek syncline and eastern Anadarko basin, so their migration would have been limited to the western Mill Creek syncline. Overall, this study confirms the antiquity of many of the Oklahoma oil accumulations interpreted by previous workers (e.g., Webb, 1976; Huffman, 1979), but interprets events in greater detail.

STRUCTURAL EVOLUTION OF SOUTH-CENTRAL OKLAHOMA

Before the timing of petroleum generation was evaluated, a review of the structural evolution of south-central Oklahoma was in order. Structural evolution controls the burial history as well as the availability of stratal (bedding-parallel) and cross-stratal (fault and fracture) migration pathways. Southern Oklahoma in the vicinity of the Arbuckle anticline was characterized by three main tectonic phases: (1) an aulacogen phase of thermally driven Late Cambrian through Mississippian subsidence (Feinstein, 1981); (2) a complex collision phase (Pennsylvanian through Early Permian) (Tomlinson and McBee, 1959; McBee, 1995); and (3) quiescence (Triassic through present), during which neither significant erosion nor sedimentation occurred.

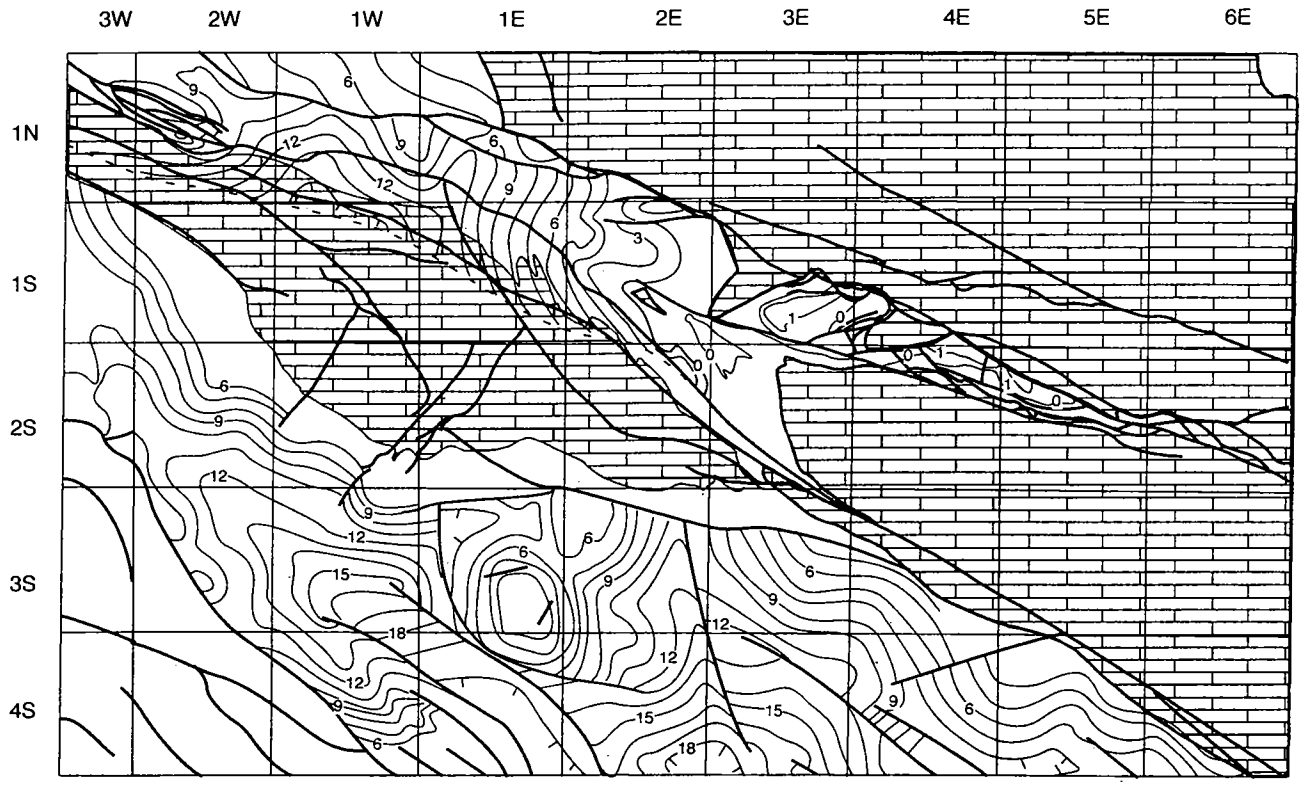

Figure 2. Structure map depicting the top of the Viola Group in the Mill Creek syncline and northern Ardmore basin in thousands of feet below sea level. Surface elevation is about 750–1,000 ft above sea level over most of the area, and the Woodford Shale is about 1,000 ft above the top of the Viola Group, so this structure map also approximates Woodford burial depth. Brick pattern indicates areas where the top of the Viola Group is eroded. The Viola Group extends under the Arbuckle thrust in the western Mill Creek syncline where brick pattern overlies contours. Other areas of possible subthrust Viola Group are not mapped owing to a lack of data. Grid pattern is township grid. Subcrop and fault data are mainly from Ham (1955) and Hicks (1972). Structural data are from many sources.

Aulacogen Phase

An east–west trend of thickened Cambrian through Devonian strata has long been recognized in southern Oklahoma. This is now referred to as the southern Oklahoma aulacogen (Johnson and Cardott, 1992). Aulacogens are characterized by a progressive decrease in accumulation rate caused by decreasing thermal subsidence as the aulacogen cools. The southern Oklahoma aulacogen shows this pattern for Late Cambrian through Middle Devonian strata (Feinstein, 1981). More than 10,000 ft of Cambrian and Ordovician strata was deposited in the Arbuckle anticline area (Ham, 1969).

The southern Oklahoma aulacogen had a renewed pulse of Late Devonian through Mississippian subsidence, which appears to have been related to flexural loading rather than to crustal cooling. The Devonian–Mississippian Woodford Shale was deposited during the rapid flooding of southern Oklahoma, followed by sediment starvation in the Ardmore basin area through the Early and middle Mississippian. Starvation was followed by a thick Chesterian–Morrowan shale-prone clastic wedge (Goddard–Springer Formations). The total Late Devonian through Mississippian section is >5,000 ft thick in the Ardmore basin but ~1,000 ft thick in the eastern Mill Creek syncline. The Mississippian section is more calcareous in the Anadarko basin.

The Woodford Shale is the main potential source rock deposited during the aulacogen phase. Other potential pre-Carboniferous source rocks were deposited in the Simpson Group (Middle Ordovician) (Wang and Philp, 1997) and in the Viola Group (Late Ordovician) (Wang and Philp, 1997). Neither of these are prolific source rocks (Jones and Philp, 1990; Brown and Senftle, 1997). All Late Ordovician through Mississippian units are close to the top of the aulacogen succession, so they were insufficiently buried to generate oil prior to the collision phase.

Collision Phase

Uplift and erosion indicating the initiation of the collision with South America started during the latest Mississippian (Johnson and others, 1988). In the Ardmore basin area, three orogenies are widely recognized: the first Wichitan orogeny (Morrowan), the second Wichitan orogeny (late Atokan), and the Arbuckle orogeny (Virgilian) (Tomlinson and McBee, 1959). Local deformation continued between the three orogenies.

The latest Mississippian deformation along the

Criner Hills uplift continued into the Morrowan to form the first Wichitan orogeny (Johnson and others, 1988). The first Wichitan orogeny mainly affected the southern Ardmore basin, the Criner Hills area, and areas south of the Criner Hills. There is no evidence for significant (several thousand feet) uplift of blocks in the northern Ardmore basin or northward (Rascoe and Adler, 1983).

Large uplifts of the second Wichitan orogeny are also concentrated in the southern area, but uplift is moderate farther north. A widespread late Atokan unconformity truncates successively older formations toward the north (Swesnik, 1950), indicating uplift of the Pauls Valley uplift and the Hunton anticline (Fig. 3). At NW Butterly field, the western end of the Mill Creek fault (separating the Mill Creek syncline from the Pauls Valley uplift) shows an offset of ~1,500 ft prior to Desmoinesian deposition (Borras, 1979).

The Desmoinesian stage marked the time of greatest Ardmore basin subsidence (Tomlinson and McBee, 1959). Desmoinesian strata transgressed onto highs north and south of the Ardmore basin. The Pauls Valley uplift was progressively buried from the west through the Desmoinesian and into the Missourian (Swesnik, 1950), whereas the Hunton anticline remained emergent through the Missourian, acting as a source of conglomerate to the Franks graben (Ham, 1955). Even with this structural readjustment, the north-to-south dip from the Hunton anticline into the Ardmore basin remained relatively uninterrupted until the end of the Missourian Stage. The Mill Creek syncline and Tishomingo anticline were probably not structurally differentiated from the Arbuckle anticline and Ardmore basin until the Arbuckle orogeny (Fig. 4). Missourian strata are absent by erosion from the Tishomingo anticline and Mill Creek syncline, with the possible exception of early Missourian conglomeratic strata at the western end of the structure (Ham, 1955).

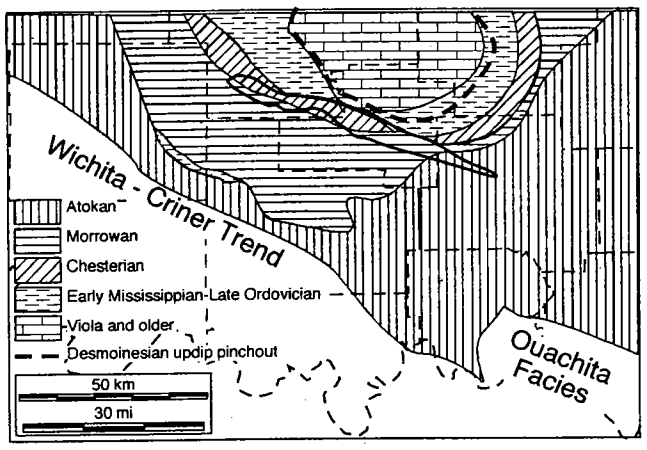

Figure 3. Reconstructed pre-Desmoinesian subcrop map for the Ardmore basin–Arbuckle Mountains area. Substantial pre-Desmoinesian erosion occurred in the Pauls Valley–Hunton anticline area and along the structural axis of Sho-Vel-Tum field (see Fig. 1). Atokan–Desmoinesian strata are relatively conformable in the eastern area, but Atokan rocks are apparently thin or absent over most of the western Ardmore basin, with the exception of the Harrisburg trough. The complex subcrop patterns in the Marietta basin, Ouachita facies, and Wichita–Criner trend are not shown. Mill Creek syncline is outlined. Data are from many sources.

Following Johnson and others (1988) and most recent workers, significant differential growth of the Arbuckle anticline relative to the Tishomingo anticline began during the early Virgilian Arbuckle orogeny. However, previous workers interpreted earlier ages for initiation of Arbuckle anticline growth. Swesnik (1950) describes detrital igneous pebbles in the basal Desmoinesian conglomerate at SW Antioch field. He interprets these pebbles as evidence for late Atokan uplift of the western end of the Arbuckle anticline sufficient to expose the igneous basement. This observation has not been confirmed in other areas. This large uplift is inconsistent with the paucity of Desmoinesian conglomerates near the western end of the uplift, so this interpretation has not been followed here. The late Desmoinesian Warren Ranch Conglomerate has been interpreted as evidence for the first significant uplift of the eastern part of the Arbuckle anticline (Tomlinson and McBee, 1959). However, the Warren Ranch Conglomerate appears from maps in Tomlinson and McBee (1959) to be an incised conglomerate channel, not a widespread fan delta like other southern Oklahoma syntectonic conglomerates. Johnson and others (1988) interpret the conglomerate to have been derived from the Hunton anticline.

The Arbuckle orogeny was the main phase of deformation in the Arbuckle anticline–Mill Creek syncline area. This was also the time of major compression of the Ardmore basin. Pre-Virgilian strata are significantly deformed, but late Virgilian strata are mildly deformed, indicating early Virgilian deformation. Early Virgilian strata are absent near the Arbuckle Mountains area, because deformation and uplift were so intense that little sediment was preserved. The combination of syntectonic-conglomerate deposition on the north side of the Arbuckle anticline and tectonic loading by the thrust sheet resulted in deep burial of middle Paleozoic strata in the western end of the Mill Creek syncline (Saxon, 1994). There is no evidence for similar burial of the eastern end of the anticline.

Permian subsidence continued in the Anadarko basin and the western Ardmore basin. More than 7,000 ft of Permian strata is preserved in the Anadarko basin. Permian strata thin to the east by both depositional thinning and by erosional truncation. Permian strata are not preserved in the Arbuckle Mountains, but Permian Wolfcampian and Leonardian rocks bury the western end of the Arbuckle anticline (Hicks, 1972). Wolfcampian rocks contain conglomerates from the eroding Arbuckle Mountains, whereas Leonardian strata are predominantly shaly (Hicks, 1972). Rocks as young as Guadalupian are preserved a short dis-

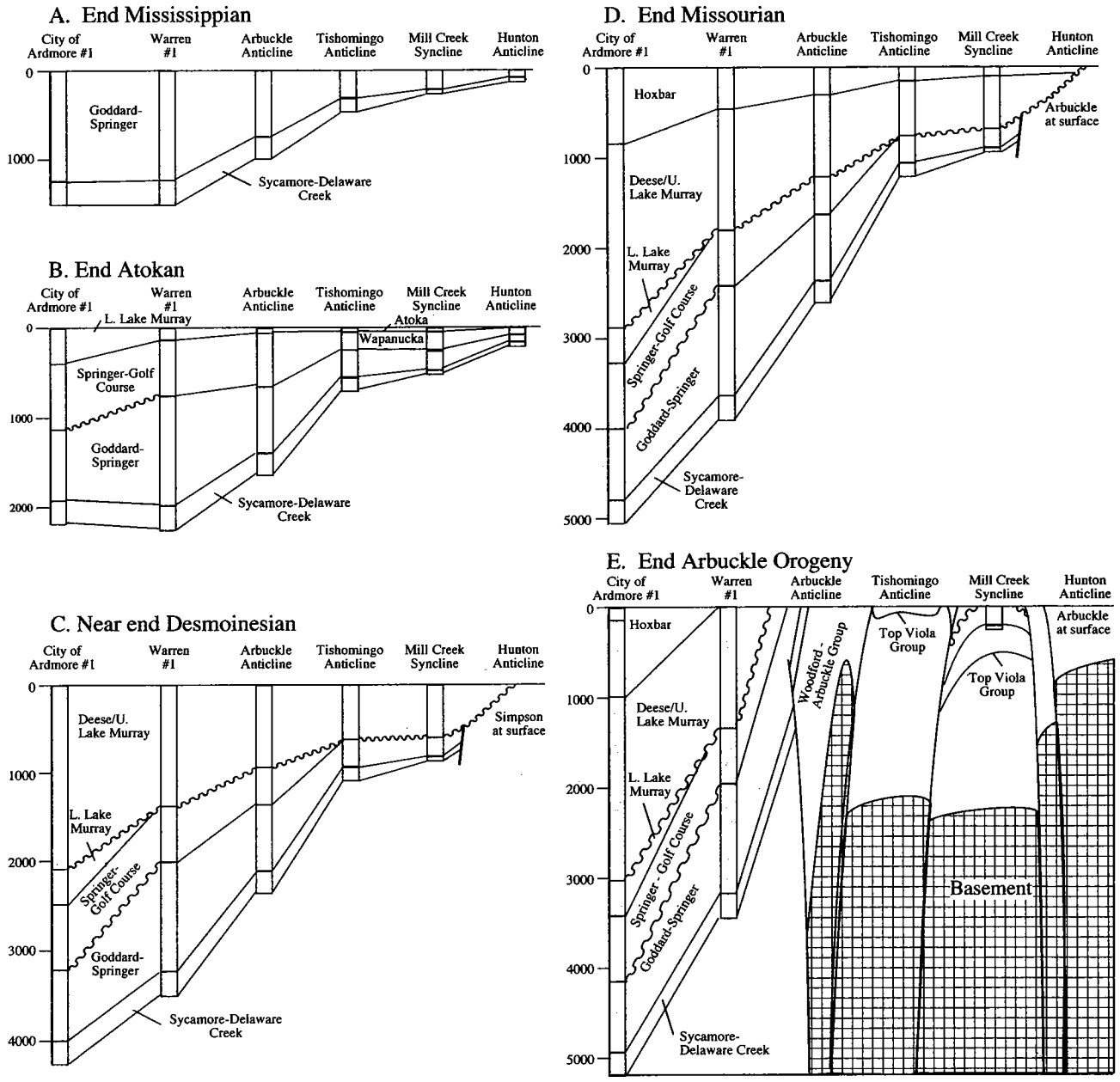

Figure 4. Generalized structural evolution of a southwest–northeast traverse between the Ardmore basin and the Hunton anticline, showing interpreted amounts of deposition and eroded strata, and time of disruption of updip-migration potential. Early Desmoinesian–late Atokan deformation (between *B* and *C*) resulted in deformation and potential trapping along the traverse but did not disrupt the northward migration of petroleum toward the Mill Creek syncline. Virgilian growth of the Arbuckle anticline (*E*) isolated the Mill Creek syncline from southerly charge. Depths are in feet. Reconstructed sections have not been decompacted, so burial during the Pennsylvanian exceeded that shown here.

tance to the west of the Arbuckle Mountains. Isopach patterns indicate that Leonardian–Guadalupian deposits once extended farther east and probably buried low areas surrounding the Arbuckle Mountains. There is little evidence of significant differential structural growth during Permian deposition. Moderate fault movement west of the Arbuckle Mountains (Hicks, 1972) offsets Permian strata. Offsets and thickening patterns are small, so they might be explained entirely by differential compaction.

Quiescent Phase

There is no evidence for Triassic, Jurassic, or pre-Albian Cretaceous deposition in southern Oklahoma (Johnson and others, 1988). After erosion of most Permian strata, Early Cretaceous strata onlapped the southern part of the Ardmore basin and Tishomingo anticline (Ham, 1955). Cretaceous strata along the Texas–Oklahoma border were deformed by modest reactivation of Paleozoic structures (Bergquist, 1949). Corrigan and others (1998) interpret a kilometer of

Cretaceous–Early Tertiary burial on the southern Tishomingo block in an area just north of the Cretaceous erosional limit. Fission-track data also indicate that exhumation began about 40 million years ago (Corrigan and others, 1998). On the basis of fission-track dates and burial-history modeling, Gallardo and Blackwell (1999) propose burial of the Anadarko basin by ~5,000 ft of Cretaceous strata. Nearby preserved Cretaceous strata are much thinner than this.

OIL DISTRIBUTION NEAR THE MILL CREEK SYNCLINE

Large oil fields demonstrate that oil has migrated into the western Mill Creek syncline, whereas asphalt and smaller oil fields indicate that oil has also migrated into the eastern Mill Creek syncline. Conventional oil has been produced from a number of fields in the central and western parts of the Mill Creek syncline (Fig. 5). Most of these fields are productive from Ordovician reservoirs. The east-central part of the Mill Creek syncline is characterized by abundant asphalt stains and deposits (Fig. 5). The asphalt is biodegraded, devolatilized petroleum derived from oil of normal thermal maturity (Cardott and Chaplin, 1993).

At least four oil types have been identified in southern Oklahoma (Zemmels and Walters, 1987; Burruss and Hatch, 1989; Jones and Philp, 1990; Wavrek, 1992). For this reason, available data on the probable source rocks for oils in fields and asphalt deposits in the Mill Creek syncline area were compiled (Fig. 5).

The majority of oils identified near the Mill Creek syncline are interpreted to have been generated in the Woodford Shale (Zemmels and Walters, 1987). The asphalts are also correlated to a Woodford source (Cardott and Chaplin, 1993). Wavrek (1992) identifies three oil types (his types A, B, and C), which he correlates with three Devonian through Carboniferous sources. Their compositions are similar, including almost identical carbon isotopic ratios. I interpret all three oil types to have been sourced from the Woodford Shale rather than from Carboniferous units. The compositional differences between these three types are interpreted to correspond to the three different facies or maturity ranges of Woodford-generated oils postulated by Zemmels and Walters (1987). The carbon isotopic ratios of the oil types are similar to each other and to Woodford shale extracts (Burruss and Hatch, 1989; Jones and Philp, 1990; Wang and Philp, 1997). Carbon isotopic ratios from all three types are dissimilar to the heavier carbon isotopic ratios from Oklahoma Carboniferous source rocks (e.g., Wang and Philp, 1997; Burruss and Hatch, 1992).

Ordovician-sourced oil is the next most abundant oil near the Mill Creek syncline (Fig. 5). This oil is easily identified by its unusual odd-dominated C_{13} to C_{19} normal paraffins and low concentrations of C_{20+} normal paraffins (Zemmels and Walters, 1987; Burruss and Hatch, 1989). This oil has been typed to the Simpson Group (Burruss and Hatch, 1989). Another Ordovician-sourced oil occurs sparsely in the area but has not been identified in the Mill Creek syncline. It has been typed to the Viola Springs Formation (Wavrek, 1992; Wang and Philp, 1997). No oil with isotopically heavy carbon and a high wax content characteristic of the Pennsylvanian oils of the Anadarko basin (Burruss and Hatch, 1992) has yet been identified from the Ardmore basin–Mill Creek syncline area.

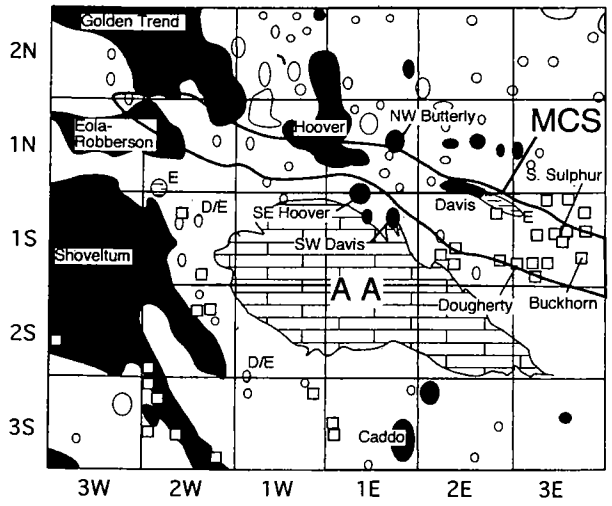

Figure 5. Petroleum accumulations near the Mill Creek syncline. Small petroleum fields are shown by ovals, large fields are outlined, and asphalt accumulations and tar-stained rock are shown by rectangles. Fields with oil of known source are indicated by black-filled outlines (Woodford source) or letters as follows: *E* = Simpson-sourced oils; *D* = Viola Springs–sourced oils; *D/E* = mixed Simpson/Viola Springs–sourced oil. Fields and asphalt accumulations referred to in the text are named. Grids are township blocks, about 10 km across. *AA* = outcrop of Viola Group and older rocks on the Arbuckle anticline; *MCS* = Mill Creek syncline. Field locations are from Burchfield (1985), and asphalt locations are from Jordan (1964).

On the basis of available data, almost all oil in the Mill Creek syncline area is derived from the Woodford Shale, with minor amounts contributed by two Ordovician source rocks. For this reason, the main modeling effort addresses Woodford oil generation and its timing.

GEOHISTORY MODELING

Modeling Methodology

One-dimensional geohistory models were constructed, using the Genesis burial-history program (available from www.Zetaware.com). Genesis is a flexible, user-friendly modeling program that allows rapid testing of different modeling scenarios of varying complexity. The user can mix lithologies in strata, use different compaction and thermal models, modify thermal conductivity of rocks to allow for local calibration, and generate petroleum using either default or custom discrete or gaussian kerogen-transformation kinetics. Models can be modified easily, so Genesis al-

lows rapid testing of different burial scenarios. For this project, the following options were used.

Lithology and thicknesses were interpreted from measured sections and well descriptions available in the public literature. In some cases, "pseudowells" were constructed from seismic and nearby well data in synclinal areas with no well coverage. Up to five lithologies were used per stratigraphic interval, with percentages estimated from the fraction of the stratigraphic unit thickness.

Porosity is modeled as an exponential function of effective stress and lithology during burial, defined by an initial (surface) porosity, a reference depth, and porosity at the effective stress of the reference depth, assuming normal pressure and lithostatic gradient. Default Genesis reference depths and porosity at reference depths were used for all lithologies. Initial porosities of sandstone and shale were reduced to 30% to match the lower porosities of the shallow Paleozoic section. Porosity rebounds 0.02% during uplift. Under this option, water is not conserved during compaction, so geopressure and formation permeability were not calculated.

The thermal conductivity of a layer is estimated by averaging the matrix thermal conductivity from the lithological components and water-filled porosity. The thermal conductivities assumed for most end-member rock types are similar to those used elsewhere (e.g., Carter and others, 1998). Because shale is the dominant rock type, it greatly influences overall thermal conductivity. Shale thermal conductivity was calibrated by using the temperature data in Gallardo and Blackwell (1999) from the nearby Anadarko basin. A steady-state heat-flow model was used to match temperatures reported in Anadarko basin wells with known heat flows (Gallardo and Blackwell, 1999) by modifying the shale conductivity. Shale conductivity was changed from the Genesis default of 1.62 W/m^2 to 1.84 W/m^2 to match the calibration. *Red bed* is not a Genesis lithology, so the "redbed" lithology used by Carter and others (1998) and Gallardo and Blackwell (1999) in the shallow Permian section was modeled by increasing the fraction of sand in excess of the reported fraction to match reported interval thermal conductivity. This is consistent with a higher fraction of quartz in red-bed shales.

Thermal maturation was modeled by discrete distribution kinetics. Vitrinite reflectance was calculated from the Lawrence Livermore model (LLVR; Burnham and Sweeney, 1989). Kerogen transformation to oil and gas was modeled by three different kinetics: the default Genesis low-sulfur marine-shale kinetics, the Woodford transformation kinetics reported by Braun and others (1991), and the Woodford transformation kinetics reported by Tegelaar and Noble (1994). The correlation between calculated transformation ratio (TR) and LLVR is almost independent of heating rate at geological heating rates, so differences in transformation kinetics can be determined by comparing calculated TR to LLVR. The three transformation models show similar but not identical transformation with increasing LLVR (Fig. 6). For consistency, the Woodford TRs reported elsewhere in this paper are results of the Tegelaar and Noble (1994) kinetics.

Because the time of interest was after the aulacogen phase, basement heat flow was assumed constant at each modeled location. This assumption was tested by comparing predicted to observed vitrinite reflectance at well-characterized locations in the Anadarko basin, as discussed below.

Pennsylvanian burial and uplift were rapid, so the transient-heat-flow assumption was also tested. Transient assumption decreases heat flow near the Woodford Shale by up to about 10% of the assumed steady heat flow during times of maximum subsidence rate. This delayed maturation in rapidly subsiding basinal areas by about 1 million years or less. However, this effect is evident only in those parts of the basin that subsided most rapidly. Time-transient heat flow does not affect present-day transformation, because adequate time had elapsed since rapid burial for vitrinite reflectance to equilibrate to the late Paleozoic thermal structure. Steady heat flow was used for the final modeling effort.

Surface temperature was assumed to have decreased from 30°C in the Paleozoic and Mesozoic to its present value of about 18°C at three steps. Surface temperature would have dropped to 28°C at the end of the Cretaceous, and would have dropped further to 22°C at the end of the Eocene. Surface temperature would have dropped to its present value at the beginning of the Pleistocene. Climatic cooling may have caused at least part of the middle Tertiary cooling in-

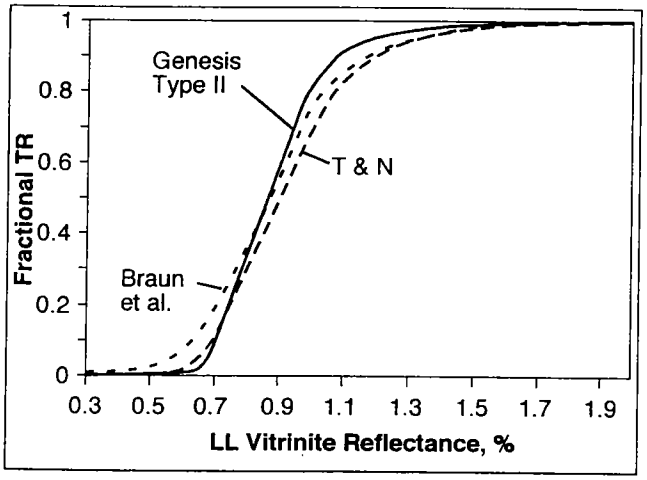

Figure 6. Comparison of calculated transformation ratio (TR), using different kerogen-transformation kinetics to Lawrence Livermore (LL) vitrinite reflectance. Genesis type II is the default kinetics for marine-shale kerogen in the Genesis modeling program. Braun and others is the Woodford Shale custom kinetics from Braun and others (1991). T & N is the Woodford Shale custom kinetics from Tegelaar and Noble (1994).

terpreted from fission-track data by Carter and others (1998) and Corrigan and others (1998).

Calibration of Thermal and Burial History for the Anadarko Basin

Few thermal data and essentially no vitrinite-reflectance data are available for the Ardmore basin. On the other hand, high-quality thermal data and thermal-maturity-indicator data are available for the Anadarko basin, and its stratigraphy and tectonic setting are similar to those of the Ardmore basin. Wells in the eastern part of the Anadarko basin with vitrinite-reflectance data were modeled to constrain Cretaceous burial as well as to evaluate timing of generation.

The philosophical approach taken here is that burial history can be better constrained than ancient heat flow in the absence of a known heating event (such as rifting or intrusion). If thermal-maturity indicators can be modeled with a stratigraphically reasonable burial history and a constant basement heat flow, then this interpretation is preferred over a variable heat flow. Changes in the paleo–heat flow will be considered only if thermal maturity cannot be matched by a stratigraphically reasonable burial history.

Vitrinite-reflectance data and heat-flow measurements available for the eastern Anadarko basin were not collected from the same wells. Three vitrinite-reflectance data sets are available: one for the Woodford Formation (Cardott, 1989), one for wells along a traverse in the eastern Anadarko basin (Pawlewicz, 1990), and one for a single well, the No. 1 Bertha Rogers (Price and others, 1981). The first step is analysis of consistency in the different data sets and their correlation to heat flow.

Heat flows were estimated for the eastern and central Anadarko basin wells with vitrinite-reflectance measurements by using the heat-flow map in Gallardo and Blackwell (1999). Wells in the critical area of transition from the Anadarko basin to the Ardmore basin were not contoured on the Gallardo and Blackwell (1999) heat-flow map, so heat flows were not assigned to these data. The other reflectance data were then separated by source and heat flow and compared (Fig. 7).

The Cardott (1989) vitrinite-reflectance data show that average vitrinite reflectance at depth is higher with a heat flow of 53–54 mW/m^2 than with a heat flow of 42–45 mW/m^2, especially in the deeper part of the section (Fig. 7A). Reflectance trends of the Bertha Rogers well fit between the two Cardott (1989) trends, consistent with its interpolated intermediate heat flow of 46 mW/m^2. A heat flow higher than the plotted values occurs only in the northern part of the basin where burial is less, so these do not have enough depth range to form a distinctive trend. Few low-heat-flow data are available because of the limited geographic extent of low heat flows, so these trends could not be characterized as well as the trend for moderate (53–54 mW/m^2) heat flow and the trend for the Bertha Rogers well.

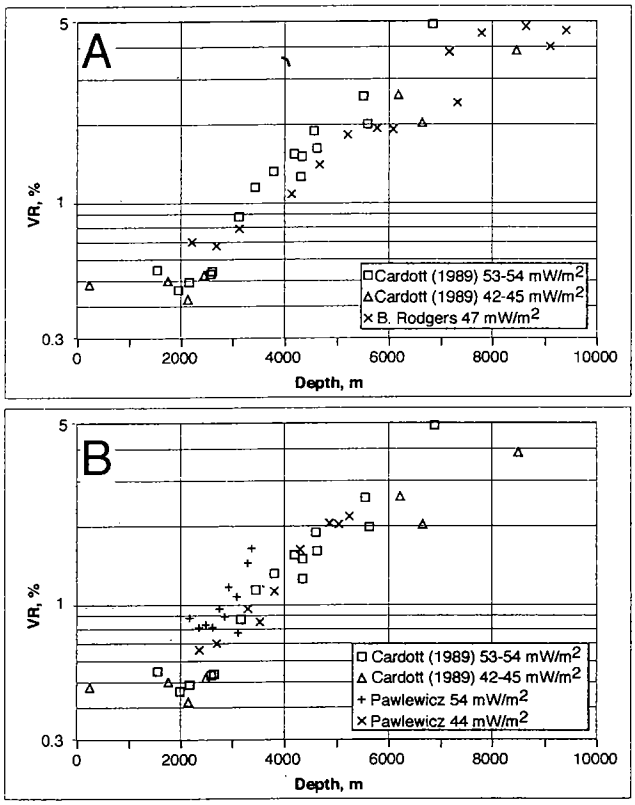

Figure 7. Observed vitrinite reflectance as a function of depth and heat flow in the Anadarko basin. (A) Comparison of variation within Cardott (1989) and Price and others (1981) data sets. (B) Comparison of Cardott (1989) and Pawlewicz (1990) data sets.

The Pawlewicz (1990) vitrinite-reflectance data also show systematic differences in reflectance–depth trends with heat flow for the wells with well-defined reflectance–depth profiles, but the reflectance–depth trend is systematically higher than the Cardott (1989) trend for similar heat flow (Fig. 7B). The Cardott (1989) data set was chosen for calibration for the following three reasons: (1) Cardott (1989) data show a systematic increase with depth, whereas some of the wells analyzed by Pawlewicz (1990) do not. Some Pawlewicz (1990) vitrinite reflectances are very high at shallow depth in areas where heat flow is low and uplift is moderate to absent. This indicates that at least some of the Pawlewicz (1990) data may not represent actual maturation states. (2) The Cardott data are consistent with those of Price and others (1981), indicating that interlaboratory calibration is probably good. Cardott's data were measured on strata deposited before uplift of surrounding areas, so samples were less likely to be contaminated by reworked vitrinite. (3) Most other studies of thermal maturity in the area use the Cardott (1989) data set or its less complete precursor (Cardott and Lambert, 1985) as calibration, so modeling results of this study can be compared better to those of other studies if Cardott's trends are used.

The Genesis program was used to calculate Anadarko basin vitrinite reflectance under varying Cretaceous paleoburial scenarios. Four wells were tested: the No. 1-28 Ferris (Gallardo and Blackwell, 1999), the No. 51-11 Weller (Pawlewicz, 1990), the No. 1 Petree Ranch (Pawlewicz, 1990), and the No. 1 Bertha Rogers (Price and others, 1981). Heat flows interpolated from figure 4 in Gallardo and Blackwell (1999) for these wells are 39, 44, 53, and 46 mW/m^2, respectively. The Petree Ranch, Weller, and Bertha Rogers models successfully matched the 53–54 mW/m^2, 40–45 mW/m^2, and Bertha Rogers vitrinite-reflectance trends, respectively, assuming 650 ft of Cretaceous burial (Fig. 8A).

In contrast, models of the No. 1-28 Ferris well could match the 40–45 mW/m^2 reflectance–depth trend only with an assumed 5,000 ft of Cretaceous burial. This result is similar to that of Carter and others (1998), verifying that the difference is not due to the modeling program. The mismatch may be caused by the fact that the No. 1-28 Ferris well is much cooler than Anadarko basin wells for which VR was measured. Heat flow in the Ferris well was low relative to other areas in the Anadarko basin (37 mW/m^2; Gallardo and Blackwell, 1999), and its corrected thermal gradient is about 1.1°F/100 ft or less. The average thermal gradient in the central and eastern Anadarko basin is about 1.3°F/100 ft, and heat flow for wells with VR data varies from about 40 to 62 mW/m^2.

The modeled match to observed vitrinite using constant heat flow is consistent with a basement heat-flow constant through time, a result similar to that of Carter and others (1998). Modeling results are not consistent with the high heat flows proposed by Garner and Turcotte (1984) for late Paleozoic burial. A high heat flow results in a vitrinite reflectance significantly higher than that observed (Fig. 9). Modeling results also indicate a relatively thin Cretaceous cover over the Anadarko basin—less than 650 ft. Cretaceous burial by 5,000 ft caused excessively high modeled VR in the Bertha Rogers well, for which both VR data and moderate-quality bottomhole-temperature data are available (Fig. 9).

Ardmore Basin and Mill Creek Syncline Heat Flow and Burial

Cardott's (1989) vitrinite-reflectance data overlap the transition from the Anadarko basin to the Ardmore basin. The reflectance-versus-data trend for this area is approximately the same as the 40–44 mW/m^2

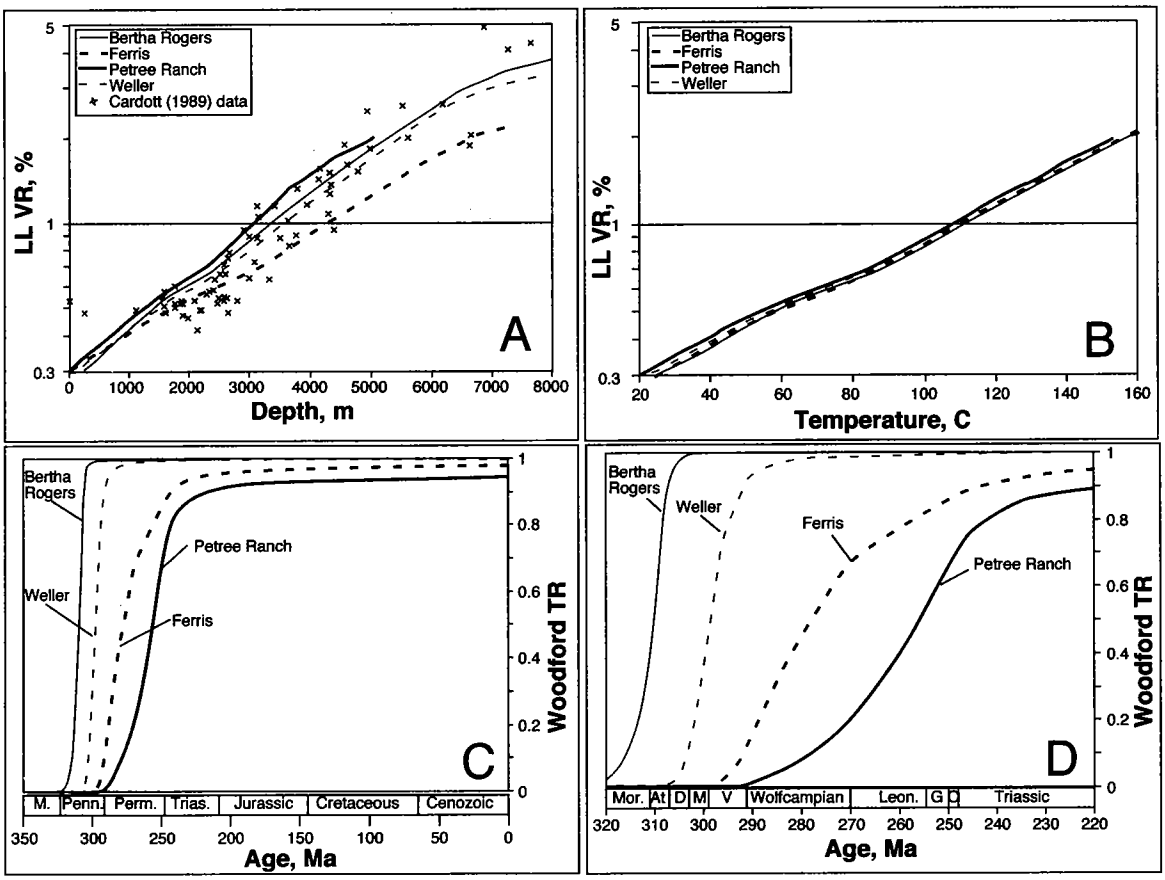

Figure 8. Modeled vitrinite reflectance (VR) and Woodford Formation transformation ratio (TR) for well locations in the Anadarko basin. (A) Modeled and observed VR versus depth. (B) Modeled VR versus temperature. (C) Petroleum generation from the Woodford Formation as indicated by fractional TR. (D) Expanded time scale, showing Pennsylvanian and Permian transformation of Woodford kerogen.

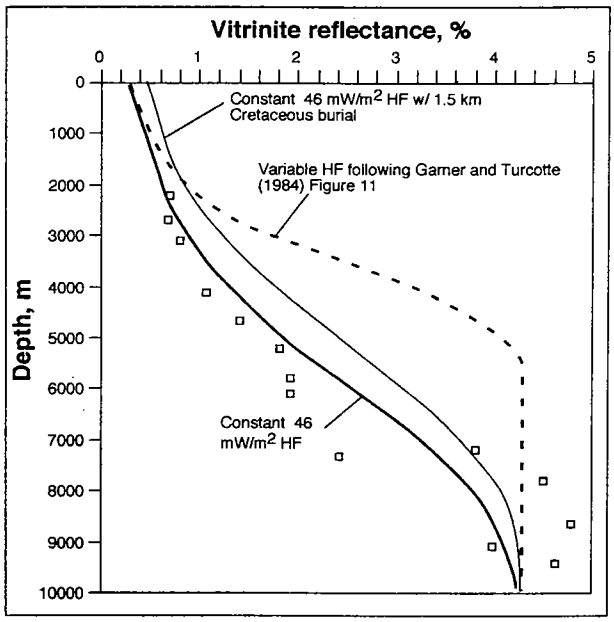

Figure 9. Comparison of predicted vitrinite reflectance (VR) in the No. 1 Bertha Rogers well, using present-day heat flow of 46 mW/m² and 650 ft of Cretaceous burial, the variable-heat-flow model proposed by Garner and Turcotte (1984), and constant heat flow with 5,000 ft (1.5 km) of Cretaceous burial. Symbols are averaged from measured VR from Price and others (1981). Lawrence Livermore VR has a maximum calculated value of 4.74% (Burnham and Sweeney, 1989), so an observed VR close to or exceeding this value is underestimated by the model.

trend, indicating relatively low heat flow. This is consistent with the low averaged thermal gradient mapped by Harrison and others (1983).

Because no accurate heat-flow or thermal data are available for the Ardmore basin, heat flow was estimated from an averaged thermal gradient (Harrison and others, 1983), using the Genesis program. Genesis calculates the heat flow that best fits the linear thermal gradient over the depth range of the model. It then uses this heat flow for calculation of thermal history and thermal indicators. The customized thermal conductivities from the Anadarko basin models were used. In most areas, the Harrison and others (1983) thermal-gradient data were calculated from relatively shallow wells. Models of structural highs extend only to the base of the Simpson Formation to avoid overestimation of heat flow by inclusion of the conductive Arbuckle Group and basement strata.

Heat flows calculated from the averaged thermal gradient and thermal-conductivity model range from about 43 to 64 mW/m² (Table 1). In basin areas from which heat-flow estimates are probably more reliable, heat flow varies from about 45 to 51 mW/m², with lower heat-flow values in the eastern Ardmore basin and western Mill Creek syncline, and higher heat-flow values in the northern central Ardmore basin. These variations are probably real. Variations in heat flow on highs with a thin sedimentary section or a conductive carbonate lithology may be artifacts of thermal-gradient averaging and the conductivity model. For instance, the Freeman Heirs model results in exceptionally high heat flow owing to the combination of its highly conductive carbonate section and the relatively high thermal gradient from SE Hoover field, which has a much less conductive section. Heat flows used for modeling petroleum generation were modified to account for these problems (right column of Table 1).

With such poor temperature and thermal-indicator control, it is impossible to assess the probable thickness of Cretaceous strata from the burial history. The Cretaceous thickness used in models was interpolated between the outcrop thickness and the Anadarko thickness, with thinning toward the west and north (Table 1). Outcropping Cretaceous strata are about 5,000 ft thick in the eastern Sherman sheet and the western Texarkana sheet of the *Geological Atlas of Texas* (Barnes, 1966, 1967), so Cretaceous burial can be no more than this amount in southern Oklahoma. Cretaceous strata thin toward the west on the Sherman sheet, so similar thinning is expected for southern Oklahoma prior to its erosional stripping. The interpolated Cretaceous thickness is approximately consistent with Tishomingo block paleoburial estimates (Corrigan and others, 1998). The date of initiation of exhumation at about 40 Ma is based on results of Corrigan and others (1998).

Time Scale and Structural Timing

Ages for late Paleozoic stages are interpolated from Harland and others (1990). Although there are uncertainties as to the absolute ages of some stage boundaries, the uncertainties do not affect the modeled time of petroleum generation as long as model results, structural events, and sedimentary events all follow the same chronostratigraphy.

The ages of some structural events were arbitrarily assigned for modeling purposes. The late Atokan deformation event (second Wichitan orogeny) was assigned to the last 1 million years of the Atokan. The Arbuckle orogeny commenced at the beginning of the Virgilian and terminated 1 million years before the end of the Virgilian, resulting in approximately 3 million years' duration. All differential uplift of the Tishomingo and Arbuckle anticlines is interpreted to have occurred during the Arbuckle orogeny.

Permian strata are interpreted to have extended over most of south-central Oklahoma prior to Mesozoic erosion, with the exception of the crest of the Arbuckle anticline. Modeled thicknesses of eroded Permian strata are shown in Table 1. Cretaceous through Cenozoic sedimentation was assumed to have begun 110 million years ago and to have terminated 40 million years ago. These strata were then stripped linearly from 40 million years ago to the present.

Table 1. — Modeled Heat Flow (HF), Thermal Gradient (TG), and Eroded Thicknesses

Model	Location	Eroded Permian (ft)	Eroded Cretaceous–Cenozoic (ft)	TG, F/100 (ft)	HF calculated from TG (mW/m^2)	HF used (mW/m^2)
Eastern Ardmore basin	sec. 24, T. 6 S., R. 4 E.	160	3,200	1.3	46.1	46
Signal City of Ardmore 1	sec. 4, T. 5 S., R. 2 E.	500	2,600	1.4	47.8	48
Caddo anticline	sec. 36, T. 3 S., R. 1 E.	120	2,300	1.4	50.6	49
Gulf Central Warren 1	sec. 11, T. 3 S., R. 2 E.	320	2,300	1.4	48.7	49
Arbuckle anticline crest	sec. 24, T. 1 S., R. 1 W.	0	2,300	1.3	49.3	49
Tishomingo	sec. 3, T. 2 S., R. 3 E.	320	2,000	1.35	46.4	47
Buckhorn	sec. 35, T. 1 S., R. 3 E.	500	2,000	1.5	47.4	48
Mill Creek	sec. 7, T. 2 S., R. 5 E.	500	2,160	1.5	48.4	48
Hunton anticline	sec. 36, T. 1 N., R. 5 E.	250	1,300	1.1	51	50
Classen	sec. 10, T. 1 N., R. 1 E.	500	1,600	1.35	42.7	45
Eola Subthrust	sec. 30, T. 1 N., R. 1 W.	320	1,600	1.3	54	46
Frankfort Freeman Heirs 1	sec. 1, T. 1 S., R. 1 W.	0	1,600	1.35	65	48
SE Hoover	sec. 4, T. 1 S., R. 1 E.	320	1,600	1.35	47	45
Eola deep	sec. 29, T. 1 N., R. 1 W.	320	1,300	1.3	44.6	45
Tishomingo	sec. 3, T. 3 S., R. 5 E.	160	4,000	1.4	51.6	50

MODELING RESULTS

Eastern Anadarko Basin

Vitrinite-reflectance depth trends show significant variation between modeled wells in the eastern Anadarko basin (Fig. 8A). These results are consistent with the scatter seen in the Cardott (1989) vitrinite-reflectance data. There is a better relationship between modeled vitrinite reflectance and modeled present-day temperature (Fig. 8B). There is only about a 5°C temperature difference between well models for a given reflectance level. Given the uncertainty of temperatures at well locations, this correlation is probably good enough to be used to predict vitrinite reflectance of zones in the eastern Anadarko basin except in areas of major uplift.

The transformation of the Woodford source rock is high in all modeled wells (Fig. 8C). The least mature, the Petree Ranch well, shows a transformation ratio (TR) of about 0.95. This means that 95% of the possible oil and gas generation has already occurred, and only 5% of the original potential is left for future generation. Most oil was generated in the Pennsylvanian and Permian Periods, and essentially all oil was generated before the end of the Triassic Period. The time of oil generation from the Woodford Shale is progressively younger where the Woodford is buried to shallower depths. Most Woodford petroleum was generated during the Early Pennsylvanian (Atokan) at the Bertha Rogers well location. Most Woodford petroleum generation in the least mature well (Petree Ranch) is of Permian Leonardian to Guadalupian age (Fig. 8D). The duration of oil generation increased at locations with shallower modern Woodford burial, owing to the overall decreasing rate of late Paleozoic subsidence. Slower subsidence caused lower heating rates and longer duration of generation. Essentially no petroleum was generated from the Woodford Shale at any of the modeled sites during the Cretaceous or the Cenozoic because of low deposition rates and high TRs of the Woodford during this time. Parts of the Anadarko basin closest to the Mill Creek syncline are characterized by Permian generation of Woodford petroleum.

Ardmore Basin

Because interpreted thermal gradients and heat flow show minor variation in the deep northern Ardmore basin, vitrinite reflectance correlates well with both depth and temperature for most modeled locations (Fig. 10A,B). The exception is the Arbuckle anticline model. Uplift of the Arbuckle anticline following Desmoinesian burial would have lowered temperatures far below those of maximum burial, so modeled vitrinite-reflectance trends reflect maximum paleotemperature, not modern temperature.

Most Ardmore basin Woodford petroleum was generated during the Desmoinesian and Missourian Stages (Fig. 10C). Where the Woodford Shale is deeply buried, essentially all petroleum was generated from the Woodford, Viola Springs, and Simpson source rocks during the Desmoinesian and Missourian Stages (Fig. 10D). The effects of Creta-

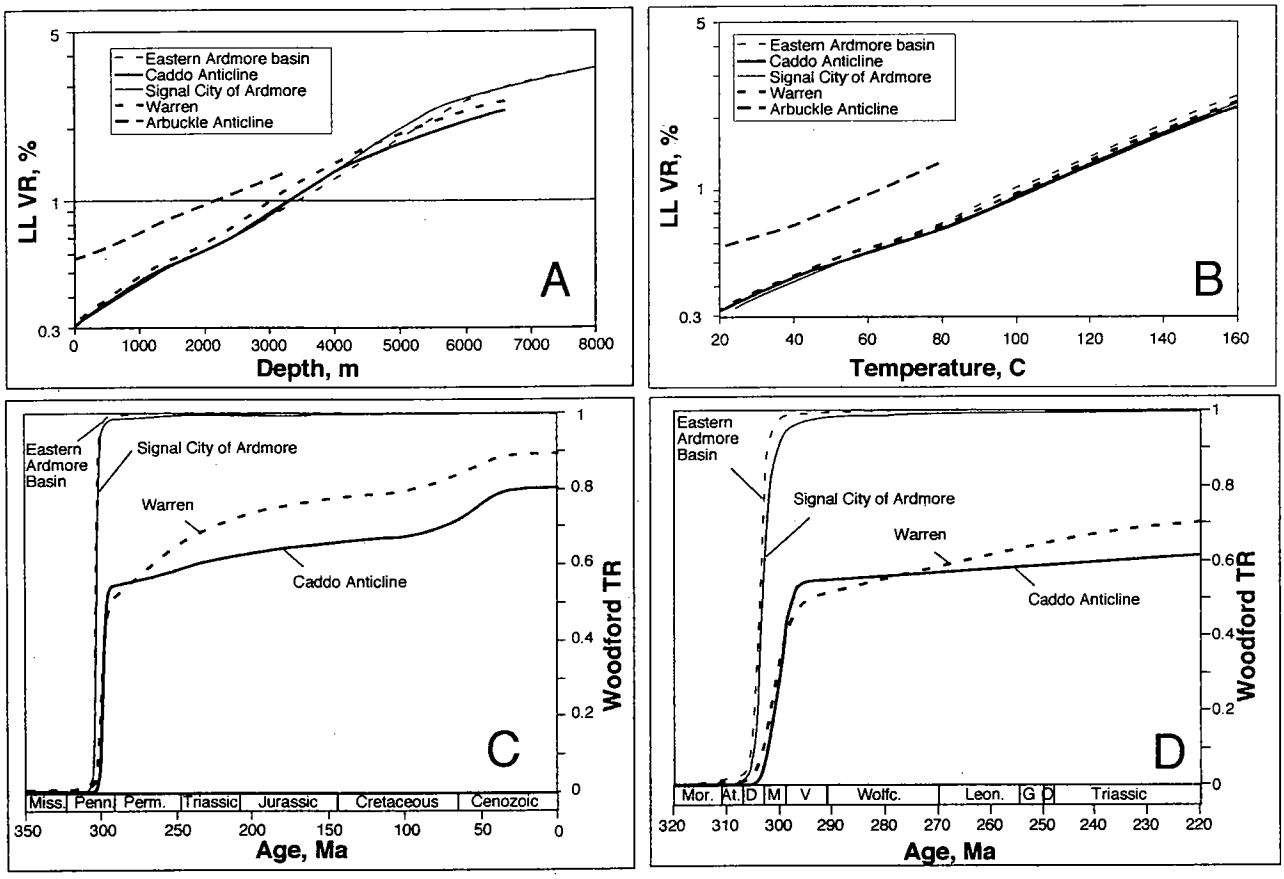

Figure 10. Modeled vitrinite reflectance (VR) and Woodford Shale transformation ratio (TR) for well locations in the Ardmore basin. (A) Modeled VR versus present depth. (B) Modeled VR versus temperature. (C) Petroleum generation from the Woodford Shale as measured by fractional TR. (D) TR on an expanded time scale, showing Pennsylvanian and Permian transformation of Woodford kerogen. Approximate model locations are listed in Table 1.

ceous through Cenozoic burial are not evident in the two deep wells, because the generation potential of Woodford and older source rocks was almost completely exhausted before initiation of Cretaceous sedimentation.

Woodford kerogen in the two modeled wells near the northern margin of the Ardmore basin has not been completely transformed. Petroleum-generation rates were high during Desmoinesian and Missourian deposition, but generation continued slowly through the Mesozoic and Cenozoic (Fig. 10D). Generation rates abruptly slowed after exhumation during the Arbuckle orogeny. Both models show modestly increased generation from Cretaceous through Cenozoic burial. Overall, about two-thirds of the total Woodford generation occurred before the end of the Pennsylvanian Period, and about 15% occurred after Cretaceous deposition began. The Warren model shows less Pennsylvanian generation than the Caddo anticline model, owing to less Pennsylvanian burial. However, this well encountered less exhumation than that indicated for the Caddo anticline model. Deeper post-Virgilian burial would have resulted in higher transformation than that of the Warren well. Similar modeled patterns are evident for the Simpson Group and Viola Springs source rocks, but these units have higher transformations because of deeper burial.

The Arbuckle anticline model and other models on the Arbuckle and Tishomingo highs indicate that the Woodford Shale, Viola Springs Formation, and Simpson Group on outcrop in these areas are thermally immature for oil generation, consistent with outcrop geochemical data. Shallow-subsurface samples are also immature. Woodford samples from the Aylesworth field are thermally immature (VR <0.5% at 930 m; Comer and Hinch, 1987; Rock-Eval production index <0.025 at 1,960 m; Kirkland and others, 1992).

Mill Creek Syncline

Models for locations in the eastern Mill Creek syncline indicate that the Woodford Shale, Viola Springs Formation, or Simpson Group have TRs significantly less than 0.1, so no petroleum was generated in this area. Four models in the western Mill Creek syncline indicate complex patterns of predominantly Permian petroleum generation in the Woodford and older formations. Two models are estimates of generation in the deeper parts of the Mill Creek syncline (Eola deep and SE Hoover), and two models evaluate maturation

where strata have been overridden by the Arbuckle thrust sheet on the south side of the Mill Creek syncline (Eola subthrust and Freeman Heirs models).

The two models for the deep parts of the western Mill Creek syncline show similar reflectance–depth and reflectance–temperature profiles, owing to similar lithology and heat flow (Fig. 11A,B). At present, the Woodford Shale in both wells is in the oil window, with a relatively high TR in the Eola deep model and marginal maturity in the shallower SE Hoover model (Fig. 11C). Petroleum generation did not initiate until the Permian Period (Fig. 11D). About 36% of the Eola deep transformation occurred during the Permian, and only about 15% occurred after initiation of Cretaceous deposition. A relatively larger fraction of generation in the SE Hoover model is associated with the Cretaceous and younger deposition, but the total generation is much lower because the final TR is low.

The two subthrust models are more complex. Subthrust strata are rapidly heated as the thrust overrides the strata. As the topographic high created by thrusting is eroded, the burial decreases and temperature cools. The Genesis program treats thrust sheets as special layers so that the effects of subthrust burial can be modeled. Thrust loading was modeled as early Virgilian. Erosion was modeled as Virgilian through Early Permian, coincident with deposition of the surrounding molasse deposits.

The Eola subthrust model has a vitrinite-reflectance trend with temperature similar to that of the Mill Creek syncline models (Fig. 11B). This results from a similar conductive model. The Eola subthrust strata are overlain by a thermally conductive carbonate thrust that is buried under a thermally resistive Permian red-bed section. The Freeman Heirs model has a higher modeled vitrinite reflectance at a given temperature than the other models (Fig. 11B). The Freeman Heirs model has the thermally conductive carbonate thrust sheet extending to the surface, so overall thermal conductivity is higher and the section is cooler than those of the other models. Vitrinite-reflectance variations with depth in the two subthrust models are similar, because the reflectance developed during thrust loading, not present temperature trends. Most Woodford petroleum generation in the subthrust models occurred during Virgilian and early Permian thrust loading (Fig. 11D). After erosion of the upper part of the thrust sheet, temperatures cooled and generation rates dropped. The deeply buried Freeman Heirs model shows almost no post-Permian petroleum generation in the Woodford Shale. The Eola subthrust model shows additional generation, owing to its lower TR after burial by the thrust sheet (Fig. 11C). About 30% of its total transformation occurred after initiation of Creta-

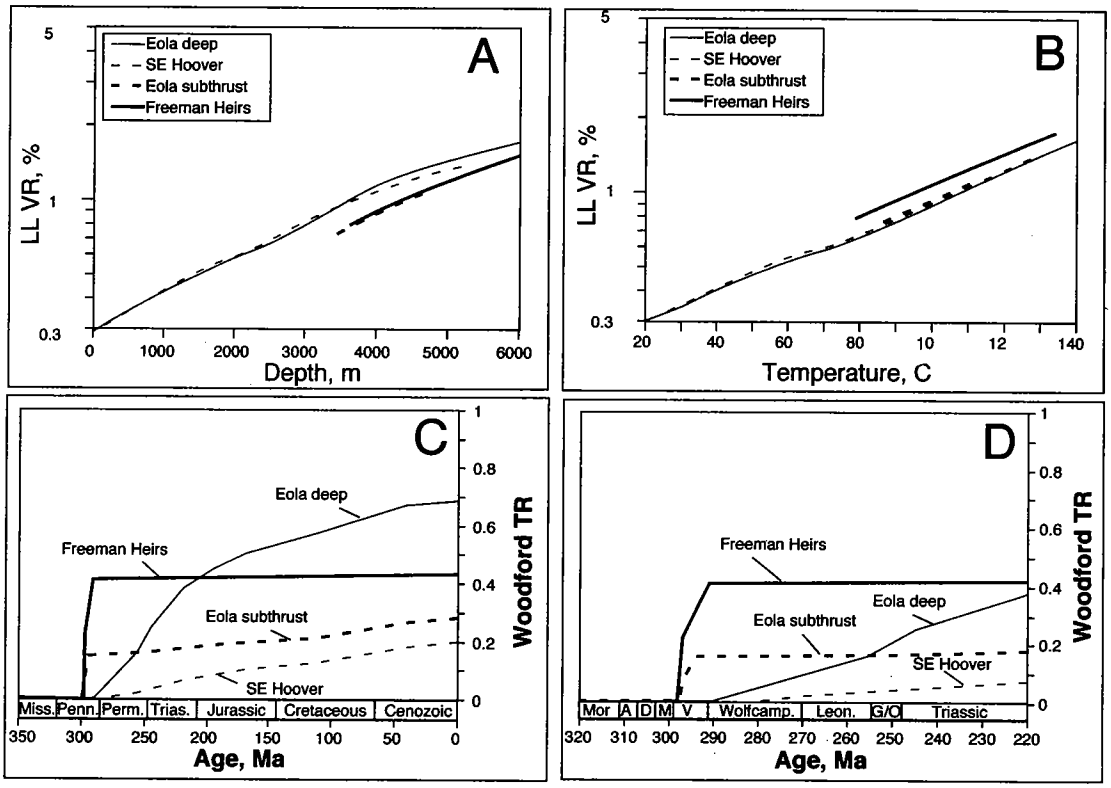

Figure 11. Modeled vitrinite reflectance (VR) and Woodford Shale transformation ratio (TR) for well locations in the Mill Creek syncline. (A) Modeled VR versus depth. (B) Modeled VR versus temperature. (C) Petroleum generation from Woodford Shale as measured by fractional TR. (D) TR on an expanded time scale, showing Pennsylvanian and Permian transformation of Woodford kerogen. Approximate model locations are listed in Table 1.

ceous deposition. The current TR is about 0.43 and 0.28 for the Freeman Heirs and Eola subthrust models, respectively.

Although the Woodford Shale is buried deeper in the subthrust models than in the Eola deep model, transformation is less as a result of the high conductivity of the thrust sheets, which lowered the temperature of the subthrust strata during post-Permian burial.

Comparison of Thermal Maturity in Different Basins

The calculated vitrinite-reflectance versus temperature trends in the different basins are similar. The Ardmore basin reflectances are slightly higher, owing to deeper Cretaceous through Cenozoic burial. The uncertainty of subsurface temperature is greater than the difference in the different reflectance versus temperature trends, so for modeling purposes, modern vitrinite reflectance and TR can be calculated directly from present-day subsurface temperature for those areas that have not been buried by thrusts and that have not been greatly exhumed since Pennsylvanian burial.

The depth range corresponding to the oil window in the central Ardmore basin lies between ~8,200 ft (Woodford TR = 0.1) and ~12,500 ft (Woodford TR = 0.95) below the surface. Because the thermal gradient decreases to the east and west, the depth of the oil window increases (Fig. 12). The shallow depth of the oil window in this cold basin is caused by its great age and by Cretaceous through Cenozoic burial. Essentially all Woodford oil generation in parts of the Ardmore basin deeper than the present-day top of the oil window occurred during the Desmoinesian and Missourian Stages. Most Woodford oil generation at locations in the present oil window occurred prior to the Arbuckle orogeny.

The vitrinite-reflectance–temperature trends for the western Mill Creek syncline and the eastern Anadarko basin are approximately the same, but the thermal gradient is more variable in these areas. The depth of the oil window is 11,000–18,000 ft for a thermal gradient of 1.1°F/100 ft and 9,000–14,500 ft for a thermal gradient of 1.4°F/100 ft. Only the deepest parts of the Mill Creek syncline are thermally mature for oil generation, and the Woodford Shale has not been buried below the oil window anywhere in the syncline (Fig. 12). In subthrust areas, almost all oil

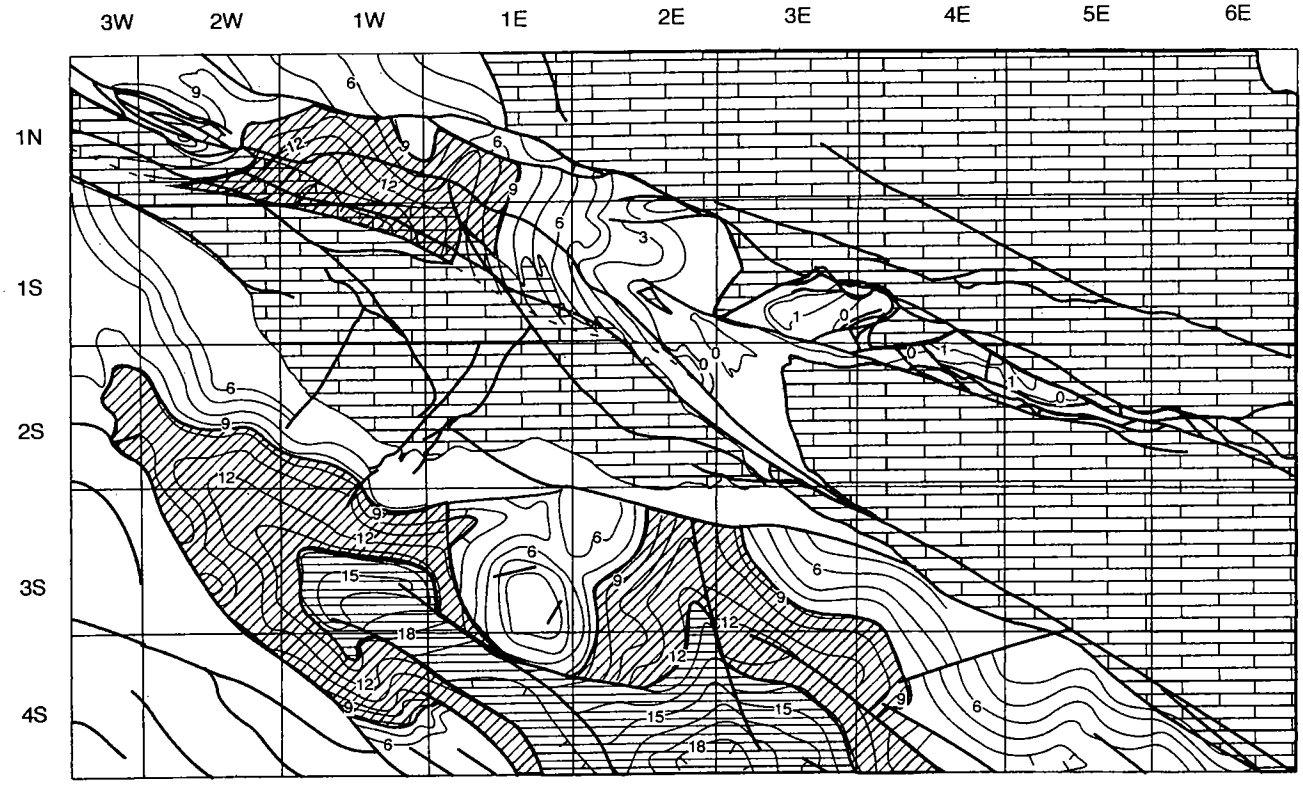

Figure 12. Modeled Woodford Shale oil window (diagonal hatching) and gas window (horizontal hatching) in the modern Ardmore basin and Mill Creek syncline. Depths of generation zones (shown by contour values in thousands of feet below sea level) are interpreted from subsurface temperatures calculated from the thermal gradient. All post-mature areas and areas near the base of the oil window in the central and eastern Ardmore basin became mature during Desmoinesian and Missourian burial. Marginally mature areas became mature after Virgilian deformation owing to long exposure to moderate temperature. This map underestimates maturity close to the Arbuckle anticline, because these areas attained maturation before uplift. Maturation zones are plotted on the structure map depicting the top of the Viola Group (Fig. 2), so post-Virgilian migration patterns can be interpreted from the structural configuration.

generation is Early Permian in age. In areas in front of the thrust, most oil was generated during the Permian and Triassic Periods, but some was generated during Jurassic to Holocene burial.

Generation in the deep eastern Anadarko basin was predominantly Permian in age, owing to less burial by Morrowan through Desmoinesian strata and greater burial by Permian strata (Fig. 8D). Most of the deep eastern Anadarko basin is characterized by a low thermal gradient, so deep areas to the west of Eola-Robberson field are still in the oil window. This area generated a significant fraction of its petroleum after the Triassic Period, but deeper, more thermally mature areas farther west are characterized by Permian–Triassic generation, like most of the eastern Anadarko basin.

Although no geohistory models were run for the complexly deformed western Ardmore basin, the temperature correlation to thermal maturity of the eastern Anadarko basin can be used to project areas of thermal maturity into this part of the basin because the stratigraphy is similar. Thermal gradients are lower here, and burial of the Woodford Shale is not as deep as in the central and eastern Ardmore basin. Areas with the Woodford Shale buried deeper than about 11,000 ft are thermally mature for oil generation, and almost no area has Woodford Shale in the gas window. Desmoinesian isopachs also thin into the western Ardmore basin, so generation began during the Permian Period, as it did in the western Mill Creek syncline and eastern Anadarko basin. However, the southern side of the basin was overridden by a thrust associated with the Criner Hills uplift (Jacobson, 1984; Cooper, 1995), so Atokan subthrust generation and charge to the south side of the Ardmore basin is probable. The axes of structural highs in Sho-Vel-Tum field prevented migration of this petroleum to areas on the north side of the Ardmore basin.

Time of Generation and Potential Charge to the Mill Creek Syncline

Most central and eastern Ardmore basin Woodford oil was generated in the Desmoinesian prior to the Arbuckle orogeny. Oil generated in the northern part of the basin could have migrated north to the central and eastern Mill Creek syncline without being blocked by the Arbuckle anticline and Tishomingo anticline. Because the Desmoinesian isopachs thin west of the Caddo anticline, the northern part of the western Ardmore basin underwent later generation, and many parts of the western basin are not thermally mature. Oil generated by Criner Hills thrust loading during the Atokan was not in a position to charge the northern side of the Ardmore basin.

Given an average content of 10% total organic carbon (TOC), a hydrogen index of 700 mg/g, and a thickness of 100 m, the Woodford Shale could have generated about 13 billion metric tonnes (MT) of oil (100 billion bbl) in the Ardmore basin prior to the Arbuckle orogeny. About 10 billion MT was probably expelled from the Woodford Shale, on the basis of average expulsion-efficiency estimates for rich-shale source rocks (Pepper, 1991). About half of this oil was in a position where it could migrate toward the north. Only about 3% of the total generation in the Ardmore basin occurred after the Arbuckle orogeny. This petroleum was generated after uplift of the Arbuckle anticline and Tishomingo anticline, so northerly migration could have extended only to the edge of the Ardmore basin.

All western Mill Creek syncline oil was generated after the Arbuckle orogeny, and most was generated after the Triassic Period. Structural deformation has been minor since the Virgilian Stage, so modern structural patterns can be used to assess oil-migration patterns for the Mill Creek syncline for its entire period of generation. Oil generated in the Mill Creek syncline could have migrated updip toward the north, northeast, and west, but it could not have migrated to the southeast to charge asphalt and oil accumulations in the eastern Mill Creek syncline. The eastern deep in the Mill Creek syncline is only marginally mature (Fig. 12), so the potential charge to traps farther east is probably overestimated. Only a total of about 600 million MT of Woodford oil has been generated in the Mill Creek syncline, using the same source-quality assumptions as those used for the Ardmore basin, so generation is minor by comparison.

The Anadarko basin charge to the area near the Mill Creek syncline conceivably could have initiated in the Atokan if the charge had been from the deep central Anadarko basin far to the west. However, pre-Desmoinesian migration from the deep central Anadarko basin was probably directed to the north and northeast, on the basis of Morrowan and Atokan isopach patterns, so an early charge was not likely. The Atokan uplift of the Pauls Valley high directed updip migration from the eastern Anadarko basin toward the northeast, not toward the east and southeast. Parts of the Anadarko basin closest to the Mill Creek syncline generated oil only after the Arbuckle orogeny. Late Pennsylvanian and modern structural configuration do not favor migration of oil from the eastern Anadarko basin to the central and eastern Mill Creek syncline. Accumulations at the western end of the Mill Creek syncline and in the Golden Trend area could have been easily charged by post-Atokan generation of Woodford oil in the eastern Anadarko basin. The Woodford Shale in the Anadarko basin generated approximately 80 billion MT of oil (600 billion bbl), of which most migrated toward the northeast, north, and northwest. Even a small fraction of this vast generation that migrated eastward could have charged traps in the Eola-Robberson and Golden Trend areas.

Modeling results indicate that petroleum charge to the eastern and central Mill Creek syncline came from the Ardmore basin during Desmoinesian and Missou-

rian time, prior to Virgilian uplift of the Arbuckle anticline and Tishomingo block. Most oil in the Golden Trend and similar fields north of the western Mill Creek syncline probably migrated from the Anadarko basin during Permian time, because these areas are unfavorably situated for charge from the western Mill Creek syncline. Much of the Eola-Robberson oil is probably also from the Anadarko basin. However, some of the oil in the Eola-Robberson and Hoover areas was probably generated in the western Mill Creek syncline. Much of the western Mill Creek syncline oil was generated during Triassic and younger time, after the present trapping configuration was established. Some of the oil could have been generated as recently as the Cretaceous Period, but this oil would be only a small fraction of total generation. The western Mill Creek syncline oils might be the youngest oils generated in Oklahoma. Most oil accumulations in southern Oklahoma are old, because most oil was generated during the Pennsylvanian and Permian Periods.

STRATIGRAPHIC EVIDENCE FOR CHARGE TIMING

Eastern Mill Creek Syncline

Two lines of evidence indicate that the Buckhorn asphalt deposit is of Desmoinesian age. If the asphalt deposit formed at this time, then oil migration to the eastern Mill Creek syncline dates back at least to the Desmoinesian.

The first line of evidence for Desmoinesian charge to the Buckhorn deposit is the presence of a well-preserved aragonite mollusk fauna (Sadd, 1990). A solid hydrocarbon soluble in organic solvents occludes porosity in porous rocks in the Buckhorn quarry. The asphalt isolated aragonite and magnesium calcite from water, preserving the aragonite and causing magnesium calcite to recrystallize under closed conditions (Sadd, 1990). There is almost no evidence of early meteoric cementation in deposits of the asphalt-impregnated quarry, so the carbonate probably was never subaerially exposed prior to oil impregnation (Sadd, 1990). Therefore, the solid hydrocarbon must have been emplaced prior to late Desmoinesian and Missourian sea-level lowstands.

The second line of evidence gives a more precise age for oil migration. An organic-rich bed in the central part of the quarry is interpreted as a fossil oil seep contemporaneous with late middle Desmoinesian deposition. This bed contains insoluble organic matter with an appearance different from the soluble organic matter common in the rest of the quarry (Squires, 1973). Vitrinite, exinite, and other structured organic matter constitute a relatively small part of the organic matter in the bed. Most of the organic matter is a brittle, amorphous, low-reflectance, nonfluorescent solid hydrocarbon insoluble in organic solvents. The solid hydrocarbon has an elevated hydrogen content, as indicated by a moderate Rock-Eval hydrogen index. These characteristics are consistent with the solid hydrocarbon albertite. Solid hydrocarbon veins cross-cut strata underlying and overlying the organic-rich bed (Eldridge, 1901). The asphalt in the veins is similar to that of the bed, indicating that the material interpreted as albertite in the bed is not just an amorphous kerogen. These veins may be the migration pathways that fed the oil seep. The vein on the north wall of the quarry has a folded appearance with irregular boundaries where it crosses a mudstone. This indicates emplacement prior to mudstone compaction, most of which occurred soon after burial.

Stratigraphic relationships in the South Sulphur asphalt district and the Dougherty asphalt quarry provide evidence for early Virgilian migration of oil. The Dougherty asphalt deposit originated as a Virgilian high associated with a double restraining bend of the Reagan fault. After charge, the trap was breached, petroleum leaked to the surface, and the breached trap was overlain by the late Virgilian Vanoss Conglomerate (Brown and Corrigan, 1997). The South Sulphur asphalt deposits were formed as an ancient fluid-level trap at the updip end of a Virgilian-aged, southwest-plunging faulted anticline (Brown and Corrigan, 1997). The Vanoss Conglomerate was deposited unconformably over the anticline after most asphalt had formed. The Dougherty deposit lies just south of the southwest end of the plunging anticline with the South Sulphur asphalt deposits. The present structural configuration is consistent with the spill of oil from the Dougherty anticline prior to its breaching and oil migration up the anticline to the South Sulphur area. The asphalt deposits indicate southwest to northeast migration under the present structural configuration. Most of the eastern Mill Creek syncline asphalt accumulations occur on this southwest-plunging faulted anticline. However, the older Buckhorn asphalt deposit lies east of the plunging anticline in a structurally low position consistent with its formation under an older structural configuration.

Western Mill Creek Syncline and Oklahoma City Field

Most structural traps in or near the western Mill Creek syncline (Eola-Robberson, NW Butterly, SE Hoover, SW Davis fields) are Virgilian structures (Hicks, 1972; Borras, 1979; Beck, 1987; Saxon, 1994), so charge to accumulations in the structures is younger than Virgilian deformation. Many of the traps north of the western Mill Creek syncline are stratigraphic updip pinch-outs or combination traps in Desmoinesian and Missourian strata (Swesnik, 1950). Pinch-outs are oriented for charge from the west or southwest. These traps could have been charged by any migration after Desmoinesian and Missourian deposition.

The Oklahoma City field, north of the study area, shows evidence for charge from Atokan to Permian or later age. Rascoe and Adler (1983) interpret the age of the initial Oklahoma City structure and other Nemaha uplift structures as late Atokan. Ordovician sandstones on the crest of the structure unconformably below the early Desmoinesian seal contain asphalt near the unconformity surface, and overlying

basal Pennsylvanian sediments contain clasts of reworked asphaltic rock (Webb, 1976). This indicates that charge initiated and the trap was breached during the late Atokan and early Desmoinesian. The early charge did not substantially contribute to the oil currently being produced from the field. This oil was emplaced when the Oklahoma City field was buried to near its present depth (Webb, 1976). Surface rocks are Permian in age, so termination of the charge must have been Permian or younger. The charge was from the west (Webb, 1976).

Comparison of Timing Estimates from Models and Stratigraphic Relationships

Both modeling results and physical stratigraphic relationships indicate an earliest petroleum charge to the central and eastern Mill Creek syncline during Desmoinesian deposition. However, the model predicts that charging would have stopped with Virgilian deformation and isolation from the Ardmore basin. This is inconsistent with the age of the South Sulphur and Dougherty asphalt deposits. However, it is possible that the oil that formed the asphalt accumulations was derived from a trap spilled by Virgilian deformation. Some Atokan-aged structures were probably present in the area now occupied by the Arbuckle anticline and Tishomingo anticline. The Caddo anticline, for example, shows stratigraphic evidence of minor (100-m) structural relief during the late Atokan (Clopine, 1991). The fact that Virgilian asphalt accumulations are localized along a single migration pathway is consistent with spillage from an older trap rather than a broad front of northerly migration.

A late charge to traps at the west end of the Mill Creek syncline can be explained by modeled charge from either the Anadarko basin or the Mill Creek syncline itself. Traps are in a position to be charged from these areas under present structural configuration, so the modeling results are consistent with the observed charge.

Because continuous petroleum charge from Atokan to Permian seemed unreasonable to Webb (1976), he proposed two distinct phases of petroleum charge to the Oklahoma City field. The first phase was related to rapid burial before the Desmoinesian unconformity, and the second phase was related to the long duration after the unconformity, which would allow the source rocks to generate in marginally mature settings. However, the physical data also support a continuous migration into the field from late Atokan through Permian. This age range corresponds approximately to the age range of predicted oil and gas generation in the Anadarko basin, the most likely source area for the Oklahoma City field oil.

Most Oklahoma oil is late Paleozoic in age, because this was the time of maximum subsidence and rate of subsidence. A small band of source rock surrounding the basins has continued to mature through the Mesozoic and Cenozoic Eras, but the volume of post-Paleozoic oil has been minor compared to that generated during the Paleozoic Era. Oil is expelled from the source rock soon after generation, so trapping generally follows soon after generation. On this basis, most oil accumulations in Oklahoma are probably Pennsylvanian or Permian in age.

EXPLORATION IMPLICATIONS

Potential oil targets in the eastern and central Mill Creek syncline must have been charged from the Ardmore basin, so older (pre-Virgilian) structures are more likely to be charged. The Virgilian charge demonstrated by the asphalt accumulations occurs along migration fairways with shows in the form of asphalt. Overall, the Mill Creek syncline is relatively poor in production in comparison to areas farther north and west, which received a charge from the prolific Anadarko basin. There should be no potential charge problems in the western Mill Creek syncline, because oil was generated in the deeper parts of the syncline, and traps at the western end of the syncline could have been charged from the Anadarko basin.

Prospects below the Arbuckle thrust have special charge problems. The Woodford Shale in depocenters overridden by the thrust are marginally mature for oil generation in most areas. The target Ordovician reservoirs lie below the main source zone (Woodford) in most areas, and their current structural position is not favorable for charging from downdip subthrust source rocks. The charge risk to Virgilian structures below the Arbuckle thrust is significant. Successful subthrust plays along the north side of the Arbuckle anticline have been in thrust sheets lying above the Arbuckle thrust, so subthrust source-rock strata could have charged them. Modeling results indicate that charge from the Ardmore basin to Ordovician reservoirs may have been possible if subthrust structure is pre-Virgilian in age. Undoubtedly, such structures would have been reactivated during Virgilian deformation, but as long as the trapping geometry remained intact, the pre-Virgilian charge would have remained in the trap. Similar considerations probably apply to other targets below basal detachment thrusts in southern Oklahoma.

In addition to direct application to local charging issues, this study demonstrates that old petroleum systems can still be quite prolific, contrary to some models that propose a short-accumulation life span (e.g., Miller, 1992). Most oil accumulations in Oklahoma are probably Pennsylvanian or Permian in age, quite old compared to the worldwide average (Macgregor, 1996). Their longevity is probably related to their position on a stable craton after Pennsylvanian deformation, so the trapping geometry and seal integrity would not have been disrupted (cf. Bois and others, 1982).

Explorationists should not avoid stable cratonic settings just because oil generation was ancient. In these settings, oil accumulations can also be ancient.

Approximately 660 billion MT of Woodford petroleum was generated from the Anadarko and Ardmore basins, and about 4.8 billion MT of recoverable petroleum reserves (oil, gas, and condensate) (Klett and others, 1997) have been discovered in areas charged by these basins. Assuming that known recoverable reserves are about 40% of the total trapped petroleum in economic accumulations, and that most of the petroleum was generated from the Woodford Shale, overall basin trapping efficiency is about 2%. This compares favorably with worldwide basin-scale trapping efficiency as summarized by Perrodon (1995).

SUMMARY AND CONCLUSIONS

Model results indicate that the central and eastern Mill Creek syncline was charged by petroleum from the Ardmore basin during rapid Desmoinesian–Missourian subsidence. Charge stopped with isolation of the Mill Creek syncline from the Ardmore basin by Virgilian uplift of the Arbuckle Mountains and Tishomingo anticline.

Although the Woodford source rock is thermally mature in the western Mill Creek syncline, it generated petroleum significantly after deformation, so migration is constrained to follow present structural configuration. At present, western Mill Creek syncline oil could charge traps directly around the western end of the syncline, but it cannot charge areas in the eastern or central Mill Creek syncline.

Woodford petroleum generation in the Anadarko basin began during Atokan deposition, and continued outward with subsidence of the basin. Woodford oil generation in the eastern Anadarko basin began during Permian deposition, so the area most likely to have charged the Mill Creek syncline did not do so until the present structural configuration had developed. Under this setting, oil migrating east from the Anadarko basin would have been diverted south to Eola-Robberson field or north by the Pauls Valley uplift.

Model results are consistent with physical stratigraphic constraints for petroleum migration. Virgilian-aged structures in the central and eastern Mill Creek syncline are likely to be charged only if oil spilled from an older structure. Subthrust areas require pre-Virgilian closure to be effectively charged.

ACKNOWLEDGMENTS

I thank Jeff Corrigan for preliminary modeling efforts and discussions on heat flow and burial history in southern Oklahoma. Weldon Beauchamp helped with discussion of structural complexities and oil occurrences north of the Mill Creek syncline.

REFERENCES CITED

Barnes, V. E. (compiler), 1966, Geologic atlas of Texas, Texarkana sheet: Texas Bureau of Economic Geology, Austin, 1 sheet, scale 1:250,000.

_____(compiler), 1967, Geologic atlas of Texas, Sherman sheet: Texas Bureau of Economic Geology, Austin, 1 sheet, scale 1:250,000.

Beck, J. H., 1987, Subsurface structural analysis of the Southeast Hoover field and vicinity, northern Arbuckle Mountain region, southern Oklahoma: Baylor University unpublished M.S. thesis, 147 p.

Bergquist, H., 1949, Geology of the Woodbine Formation of Cooke, Grayson, and Fannin Counties, Texas: U.S. Geological Survey Oil and Gas Investigations Preliminary Map 98, 2 sheets.

Bois, C.; Bouche, P.; and Pelet, R., 1982, Global geologic history and distribution of hydrocarbon reserves: American Association of Petroleum Geologists Bulletin, v. 66, p. 1248–1270.

Borras, J. B., 1979, Genetic study of the Northwest Butterly field, Garvin County, Oklahoma: Shale Shaker, v. 30, p. 58–76.

Braun, R. L.; Burnham, A. K.; Reynolds, J. G.; and Clarkson, J. E., 1991, Pyrolysis kinetics for lacustrine and marine source rocks by programmed micropyrolysis: Energy and Fuels, v. 5, p. 192–204.

Brown, A. A.; and Corrigan, J., 1997, Petroleum systems, Ardmore basin and Arbuckle Mountains, Oklahoma: American Association of Petroleum Geologists, 1997 Annual Meeting, Field Trip 32, 88 p.

Brown, A. A.; and Senftle, J. T., 1997, Source potential of the Viola Springs Formation, southern limb of the Arbuckle anticline, Arbuckle Mountains, Oklahoma [abstract], *in* Johnson, K. S. (ed.), Simpson and Viola Groups in the southern Midcontinent, 1994 symposium: Oklahoma Geological Survey Circular 99, p. 102.

Burchfield, M. R. (compiler), 1985, Map of Oklahoma oil and gas fields: Oklahoma Geological Survey Map GM-28, 1 sheet, scale 1:500,000.

Burnham, A. K.; and Sweeney, J. J., 1989, A chemical kinetic model of vitrinite maturation and reflectance: Geochimica et Cosmochimica Acta, v. 53, p. 2649–2657.

Burruss, R. C.; and Hatch, J. R., 1989, Geochemistry of oils and hydrocarbon source rocks, greater Anadarko basin: evidence for multiple sources of oils and long-distance oil migration, *in* Johnson, K. S. (ed.), Anadarko basin symposium, 1988: Oklahoma Geological Survey Circular 90, p. 53–64.

_____1992, Geochemistry of oils and hydrocarbon source rocks, greater Anadarko basin, Oklahoma, Texas, Kansas, Colorado, and Nebraska: an update [abstract], *in* Johnson, K. S.; and Cardott, B. J. (eds.), Source rocks in the southern Midcontinent, 1990 symposium: Oklahoma Geological Survey Circular 93, p. 197.

Cardott, B. J., 1989, Thermal maturation of the Woodford Shale in the Anadarko basin, *in* Johnson, K. S. (ed.), Anadarko basin symposium, 1988: Oklahoma Geological Survey Circular 90, p. 32–46.

Cardott, B. J.; and Chaplin, J. R., 1993, Guidebook for selected stops in the western Arbuckle Mountains, southern Oklahoma: Oklahoma Geological Survey Special Publication 93-3, 55 p.

Cardott, B. J.; and Lambert, M. W., 1985, Thermal maturation by vitrinite reflectance of Woodford Shale, Anadarko basin, Oklahoma: American Association of Petroleum Geologists Bulletin, v. 69, p. 1982–1998.

Cardott, B. J.; Metcalf, W. J.; and Ahern, J. L., 1990, Thermal maturation by vitrinite reflectance of Woodford Shale near Washita Valley fault, Arbuckle Mountains, Oklahoma, *in* Nuccio, V. F.; and Barker, C. E. (eds.), Applications of thermal maturity studies to energy exploration: Society of Economic Paleontologists and Mineralogists, Rocky Mountain Section, p. 139–146.

Carter, L. S.; Kelley, S. A.; Blackwell, D. D.; and Naeser, N., 1998, Heat flow and thermal history in the Anadarko basin, Oklahoma: American Association of Petroleum Geologists Bulletin, v. 82, p. 291–316.

Clopine, W. W., 1991, Lithostratigraphic and biostratigraphic analysis of the Atokan Series (Middle Pennsylvanian) in the Ardmore basin, Oklahoma: Compass, v. 68, p. 221–232.

Comer, J. B.; and Hinch, H. H., 1987, Recognizing and quantifying expulsion of oil from the Woodford Formation and age equivalent rocks in Oklahoma and Arkansas: American Association of Petroleum Geologists Bulletin, v. 71, p. 844–858.

Cooper, J. C., 1995, Geological evolution of the Criner Hills trend, Ardmore basin, Oklahoma, *in* Johnson, K. S. (ed.), Structural styles in the southern Midcontinent, 1992 symposium: Oklahoma Geological Survey Circular 97, p. 144–160.

Corrigan, J.; Cervany, P. F.; Donelick, R.; and Bergman, S., 1998, Postorogenic denudation along the late Paleozoic Ouachita trend, south central United States of America: magnitude and timing constraints from apatite fission track data: Tectonics, v. 17, p. 587–603.

Eldridge, G. H., 1901, Asphalt and bituminous rock deposits: U.S. Geological Survey, 22nd annual report, pt. 1, p. 262–320.

Feinstein, S., 1981, Subsidence and thermal history of southern Oklahoma aulacogen: implications for petroleum exploration: American Association of Petroleum Geologists Bulletin, v. 65, p. 2521–2533.

Gallardo, J.; and Blackwell, D. D., 1999, Thermal structure of the Anadarko basin: American Association of Petroleum Geologists Bulletin, v. 83, p. 333–361.

Garner, D. L.; and Turcotte, D. L., 1984, The thermal and mechanical evolution of the Anadarko basin: Tectonophysics, v. 107, p. 1–24.

Glash, S. J.; and Friedman, G. M., 1988, Paleodepth of burial: case history of exposed Paleozoic carbonates in Arbuckle Mountains, Oklahoma: American Association of Petroleum Geologists Bulletin, v. 72, p. 962–963.

Ham, W. E., 1955, Regional stratigraphy and structure of the Arbuckle Mountain region, *pt. 2 of* Ham, W. E., Geology of the Arbuckle Mountain region: Oklahoma Geological Survey Guidebook 3, p. 29–61.

_____1969, Regional geology of the Arbuckle Mountains, Oklahoma: Oklahoma Geological Survey Guidebook 17, 52 p.

Harland, W. B.; Armstrong, R. L.; Cox, A. V.; Craig, L. E.; Smith, A. G.; and Smith, D. G., 1990, A geologic time scale, 1989: Cambridge University Press, New York, 263 p.

Harrison, W. E.; Luza, K. V.; Prater, M. L.; and Cheung, P. K., 1983, Geothermal resource assessment in Oklahoma: Oklahoma Geological Survey Special Publication 83-1, 42 p.

Hicks, I. C., 1972, Southern Oklahoma folded belt, *in* Cram, I. H. (ed.), Future petroleum provinces of the United States—their geology and potential: American Association of Petroleum Geologists Memoir 15, v. 2, p. 1070–1076.

Huffman, G. G., 1979, Oil and gas in Bryan County, *in* Huffman, G. G.; and others, Geology and mineral resources of Bryan County, Oklahoma: Oklahoma Geological Survey Bulletin 126, p. 53–81.

Jacobson, M. I., 1984, The Harrisburg trough, Stephens County, Oklahoma—an update, *in* Borger, J. G. (ed.), Technical proceedings of the American Association of Petroleum Geologists, Mid-Continent Section, 1981 regional meeting: Oklahoma City Geological Society, p. 127–137.

Johnson, K. S.; and Cardott, B. J., 1992, Geologic framework and hydrocarbon source rocks of Oklahoma, *in* Johnson, K. S.; and Cardott, B. J. (eds.), Source rocks in the southern Midcontinent, 1990 symposium: Oklahoma Geological Survey Circular 93, p. 21–37.

Johnson, K. S.; Amsden, T. W.; Denison, R. E.; Dutton, S. P.; Goldstein, A. G.; Rascoe, Bailey, Jr.; Sutherland, P. K.; and Thompson, D. M., 1988, Southern Midcontinent region, *in* Sloss, L. L. (ed.), Sedimentary cover—North American craton; U.S.: Geological Society of America, Boulder, The Geology of North America, v. D-2, p. 307–359. [Reprinted as Oklahoma Geological Survey Special Publication 89-2, 53 p.]

Jones, P. J.; and Philp, R. P., 1990, Oils and source rocks from Pauls Valley, Anadarko basin, Oklahoma, U.S.A.: Applied Geochemistry, v. 5, p. 429–448.

Jordan, Louise, 1964, Petroleum-impregnated rocks and asphaltite deposits of Oklahoma: Oklahoma Geological Survey Map GM-8, 1 sheet and text booklet, scale 1:750,000.

Kirkland, D. W.; Denison, R. E.; Summers, D. M.; and Gormly, J. R., 1992, Geology and organic geochemistry of the Woodford Shale in the Criner Hills and western Arbuckle Mountains, Oklahoma, *in* Johnson, K. S.; and Cardott, B. J. (eds.), Source rocks in the southern Midcontinent, 1990 symposium: Oklahoma Geological Survey Circular 93, p. 38–69.

Klett, T. R.; Ahlbrandt, T. S.; Schmoker, J. W.; and Dolton, G. L., 1997, Ranking of the world's oil and gas provinces by known petroleum volumes: U.S. Geological Survey Open File Report 97-463 [CD-ROM distribution].

Macgregor, D. S., 1996, Factors controlling the destruction and preservation of giant light oil fields: Petroleum Geoscience, v. 2, p. 197–217.

McBee, William, Jr., 1995, Tectonic and stratigraphic synthesis of events in the region of the intersection of the Arbuckle and Ouachita structural systems, Oklahoma, *in* Johnson, K. S. (ed.), Structural styles in the southern Midcontinent, 1992 symposium: Oklahoma Geological Survey Circular 97, p. 45–81.

Miller, R. G., 1992, The global oil system: the relationship between oil generation, loss, half-life, and the world crude oil resource: American Association of Petroleum Geologists Bulletin, v. 76, p. 489–500.

Pawlewicz, M. J., 1990, Chapter C: Thermal maturation of the eastern Anadarko basin, Oklahoma: U.S. Geological Survey Bulletin 1866, p. C1–C12.

Pepper, A., 1991, Estimating the petroleum expulsion behaviour of source rocks: a novel quantitative approach, *in* England, W. A.; and Fleet, A. J. (eds.), Petroleum migration: Geological Society [London] Special Publication 59, p. 9–31.

Perrodon, A., 1995, Petroleum systems and global tectonics: Journal of Petroleum Geology, v. 18, p. 471–476.

Price, L. C.; Clayton, J. L.; and Rumen, L. L., 1981, Organic geochemistry of the 9.6 km Bertha Rogers No. 1 well, Oklahoma: Organic Geochemistry, v. 3, p. 59–77.

Quigley, T. M.; and Mackenzie, A. S., 1988, The temperatures of oil and gas formation in the sub-surface: Nature, v. 333, p. 549–552.

Rascoe, Bailey, Jr.; and Adler, Frank, 1983, Permo–Carboniferous hydrocarbons, Mid-Continent, U.S.A.: American Association of Petroleum Geologists Bulletin, v. 67, p. 979–1001.

Sadd, J. L., 1990, Tectonic influences on carbonate deposition and diagenesis, Buckhorn asphalt, Deese Group (Desmoinesian), Arbuckle Mountains, Oklahoma: Journal of Sedimentary Petrology, v. 61, p. 28–42.

Saxon, C. P., 1994, Surface to subsurface structural analysis, northwest Arbuckle Mountains, southern Oklahoma: Baylor University unpublished M.S. thesis, 191 p.

Squires, R. L., 1973, Burial environment, diagenesis, mineralogy, and Mg and Sr contents of skeletal carbonates in the Buckhorn asphalt of Middle Pennsylvanian age, Arbuckle Mountains, Oklahoma: California Institute of Technology unpublished Ph.D. dissertation, 226 p.

Swesnik, R. M., 1950, Golden trend of south-central Oklahoma: American Association of Petroleum Geologists Bulletin, v. 34, p. 386–422.

Tegelaar, E. W.; and Noble, R. A., 1994, Kinetics of hydrocarbon generation as a function of the molecular structure of kerogen as revealed by pyrolysis–gas chromatography: Organic Geochemistry, v. 22, p. 543–574.

Tomlinson, C. W.; and McBee, William, 1959, Pennsylvanian sediments and orogenies of Ardmore district, Oklahoma, *in* Mayes, J. W.; and others (eds.), Petroleum geology of southern Oklahoma: American Association of Petroleum Geologists, Tulsa, v. 2, p. 3–52.

Wang, H. D.; and Philp, R. P., 1997, Geochemical study of potential source rocks and crude oil in the Anadarko basin, Oklahoma: American Association of Petroleum Geologists Bulletin, v. 81, p. 249–275.

Wavrek, D. A., 1992, Characterization of oil types in the Ardmore and Marietta basins, southern Oklahoma aulacogen, *in* Johnson, K. S.; and Cardott, B. J. (eds.), Source rocks in the southern Midcontinent, 1990 symposium: Oklahoma Geological Survey Circular 93, p. 185–195.

Webb, G., 1976, Oklahoma City oil—second crop from preserved sub-unconformity source rocks: American Association of Petroleum Geologists Bulletin, v. 60, p. 115–122.

Zemmels, I.; and Walters, C. C., 1987, Variation of oil composition in the vicinity of Arbuckle Mountains, OK [abstract]: American Association of Petroleum Geologists Bulletin, v. 71, p. 998–999.

Computer Modeling of a Small-Scale Inversion Feature: Milroy Field, Southern Oklahoma

Robert E. Harmon
C. E. Harmon Oil, Inc.
Tulsa, Oklahoma

Richard Banks
Scientific Computer Applications, Inc.
Tulsa, Oklahoma

Raymond W. Suhm
Consulting Geophysicist and Geologist
Oklahoma City, Oklahoma

ABSTRACT.—Milroy field is a small, structurally complex southern Oklahoma feature with multiple pay zones. The field extends from northeastern Stephens County to northwestern Carter County. Overlooked areas of pay are continually being found in and near the Milroy field area, owing to reevaluations of previous geologic interpretations. This paper offers a new interpretation of the regional geology of Milroy field derived from an evaluation of an electric-log cross section.

A 13-well electric-log cross section that extends from secs. 23 and 24, T. 2 S., R. 4 W., to sec. 18, T. 2 S., R. 3 W., was modeled in the tradition of Schweers (1959) as a "rabbit-ear" anticline with three vertical faults, whereas another model shows thrust faults in a fault-rejuvenation mode. To determine if one or both models are reasonable, both were balanced. The model of Schweers (1959) did not balance, whereas the model proposed here did balance. The balanced model exhibits faulting from the north, such as might have been caused by a backthrust from the Arbuckle Mountains. This backthrust could have resulted from inversion in the Arbuckle Mountains. Interpreted seismic data agree closely with the balanced model.

Additionally, computer modeling of this project suggests that (1) the basal Morrowan unconformity is continuous beneath either the upper Dornick Hills or, in its absence, the Tussy limestone; (2) the upper Dornick Hills and Springer are not present between the two anticlines shown on the 11-well cross section, and a single fault separates the two anticlines; (3) computer-generated contour maps from the Goddard Shale to the Arbuckle show fault displacements on the Milroy anticline to lessen in progressively deeper and older formations.

INTRODUCTION

Milroy field is a small, structurally complex southern Oklahoma feature with multiple pay zones. The field traverses northeastern Stephens County and northwestern Carter County and consists of about 2,650 acres (Fig. 1). Discovered in 1917, Milroy field is one of many fields found near regional, northwest–southeast-trending faults (Schweers, 1959). In 1962, Milroy field was grouped together with more than 40 previously named smaller fields to form the giant Sho-Vel-Tum field (Lacina, 1979). In an *Oil and Gas Journal* article compiled by Johnson and others (1986), primary oil production in Sho-Vel-Tum field began a rapid decline in 1953. Waterflooding began in 1955, and as of 1986, about 59,000 of the 75,000 total acres in the field were being flooded. At the close of 1984, Pennsylvanian reservoirs had produced about 1,133 million stock-tank barrels, representing 92% of Sho-Vel-Tum's total production (Johnson and others, 1987).

One of the more prominent wells in Milroy field, the Carter No. 1 Harley C-49, in the NE¼NE¼ sec. 24, T. 2 S., R. 4 W., was drilled to a depth of 8,157 ft in 1937. This well was completed for 1,215 barrels of oil per day in the Ordovician Oil Creek Formation (Schweers, 1959). Productive zones extend from the Permian at depths <1,000 ft down to the Oil Creek Formation at depths >7,000 ft.

Harmon, R. E.; Banks, Richard; and Suhm, R. W., 2002, Computer modeling of a small-scale inversion feature: Milroy field, southern Oklahoma, *in* Cardott, B. J. (ed.), Revisiting old and assessing new petroleum plays in the southern Midcontinent, 2001 symposium: Oklahoma Geological Survey Circular 107, p. 37–54.

New technological advances have prolonged the life of Milroy field. Additionally, overlooked areas of pay are continually being found in and near the Milroy field area as a result of reevaluations of previous geologic interpretations.

CROSS-SECTION MODELS

This paper evaluates a 13-well electric-log cross section by Schweers (1959) that extends from secs. 23 and 24, T. 2 S., R. 4 W., Stephens County, to sec. 18, T. 2 S., R. 3 W., Carter County. Schweers interpreted

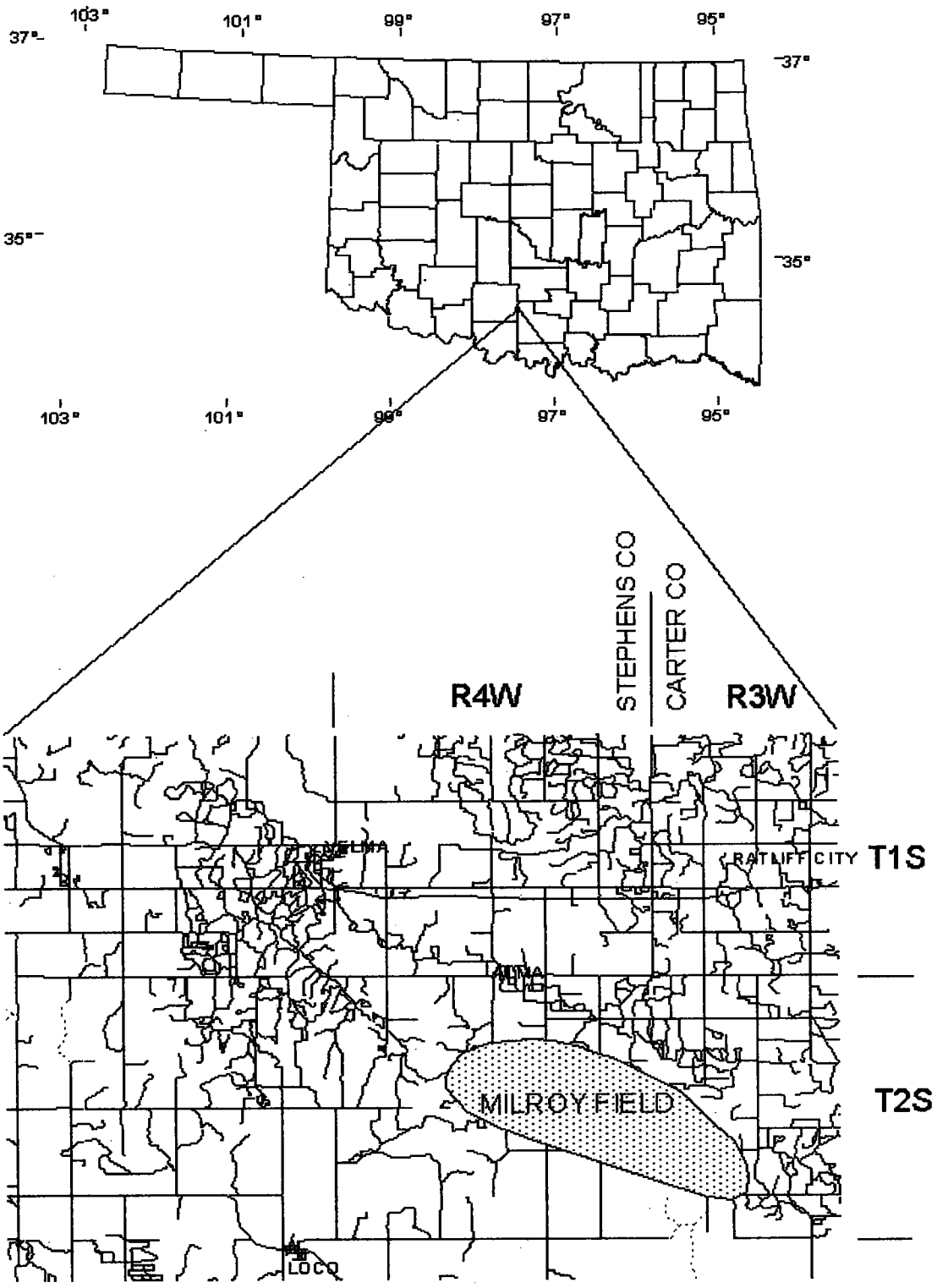

Figure 1. Location map of Milroy field, modified by Harmon and Tapp (2001) from Schweers (1959).

the structure seen in his cross section as a "rabbit-ear" anticline with three vertical faults. The same cross section is reinterpreted by Harmon (Harmon and Tapp, 2001) as one with two thrust faults, preserving the same formation intervals seen in the 13 wells of Schweers' cross section (Fig. 2).

Balancing

A good method to determine the geological validity of a cross-section model is to balance it. Balancing a cross section is the process of reconstructing a deformed structure to its original geometry (Mitra, 1993); it is a method used to flatten deformed beds and return them to their original horizontal (depositional) positions.

Cross sections can be balanced by (1) the *area* method or (2) the *line-length* method. The area method measures areas of bed layers before and after deformation. This method is the most difficult method to use where a loss of material has occurred, such as through faulting.

The line-length method is the best choice for measuring deformation in regions such as Milroy field, where areas are unknown. This method measures lengths of beds by using a string or rolling map measure. Distances are measured from a specific point called a pin line. Line-length balancing can be measured from pictures as well as from the actual outcrop (Price and Cosgrove, 1990).

A cross section is considered to be balanced if bed lengths in the deformed and restored (horizontal) sections are equal within 5–10% (Rowland and Duebendorfer, 1994). One cross section could be said to be better than another in a particular region if that cross section "balances." This is the case with the cross-section comparison between Schweers (1959) and Harmon (2000). When both cross sections are evaluated and reevaluated according to fault placement and bed length, Schweers' section did not balance, whereas Harmon's did, according to the 5–10% rule of Rowland and Duebendorfer (1994), as applied with the line-length method (Harmon, 2000).

Inversion

Harmon's cross section shows two thrust faults dipping to the north. The best explanation for this dip direction would be thrust faulting from the north, such as a backthrust—a backthrust from the Arbuckle Mountains—into the Ardmore basin. For a backthrust to have occurred, the Arbuckle Mountains must have undergone inversion.

Tapp (1995) suggests that the dominant form of deformation in the Arbuckle Mountain region is positive, left-lateral-oblique, contractional inversion. Inversion is the reversal of direction along basin-controlling faults. According to Tapp (1995), evidence of positive inversion is seen in the Arbuckle region in the form of room-accommodation backthrusts formed as a result of rollover anticlines. Other evidence for inversion in the region can be found in interpretations by Gold (1997), who also states that inversion-produced backthrusts are common in the region. Additionally, a cross section developed by Reedy and Sykes (1959) for the Carter-Knox field looks similar to the backthrust model presented in this paper. Finally, Mitra (1990) showed translation of fault-propagation folds along thrusts where the propagation is through the axial plane of the syncline, as shown in Harmon's (2000) cross section.

SEISMIC INTERPRETATION

To test the accuracy of the proposed model, two-dimensional (2-D) seismic lines were obtained and tied into the subsurface network of wells within and near Milroy field. The interpreted seismic data agree closely with the model proposed in this paper. However, faults of minor displacement and narrow fault wedges were observed on seismic data that were not seen through electric-log interpretation.

Seismically, Milroy is an anticlinal block, almost horst-like, with a shallow Tussy-to-Fusulinid anticline located generally south and west of a deep-faulted anticlinal core of pre-Pennsylvanian strata. The deep structure formed during the Morrowan Wichita orogeny. The deep core of the horst complex exhibits at least two northeast-dipping reverse faults. The structurally highest block was later truncated, with the Sycamore, Caney, Goddard, and Springer sequences removed through erosion. The Tussy was deposited in angular discordance at the interface with the "bald-headed" structure. The adjoining downthrown blocks (southwest of the high block) do not exhibit a bald-headed geometry; rather, they consist of a normal stratigraphic section up through the Springer with little angular discordance with the overlapping Dornick Hills and Tussy.

During the Arbuckle orogeny (Virgilian), the major faults reversed direction (the upthrown block moved down and the downthrown block moved up). The newly raised downthrown block uplifted the overlying Fusulinid and Tussy units into anticlinal form. The structure attained its highest position at the end of the Pennsylvanian Period. The structure was peneplained, and then Permian red beds were deposited with slightly dipping strata (Fig. 3).

DATA SELECTION FOR COMPUTER MODELING

Computer modeling of this project has regional applications, such as the backthrust-oriented faulting observed in Harmon's (2000) cross section. Regional modeling based strictly on deformation, as seen in the cross section, is probably too simple to define all of the deformational events in the area. However, what the computer modeling should (and did) achieve was to show the influence of deformation on the region.

Wells were chosen with the sole purpose of showing the deformation style in the 13-well cross section. This meant that, first, wells were chosen in and around the line of the cross section, and second, wells were selected by depth, fault presence, fault displacements,

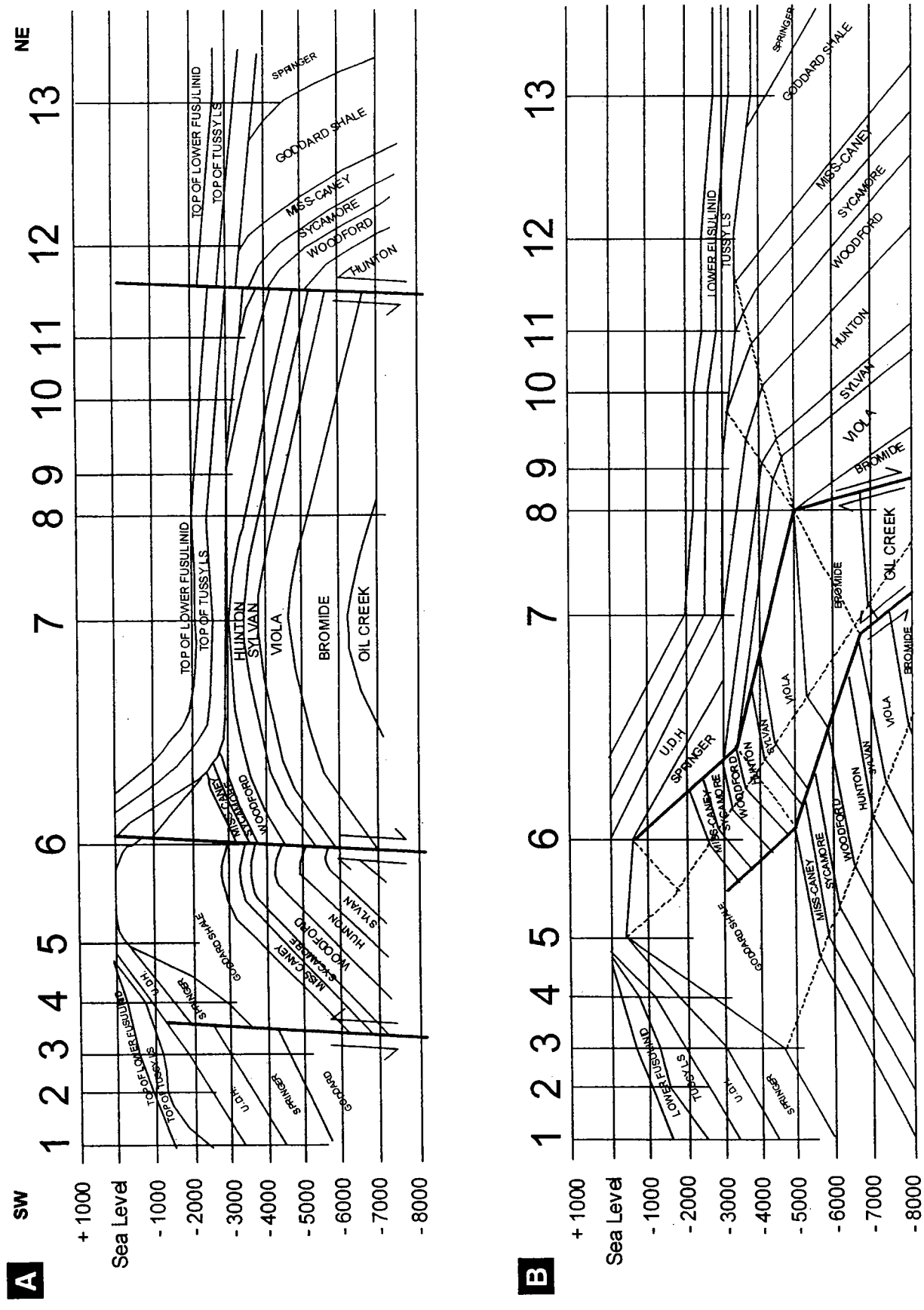

Figure 2. (A) "Rabbit-ear" anticline model, modified by Harmon and Tapp (2001) from Schweers (1959). (B) Inversion-produced backthrust model (Harmon and Tapp, 2001). Well information given in Table 1 (13-well cross section).

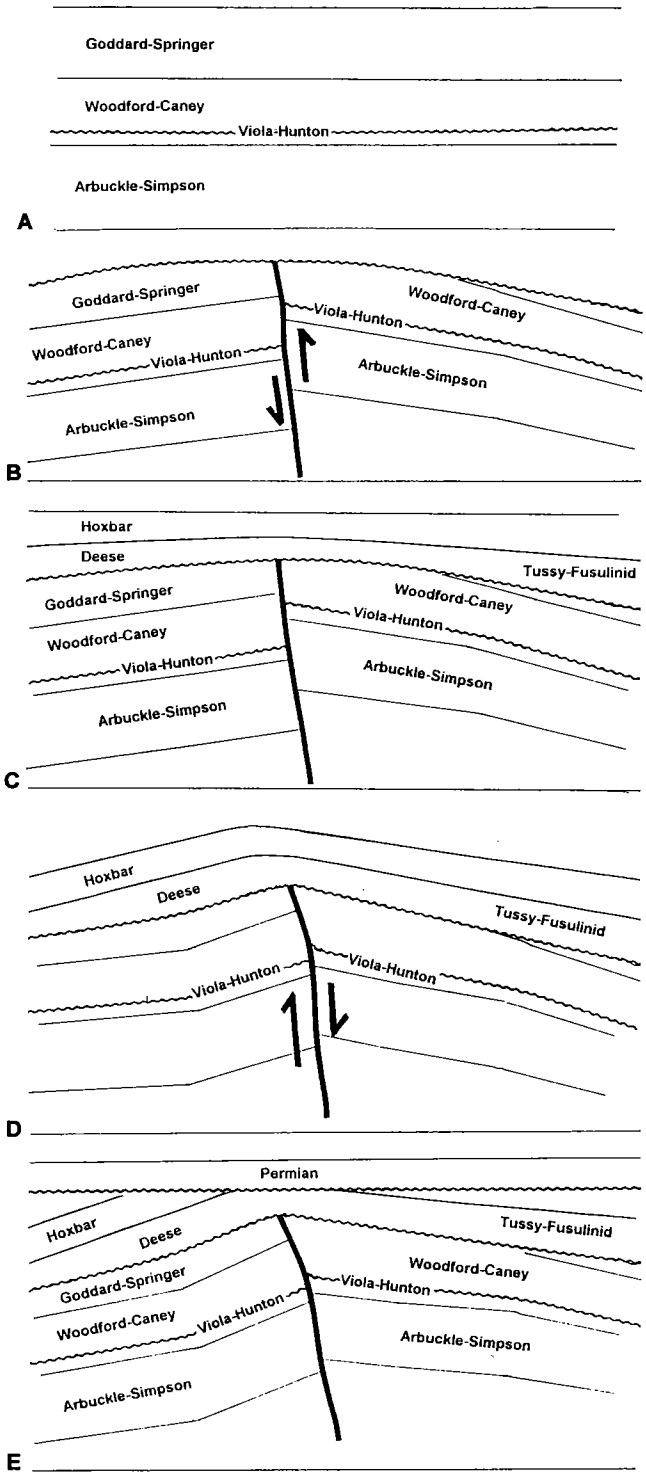

Figure 3. Sequential cross sections that illustrate the geologic history of the Milroy area. (A) Deposition of Arbuckle through Springer Groups. (B) Formation of horst block during post-Morrowan Wichita deformation and corresponding Dornick Hills fill, followed by peneplaination. (C) Deposition of Deese and Hoxbar, with slight depositional thinning on crest of Milroy structure. (D) Generation of the Deese/Hoxbar anticline of Milroy field through a reversal of fault-movement direction (inversion) during Arbuckle deformation. (E) Post-Pennsylvanian truncation, followed by deposition of Permian red beds, as evidenced by interpreted seismic data.

and location. A total of 122 wells were used. This large number of wells enabled computer-generated maps to be constructed that could track the deformation as deeply and completely as possible over a 20-mi^2 area. From the start, the project attempted to achieve a maximum amount of quality maps with a minimum investment of time to obtain reasonable results.

Stratigraphic units selected for insertion on the cross section are the same as those used by Schweers (1959), thereby closely approximating the appearance of his cross section. From youngest to oldest, those units are lower Fusulinid, Tussy limestone, upper Dornick Hills, Springer, Goddard Shale, Mississippi–Caney, Sycamore, Woodford, Hunton, Sylvan, Viola, Bromide, and Oil Creek. However, it was decided to include the Arbuckle Group in our study, since it is important to show the deepest formations affected by the backthrust. Schweers (1959) mapped the shallower unconformity at the base of the Permian red beds. The depth of this unconformity approximated sea-level datum and is so marked as the horizontal line on our cross section (Fig. 2B). The deeper unconformity was the Morrowan unconformity, which separates the Dornick Hills and Tussy from the Springer and older units. Finally, fault depth and fault vertical displacement needed to be quantified and modeled.

COMPUTER-MODELING PROGRAM

The program chosen to model fault data with multiple surfaces was the Mapping-Contouring System (MCS) computer-modeling software, a commercial computer program from Scientific Computer Applications. MCS processes all surfaces simultaneously. Fault depths and fault vertical separations are used to palinspastically restore the system to paleosurfaces before rebreaking.

Fault-Contouring Procedure

Banks and Sukkar (1992, p. 58), indicated that the "data needed [consist] of X-Y-Z points for all formation tops (in their faulted position) plus three or more X-Y-Z points for each fault and its vertical displacement. The non-gridded (triangular), multi-surface program handles multiple non-vertical, intersecting faults among multiple surfaces. Interpolations are performed within the triangles, using functions that make the resulting maps appear hand-contoured."

Multi-Surface Stacking

"The principle of conformable geology is the backbone of the multi-surface process. MCS first calculates isochores (differences in value between adjacent surfaces) wherever possible. These isochores are interpolated or extrapolated over the entire area for all isochore intervals. Calculated isochore values are added or subtracted from known datums in order to reconstruct a complete set of Z values at all data points. This 'stacking' proceeds downward first and upward second" (Banks and Sukkar, 1992, p. 60).

METHODOLOGY

Each selected well possessed an electric (induction) log and data such as a completion (scout) ticket and/or Oklahoma Corporation Commission form 1002A. Each well entered in the computer database was given a four-digit number to identify the well on the base map. A well with an ID of 2401, for example, implies that the well is in sec. 24 and was the first well chosen in that section. The well name, kelly-bushing elevation, well status (oil, gas, dry), all available formation tops, and fault depths and displacements were also included in the file.

A base map was drawn by hand, and well spots were digitized into the computer-modeling program. Well information, such as formation tops, was entered into an Excel spreadsheet, which was then entered into the MCS computer-modeling software. MCS is a multisurface system that can store and sort fault depths and fault vertical separations while processing all surfaces simultaneously. Many MCS maps were constructed to track the deformation observed in the cross section as deeply and completely as possible over a 20-mi^2 area.

Various types of geologic maps were then constructed and fine-tuned to most accurately depict deformation seen in the area. Isochore maps and cross sections, as well as contour maps, were made and refined to help define and resolve problems that would lead to a final cross section and contour maps.

The MCS cross section consists of 11 wells, whereas Schweers' (1959) and Harmon's (2000) cross sections consisted of 13 wells (Table 1). The MCS 11-well cross section approximated Schweers' 13-well cross section and added length to both ends (Fig. 4).

COMPUTER-GENERATED MAPS

The base map includes the four-digit well-identification numbers (Fig. 5). Contour maps do not include these numbers so as to present a less cluttered appearance.

The contour map of fault "A" shows where the fault subcrops against the Morrowan unconformity (Fig. 6). Figure 7 is a map of fault vertical displacement; since this is a reverse fault, vertical displacement is negative.

The other 15 contour maps are structure maps depicting the tops of stratigraphic units from the lower Fusulinid to the Arbuckle. The only unbreached and continuous units mapped are the lower Fusulinid, the Tussy limestone, and the Morrowan unconformity. The 15 contour maps include those of the lower Fusulinid, Tussy limestone, upper Dornick Hills, Morrowan unconformity, Springer, Goddard Shale, Mississippi–Caney, Sycamore, Woodford, Hunton, Sylvan, Viola, Bromide, Oil Creek, and Arbuckle (Figs. 8–22).

MODELING—MAIN CONCEPTS

Computer modeling of this project resulted in the discovery of three main concepts:

1. The Morrowan unconformity is continuous beneath the upper Dornick Hills, where present. In the absence of the upper Dornick Hills, the Morrowan unconformity lies beneath the Tussy limestone.

2. The 11-well cross section illustrates a large northwest–southeast Fusulinid/Tussy anticline, with the Harrisburg trough to the south and west. A control well, no. 2702, was used to correct for the steepness of beds in the Harrisburg trough. A fault separates this shallow anticline from a deeper truncated anticline to the east. The upper Dornick Hills and Springer are not present between the two anticlines shown on the 11-well cross section.

3. Stratigraphic units, from the Goddard Shale to the Arbuckle, move "closer together" in axial form as the computer-generated contours model progressively deeper and older units on the crest of the deeper, truncated anticline.

This paper lengthens the original 13-well cross section, as well as corrects errors in the poster presentation of Harmon and Tapp (2001). That previous project, for example, showed the unconformity in the cross section to be at the top of the Goddard Shale. This was for balancing purposes; it is somewhat valid, however, as deposition of the Goddard and Springer units was apparently continuous and occurred with little interruption (Prestridge, 1957). If previous balancing on the Goddard Shale had included the Springer Group, the balancing would have been on the continuous Morrowan unconformity—the same unconformity thought not to have been continuous in the investigation for the previous project. Additionally, the cross section by Harmon (Harmon and Tapp, 2001) should not have shown upper Dornick Hills or Springer on the truncated area between the two anticlines. Their absence is substantiated from the electric logs (Fig. 2B).

ACKNOWLEDGMENTS

We wish to recognize the people and groups that have been so helpful to this project. First, we express our gratitude to Dr. Joseph Sukkar, an independent consultant who works with Dick Banks and was so generous to give of his time to assist us with problems in computer modeling. We wish to thank Vance Hall, a Tulsa consulting geologist, who provided insight and an earlier Milroy project he had worked on. We also wish to express our gratitude to Dr. Bryan Tapp of the University of Tulsa, who gave advice and reviewed this document prior to publication.

Sources of data for this report include the University of Tulsa's McFarlin Library and various theses, dissertations, and books from libraries across the United States; the American Association of Petroleum Geologists Library in Tulsa; the Oklahoma Well Log Library in Tulsa; the Oklahoma City Geological Society Library; the Ardmore Sample Cut and Log Library; Riley Electric Log, Inc.; and NRIS Data (well-log

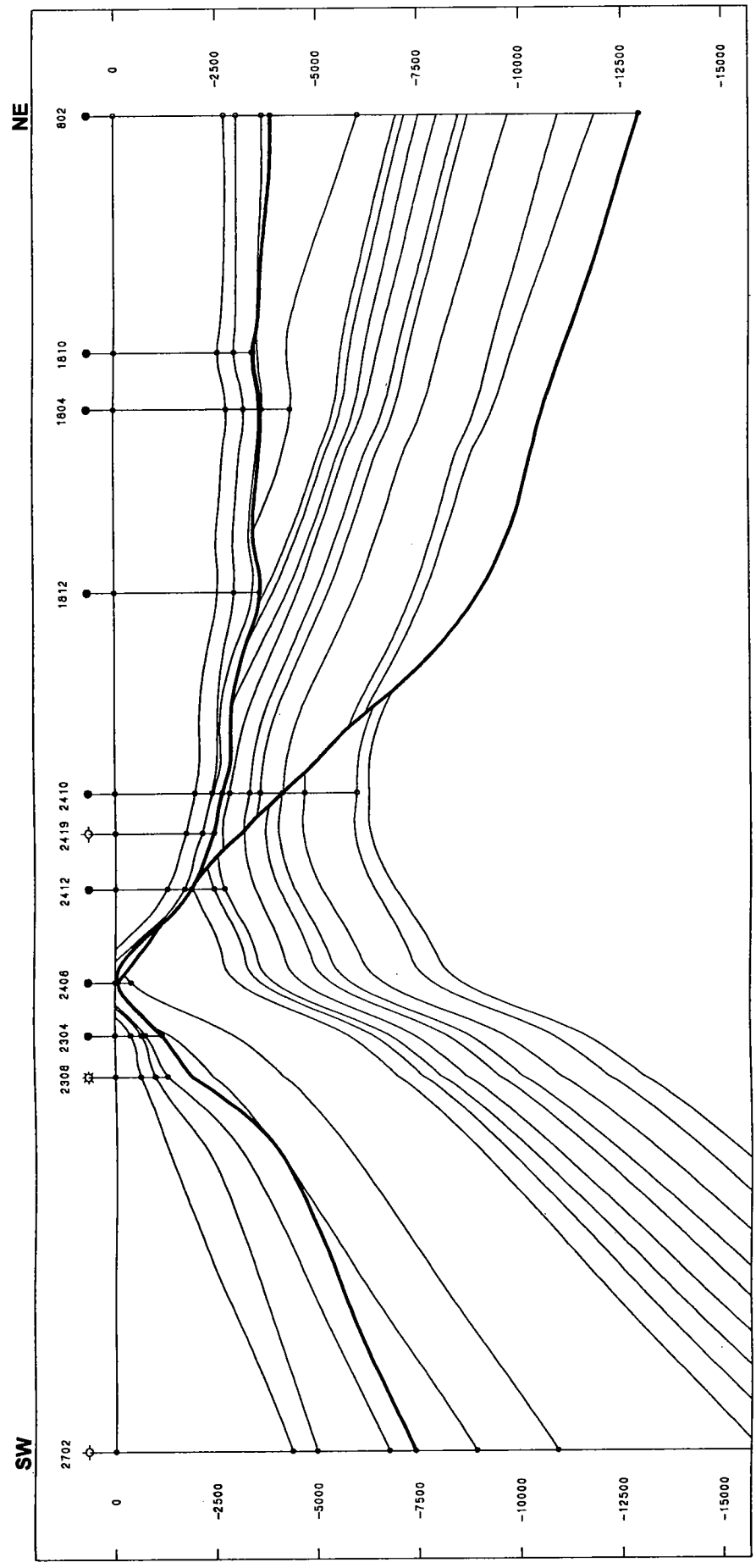

Figure 4. Eleven-well Mapping-Contouring System (MCS) cross section approximating Schweers' (1959) cross section, with fault (heavy line) shown as being backthrust from the north, below the top of the Arbuckle Group. Line of section (southwest to northeast) is shown in Figures 5–22. Scale is 1:1; depths are in feet. Stratigraphic units used by Schweers were modeled first. Later, the Arbuckle Group, the Morrowan unconformity (heavy line), and the base of the red beds (horizontal line) were added.

Table 1. — Identification of Wells in 11-Well and 13-Well Cross Sections

Well no.	4-digit ID	Well name	Operator	Section, township, range
			11-Well Cross Section	
1	2702	#1 Dockall	L. E. Jones	C NE¼NE¼ sec. 27, T. 2 S., R. 4 W.
2	2308	#10 R A Hefner E	Amoco	SW¼SE¼NE¼ sec. 23, T. 2 S., R. 4 W.
3	2304	#3 Hefner A	Hefner	SE¼SE¼NE¼ sec. 23, T. 2 S., R. 4 W.
4	2408	16 W M Elmore	McGraw	NW¼SW¼NW¼ sec. 24, T. 2 S., R. 4 W.
5	2412	#2 Harley	M & P	NW¼SW¼NE¼NW¼ sec. 24, T. 2 S., R. 4 W.
6	2419	#4-A Fisher	Gen. Amer.	C NE¼NE¼NW¼ sec. 24, T. 2 S., R. 4 W.
7	2410	#1 Alfred	M & P	NW¼NW¼NE¼ sec. 24, T. 2 S., R. 4 W.
8	1812	#1 Mattie Elmore	Stanolind	SW¼NW¼SW¼ sec. 18, T. 2 S., R. 3 W.
9	1804	#2 Sturm	Schermerhorn	SW¼SW¼NE¼ sec. 18, T. 2 S., R. 3 W.
10	1810	#15 H Wallace	Continental	NE¼SW¼NE¼ sec. 18, T. 2 S., R. 3 W.
11	802	#11 Scott	Kirkpatrick	SW¼NW¼SW¼ sec. 8, T. 2 S., R. 3 W.
			13-Well Cross Section	
1	2301	#1 Horton A	Continental	SE¼NW¼SE¼ sec. 23, T. 2 S., R. 4 W.
2	2302	#5 Hefner E	Stanolind	NW¼NE¼SE¼ sec. 23, T. 2 S., R. 4 W.
3	2303	#1 Hefner E	Stanolind	NE¼NE¼SE¼ sec. 23, T. 2 S., R. 4 W.
4	2401	#8 Harley	Texas	NW¼NW¼SW¼ sec. 24, T. 2 S., R. 4 W.
5	2402	#23 Harley A	Skelly	SE¼SW¼NW¼ sec. 24, T. 2 S., R. 4 W.
6	2403	#26 Elmore	Magnolia	SW¼NW¼NW¼ sec. 24, T. 2 S., R. 4 W.
7	2404	#1-D Harley	Magnolia	NW¼NE¼ sec. 24, T. 2 S., R. 4 W.
8	2405	#1 Harley C-49	Carter	NE¼NE¼ sec. 24, T. 2 S., R. 4 W.
9	2406	#2 Harley C-49	Carter	NE¼NE¼NE¼ sec. 24, T. 2 S., R. 4 W.
10	1801	#1 Fish	Mercury	SW¼SW¼SW¼ sec. 18, T. 2 S., R. 3 W.
11	1802	#2 Fish	Mercury	NE¼SW¼SW¼ sec. 18, T. 2 S., R. 3 W.
12	1803	#1 Williams	Goldsmith and Perkins	NE¼NW¼SW¼ sec.18, T. 2 S., R. 3 W.
13	1804	#2 Sturm	Schermerhorn	SW¼SW¼NE¼ sec. 18, T. 2 S., R. 3 W.

internet data) from GEO Information Systems at the University of Oklahoma to be used with the GIS program ARCVIEW 3.2.

Finally, we wish to express our thanks to Charles E. Harmon of C. E. Harmon Oil, Inc., for allowing Robert Harmon the freedom to work on this project. Loving appreciation is given to Robert's wife, Angela, and to his children for their patience during this project on the many occasions in which he brought work home.

REFERENCES CITED

Banks, R.; and Sukkar, J., 1992, Computer processing of multiple 3-D fault blocks containing multiple surfaces: Geobyte, v. 7, no. 4, p. 58–62.

Gold, J., 1997, Inversion tectonics: applications in the southern Oklahoma aulacogen, Criner Hills region, Carter and Love Counties, Oklahoma: University of Tulsa unpublished M.S. thesis, 63 p.

Harmon, R. E., 2000, Small-scale inversion features on the flanks of the Ardmore basin: structural study of the Milroy field: University of Tulsa unpublished M.S. thesis, 31 p.

Harmon, R. E.; and Tapp, Bryan, 2001, Small-scale inversion feature on the flanks of the Ardmore basin: structural study of the Milroy field, *in* Johnson, K. S.; and Merriam, D. F. (eds.), Petroleum systems of sedimentary basins in the southern Midcontinent, 2000 symposium: Oklahoma Geological Survey Circular 106, p. 187–190.

Johnson, H. R.; Biglarbigi, K.; Schmidt, L.; Ray, R. M.; and Kyser, S. C., 1986, Profile of a giant: rising again; part 1: Oil and Gas Journal, Dec. 15, p. 47.

_____1987, Reservoir/fluid characteristics favor enormous long-term recovery potential; conclusion: Oil and Gas Journal, Jan. 19, p. 38–43.

Lacina, J. L., 1979, Index to names of oil and gas fields in Oklahoma, 1978: Bartlesville Energy Technology Center, U.S. Department of Energy, 250 p.

Mitra, S., 1990, Fault-propagation folds: geometry, kinematic evolution, and hydrocarbon traps: American Association of Petroleum Geologists Bulletin, v. 74, p. 921–945.

_____1993, Geometry and kinematic evolution of inversion structures: American Association of Petroleum Geologists Bulletin, v. 77, p. 1159–1191.

Prestridge, J. D., 1957, A subsurface stratigraphic study of the Sycamore Formation in the Ardmore basin: University of Oklahoma unpublished M.S. thesis, 59 p.

Price, N. J.; and Cosgrove, J. W., 1990, Analysis of geological structures: Great Britain: Cambridge University Press, 502 p.

Reedy, H. J.; and Sykes, H. A., 1959, Carter-Knox oil field, Grady and Stephens Counties, Oklahoma, *in* Mayes, J. W.; Westheimer, J.; Tomlinson, C. W.; and Putman, D. M. (eds.), Petroleum geology of southern Oklahoma, v. 2: American Association of Petroleum Geologists, Tulsa, p. 198–219.

Rowland, S. M.; and Duebendorfer, E. M., 1994, Structural analysis and synthesis: a laboratory course in structural geology: Blackwell Scientific Publications, Cambridge, Massachusetts, 279 p.

Schweers, F. P., 1959, Milroy field, Stephens and Carter Counties, Oklahoma, *in* Mayes, J. W.; Westheimer, J.; Tomlinson, C. W.; and Putman, D. M. (eds.), Petroleum geology of southern Oklahoma, v. 2: American Association of Petroleum Geologists, Tulsa, p. 220–226.

Tapp, Bryan, 1995, Inversion model for the structural style of the Arbuckle region, *in* Johnson, K. S. (ed.), Structural styles in the southern Midcontinent, 1992 symposium: Oklahoma Geological Survey Circular 97, p. 113–118.

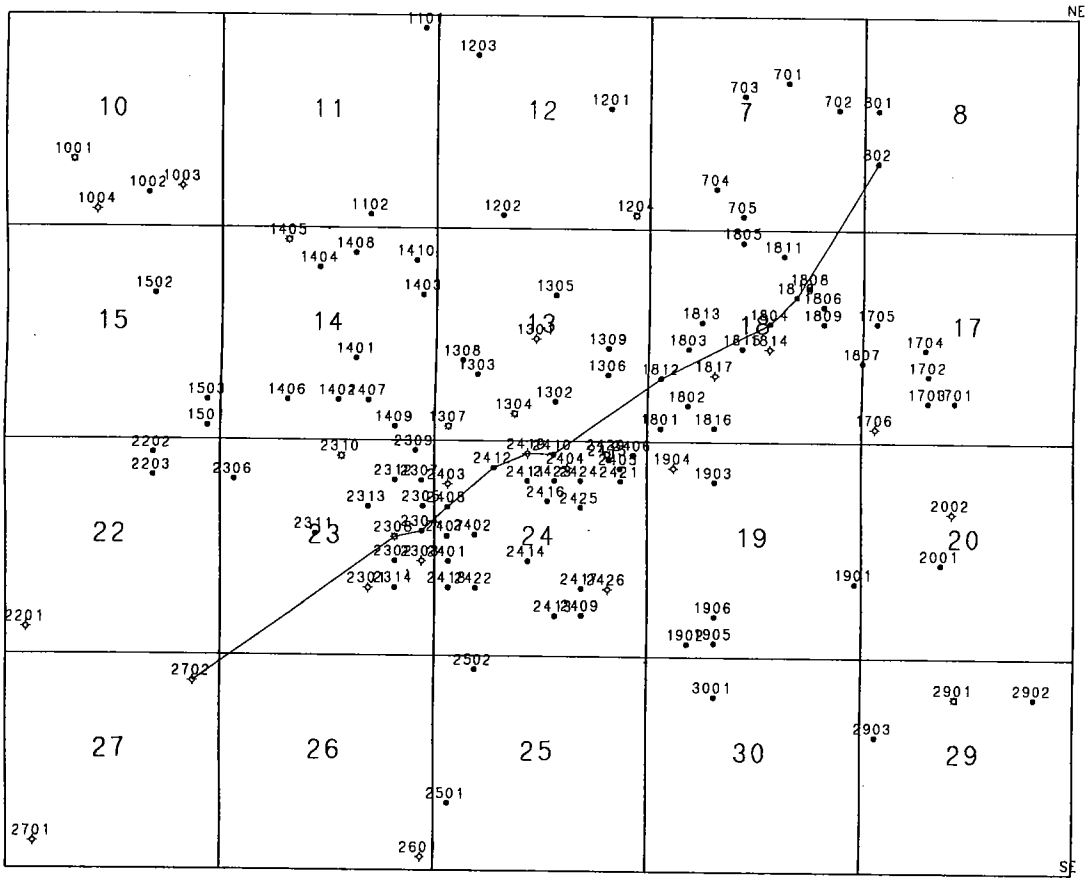

Figure 5. Milroy field base map (MCS).

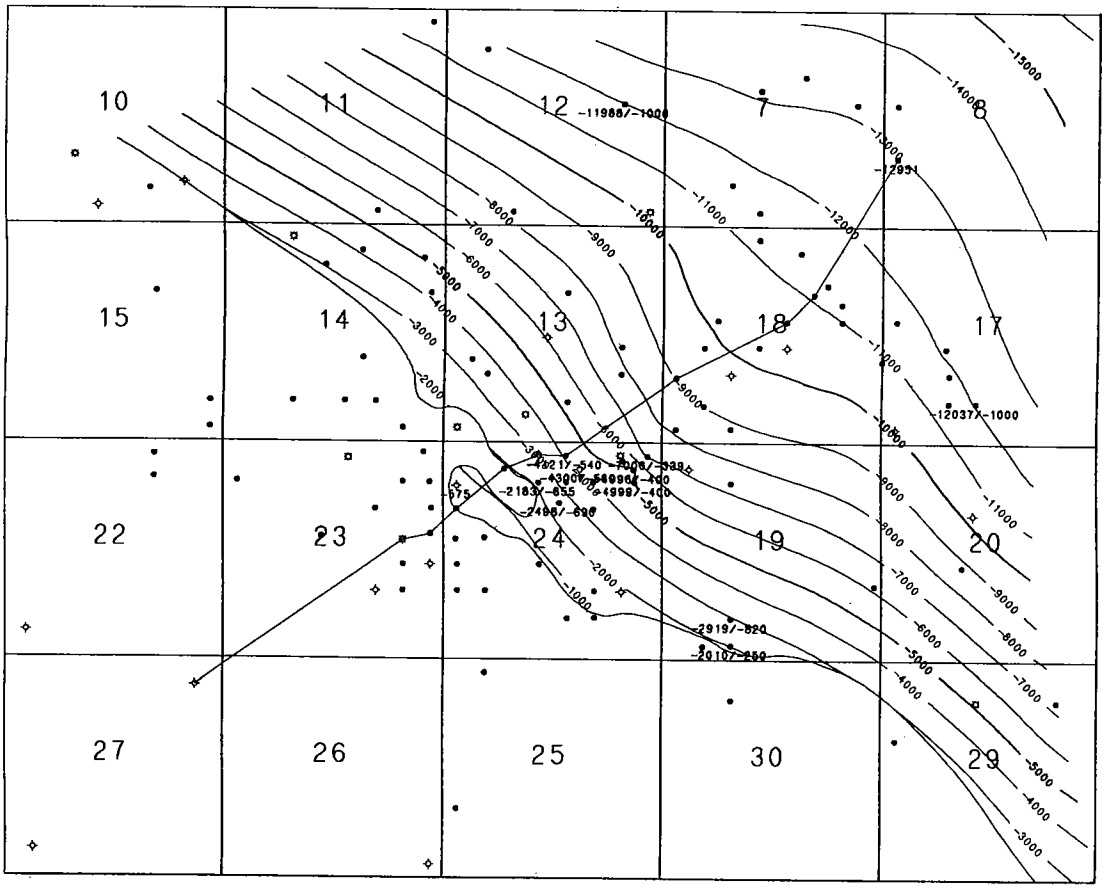

Figure 6. Fault "A" contour map (MCS). Contour interval is 1,000 ft.

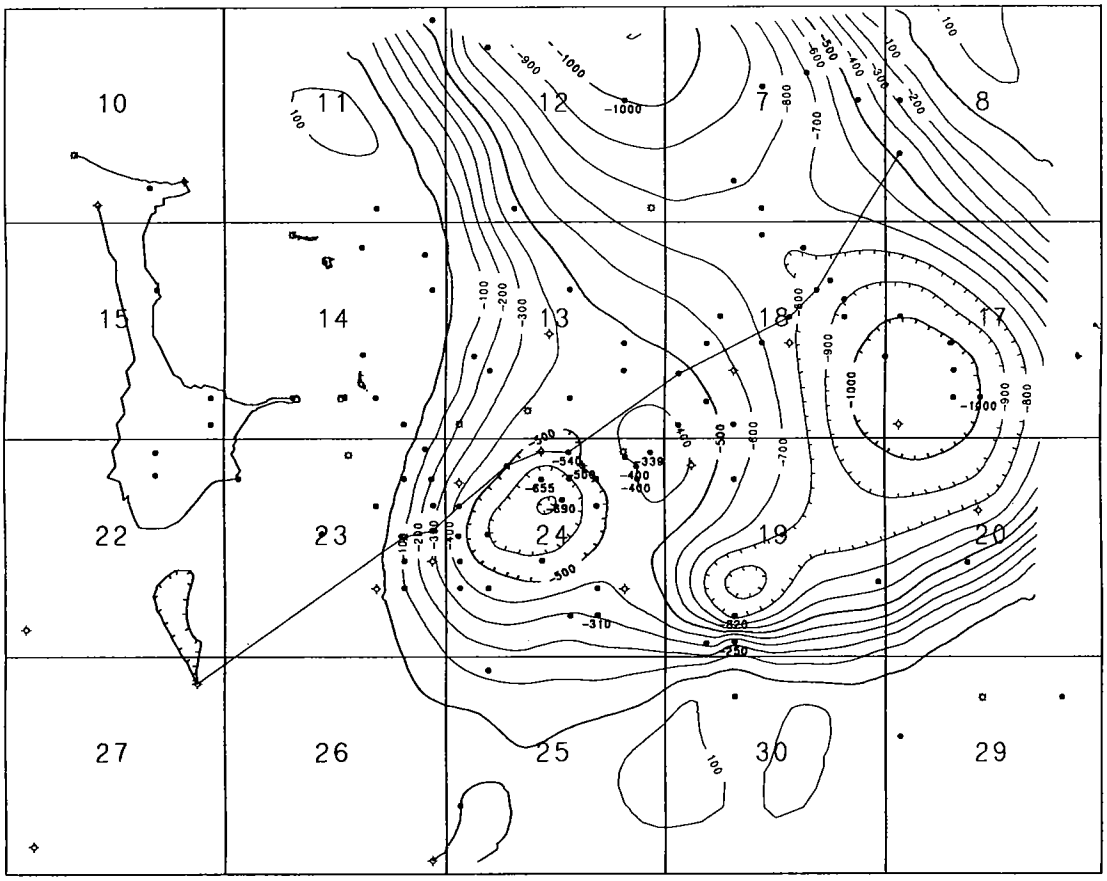

Figure 7. Fault "A" displacement contour map (MCS). Contour interval is 100 ft.

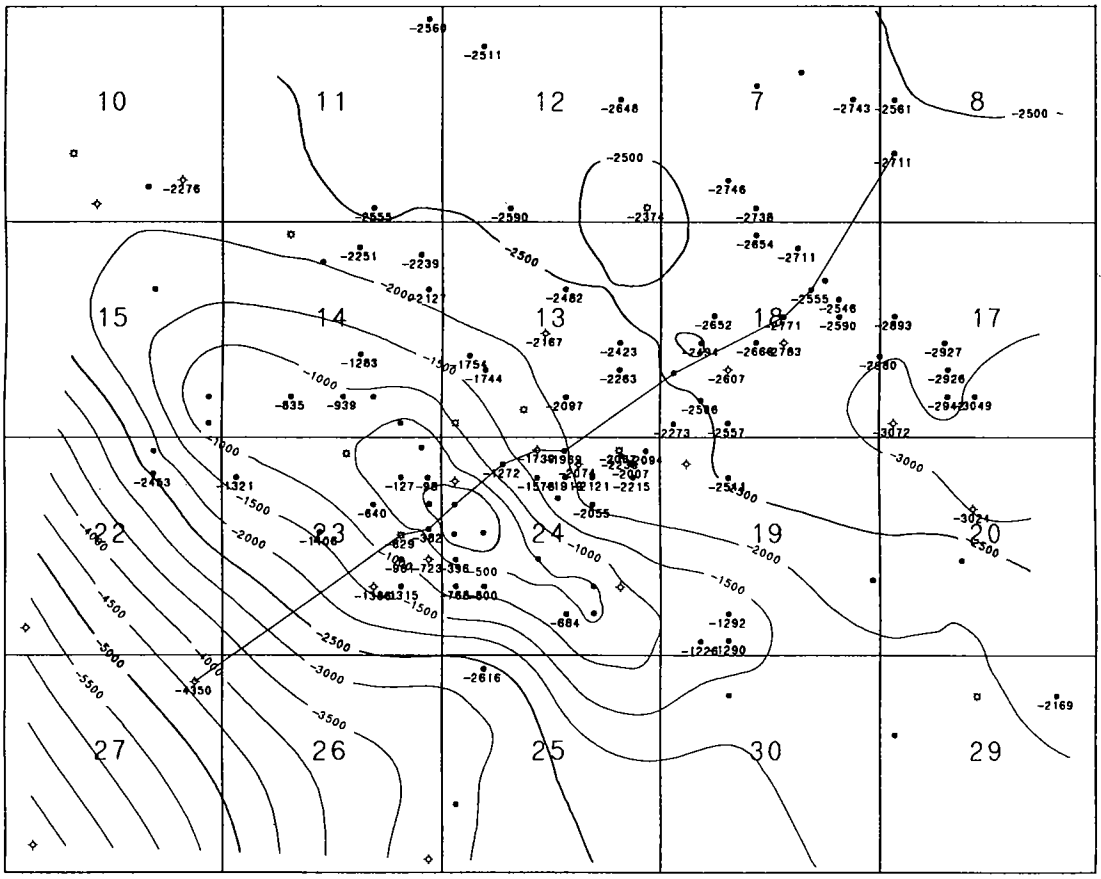

Figure 8. Top of lower Fusulinid contour map (MCS). Contour interval is 500 ft.

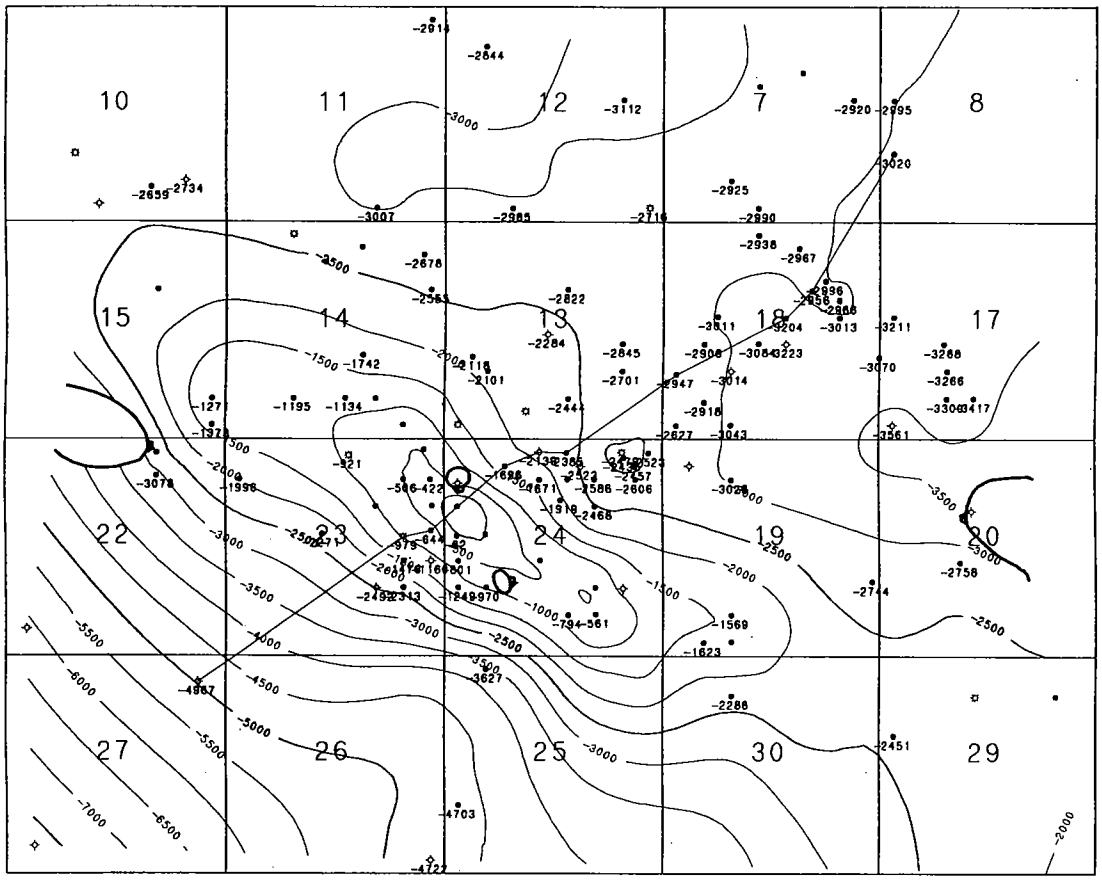

Figure 9. Top of Tussy limestone contour map (MCS). Contour interval is 500 ft.

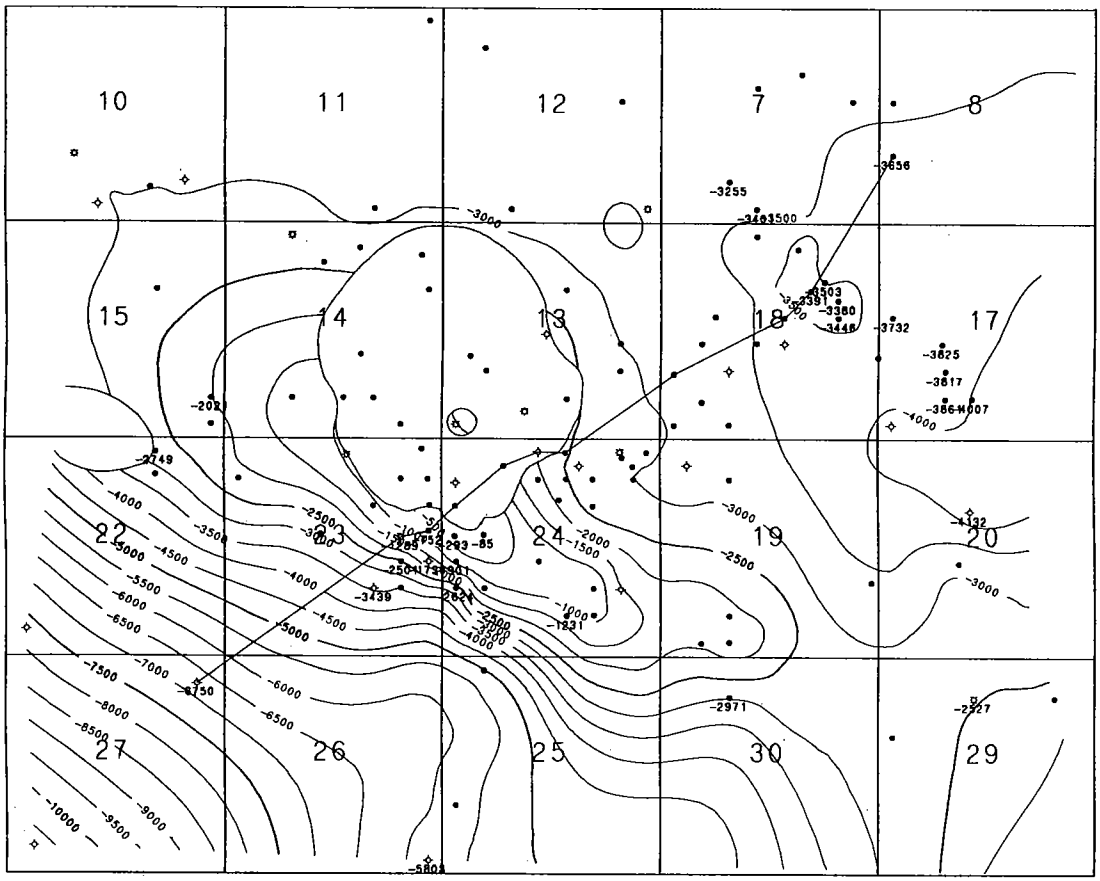

Figure 10. Top of upper Dornick Hills contour map (MCS). Contour interval is 500 ft.

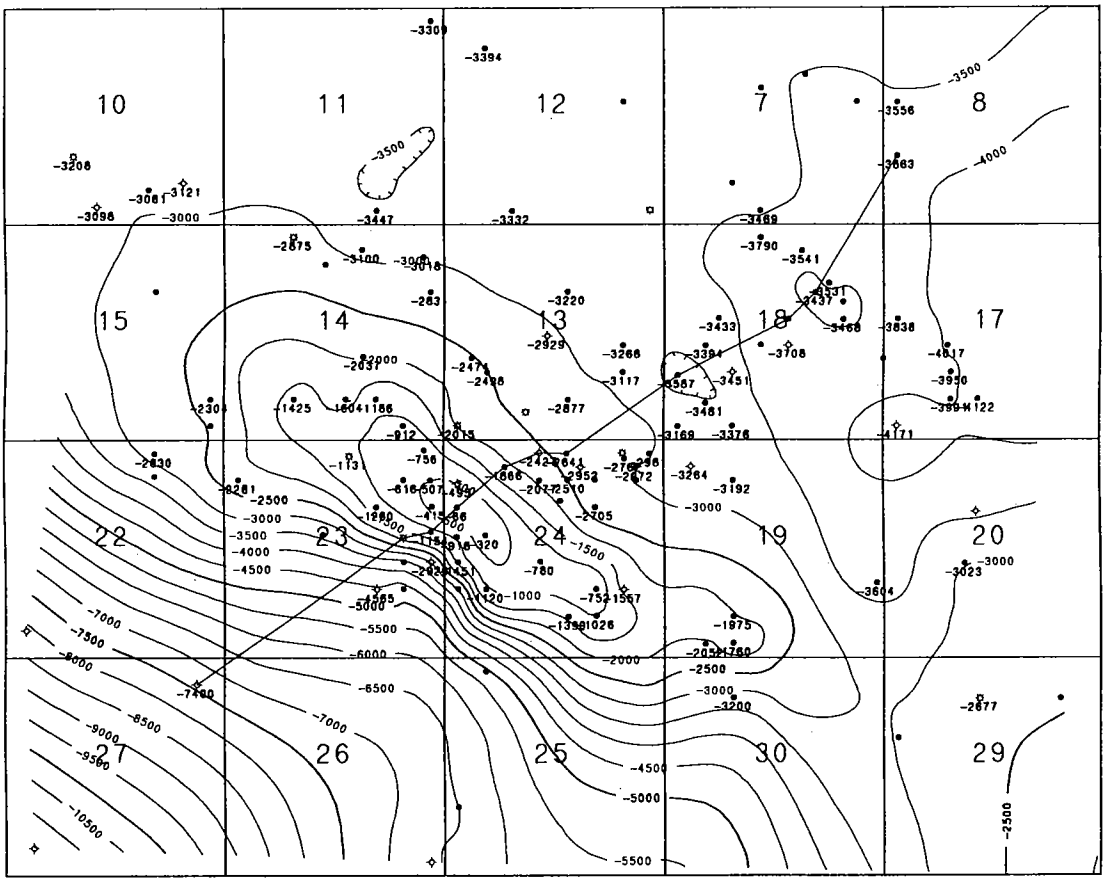

Figure 11. Top of Morrowan unconformity contour map (MCS). Contour interval is 500 ft.

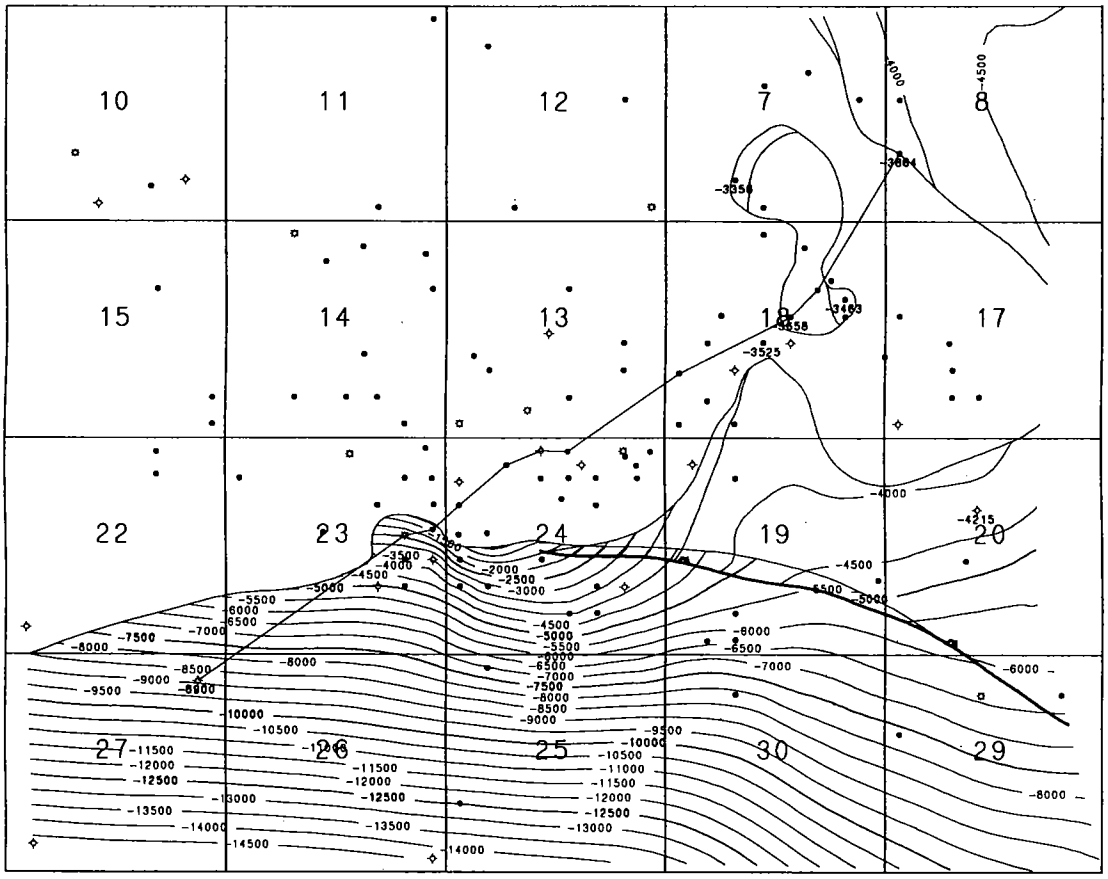

Figure 12. Top of Springer contour map (MCS). Contour interval is 500 ft.

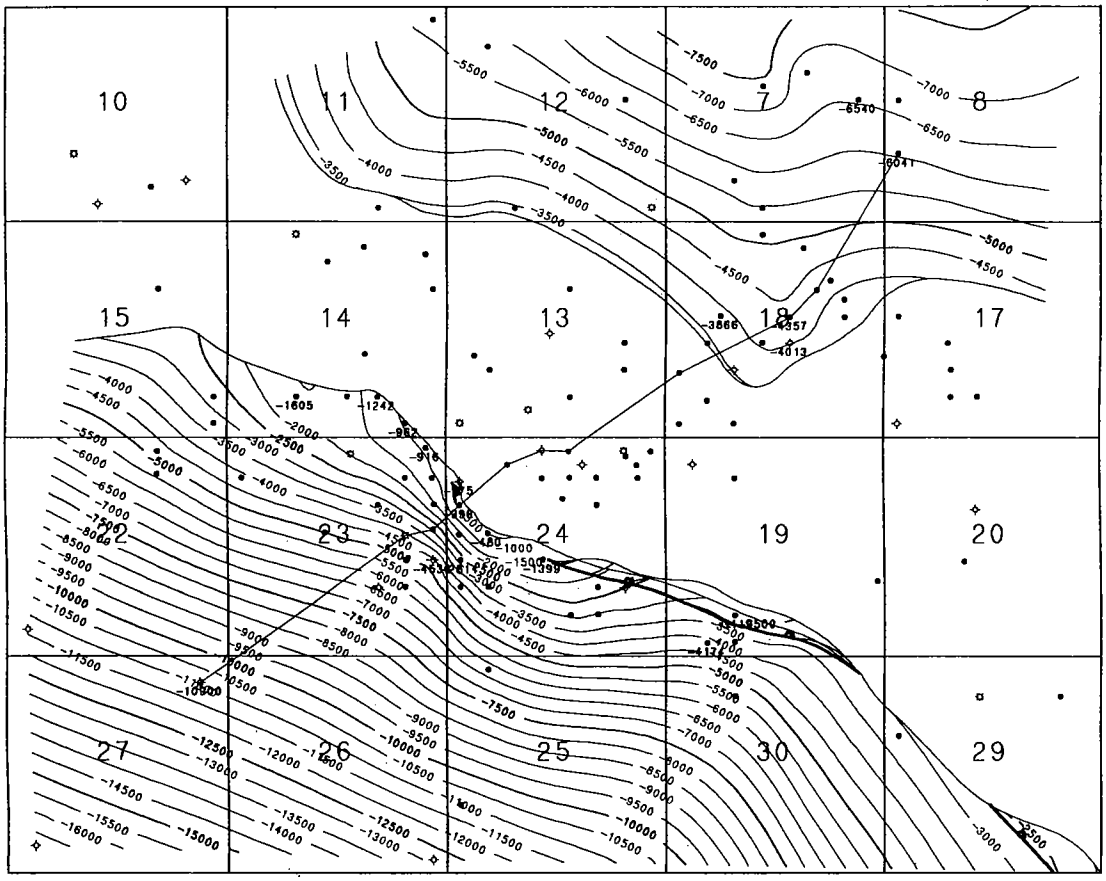

Figure 13. Top of Goddard Shale contour map (MCS). Contour interval is 500 ft.

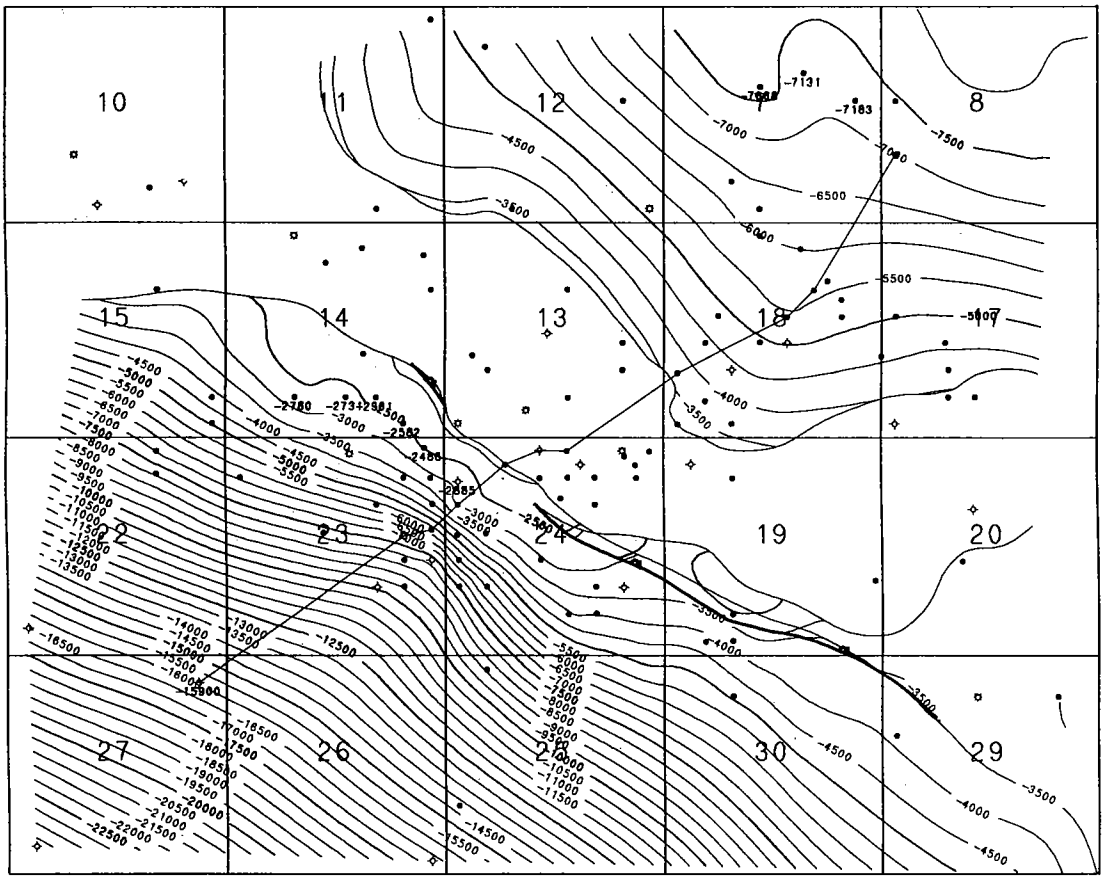

Figure 14. Top of Mississippi–Caney contour map (MCS). Contour interval is 500 ft.

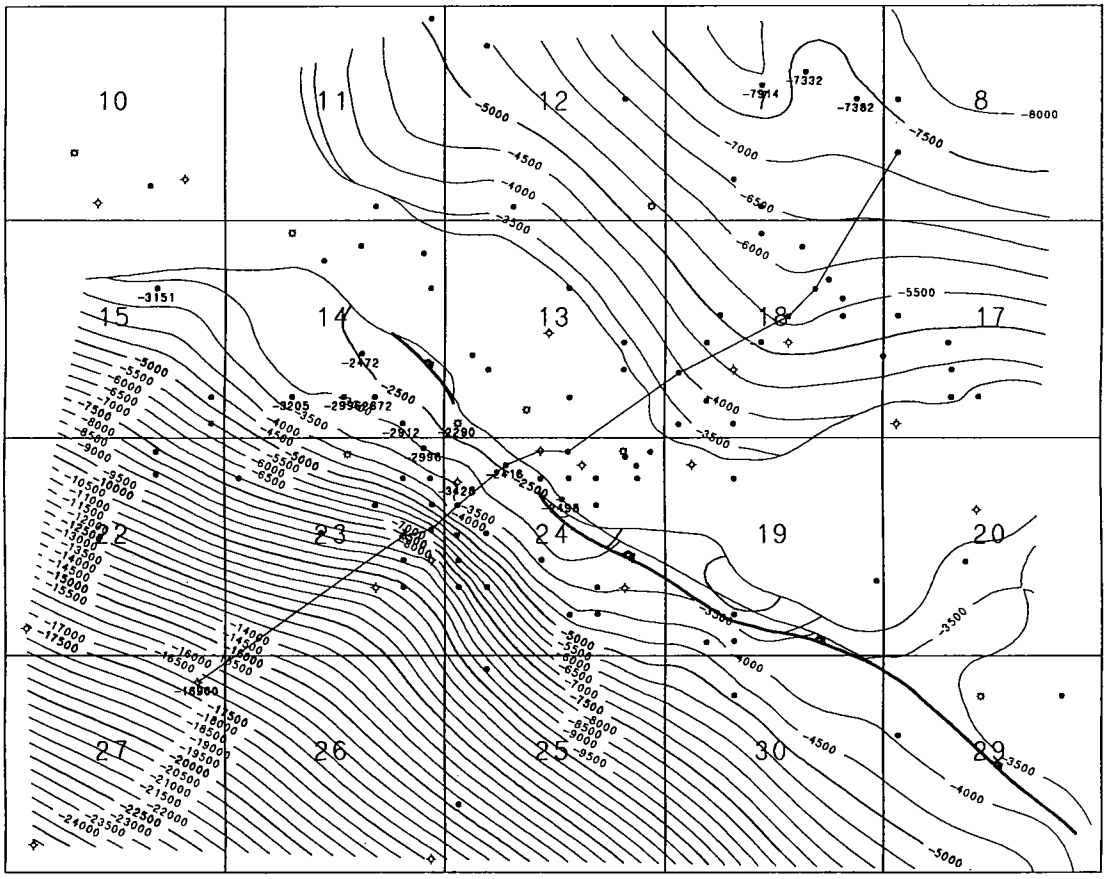

Figure 15. Top of Sycamore contour map (MCS). Contour interval is 500 ft.

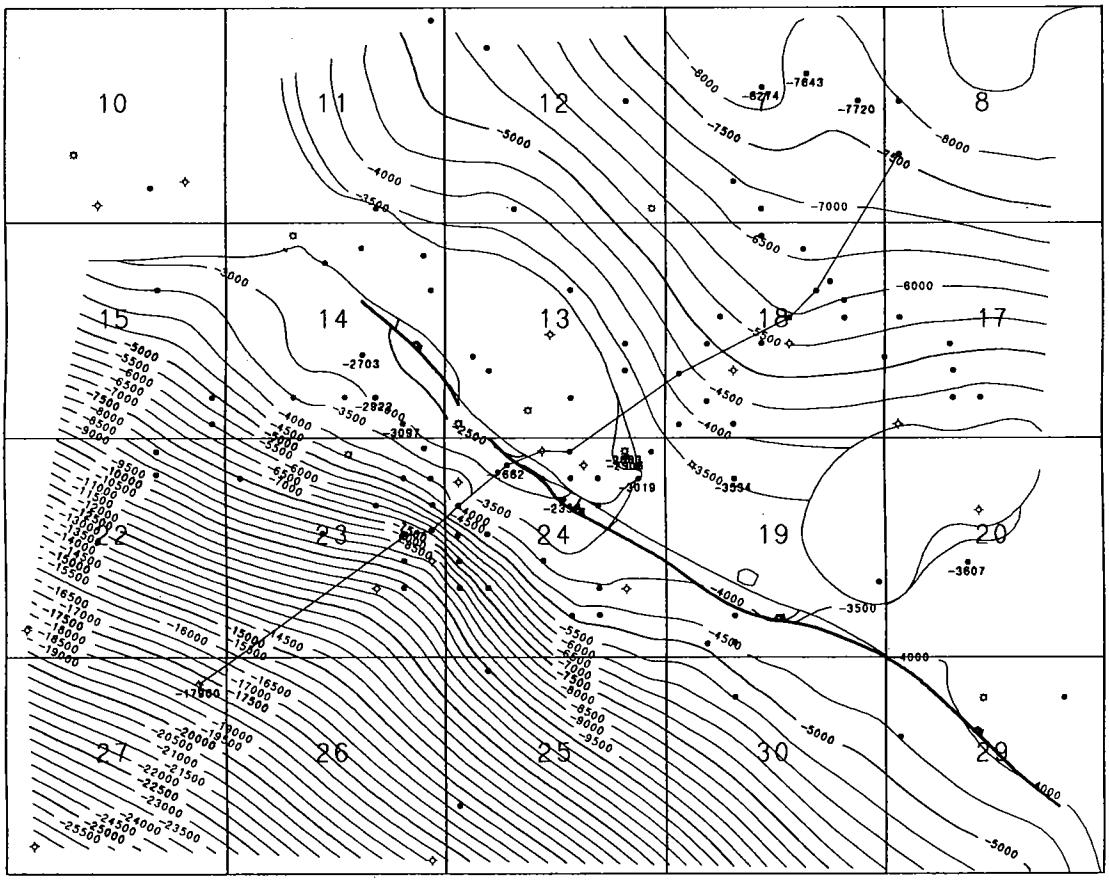

Figure 16. Top of Woodford contour map (MCS). Contour interval is 500 ft.

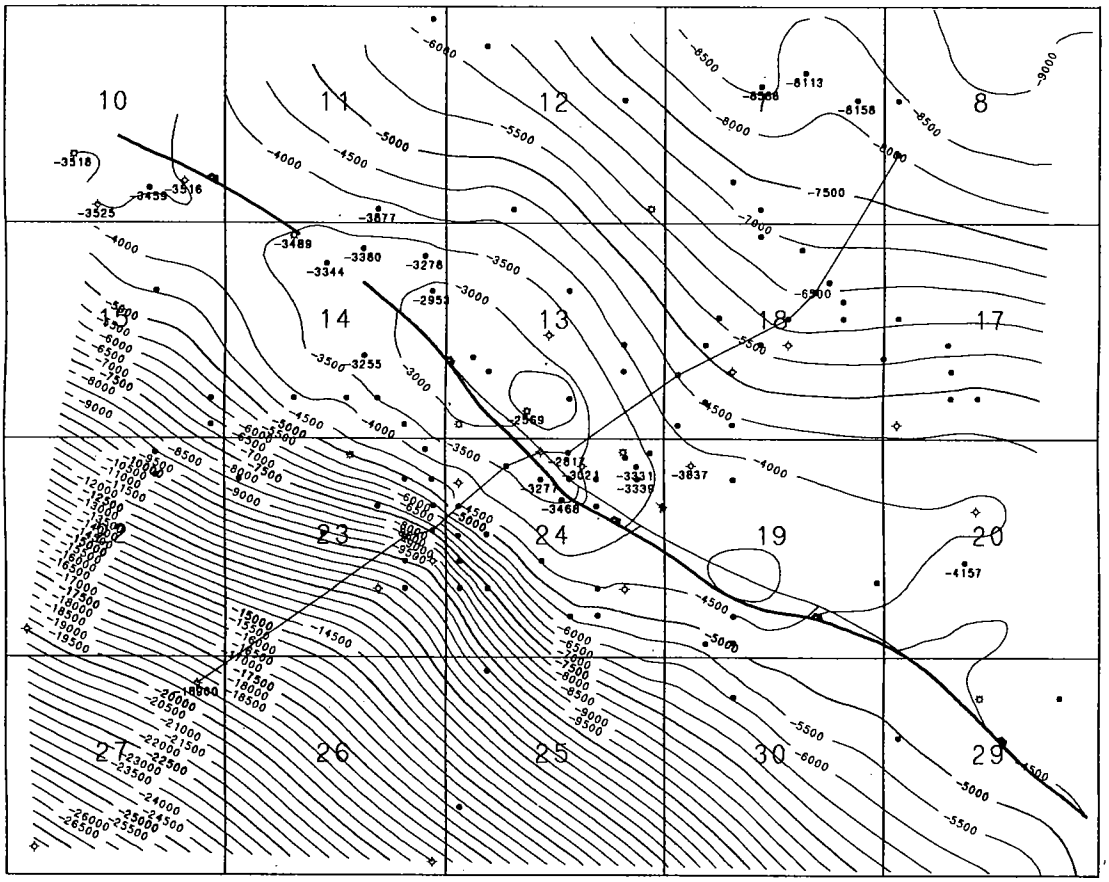

Figure 17. Top of Hunton contour map (MCS). Contour interval is 500 ft.

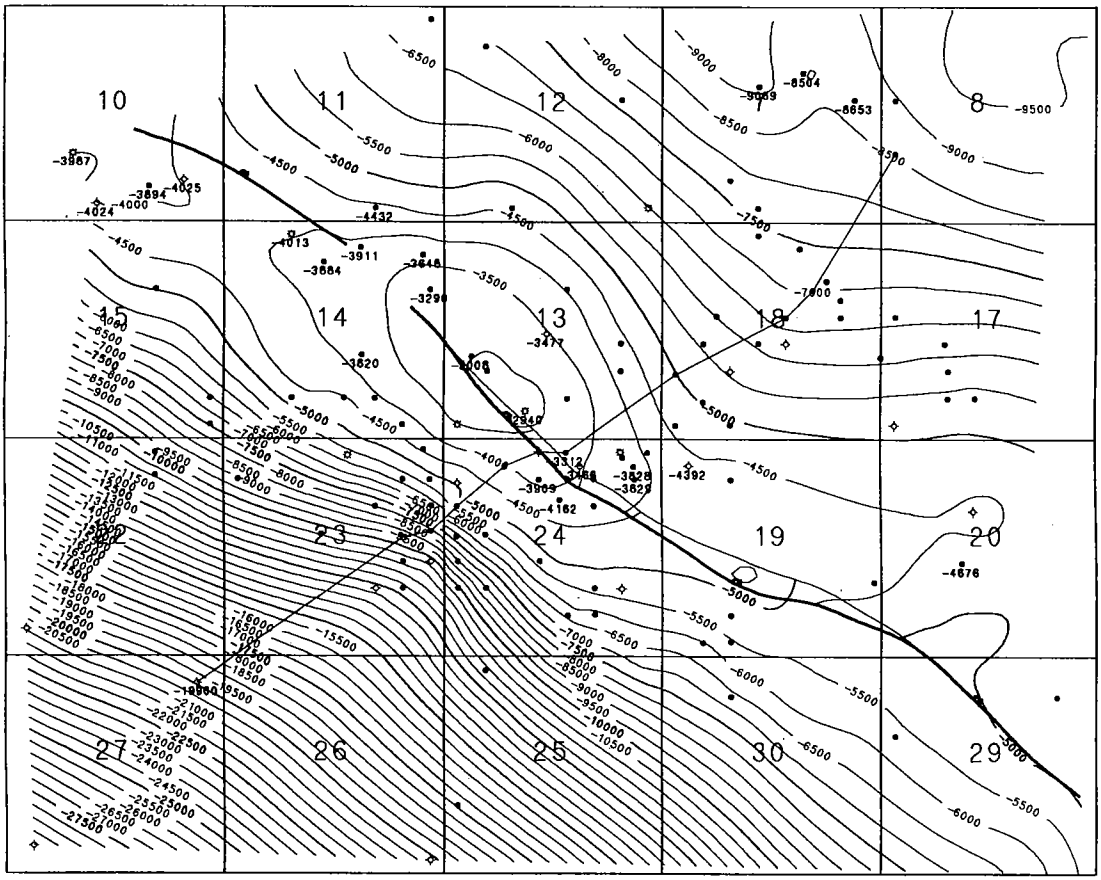

Figure 18. Top of Sylvan contour map (MCS). Contour interval is 500 ft.

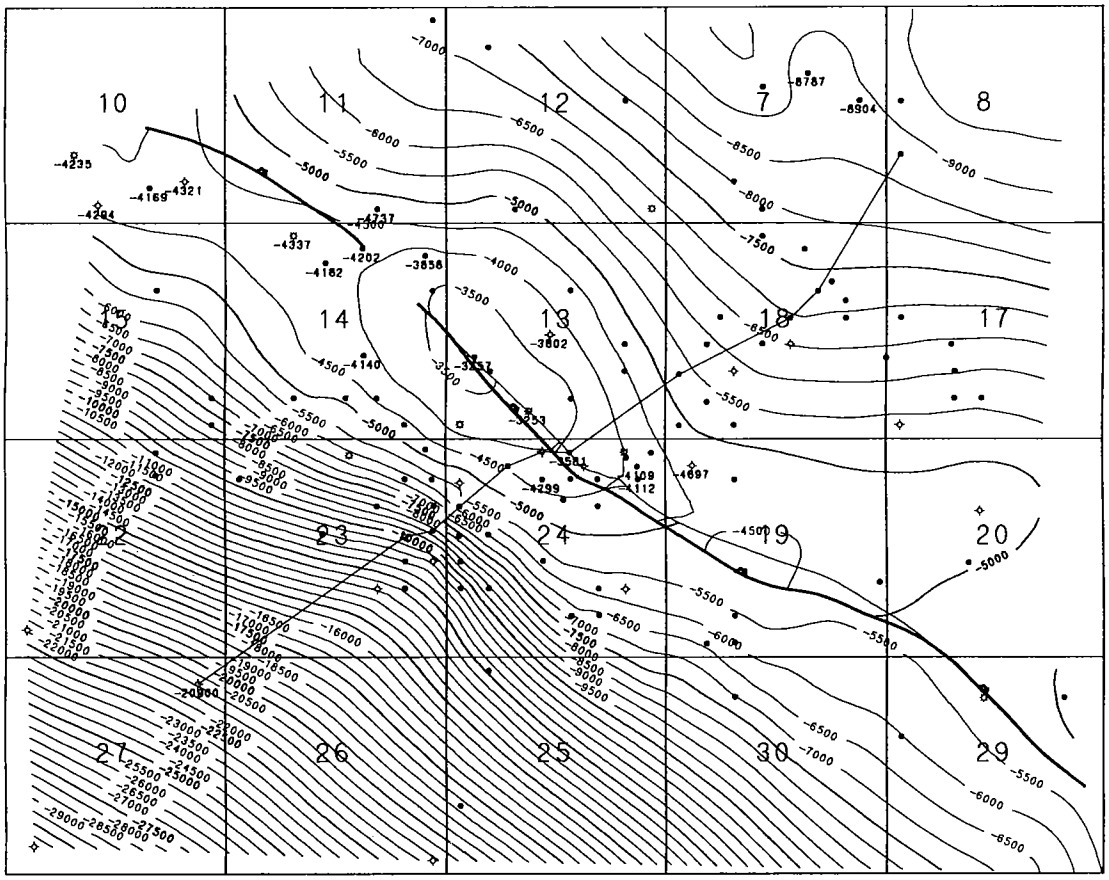

Figure 19. Top of Viola contour map (MCS). Contour interval is 500 ft.

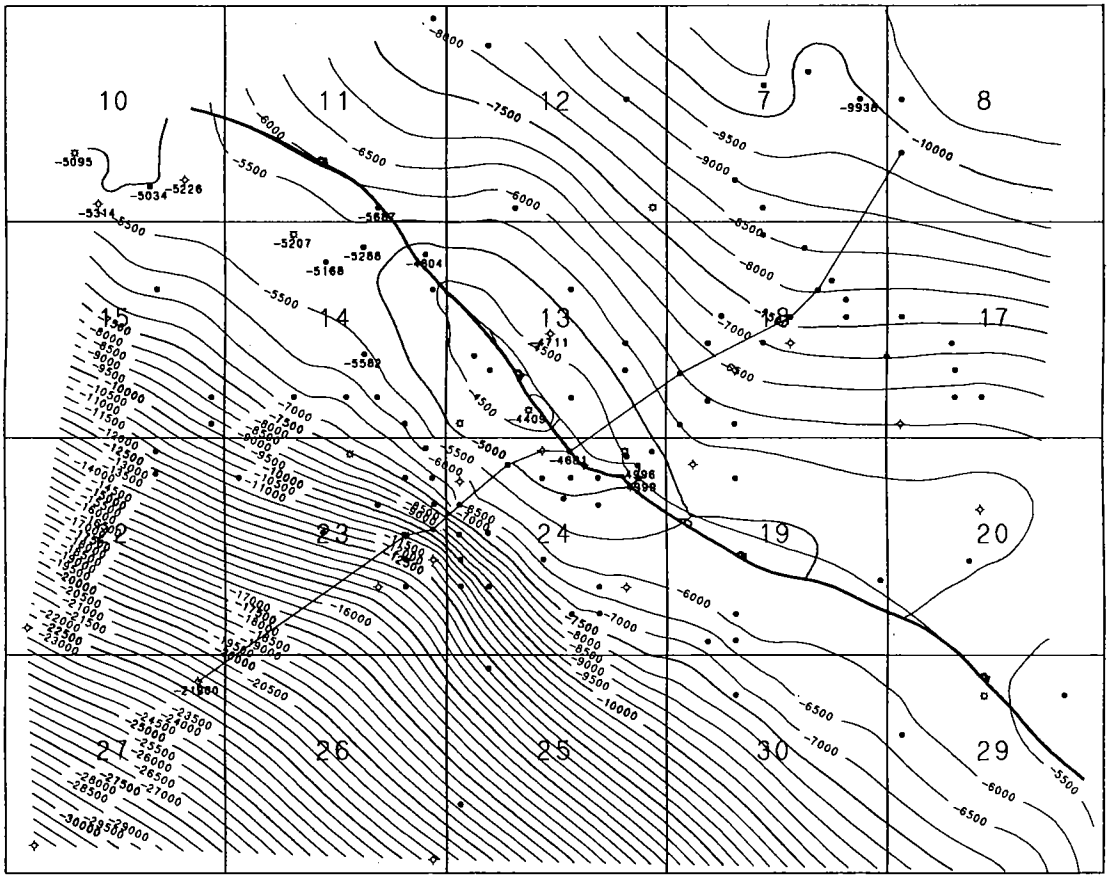

Figure 20. Top of Bromide contour map (MCS). Contour interval is 500 ft.

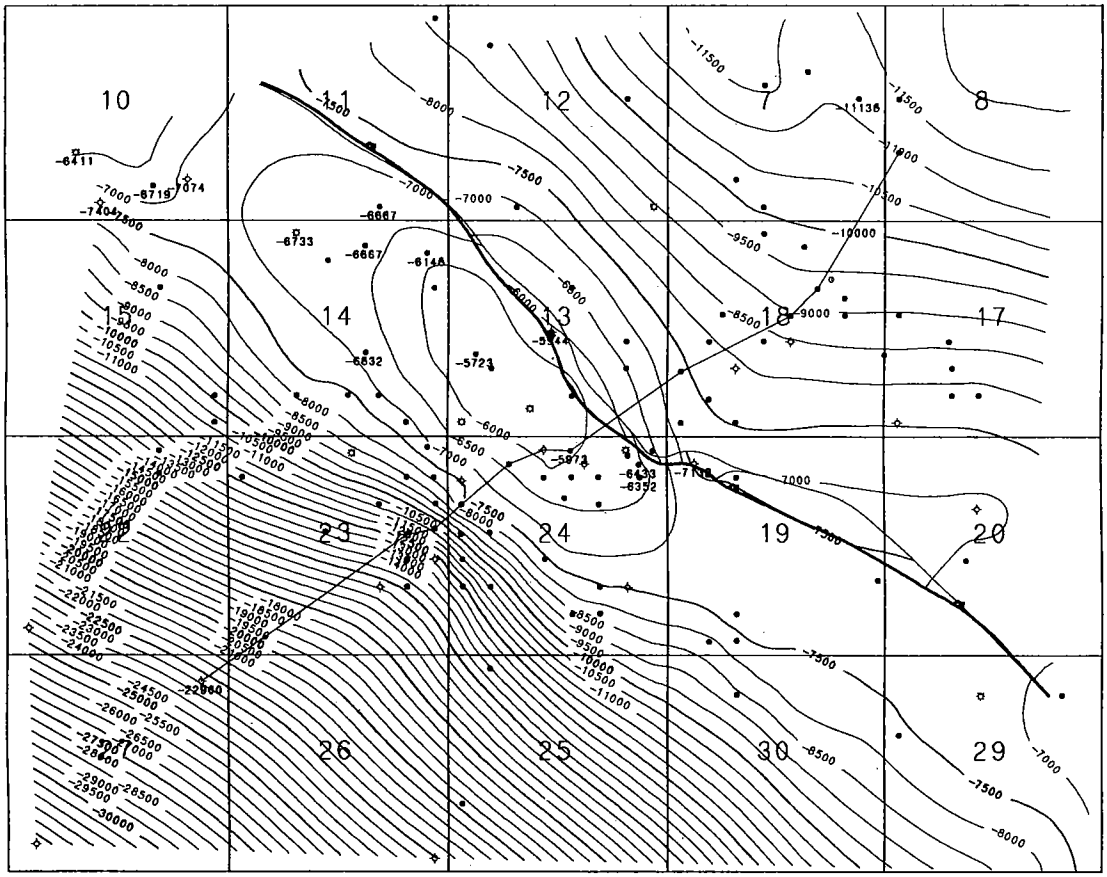

Figure 21. Top of Oil Creek contour map (MCS). Contour interval is 500 ft.

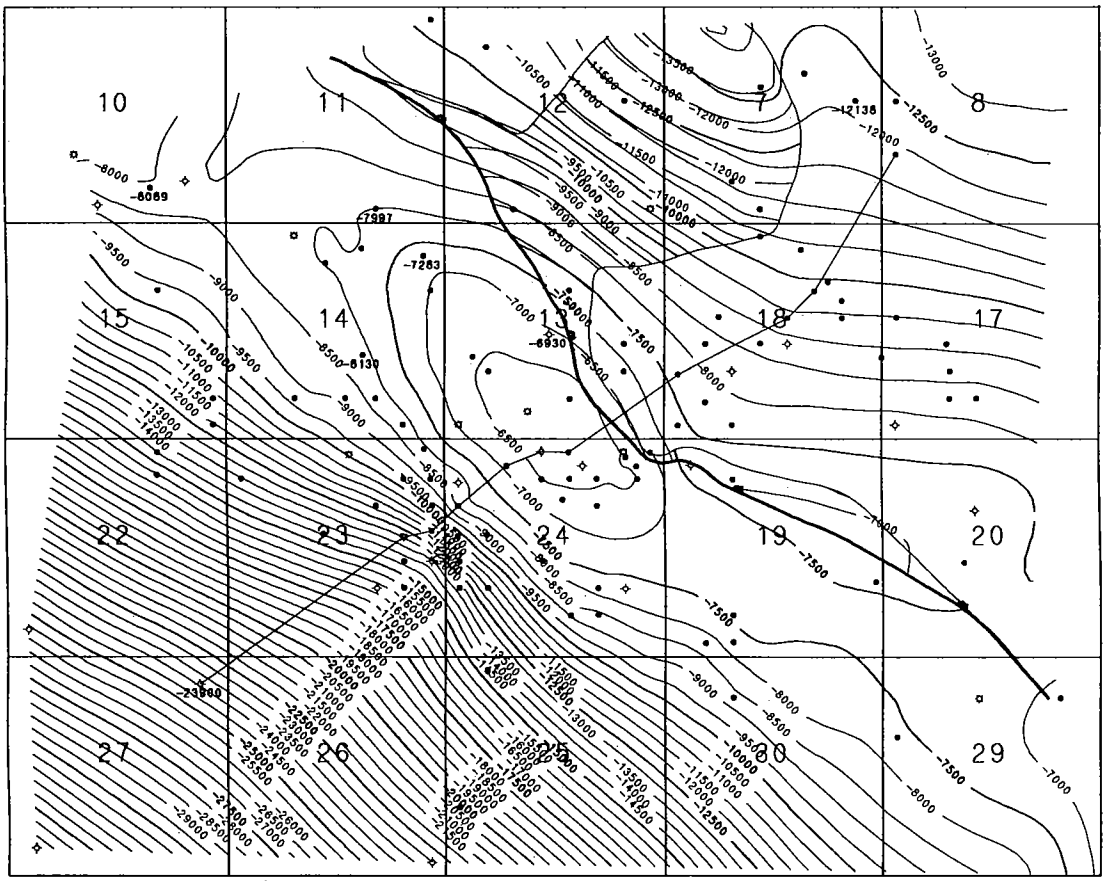

Figure 22. Top of Arbuckle contour map (MCS). Contour interval is 500 ft.

Finding Producible Simpson Sandstones (Middle Ordovician) in Southern Oklahoma with Three-Dimensional Seismic Data

Bob Springman
Independent Geophysicist
Edmond, Oklahoma

ABSTRACT.—The Simpson Group sandstones of Middle Ordovician age are the best reservoir-quality sands in the Midcontinent and are productive across south-central and southeastern Oklahoma. The purpose of this paper is to identify where 3-D seismic data would or would not be the right tool for discovering additional areas of producible hydrocarbons in these sandstones.

North Brady oil field was the first Simpson sand discovery in Garvin County, Oklahoma, using the 3-D seismic method. Also in Garvin County, Whitebead, Brady, and South Brady oil fields were discovered by 2-D methods. Subsequent 3-D seismic surveys in the area of these fields produced enhanced data, thereby enabling better interpretation of the subtle, complex geology. This resulted in several field extensions.

Future areas for new Simpson sand discoveries with 3-D seismic techniques appear to be the southern Pauls Valley uplift, the Lawrence uplift, the extension of the Franks graben into the Arkoma basin, the subthrust of the Ouachitas, the Sherman basin, and the eastern Ardmore and Marietta basins.

INTRODUCTION

The Simpson Group sandstones (Middle Ordovician) have been prolific petroleum reservoirs in southern Oklahoma. In south-central Oklahoma the basal Oil Creek sand is capable of producing >1,000,000 barrels of oil per well (BOPW), with recovery factors as high as 800 BO per acre-foot (ac-ft) at depths <7,000 ft. The Bromide sands are capable of producing >600,000 BOPW, with recovery factors as high as 400 BO/ac-ft at depths <6,000 ft. In southeastern Oklahoma the basal Oil Creek sand is capable of producing >400,000 BOPW, and the McLish sand is capable of producing >300,000 BOPW.

These sands are the best reservoir-quality sands in the Midcontinent and are productive across most of south-central and southeastern Oklahoma (Fig. 1). The recovery factors per acre-foot rival some of the recovery factors of prolific unconsolidated sands in the Gulf Coast region. Numerous secondary producing formations are also present in southern Oklahoma (Fig. 2).

WOULD 3-D SEISMIC DATA BE THE RIGHT TOOL?

Since the days of single-fold seismic data, southern Oklahoma (excluding the mountain front) has been known as an area of good-quality seismic data (Fig. 3). No adverse surface conditions exist that would cause severe attenuation of energy transmission or static problems to hinder accurate structural mapping. Also, in parts of southern Oklahoma the prolific Simpson sands are excellent seismic reflectors.

With the information provided so far, the answer to the question asked would be an obvious "yes." However, more information needs to be considered. The purpose of this paper is to delineate where three-dimensional (3-D) seismic data would or would not be the right tool.

WHERE ARE 3-D SEISMIC DATA MOST SUCCESSFULLY USED?

Three-dimensional seismic data are most successful where 2-D seismic data have been proven successful. Even further, 2-D seismic data have been most successful where single-fold (1-D) seismic data have been proven successful. In Garvin County, Oklahoma, significant Simpson sand oil fields were discovered with 1-D and common-depth-point (CDP) 2-D seismic techniques in the late 1960s and early 1970s (see Fig. 4). Empirical observation indicates that seismic data make a successful exploration tool in Garvin County for Simpson sand structural traps.

Today, with the benefit of basic geophysical modeling, the explorationist should be able to confidently predict where the seismic data will be most successful without the expense of a costly empirical approach, as in the past.

On the regional locator map (Fig. 5) the area where the Simpson sands are good seismic reflectors lies south of the heavy curved line. The shaded circles mark locations of wells from which synthetic seismograms

Springman, Bob, 2002, Finding producible Simpson sandstones (Middle Ordovician) in southern Oklahoma with three-dimensional seismic data, *in* Cardott, B. J. (ed.), Revisiting old and assessing new petroleum plays in the southern Midcontinent, 2001 symposium: Oklahoma Geological Survey Circular 107, p. 55–80.

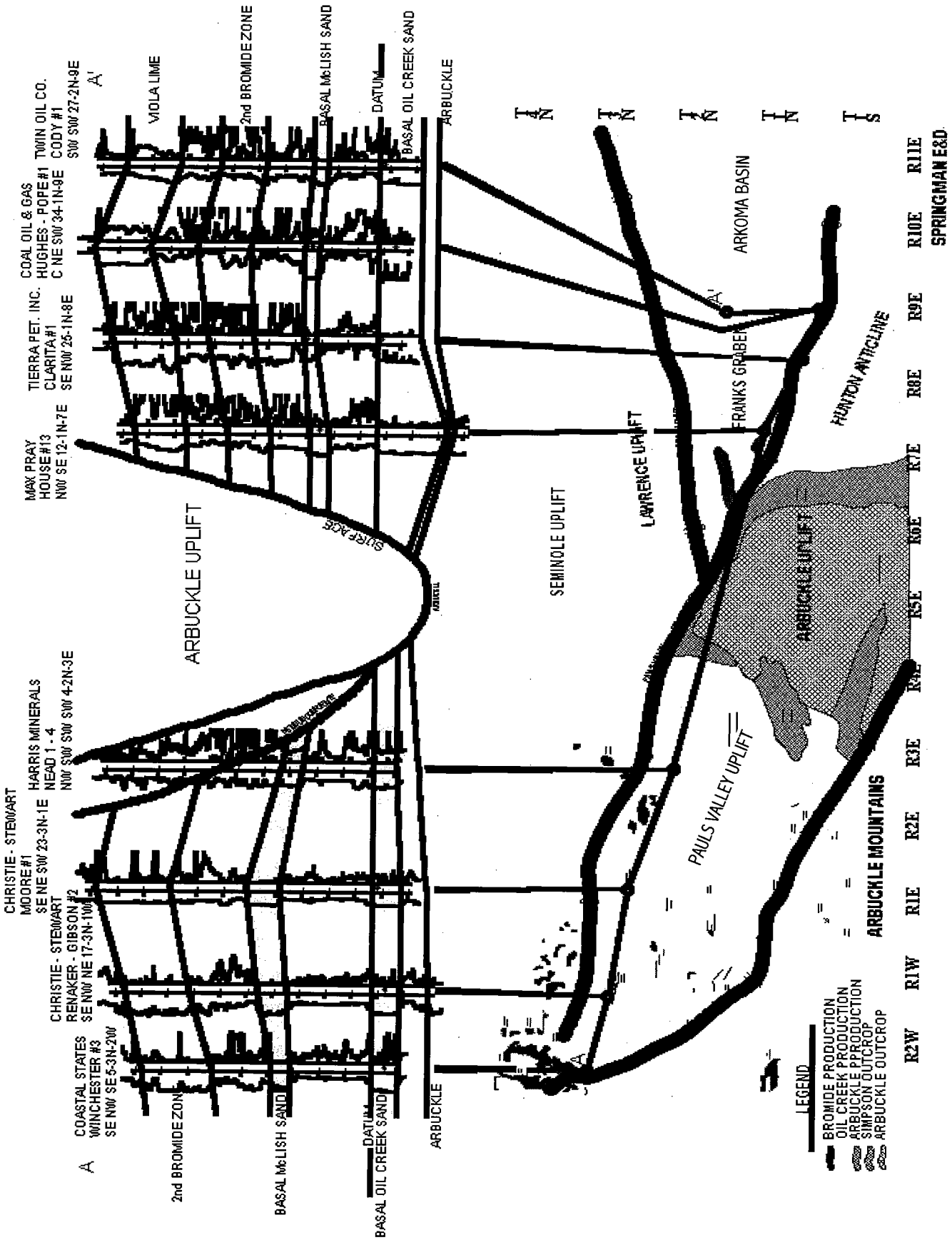

Figure 1. Cross section A–A′, from west to east, in southern Oklahoma. Map at bottom shows line of section.

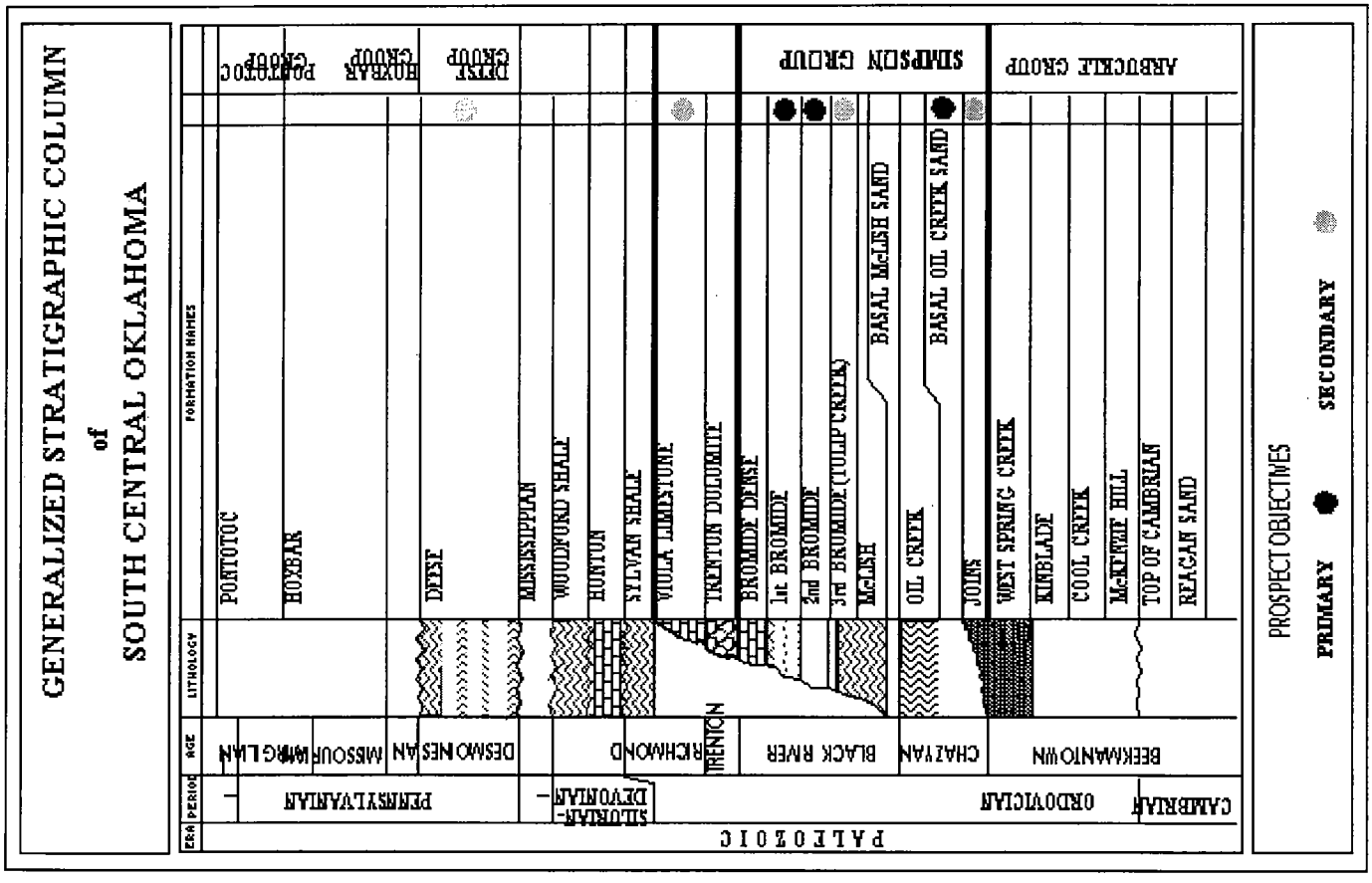

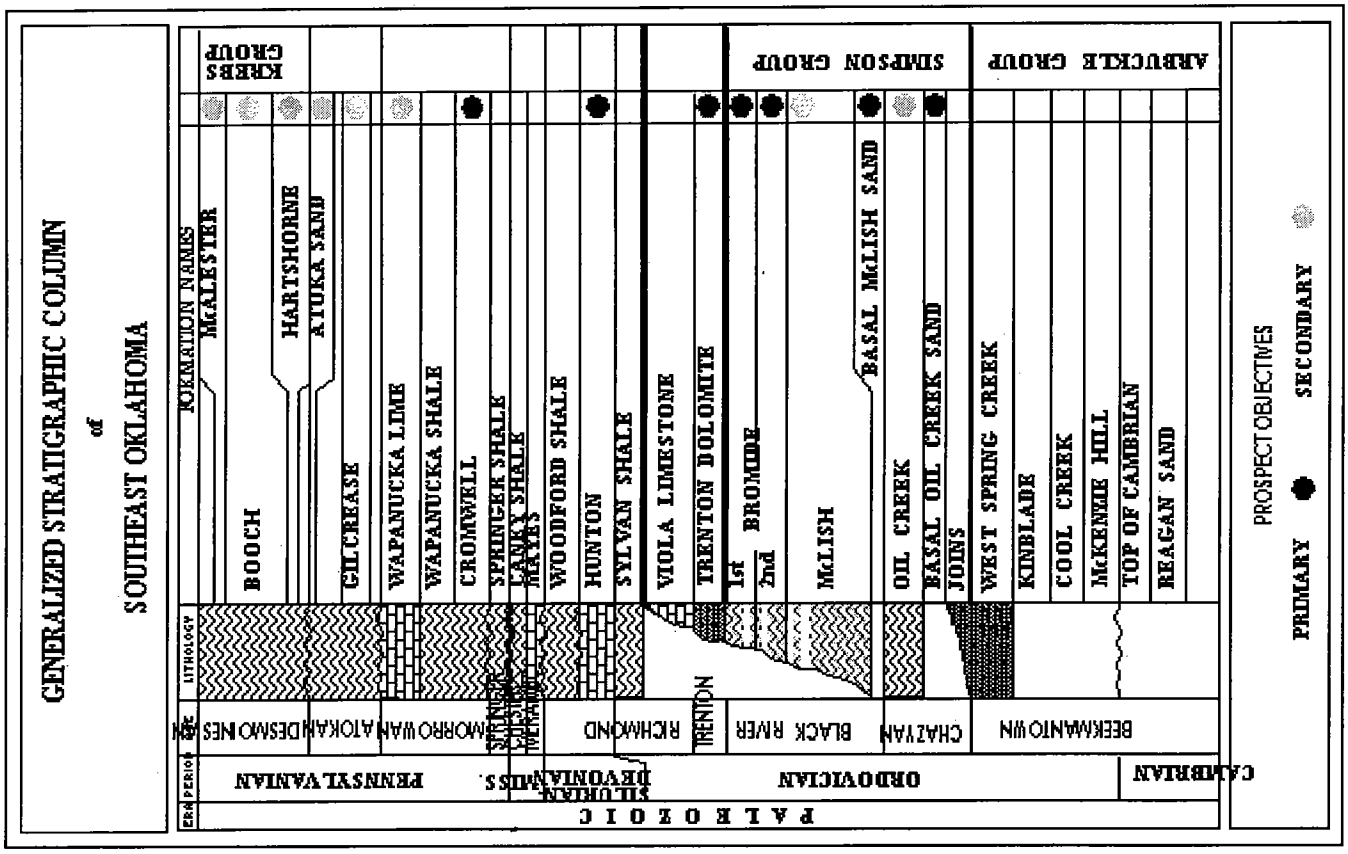

Figure 2. Stratigraphic columns for south-central and southeastern Oklahoma, indicating prospect objectives.

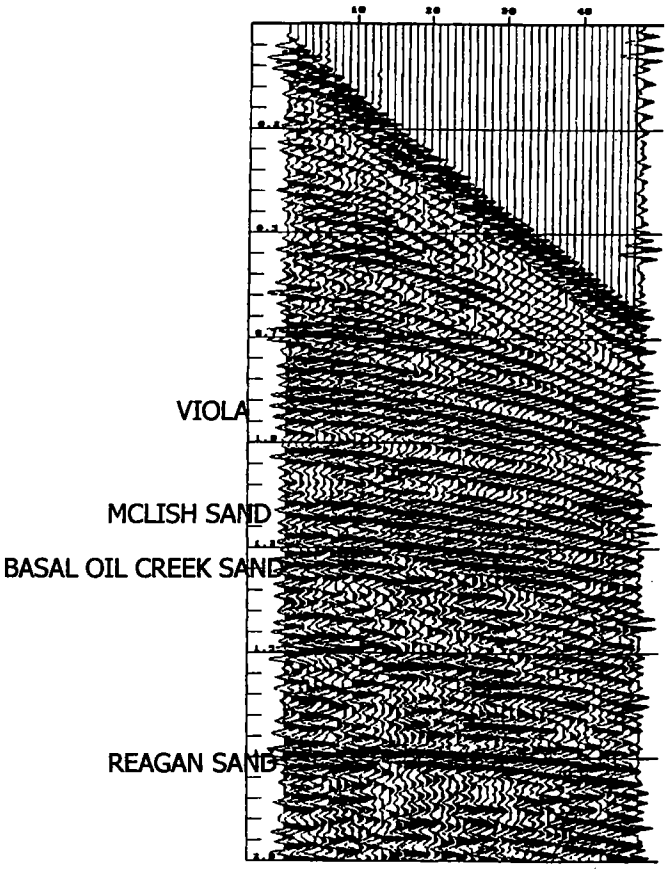

Figure 3. Single-fold (1-D) seismic profile, showing prominent Cambrian (Reagan Sandstone), Middle Ordovician (McLish and basal Oil Creek sandstones), and Upper Ordovician (Viola Limestone) reflectors.

were constructed from sonic logs, and the darker symbols mark locations where 3-D seismic data have been successfully used to define Simpson sand structures.

The following synthetic-seismogram examples do an excellent job of defining where the Simpson sands are good mappable reflectors. These 1-D models are the key for predicting where the 3-D seismic data will be the most successful. Note that none of the Simpson sands are good mappable reflectors throughout the entire area of study, and at some locations the top of the sand is not directly on the peak or trough of the wavelet. It is important to know this early in the exploration phase of a project to gain a better understanding of the risk involved in defining the objectives.

In Figure 6 (Christie-Stewart Oil Co. No. 1 Butt "C"well) the upper Simpson massive second Bromide sand (upper arrow) is not a good mappable reflector, but the lower Simpson basal McLish sand (middle arrow) and the basal Oil Creek sand (lower arrow) are excellent reflectors. The seismic data should be able to image the lower Simpson sands accurately, but the upper Simpson massive Bromide sands are transparent on the seismic data.

In Figure 7 (Perry Larson No. 1 Kennedy well) the massive Bromide sand and the basal Oil Creek sand are both good mappable reflectors (upper and lower arrows, respectively). Note that the massive Bromide sand is a peak on the wavelet, and the basal Oil Creek is a trough.

Figure 8 (Coastal Oil and Gas No. 4 Winchester well) is similar to Figure 7. Both the massive Bromide sand and basal Oil Creek sand are excellent reflectors (upper and lower arrows, respectively). The massive Bromide sand is a peak, and the basal Oil Creek sand is a trough.

In Figure 9 (Union Texas No. 1 Frady well) the upper Simpson second "Wilcox" sand (synonymous with the second Bromide sand; upper arrow) is not at the peak or trough of the wavelet but halfway between. The lower Simpson sands are not good reflectors and cannot be confidently imaged. The lower arrow marks the basal Oil Creek sand.

In Figure 10 (Chesapeake No. 1 Diane well), good reflectors are present in the upper and lower Simpson sands. Unfortunately, the sonic log was not run deep enough to sample the basal Oil Creek sand adequately.

Figure 11 (Getty Oil No. 1 Marlow well) shows that the upper and lower Simpson sands can be imaged at depths as great as 25,000 ft. Upper and lower arrows mark the first Bromide and Oil Creek sands, respectively.

In Figure 12 (Ardmore Drilling No. 1 Eskridge well) the upper Simpson sand reflectors are weak, but the lower Simpson sand reflectors are strong and are easily identified. Upper and lower arrows mark the second Bromide and basal Oil Creek sands, respectively.

In Figure 13 (Tenneco No. 1 Sarkeys well) the upper Simpson sands are transparent on the seismic data, but the lower Simpson sands are excellent reflectors. The arrow marks the basal Oil Creek sand.

Figure 14 (Hamilton Brothers No. 1-35 Pine Mountain well) indicates that lower Simpson sand reflectors can be identified and mapped beneath the Ouachita frontal thrust faults. The arrow marks the Oil Creek sand.

SOME EXAMPLES OF SUCCESSFUL 3-D SEISMIC APPLICATIONS

Whitebead Oil Field

Whitebead oil field was discovered in the early 1970s with some of the first CDP 2-D seismic work done in Garvin County, Oklahoma. The CDP method had become a proven technical tool in the oil industry a decade before this time but was late coming to Garvin County. Since the discovery of Whitebead oil field the prolific Simpson sands made Garvin County a hot spot for seismic activity for years to come, leading to the discovery of numerous Simpson sand reservoirs. With the development of Whitebead oil field, a well was eventually drilled at least every 40 acres, and more CDP seismic data were recorded to aid in field development.

Because of the subtle complexity of Simpson sand structural traps, the accuracy of the CDP seismic data could no longer successfully aid in further develop-

ment of Whitebead oil field. A west-to-east cross section across the field illustrates that this subtle, complex structure has at least four separate levels of reservoirs in the field proper (Fig. 15). From this interpretation, one would conclude that the oil field would continue to be depleted, with no additional drilling locations possible.

After 3-D seismic data were recorded over the field, a new location was staked updip from the previous highest well in the field. Figure 16 is a vertical slice from the 3-D seismic data, indicating that this well, the No. 4-5 West Whitebead, is ~15 ms (90 ft) updip from the No. 2 Rennicker-Gibson (the previous structurally highest well). Figure 17 is the final interpretation of the 3-D seismic data, illustrating the remaining "attic" oil. Figure 18 is the log from the No. 4-5 West Whitebead well, proving a 90-ft oil column updip from the previously known oil column in the field.

North Brady Oil Field

North Brady oil field was the first Simpson sand field discovery in Garvin County using the 3-D seismic method. Before the 3-D data were recorded, a basal Oil Creek sand discovery was made in sec. 15, T. 2 N., R. 1 W. Less than 10 ft of oil column was present, so this discovery well made less than 5,000 BO. Numerous operators tried to find possible updip oil to this noncommercial discovery. Nine dry holes were drilled before 3-D seismic data were finally recorded to image this subtle, complex structure adequately.

Figure 19 is a comparison of the structural interpretation before and after acquisition of the 3-D seismic data. Without the benefit of the 3-D data, this field would not have been discovered. Figure 20 is a vertical slice from the 3-D seismic survey, illustrating the Simpson sand reflectors and the faulted basal Oil Creek sand structural roll. Figure 21 is the log of the basal Oil Creek sand discovery well (Morris E. Stewart No. 1 Cassell), showing the obvious oil–water contact.

Brady and South Brady Oil Fields

Brady and South Brady oil fields were discovered with the 2-D seismic method. Many miles of 2-D seismic data were recorded in an effort to find additional offset drilling locations to extend these two fields. Even with the high density of 2-D data, it was decided that the 2-D data could not adequately evaluate the potential for possible locations because of the complex, subtle structural attitude. The previous 2-D interpretation was changed considerably after the 3-D seismic data were interpreted. Figure 22 is a vertical slice across South Brady field, illustrating how a dry hole could have been prevented with the 3-D seismic data. Figure 23 is a vertical slice from the 3-D seismic data across Brady field, illustrating how subtle some of the productive Simpson sand structures can be.

WHERE ARE THE FUTURE AREAS?

The future areas for significant new Simpson sand discoveries with 3-D seismic techniques over the next few years appear to be the southern Pauls Valley uplift area, the Lawrence uplift, the extension of the Franks graben into the Arkoma basin, the subthrust of the Ouachitas, the Sherman basin, and the eastern Ardmore and Marietta basins.

SOME PITFALLS IN THE USE OF 3-D SEISMIC DATA

Several pitfalls must be guarded against in the use of 3-D seismic data in southern Oklahoma, as follows:

1. Inadequate acquisition parameters, including (a) insufficient offsets and (b) inadequate imaging of mapping horizons;
2. Inadequate data processing;
3. Inadequate geological modeling in geophysical interpretation;
4. Inadequate geophysical experience in geophysical interpretation.

CONCLUSION

A major exploration effort over the next few years in southern Oklahoma would be justified, focusing on the prolific Simpson sands alone. However, these sands are not the only productive sands. Many more sands uphole from the Simpson significantly improve the chance of finding prolific reserves (Fig. 24).

ACKNOWLEDGMENTS

I thank the following persons and organizations for their assistance in the preparation of this paper: Clair C. Bingham for geologic support, James McCall for help with the PowerPoint presentation, Western Geophysical for data samples, and M.E.S.O.C. for data and maps.

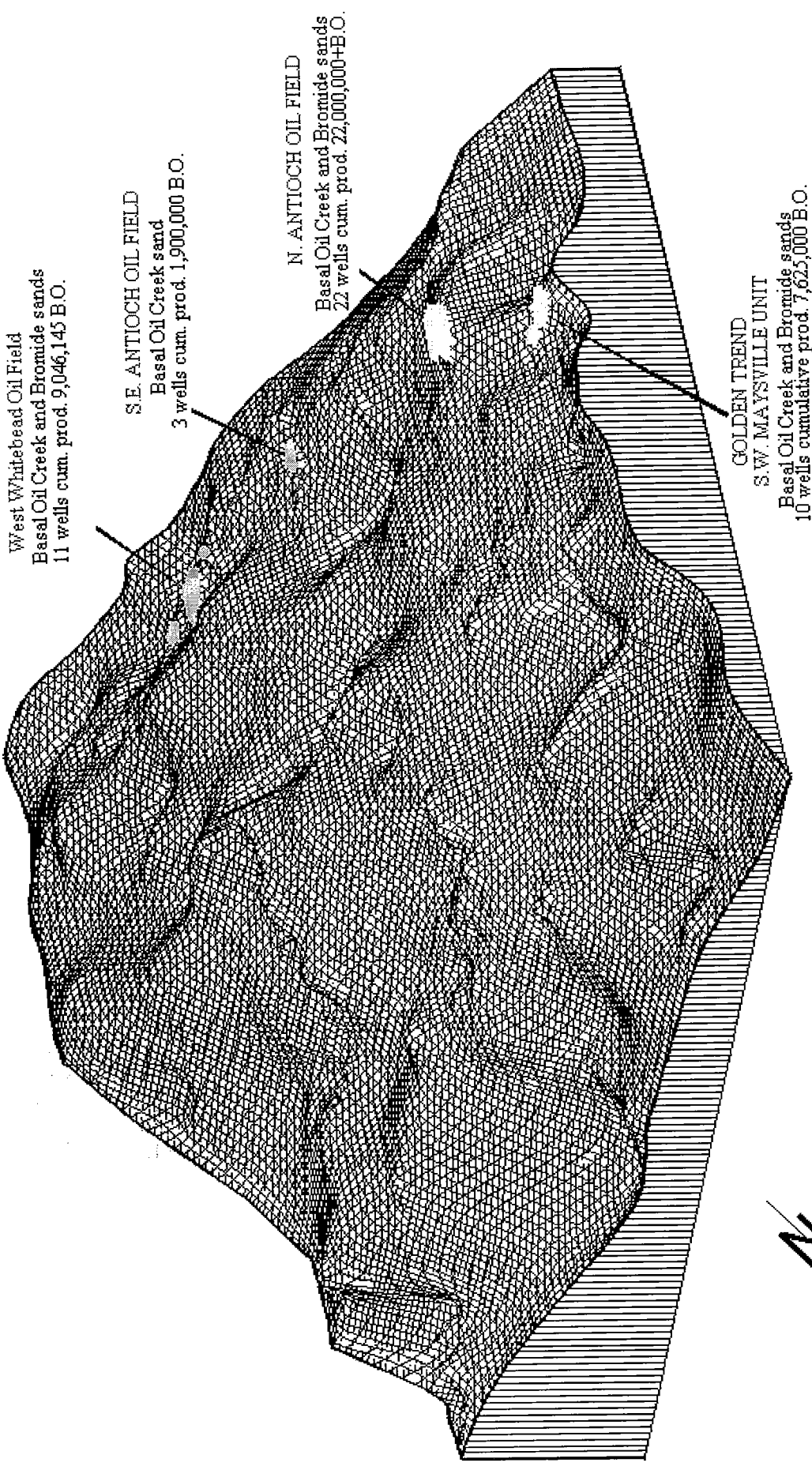

Figure 4. Diagram illustrating success in finding producible Simpson sands with 3-D seismic techniques.

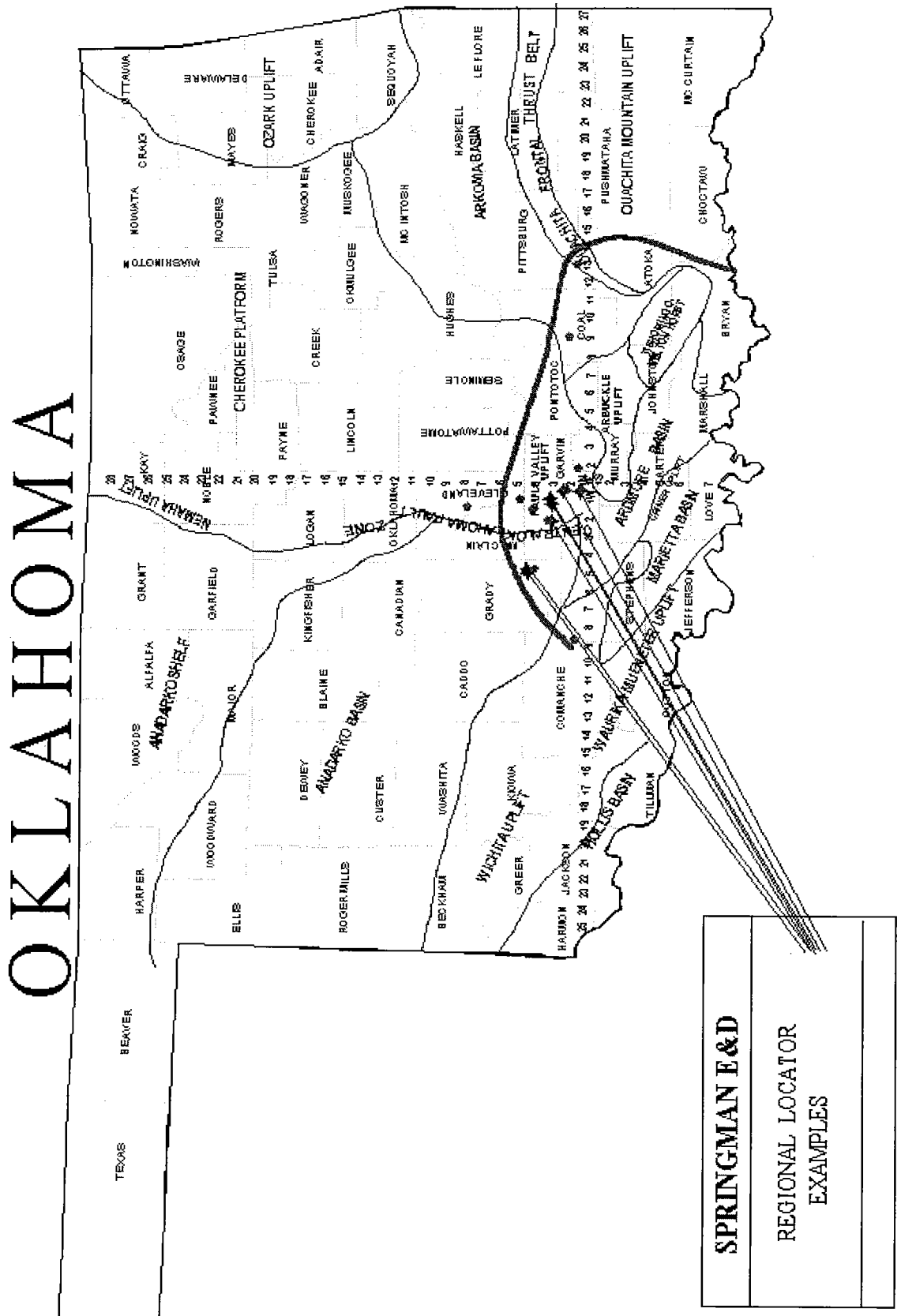

Figure 5. Regional locator map, showing the area where Simpson sands are good seismic reflectors (south of heavy curved line).

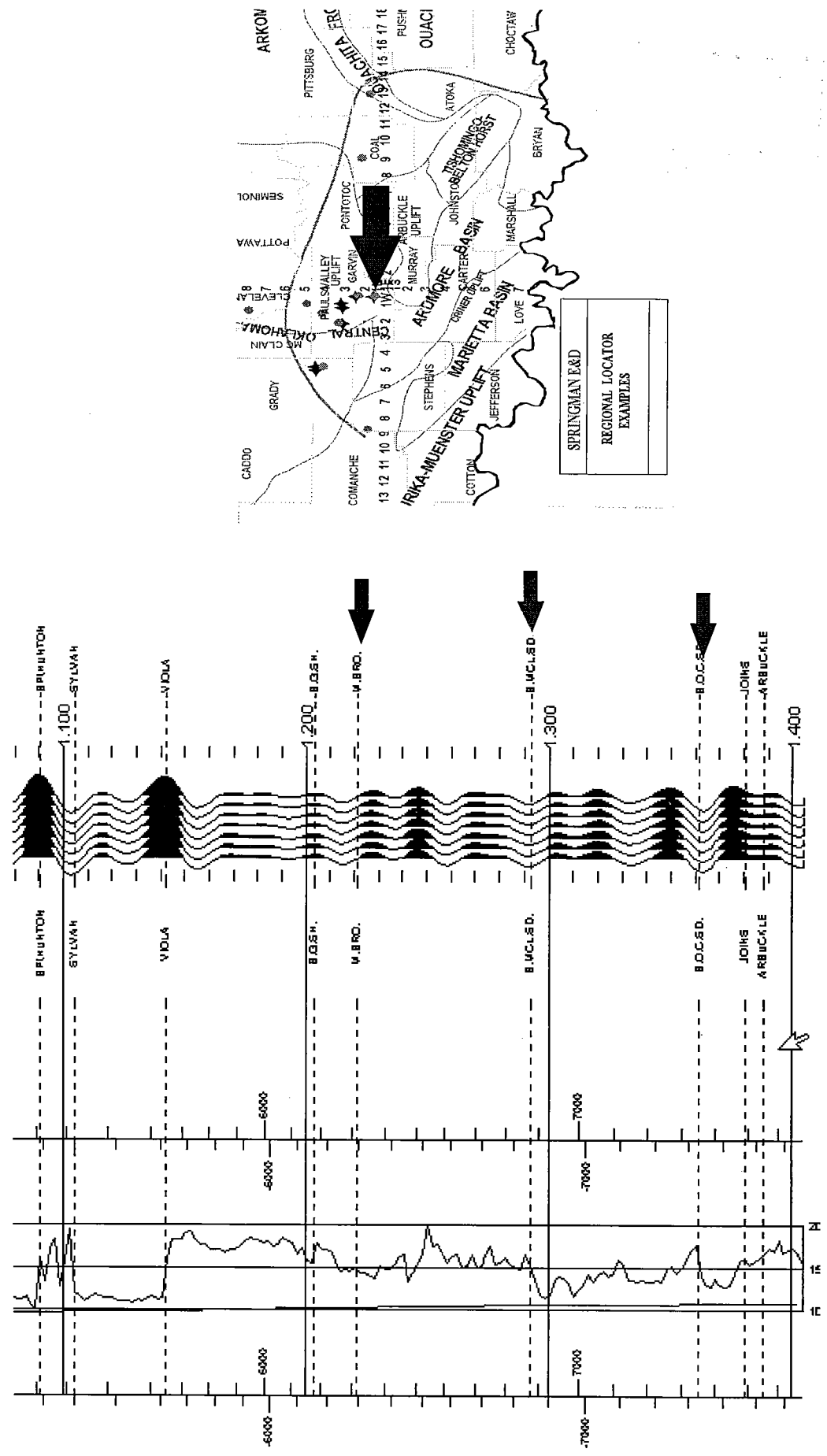

Figure 6. Sonic log and synthetic seismogram of Christie-Stewart Oil Co. No. 1 Butt "C" well, sec. 3, T. 2 N., R. 1 W., Garvin County. Upper arrow indicates massive second Bromide sand, which is not a good mappable reflector; middle and lower arrows indicate basal McLish and basal Oil Creek sands, respectively, which are excellent reflectors.

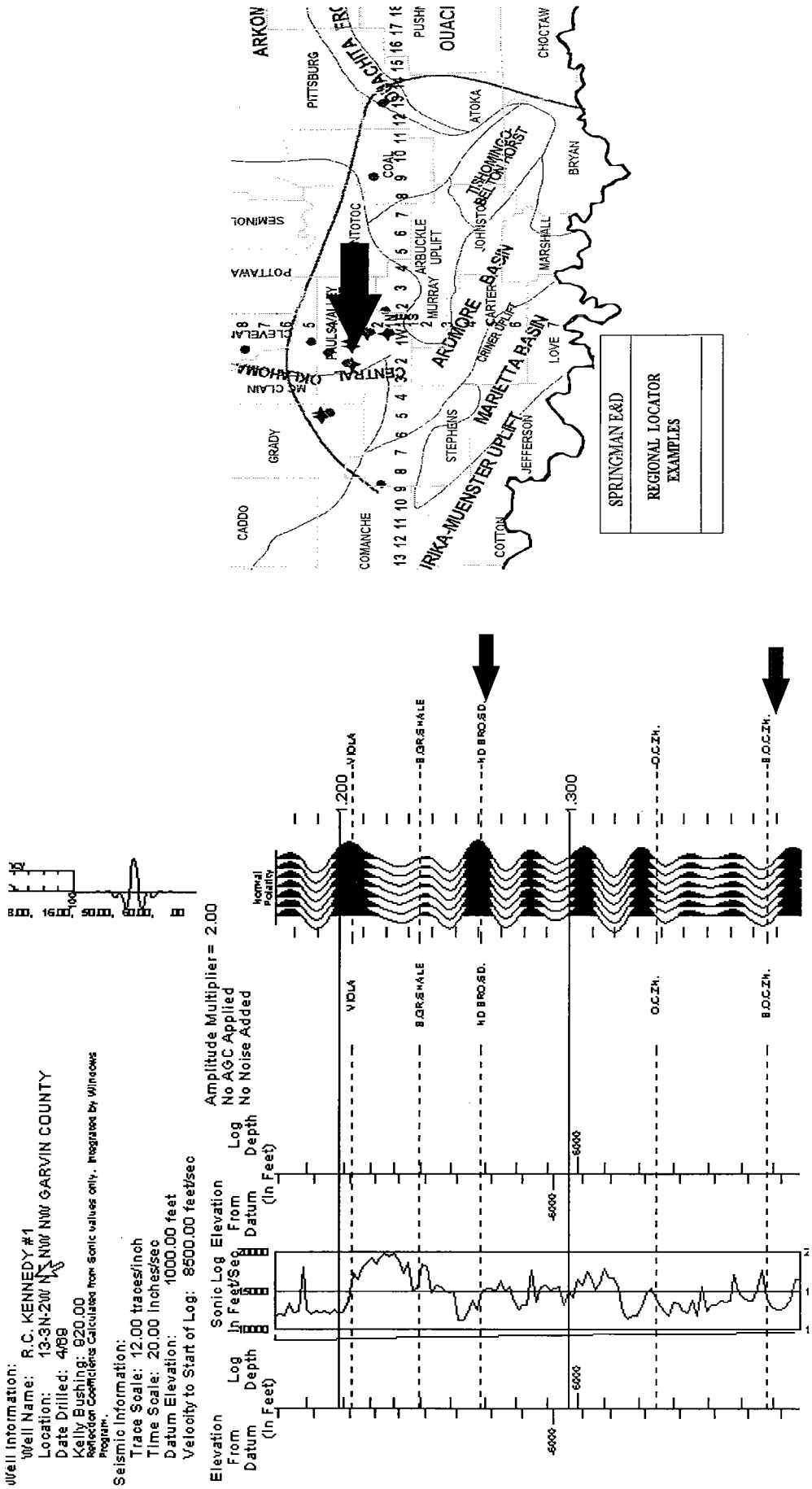

Figure 7. Sonic log and synthetic seismogram of Perry Larson No. 1 Kennedy well, sec. 13, T. 3 N., R. 2 W., Garvin County. Upper and lower arrows indicate, respectively, massive Bromide sand (a peak on wavelet) and basal Oil Creek sand (a trough on wavelet). Both sands are good reflectors.

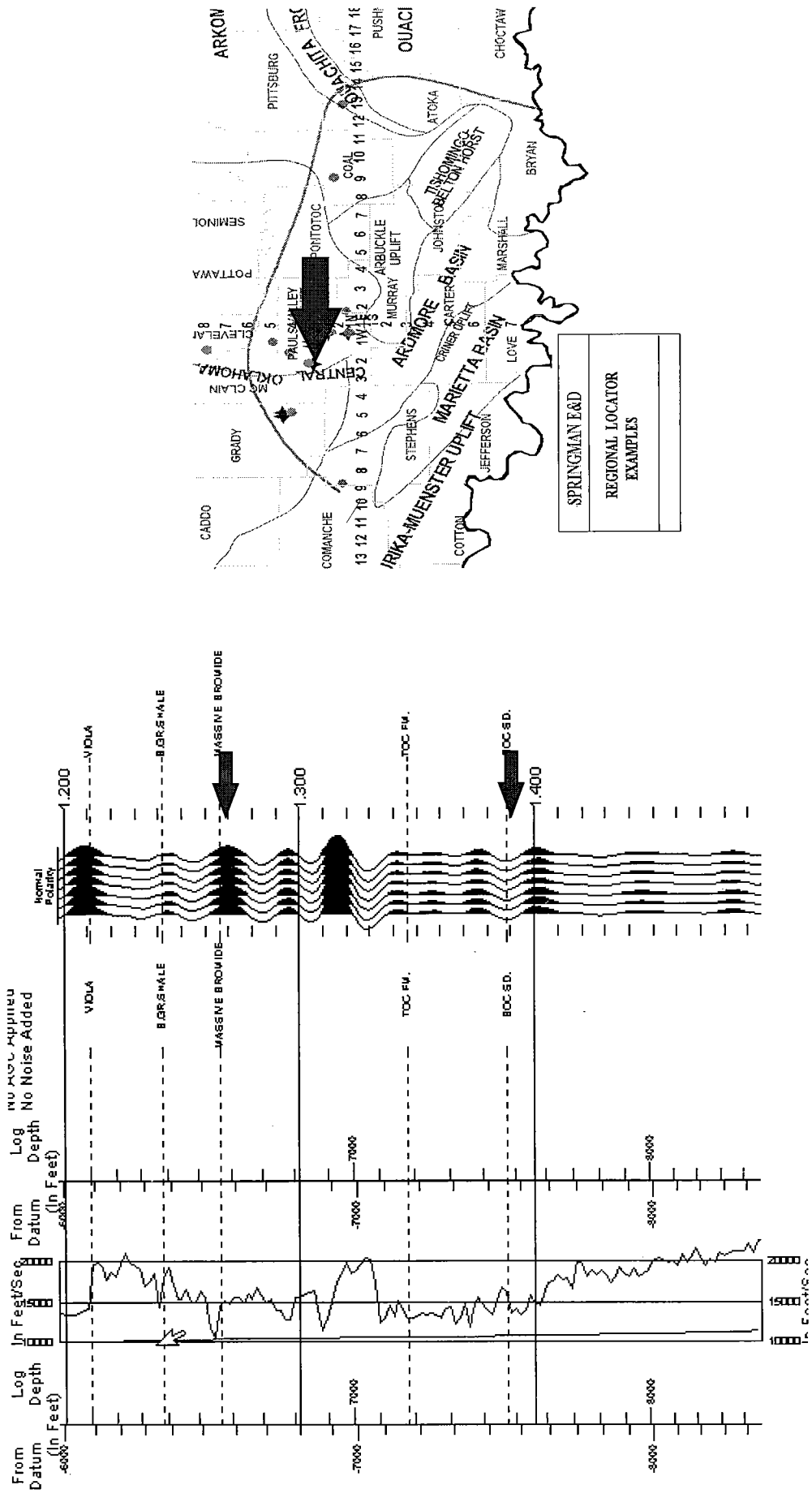

Figure 8. Sonic log and synthetic seismogram of Coastal Oil and Gas Co. No. 4 Winchester well, sec. 5, T. 3 N., R. 2 W., Garvin County, similar to Figure 7. Upper and lower arrows indicate, respectively, massive Bromide sand (a peak on wavelet) and basal Oil Creek sand (a trough on wavelet). Both sands are excellent reflectors.

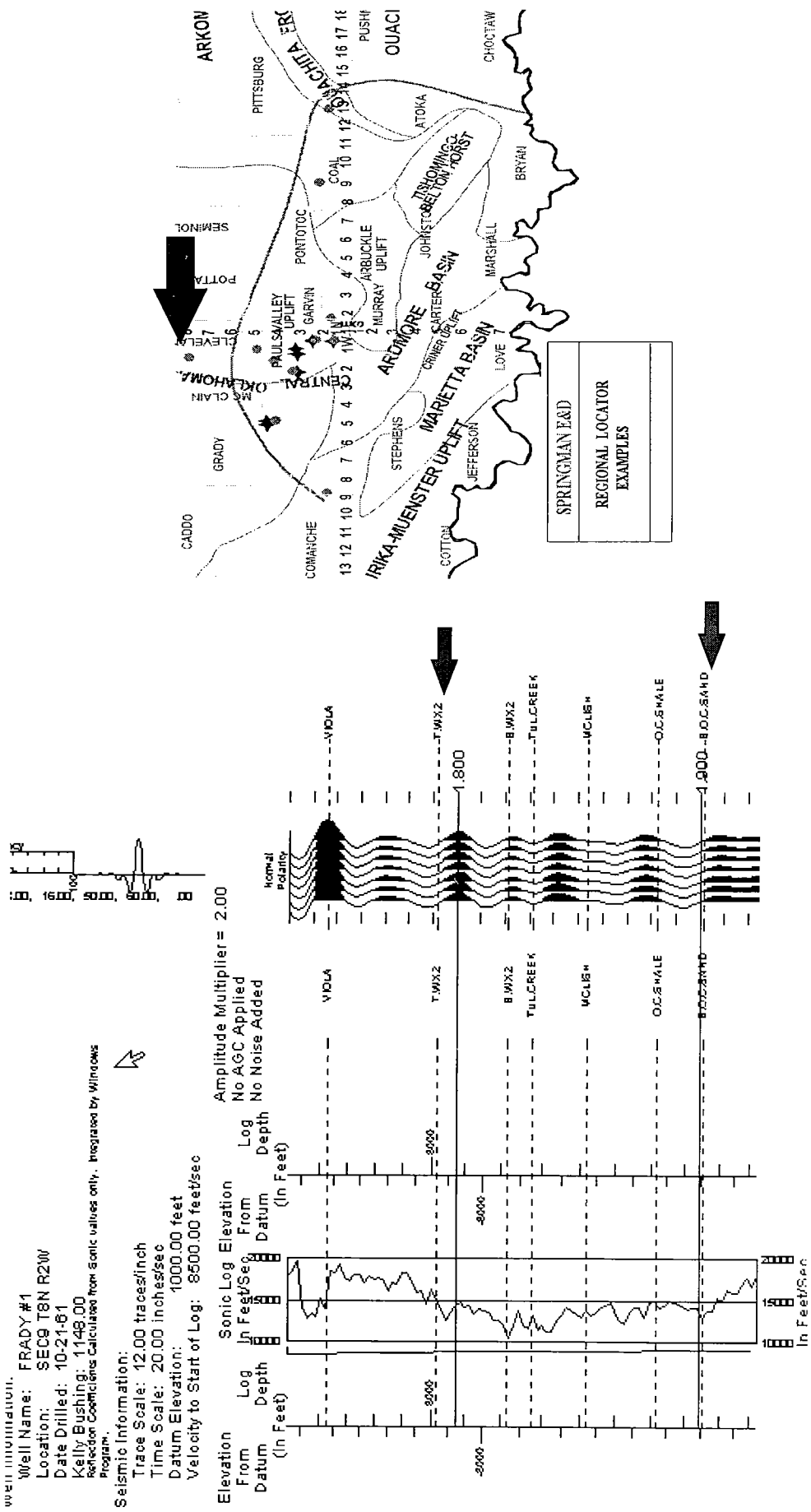

Figure 9. Sonic log and synthetic seismogram of Union Texas No. 1 Frady well, sec. 9, T. 8 N., R. 2 W., Cleveland County. Upper arrow marks second "Wilcox" sand (second Bromide sand); this sand is not at the peak or trough of the wavelet but halfway between. Lower arrow marks basal Oil Creek sand. The lower Simpson sands are poor reflectors.

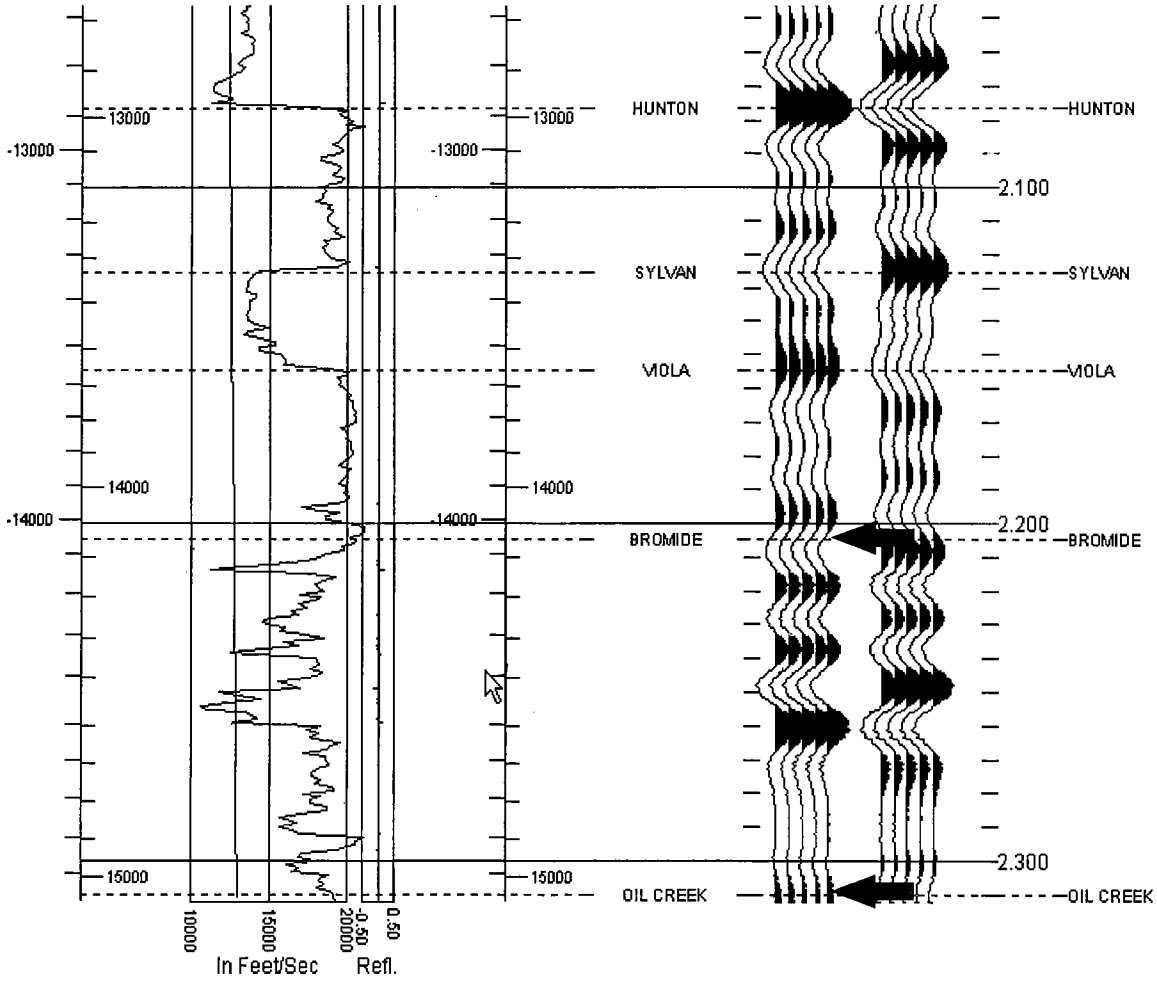

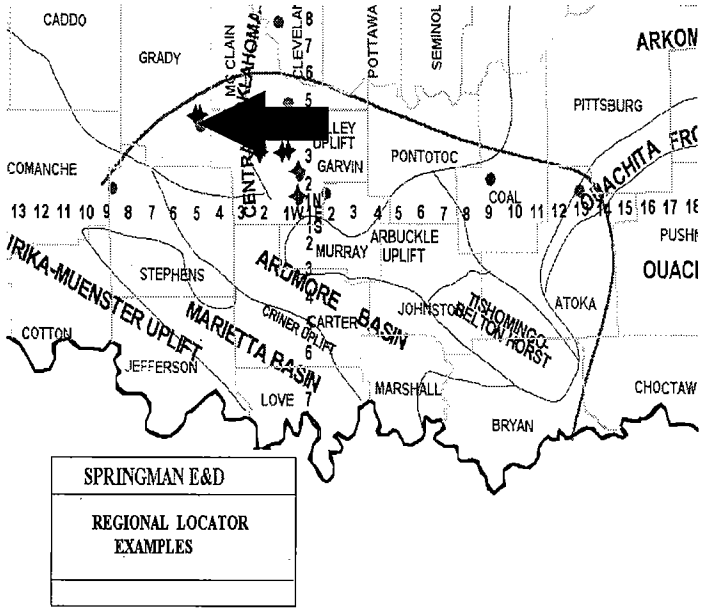

Figure 10. Sonic log and synthetic seismogram of Chesapeake No. 1 Diane well, sec. 28, T. 5 N., R. 5 E., Grady County. Good reflectors are present in upper and lower Simpson sands. Note that sonic log was not run deep enough to sample basal Oil Creek sand adequately.

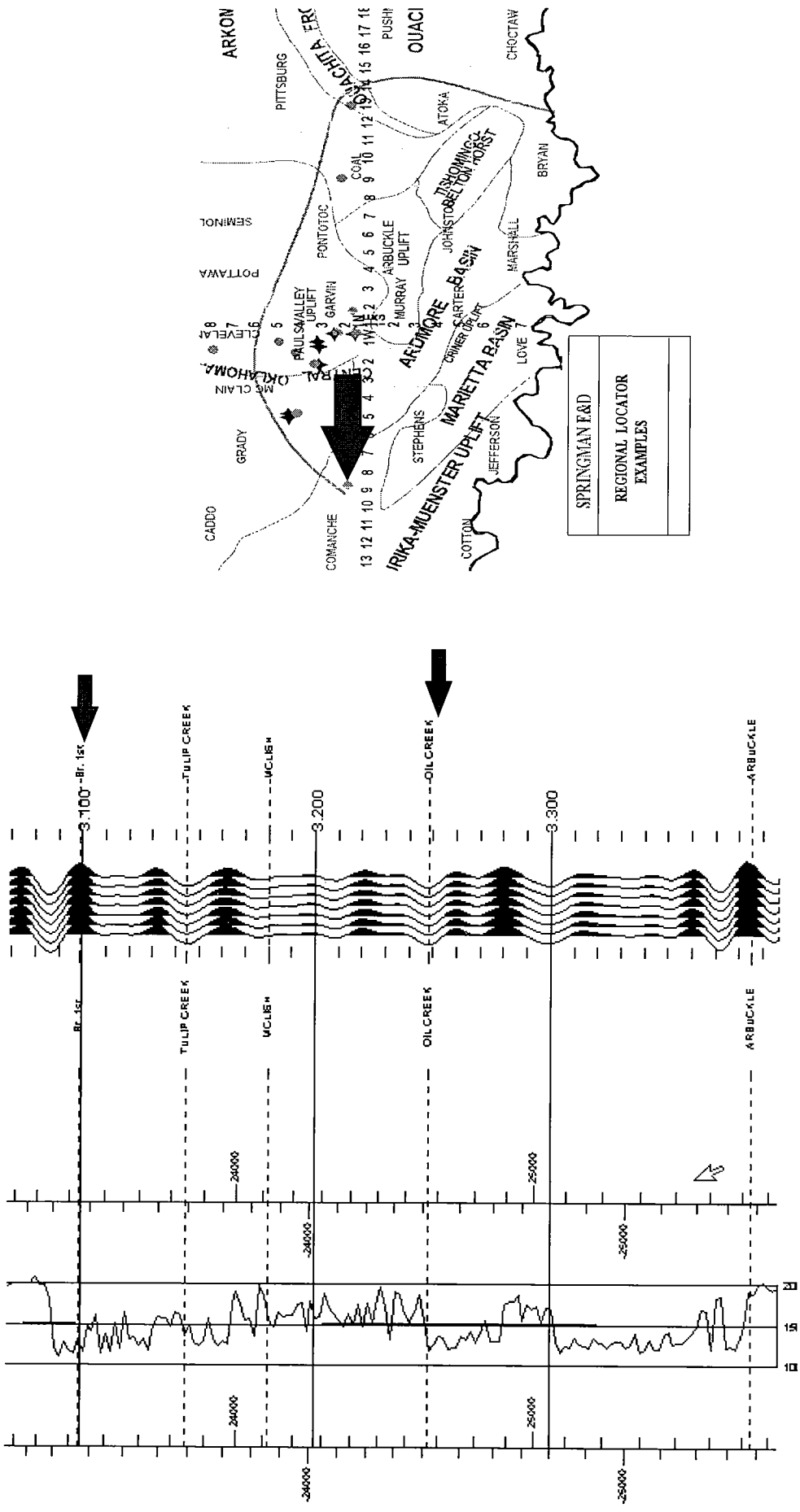

Figure 11. Sonic log and synthetic seismogram of Getty Oil No. 1 Marlow well, sec. 2, T. 2 N., R. 9 W., Stephens County. These images show that upper and lower Simpson sands can be imaged at depths as great as 25,000 ft. Upper and lower arrows mark, respectively, first Bromide and Oil Creek sands.

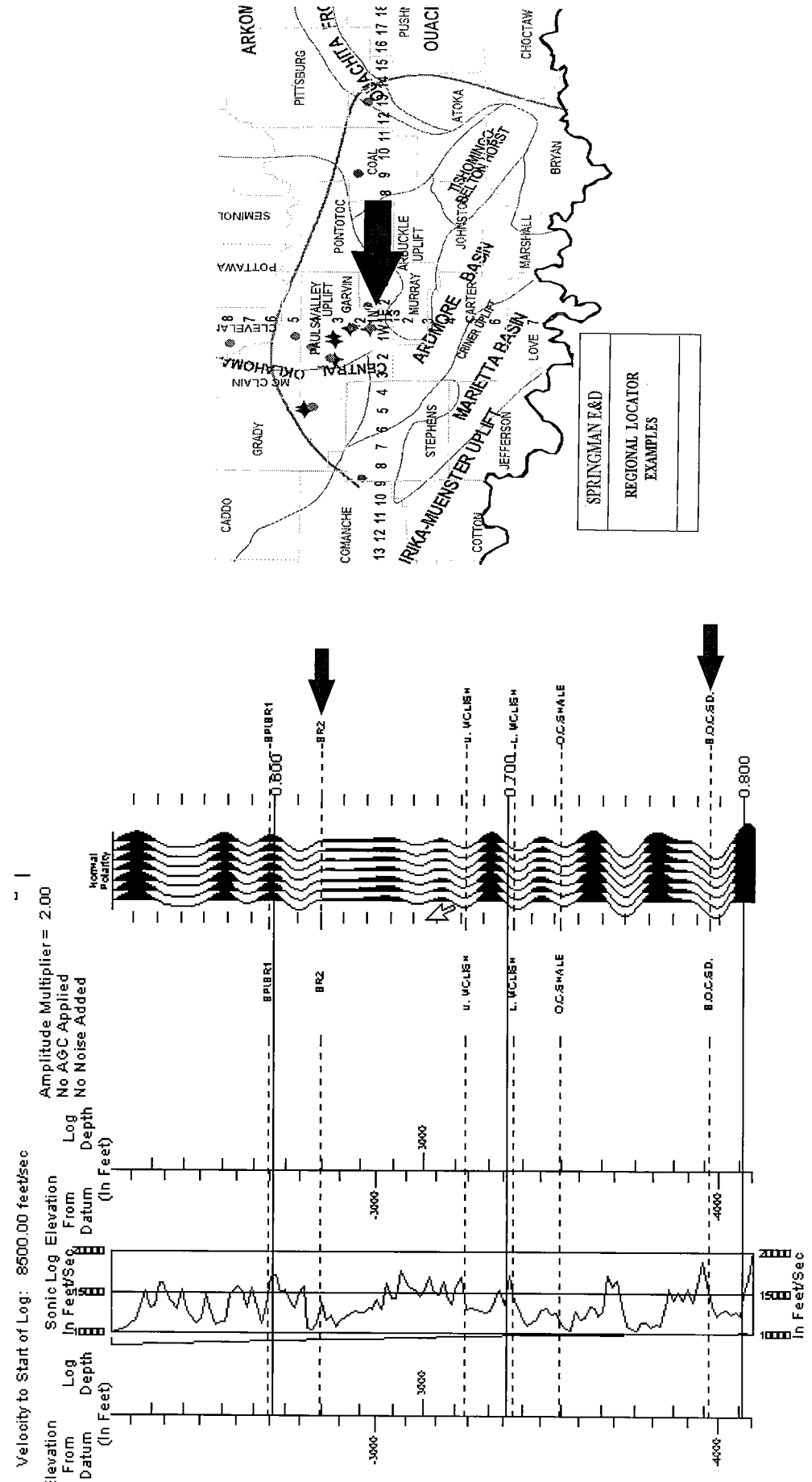

Figure 12. Sonic log and synthetic seismogram of Ardmore Drilling No. 1 Eskridge well, sec. 36, T. 2 N., R. 1 E., Murray County. Upper Simpson sand reflectors are weak, but lower Simpson sand reflectors are strong and easily identified. Upper and lower arrows mark, respectively, second Bromide and basal Oil Creek sands.

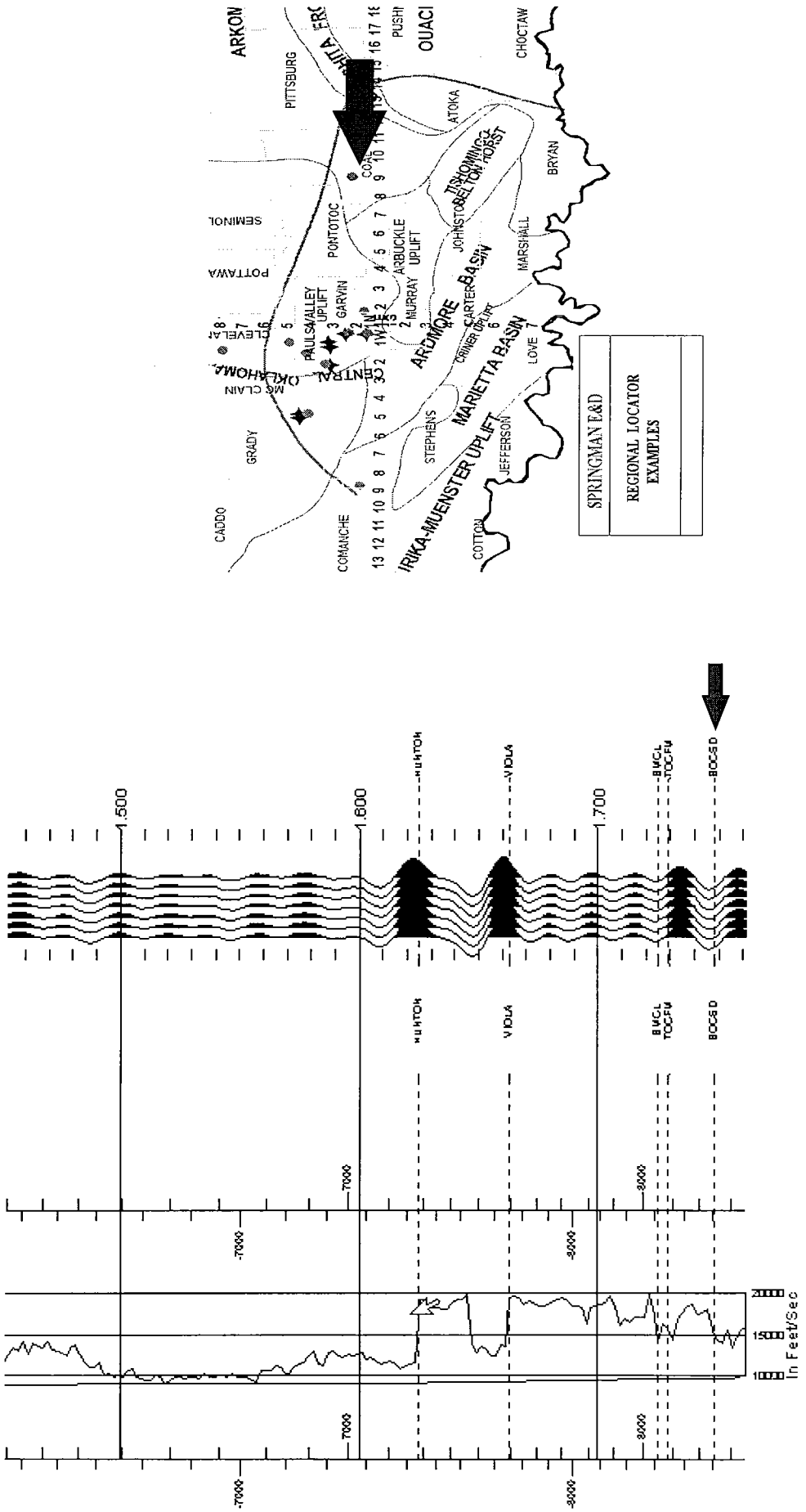

Figure 13. Sonic log and synthetic seismogram of Tenneco No. 1 Sarkeys well, sec. 35, T. 2 N., R. 9 E., Coal County. Upper Simpson sands are transparent on seismic data, but lower Simpson sands are excellent reflectors. Arrow marks basal Oil Creek sand.

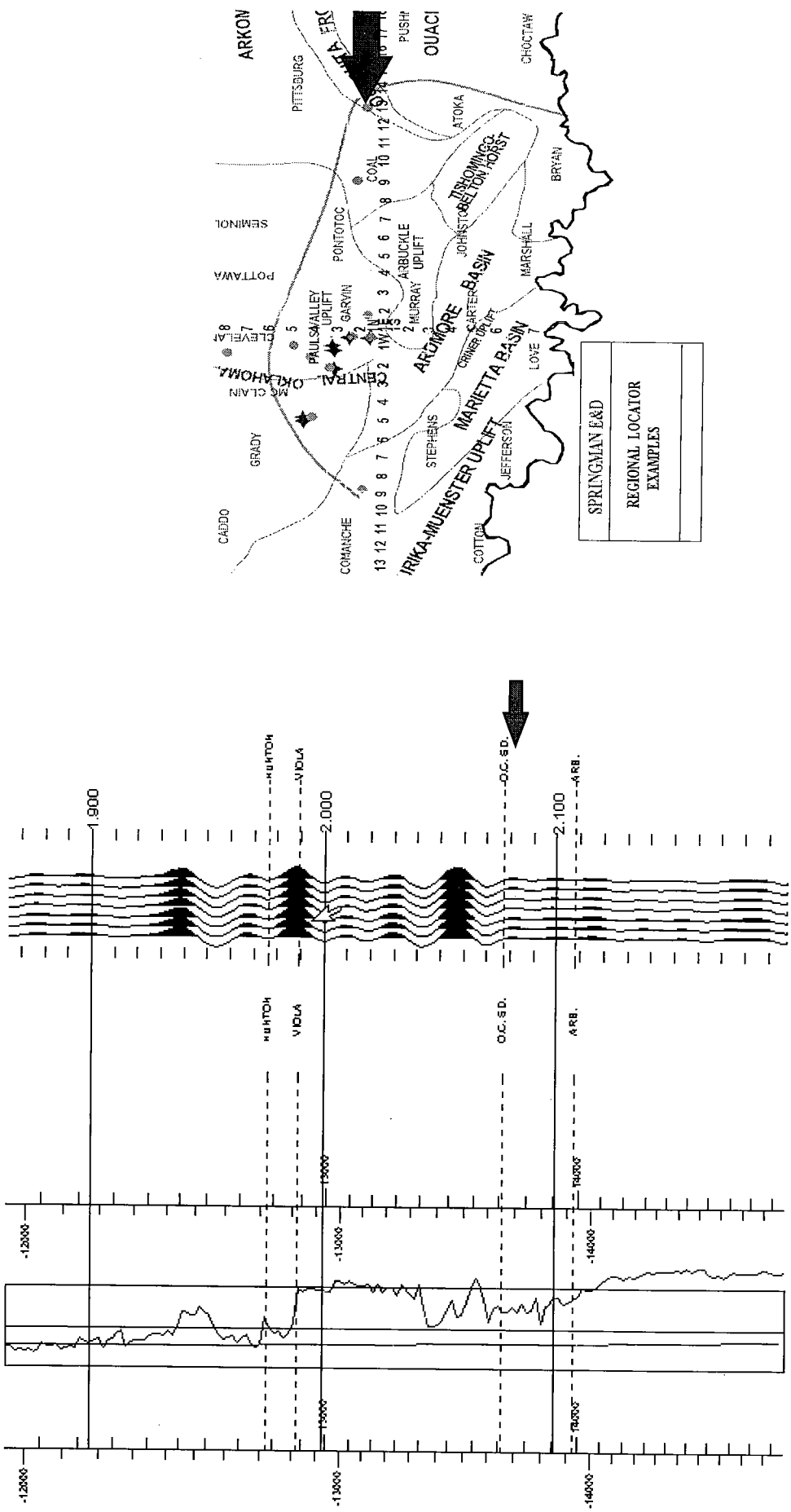

Figure 14. Sonic log and synthetic seismogram of Hamilton Brothers No. 1-35 Pine Mountain well, sec. 35, T. 2 N., R. 13 E., Atoka County, indicating that lower Simpson sand reflectors can be identified and mapped beneath Ouachita frontal thrust faults. Arrow marks Oil Creek sand.

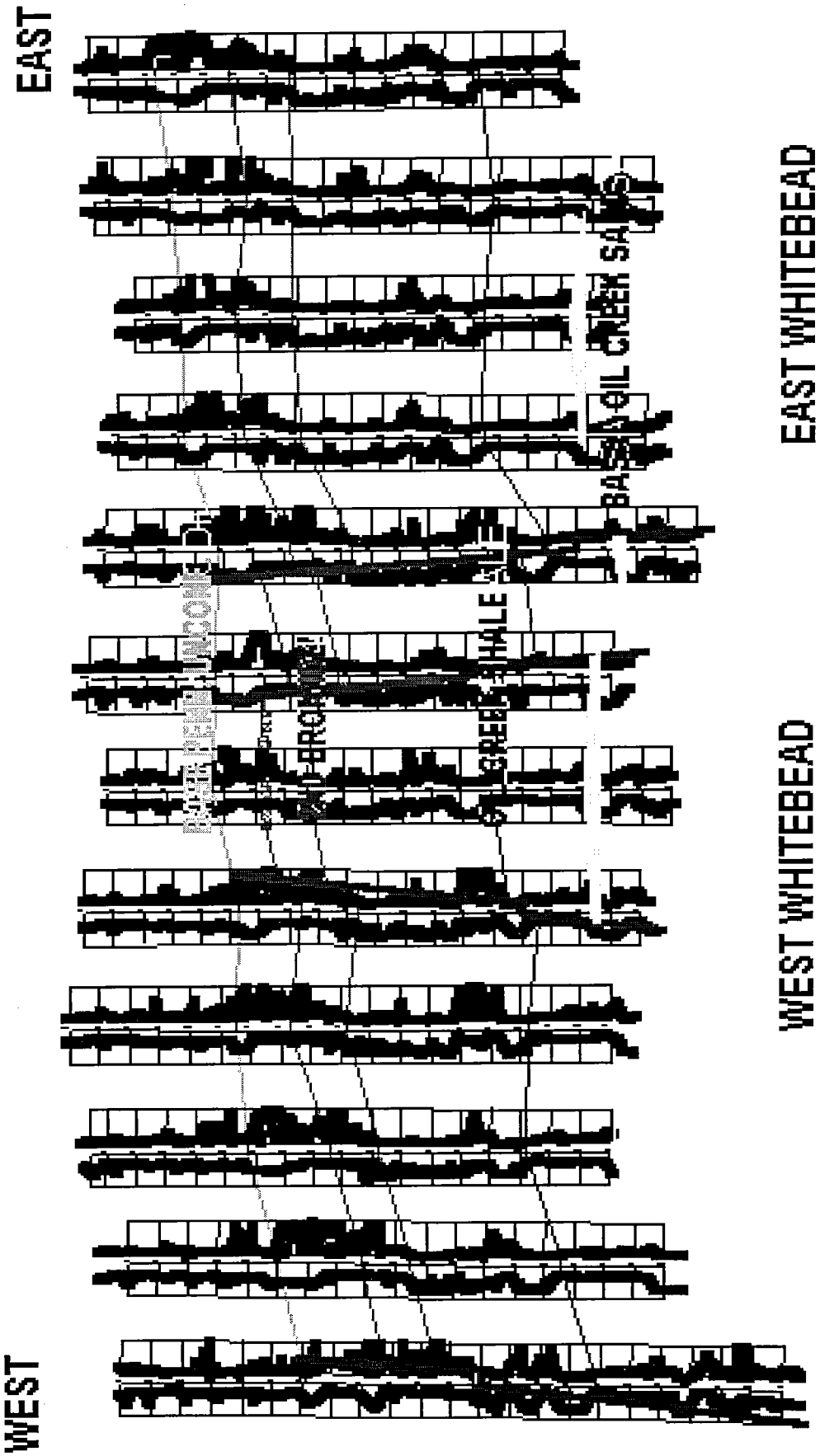

Figure 15. Cross section from west to east across Whitebead oil field, illustrating four separate levels of reservoirs.

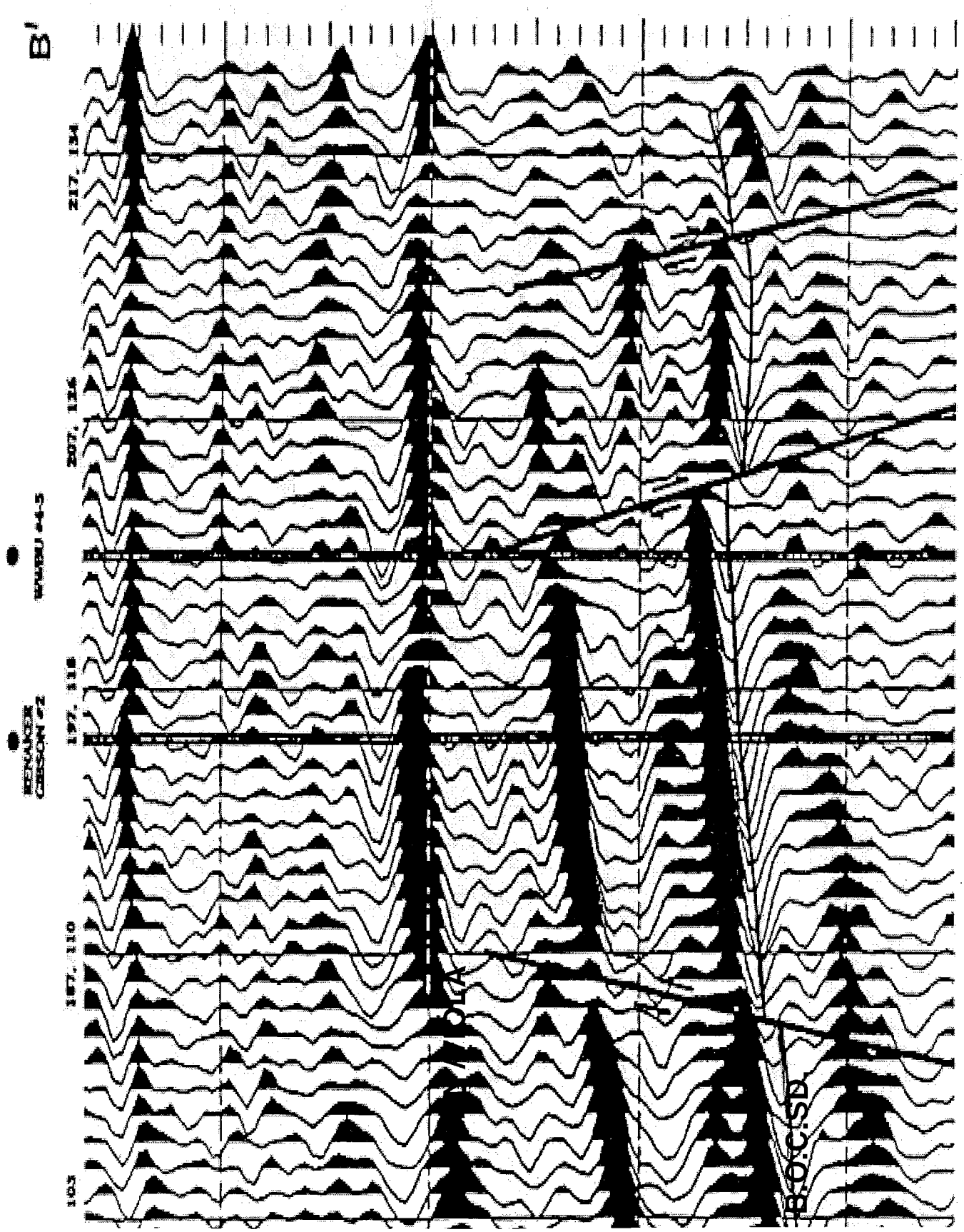

Figure 16. Vertical slice of 3-D seismic survey, indicating that No. 4-5 West Whitebead well is ~15 ms (90 ft) updip from No. 2 Rennicker-Gibson (the previous structurally highest well).

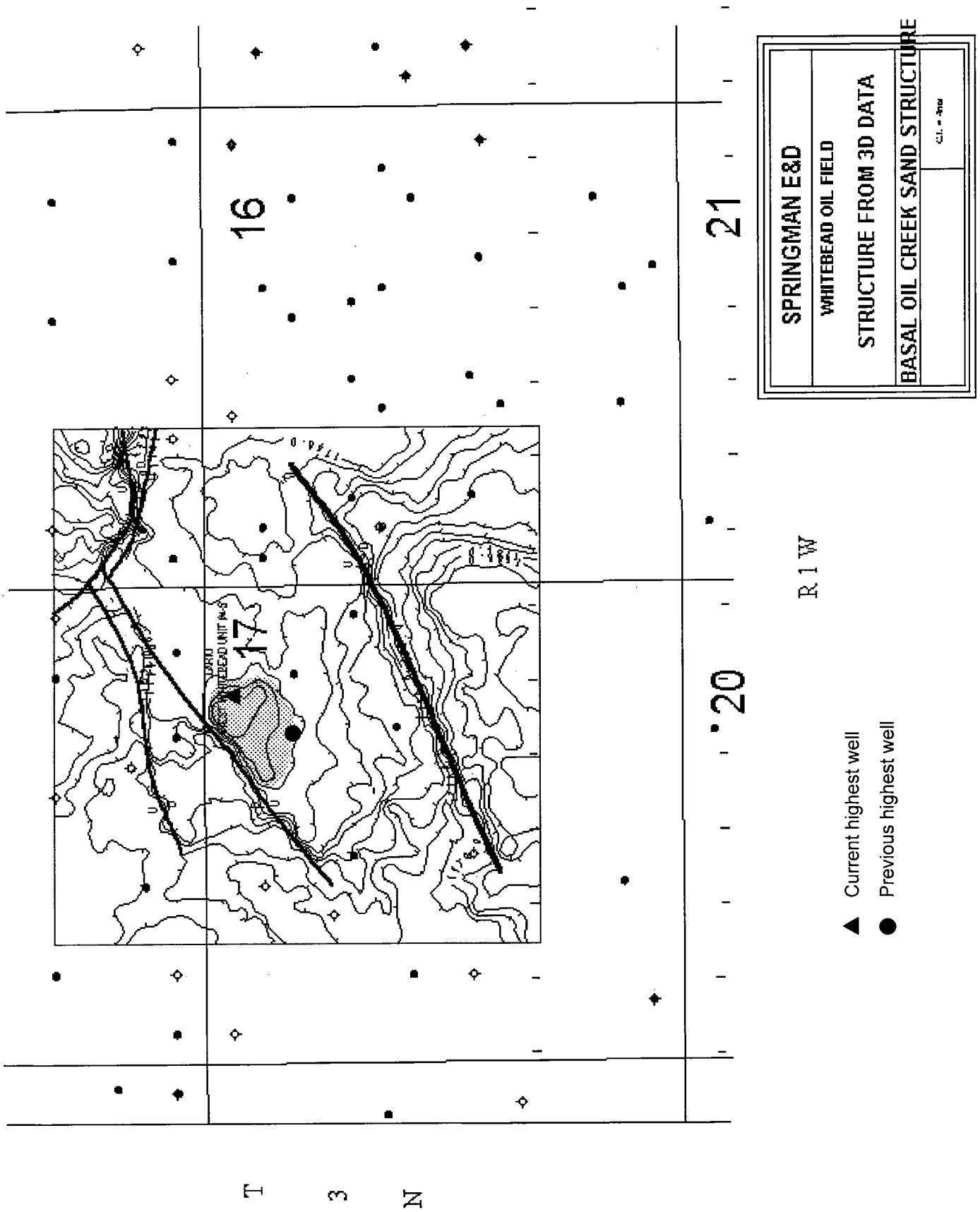

Figure 17. Final interpretation of 3-D seismic survey in Whitebead oil field, illustrating remaining "attic" oil. Contour interval, 4 ms (approximately 25 ft).

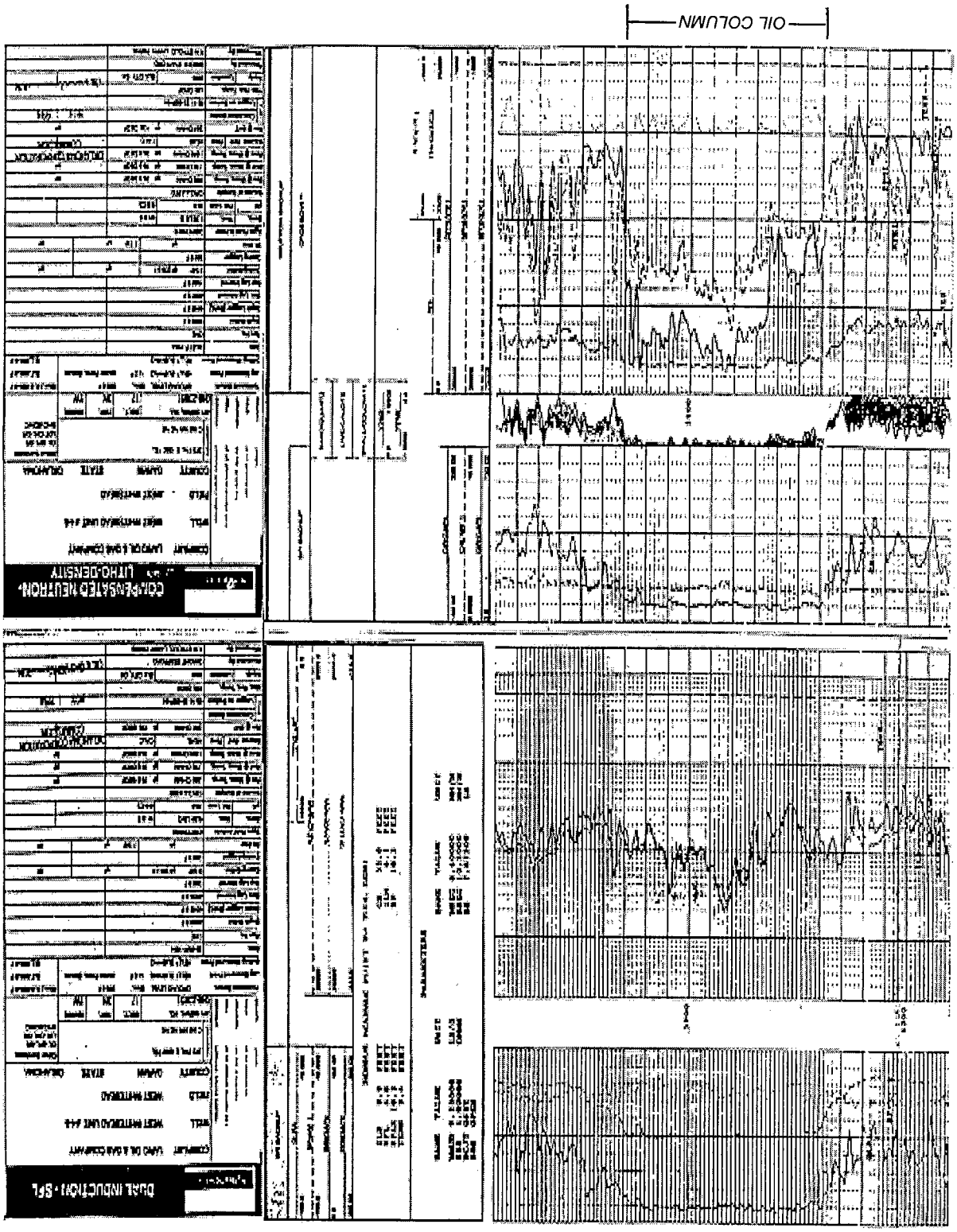

Figure 18. Log from No. 4-5 West Whitebead well, proving a 90-ft oil column updip from previously known oil column.

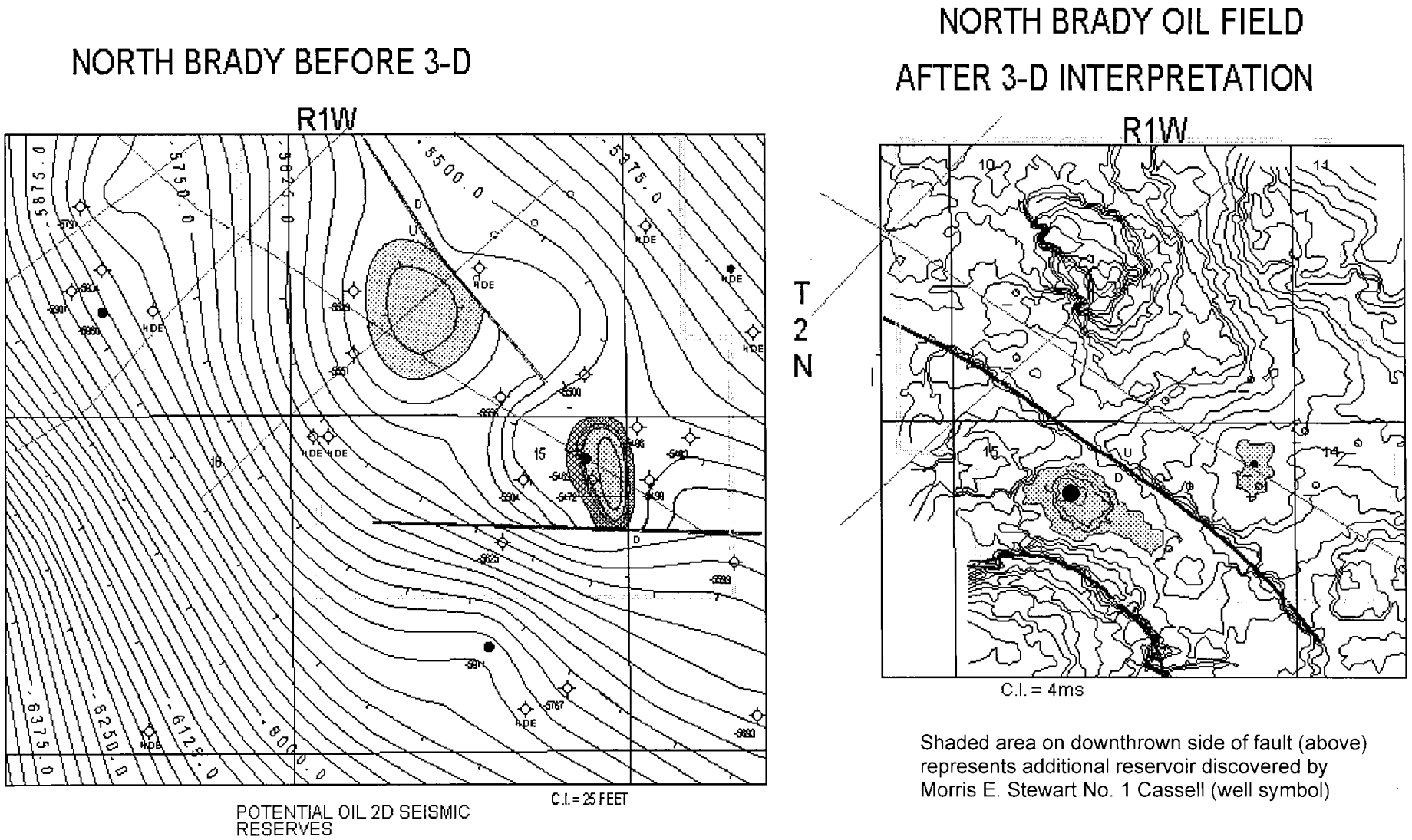

Figure 19. Maps of North Brady oil field area, showing comparison of structural interpretation before and after acquisition of 3-D seismic data.

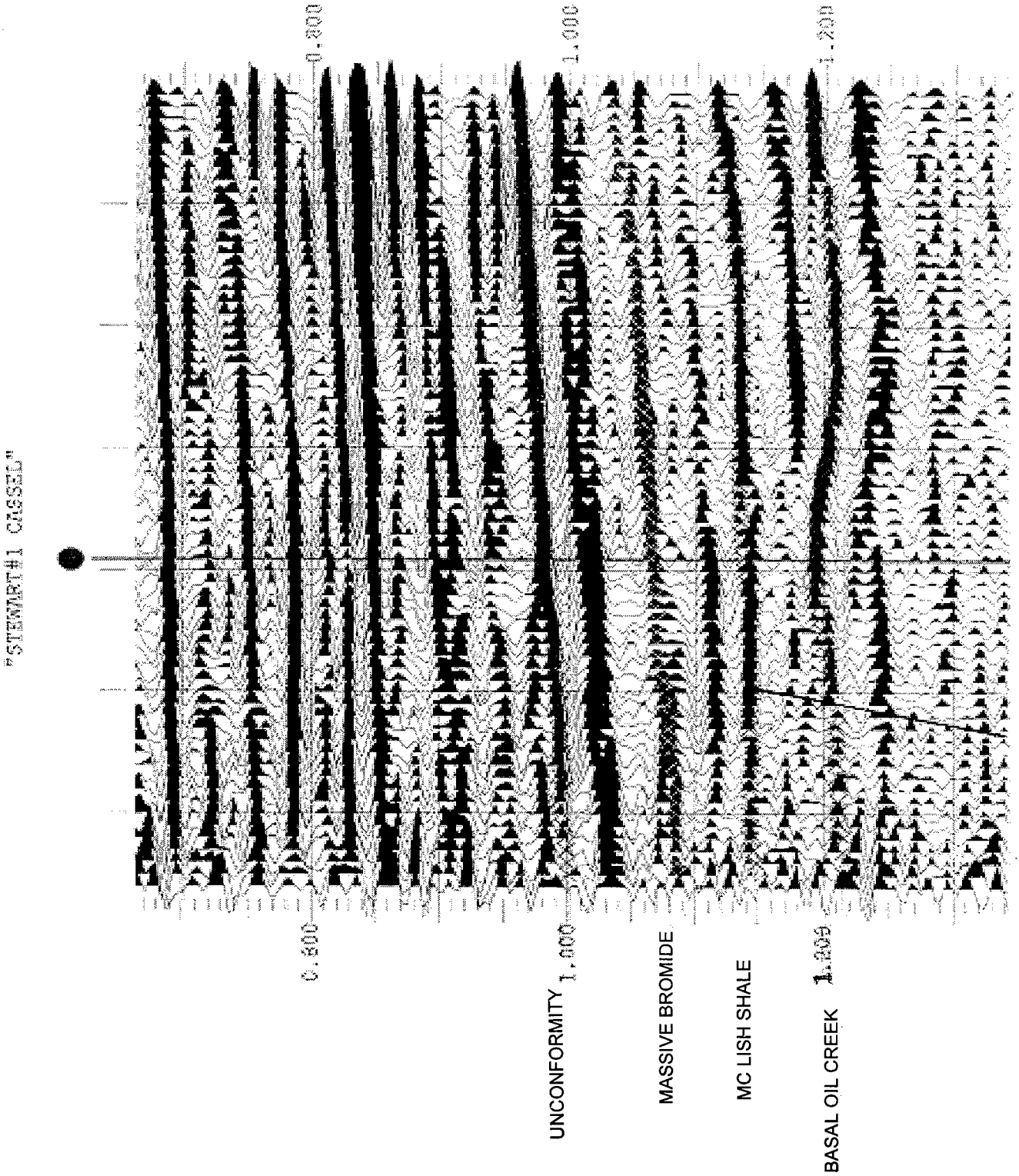

Figure 20. Vertical slice of 3-D seismic survey of North Brady field, showing Simpson sand reflectors and faulted basal Oil Creek sand structural roll.

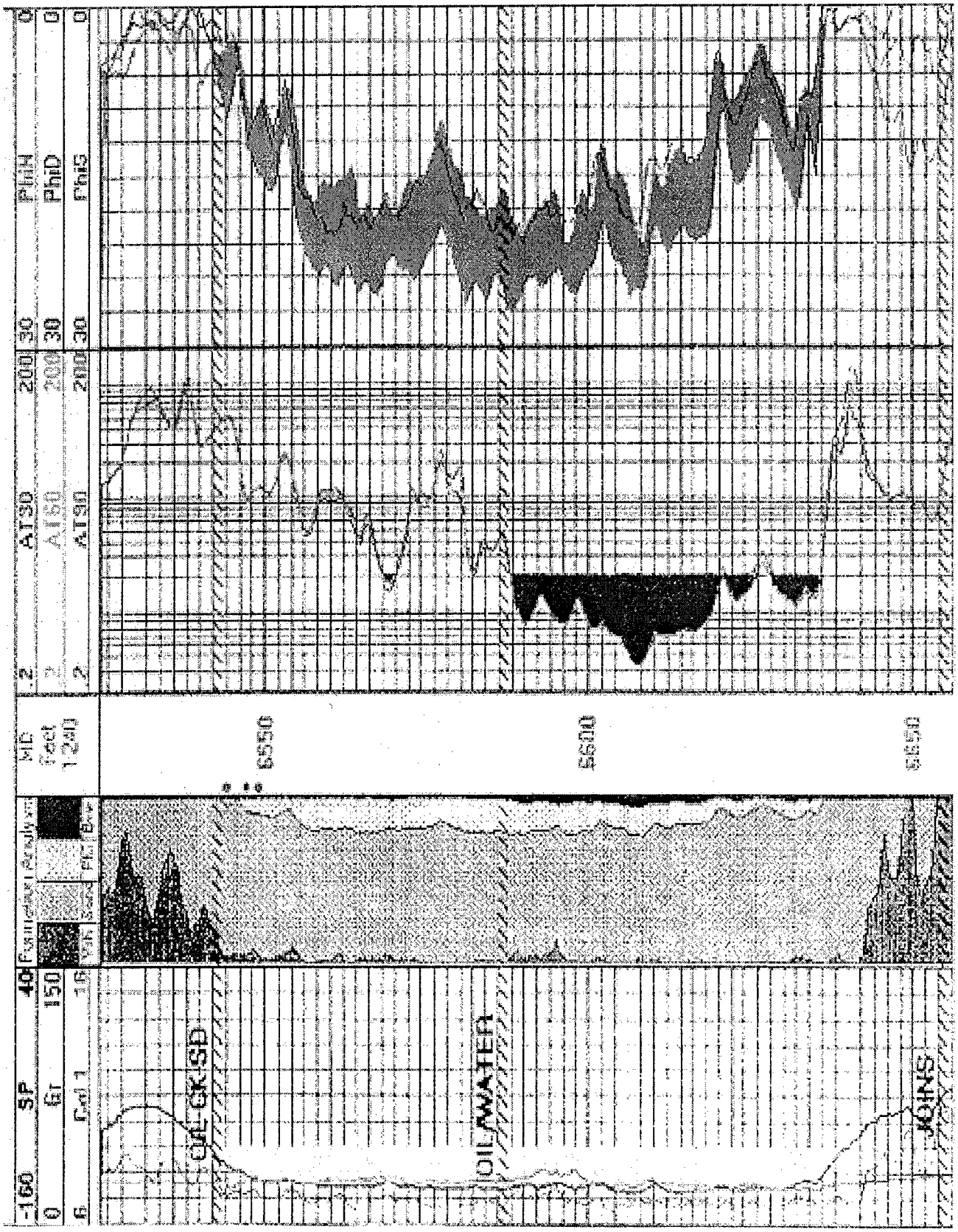

Figure 21. Log of Morris E. Stewart No. 1 Cassell well, showing obvious oil–water contact.

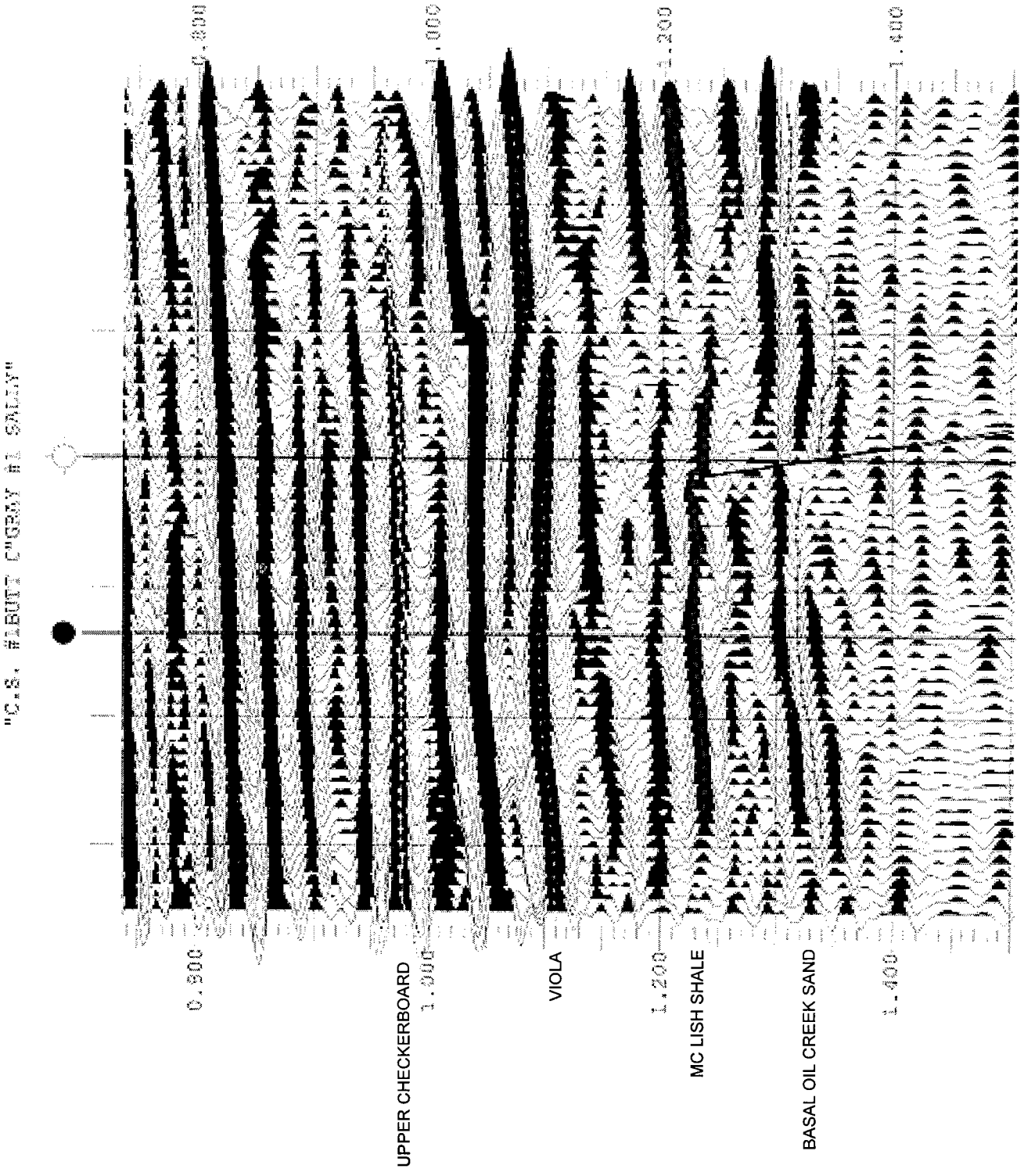

Figure 22. Vertical slice of 3-D seismic survey across South Brady oil field, illustrating how a dry hole could have been prevented with 3-D data.

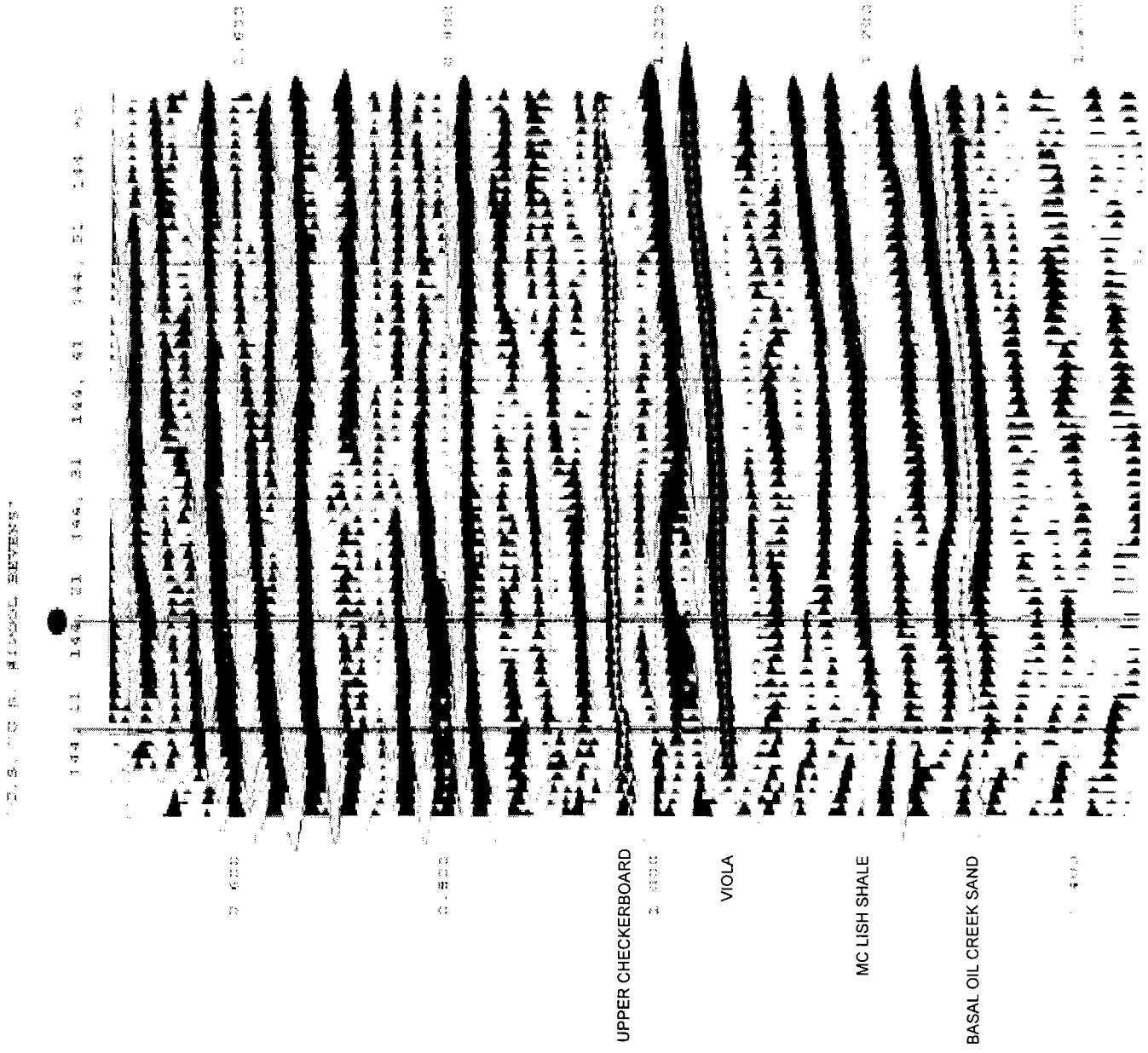

Figure 23. Vertical slice of 3-D seismic survey across Brady oil field, illustrating the subtlety of some productive Simpson sand structures.

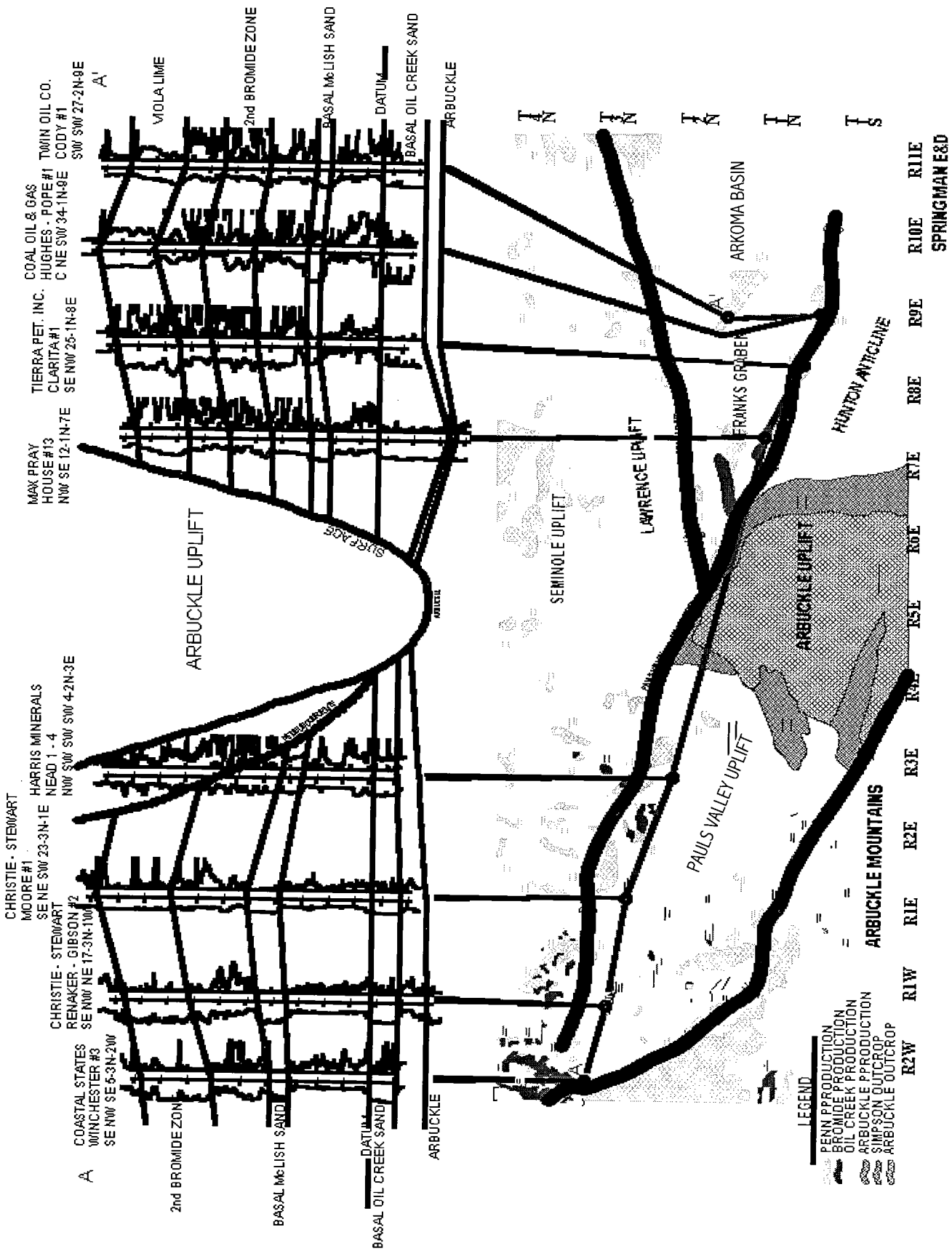

Figure 24. Cross section A–A´ and accompanying map (see Fig. 1), illustrating areas of Pennsylvanian production in addition to areas of production from Middle Ordovician and older reservoirs.

Remote Sensing of Geologic Structures in Highly Vegetated Areas: Digital Mapping in the Potato Hills, Southeastern Oklahoma

Galen W. Miller and Kevin J. Smart
University of Oklahoma
Norman, Oklahoma

ABSTRACT.—The use of remote sensing in highly vegetated areas for geologic mapping is a tool that geologists can use to save money and time. Remote sensing has been used in arid regions like the southwestern United States for decades. Recent advances now allow the techniques to be applied to densely vegetated regions of the country, and satellite images are more accurate and less expensive to purchase. Also, computers and software are more powerful and easier to use. These developments will lead to faster production and more accurate geologic maps.

The Potato Hills, in southeastern Oklahoma, is a region of dense vegetation and structural complexity. The Potato Hills, therefore, constitute a good case example for which to show these techniques.

INTRODUCTION

Remote sensing and geologic mapping are not new as individual entities. Combining the two, and the production of digital geologic maps, however, are new. The development of faster computers, the refinement of the software, and the quality of the images now available have made the process of creating digital geologic maps faster, cheaper, and more accurate. The use of satellite images can give new insight into problems faced in geologic mapping that cannot be observed while mapping on foot.

This project is part of a study of the mesoscale structures (1 cm to hundreds of meters) in the Potato Hills in an attempt to derive the origins of these hills. One of the tools required to perform this analysis is the creation of an accurate geologic map. Preliminary geologic mapping of the Potato Hills was performed with the aid of satellite images, digital elevation models (DEM), and digital raster graphics (DRG).

This paper consists of two sections: (1) a look at the use of satellite images to aid in the geologic mapping of an area of structural complexity and with large amounts of vegetation, and (2) the ways in which remote sensing and geographic information systems (GIS) software can aid in the creation of digital geologic maps.

PHYSICAL SETTING

The Potato Hills are in the Ouachita Mountains of southeastern Oklahoma. The Potato Hills are a roughly elliptical exposure of Ordovician through Mississippian rock units (Arbenz, 1968, 1989; Viele, 1989; Allen, 1990). They are in the central zone of the Ouachita Mountains fold and thrust belt (Fig. 1). This belt is characterized by mostly Mississippian and Pennsylvanian rocks folded into broad, open synclines and anticlines (Arbenz, 1968, 1989; Viele, 1989). The Ordovician through Mississippian rocks that constitute the hills were folded into a series of doubly plunging anticlines and synclines with a northwest vergence (Arbenz, 1989). The rocks consist of alternating siliceous shale and chert units (Fig. 2). These rock units were deposited as deep-marine sediments (Arbenz, 1989; Hatcher, 1989). The Potato Hills represent a window through the younger rocks, exposing the older rocks (Arbenz, 1968; Miller, 1955; Roe, 1955). The window was created when the thrust fault below the Potato Hills was folded, following movement on the fault (Miller and Smart, 2001).

The Potato Hills region is characterized by dense vegetation. A mixture of pines and oaks makes up the major species of trees in the region. Fields groomed for agriculture or pasture for cattle surround the Potato Hills. This region has an average annual rainfall of 46 in. per year (Pitt and others, 1982).

IMAGES FROM SPACE

Images from satellites are becoming better visually (both spectrally and spatially) and are less expensive to purchase. Also, the software programs used to manipulate the images have become easier to use and less expensive to purchase. This has led to a dramatic increase in the use of satellite imagery as a preliminary geologic-mapping tool. Most of the work done to this point has been in areas of low vegetation like the American Southwest or other desert regions around the world. The large amounts of vegetation in the Potato Hills hide the light-reflecting surfaces of rocks from the satellite sensors, cre-

Miller, G. W.; and Smart, K. J., 2002, Remote sensing of geologic structures in highly vegetated areas: digital mapping in the Potato Hills, southeastern Oklahoma, *in* Cardott, B. J. (ed.), Revisiting old and assessing new petroleum plays in the southern Midcontinent, 2001 symposium: Oklahoma Geological Survey Circular 107, p. 81–86.

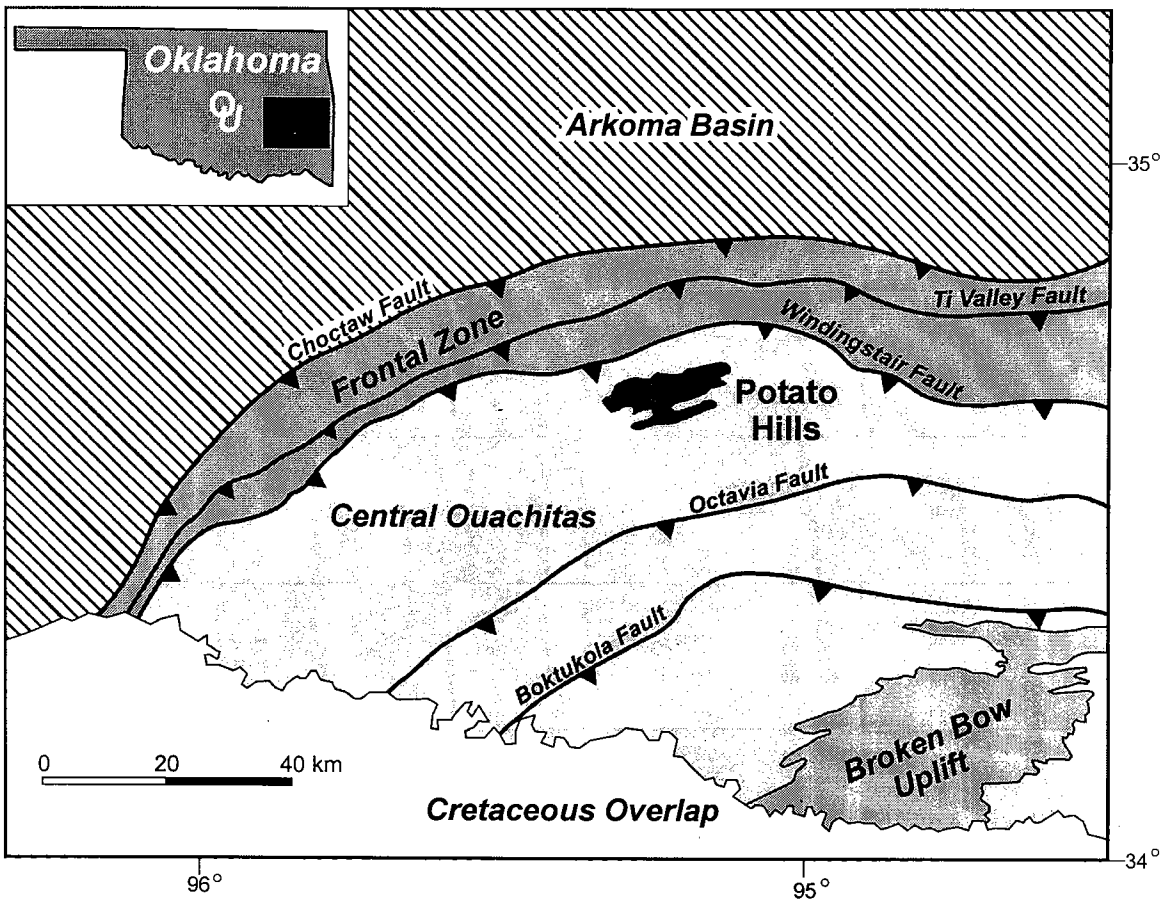

Figure 1. Schematic map showing the three structural zones of the Ouachita Mountains and the major thrust faults. Modified from Suneson and others (1990).

ating problems in mapping the rock units (Smart and others, 2000). Thus, techniques used in areas of dense vegetation differ from those used in desert areas. For example, variations in vegetation can be used to help determine rock types. Coniferous trees, such as pines, tend to grow in sandy soils, whereas deciduous trees tend to grow in shaly areas (Rowan, 1998). Some species, like the bristlecone pine (*Pinus longaeva*) of the western United States, favor only carbonate rocks like limestone or dolomite, and actually prefer dolomite over limestone (Fig. 3).

For this project, we acquired a Landsat image from August 23, 1995, and an Indian Remote Sensing (IRS) 1C LISS-3 image from March 22, 1997 (images courtesy of Space Imaging, Norman, Oklahoma). Each image has its advantages and disadvantages (see Table 1). The IRS image (Fig. 4) shows the progress of GHK, Inc., which is the most active gas-exploration company in the Potato Hills. The road used to bring the drilling equipment in on was reinforced with crushed limestone. This freshly crushed limestone is highly reflective. (Limestone is brought in, even though the Potato Hills are loaded with "natural gravel" in the form of fractured Arkansas Novaculite of Silurian through Mississippian age. The dust from this novaculite wears the teeth of horses and cattle prematurely.)

The spatial resolution of the IRS image is better at 23 m, re-sampled to 20 m, versus the 30-m resolution of the Landsat image (Table 1). Disadvantages of the IRS image include only four spectral bands, versus seven spectral bands for the Landsat image; also, the IRS image appears hazier than the Landsat image, almost eliminating the advantage of the higher resolution of the IRS image.

The images were very helpful from the start. The raw images showed quite a bit of information about the area even before manipulation. The IRS image shows the crest of a ridge formed by the Arkansas Novaculite that can be traced throughout most of the image (Fig. 4).

Manipulating the images brought a few more features into view. The major fault that created the window in the Potato Hills actually has two names at this point: the North Potato Hills thrust fault and the South Potato Hills thrust fault, which are actually the north and south exposures of the same fault. This one fault was given the two names before the theory of a window-type structure was advanced. Erosion through the upper stratigraphic units exposed the fault that helped to create the window (Miller and Smart, 2001).

CREATION OF THE DIGITAL MAP

When the region to be mapped is selected, the scale of mapping has to be decided upon. Mapping on 7.5-

PERIOD	SERIES	ARKOMA BASIN		OUACHITA MOUNTAINS
PENNSYLVANIAN	Desmoinesian	Krebs Gp.	Boggy Fm Savanna Fm. McAlester Fm. Hartshorne Fm.	
	Atokan	Atoka Fm.		Atoka Fm.
	Morrowan	Wapanucka Ls.		Johns Valley Sh.
		Union Valley Ls. Cromwell Ss.		Jackfork Group
MISSISSIPPIAN	Chesterian Meramecian Osagean Kinderhookian	Caney Sh.		Stanley Sh.
DEVONIAN	Upper	Woodford Sh.		Arkansas Novaculite
	Lower	Hunton Gp.	Frisco Ls. Bois d'Arc Ls. Haragan Ls.	
SILURIAN	Upper	Hunton Gp.	Henryhouse Fm.	Missouri Mountain Sh.
	Lower	Hunton Gp.	Chimneyhill Subgroup	
ORDOVICIAN	Upper	Sylvan Sh.		Polk Creek Sh.
		Viola Gp.	Welling Fm. Viola Springs Fm	Bigfork Chert
	Middle	Simpson Gp.	Bromide Fm. Tulip Creek Fm. McLish Fm. Oil Creek Fm. Joins Fm.	Womble Sh.
				Blakely Ss.
	Lower	Arbuckle Gp.	West Spring Creek Fm. Kindblade Fm. Cool Creek Fm. McKenzie Hill Fm. Butterly Dol.	Mazarn Sh. Crystal Mountain Ss.
CAMBRIAN	Upper	Arbuckle Gp.	Signal Mountain Ls. Royer Dol. Fort Sill Ls.	Collier Sh. ----?----
		Timbered Hills Gp.	Honey Creek Ls. Reagan Ss.	

Stratigraphy exposed in the Potato Hills

Figure 2. Stratigraphic column showing units exposed in the Potato Hills. Modified from Suneson and others (1990).

minute quadrangles would be at a 1:24,000 scale. Digital mapping enables data to be mapped at a 1:12,000 scale.

The acquisition of a base map should be the next step in producing a digital geologic map. The base map is usually provided in one of two formats. The U.S. Geological Survey prefers using USGS 7.5-minute topographic maps as a base. Digital raster graphics (DRG) files are the format in which standard 7.5-minute topographic maps are digitally available. These DRG maps were scanned into a digital format from paper maps. The resolution is usually low (150 dpi) and is therefore pixilized and not very good for field mapping.

The other useful format is the digital elevation model (DEM). The DEM is a highly useful format for a topographic base map. The contour lines can be scaled automatically, and the lines representing the contours remain the same as the map is viewed at various scales. This is very helpful when sections of the map are enlarged and printed for field-checking data. The contour lines on the DRG cannot be scaled with the image, and therefore the images get larger and smaller as you zoom in and out. This becomes a problem when performing detailed mapping, because there is no room to display the geologic data.

The aspect view of the DEM proved to be most helpful for mapping in the Potato Hills. Aspect viewing gives the slope direction by identifying the downslope direction of the maximum rate of change in value from each cell to its neighbors. The two ridge-forming units—the Arkansas Novaculite and Bigfork Chert (see Fig. 2)—are easy to see in the DEM format. The Ordovician Bigfork Chert forms the high ridges, and the Arkansas Novaculite the low ridges. The DEM shows the Bigfork as dark gray to black and the Arkansas Novaculite as lighter gray (Fig. 5).

The DRG and DEM images can be manipulated to become transparent and placed to "geo-rectify" a satellite image. The geo-rectification of the image allows the features on the satellite to be aligned with geographic features like roads on the topographic base maps. This allows maps created for the field to be spot-checked much more easily, and things you think you see can be confirmed with the placement of the topographic map over the satellite image.

Drawing the geologic map in Arc View GIS software is a process that requires some practice. It takes time to learn how to manipulate the polygons that are used to create the units exposed at the surface. The first map was created by using the Micrografx Designer program. The process is basically the same as drawing the map in Arc View but with much better drafting tools. Micrografx Designer allows greater control when creating the polygons, because the curves are easier to manipulate. The disadvantage of the Micrografx Designer program is the inability to import satellite images from the DEM and DRG files. The drawing utilities in Arc View are poor and will not enable the

Figure 3. When the substrate is hidden, plants can provide clues to the location of geologic features. This example from California shows bristlecone pines growing rather well on the Reed Dolomite and not growing on the overlying shale of the Deep Springs Formation. Photograph by Galen Miller.

Table 1. — Comparison of Spatial and Spectral Satellite Capabilities[a]

Satellites	Landsat 5 TM	IRS LISS - 3
Image date	08-23-95	03-22-97
Resolution	30 m	23.5 re-sampled to 20 m
Scene width	185 km	142 km
Revisit coverage at equator	16 days	24 days
Blue	0.45–0.52 μm	—
Green	0.52–0.60 μm	0.52–0.59 μm
Red	0.63–0.69 μm	0.62–0.68 μm
Near IR[b]	0.76–0.90 μm	0.77–0.86 μm
Mid IR	1.55–1.75 μm	1.55–1.70 μm
Thermal	10.4–12.4 μm	—
Mid IR	2.08–2.35 μm	—

[a]Data courtesy of Space Imaging, Inc.
[b]Infrared.

creation of curves. Curves can be created in Arc View, however, by placing many flexure points closely together to give the illusion of a smooth curve. In reality, Arc View creates a series of small straight-line segments, and magnification of these contacts reveals the problem of using such segments in creating curves.

CONCLUSIONS

The new technology available for mapping has made it possible to create a geologic map that is almost too accurate in the sense that rock-unit contacts can be placed on maps with such accuracy that the drafted contact line is wide enough to create error on the map. The technology in the long run will make geologic maps much easier, cheaper, and faster to make. Geologists will be able to perform much of the mapping before going into the field with the aid of this new technology.

The use of digital imagery is another tool for geologists to use but should never replace good field work. Geologists will always perform field work, and the new techniques will enable field geologists to concentrate on the more structurally complex areas of the study zone and not waste time and money on areas lacking such complexity.

REFERENCES CITED

Allen, M. W., 1990, An analysis of mesoscopic structures in selected areas within the Potato Hills, Ouachita Mountains: Fort Hays State University, Hays, Kansas, unpublished M.S. thesis, 59 p.

Arbenz, J. K., 1968, Structural geology of the Potato Hills, Ouachita Mountains, *in* Cline, L. M. (ed.), A guidebook to the geology of the western Arkoma basin and Ouachita Mountains: Oklahoma City Geological Society Guidebook, p. 109–121.

_____1989, Ouachita thrust belt and Arkoma basin, *in* Hatcher, R. D., Jr.; Thomas, W. A.; and Viele, G. W. (eds.), The Appalachian–Ouachita orogen in the United States: Geological Society of America, Boulder, Colorado, The Geology of North America, v. F-2, p. 621–634.

Hatcher, R. D., Jr., 1989, Tectonic synthesis of the U.S. Appalachians, *in* Hatcher, R. D., Jr.; Thomas, W. A.; and Viele, G. W. (eds.), The Appalachian–Ouachita orogen in the United States: Geological Society of America, Boulder, Colorado, The Geology of North America, v. F-2, p. 511–535.

Miller, B. W., 1955, The geology of the western Potato Hills, Pushmataha and Latimer Counties, Oklahoma: University of Oklahoma unpublished M.S. thesis, 55 p.

Miller, G. W.; and Smart, K. J., 2001, Structural development of the Potato Hills: how meso- and macro-scale studies aid in the understanding of the development of the Ouachita orogeny, southeastern Oklahoma [abstract]: Geological Society of America Abstracts with Programs, v. 33, no. 5, p. A19.

Pitt, W. D.; Fay, R. O.; Wilson, L. R.; and Curiale, J. A., 1982, Geology of Pushmataha County, Oklahoma: Eastern New Mexico University Studies in Natural Sciences Special Publications 2, Portales, New Mexico, 101 p.

Roe, N. C., 1955, Geology of the eastern Potato Hills, Pushmataha and Latimer Counties, Oklahoma: University of Oklahoma unpublished M.S. thesis, 63 p.

Rowan, L. C., 1998, Remote sensing in the USGS Mineral Resources Surveys Program in the eastern United States: U.S. Geological Survey Information Handout, accessed August 1998, http://pubs.usgs.gov/info-handout/rowan/.

Smart, K. J.; Miller, G. W.; and Dewars, T. A., 2000, Integration of digital techniques into traditional geologic mapping: case studies of teaching and research applications [abstract]: Geological Society of America Abstracts with Programs, v. 32, no. 7, p. A515.

Suneson, N. H.; Campbell, J. A.; and Tilford, M. J., 1990, Geologic setting and introduction, *in* Suneson, N. H.; Campbell, J. A.; and Tilford, M. J. (eds.), Geology and resources of the frontal belt of the western Ouachita Mountains, Oklahoma: Oklahoma Geological Survey Special Publication 90-1, p. 1–4.

Viele, G. W., 1989, The Ouachita orogenic belt, *in* Hatcher, R. D., Jr.; Thomas, W. A.; and Viele, G. W. (eds.), The Appalachian–Ouachita orogen in the United States: Geological Society of America, Boulder, Colorado, The Geology of North America, v. F-2, p. 555–561.

Figure 4. IRS LISS-3 satellite image, acquired March 22, 1997. The image shows the progress of GHK, Inc., at the time of image acquisition. Two well pads and the supply road can be seen clearly (*A*), and the image shows most of the folds in the Arkansas Novaculite south of the well pads (*B*). Image courtesy of Space Imaging, Norman Oklahoma.

Figure 5. Digital elevation model (DEM) of the Potato Hills. This image comprises the Albion, Kiamichi, and Yanush 1:24,000-scale (7.5-minute) quadrangles from east to west. The image shows how a DEM can be used to identify rock units on the basis of ridge-forming characteristics. The Bigfork Chert (*Ob*) is the highest ridge former and therefore the darkest in color. The Arkansas Novaculite (*MDSa*) is a lower ridge former and is lighter in color.

Arkoma Basin Coalbed Methane—Potential and Practices

John H. Wendell, Jr.
Wendell Consulting, LLC
Fort Worth, Texas

ABSTRACT.—Coalbed methane (CBM) from the Hartshorne, Upper Hartshorne, and Lower Hartshorne coal beds of the Hartshorne Formation (Pennsylvanian, Desmoinesian) has been successfully and economically produced in the Oklahoma portion of the Arkoma basin. In the Kinta–Stigler area the average coal thickness is ~5 ft at depths of 600–2,400 ft. In the Poteau area coal thicknesses are 4–10 ft at depths of <700–4,500+ ft.

The produced gas is 97–98% methane, with about 970–990 Btu per thousand cubic feet. Ultimate recoverable reserves for the average CBM well in the Kinta area are estimated to be 350 million cubic feet of gas.

Air-drilling with small, mobile rigs is generally used for the CBM wells, with few problems encountered. Most downhole surveys consist of gamma-ray and density logs.

Well-completion practices usually include hydraulic fracturing with sand as a proppant. Experience has shown that injection of most chemicals is detrimental to coal permeability, in many cases significantly curtailing production. The most successful fracture treatments are straight water "fracs" with the largest diameter proppant that can be successfully carried and placed deep within the frac channels and continuously to a packed wellbore.

INTRODUCTION

The Arkoma basin has become a very active area for coalbed-methane (CBM) exploration. This paper describes the items that I believe are important to understand in developing this resource properly. The geologic setting and engineering and economic factors are covered, as well as lessons learned from practicing in the development of CBM since 1989 in the basin.

GEOLOGY

Coal beds and sandstones of the Hartshorne Formation, part of the Pennsylvanian Desmoinesian (Strawn) Series, are present beneath a large portion of the acreage in the Arkoma basin. Within the area of consideration, the depth of the Upper Hartshorne coal member below the surface varies from about 650 ft to 4,000 ft, and the thickness of coal in the Arkoma basin varies from a low of 3+ ft to >9 ft in the Upper Hartshorne coal seam alone. The Kinta–Stigler area exhibits an average coal thickness of ~5 ft at a 600–2,400-ft depth. In the Poteau area, the Lower Hartshorne coal seam ranges in depth from <700 ft (Hartford anticline) to >4,500 ft (Cavanal syncline), with thicknesses from 4 to 10 ft.

In the CBM prospective areas, the upper Hartshorne sandstone is sporadically present and exhibits porosity that is generally <8%, which denotes the productive limit to most operators. Some high-porosity intervals of producible Hartshorne sandstone have been found while drilling for Hartshorne coals. Additional potentially productive coals and sands overlie the Hartshorne, notably the Booch sandstone of the McAlester Formation, but are not included in this discussion.

Background and supporting geologic data were obtained from four definitive published reports that encompass the area of interest: Friedman (1982), Houseknecht and Iannacchione (1982), Rieke and Kirr (1984), and Iannacchione and Puglio (1979).

The cross section in Figure 1 was reproduced from Hemish and Suneson (1997, fig. 4). It depicts generalized north–south geology across the Arkoma basin. The singular upper and split lower coals exist across the basin from the Eufaula area to the Poteau–Howe region. In actual drilling experience, in Haskell County, the coal bed encountered appears to be the "undivided" coal, and multiple coals are found in Le Flore County. The geology can be described as follows.

The Hartshorne Formation consists of the basal Desmoinesian strata of the Arkoma basin geologic column and is the basal member of the Krebs Group. Predominant marine strata of the Atoka Formation unconformably underlie nonmarine coal-bearing strata of the Hartshorne Formation. The McAlester Formation overlies the Hartshorne Formation.

The Hartshorne Formation is composed of a complex sequence of coal, shale, siltstone, and sandstone. It is generally accepted that these sediments were part of a prograding deltaic system that comprised a distributary-channel system, levee and overbank depos-

Wendell, J. H., Jr., 2002, Arkoma basin coalbed methane—potential and practices, *in* Cardott, B. J. (ed.), Revisiting old and assessing new petroleum plays in the southern Midcontinent, 2001 symposium: Oklahoma Geological Survey Circular 107, p. 87–100.

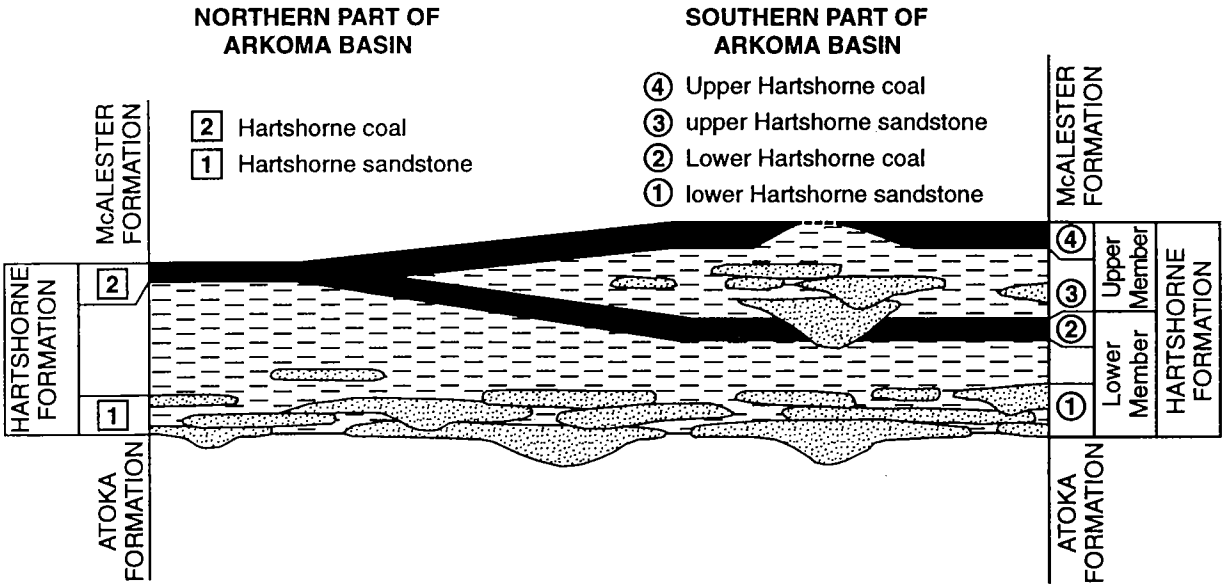

Figure 1. Generalized stratigraphic cross section, northern and southern Arkoma basin (from Hemish and Suneson, 1997, fig. 4).

its, interdistributary-bay sediments, crevasse splays, and wooded and peat swamps. The current analog of this environment is similar to that of the Lower Mississippi River–Atchafalaya River deltas, channels, and swamp complexes.

The Hartshorne Formation is subdivided into the lower Hartshorne sandstone, Lower Hartshorne coal, upper Hartshorne sandstone, and Upper Hartshorne coal. Houseknecht and Iannacchione (1982) postulated that most of the Hartshorne facies were deposited within a deltaic system, an interpretation that agrees in general with previous work by Hendricks (1937), Scruton (1950), and McDaniel (1968). Some geologists define a thickened Hartshorne sediment series with an additional delineation of a "Middle Hartshorne" coal and sandstone, but most recognize only the terms *upper* and *lower*, with the thickened middle as part of either. Westward migration of this depositional system resulted in a wide-area development of deltaic- and prodeltaic-front facies that were capped by distributary-channel sandstones ranging up to 250 ft thick.

Lateral facies deposition and gradation were governed, as in normal deltaic environs, by the development of lenses and channels in distributary-channel fashion. When the delta progressed to the present southwest, sand, silt, and carboniferous sediments were in competition. In general, where large sand channels exist, the coal thins or is not present. This could have occurred because the peat could not have accumulated in areas where higher energy water velocity, either from or near channels, would have carried the carbonaceous materials away, resulting in nondeposition. Conversely, in areas where peat accumulations did occur, the redirection of flow channels eroded the coal-generating deposits and replaced them with channel sands. Therefore, the coal is thicker and of higher quality away from massive deposits of the upper Hartshorne sandstone. However, thicker Lower Hartshorne coals (5–8 ft) have been found in the area southeast of Poteau, Oklahoma, overlying high-resistivity lower Hartshorne sands with thicknesses of 60–100 ft and with porosities of 8–16%. These sands lie directly south of the Poteau-Gilmore gas field, which has produced 40 billion cubic feet of gas (BCFG) from 105 wells in thick channels of the lower Hartshorne sands. Farther north, in the Cameron area, a prolific field from the upper Hartshorne sand has produced since the 1930s.

The Lower Hartshorne peat accumulated in a lagoonal environment until the lower Hartshorne delta slowly sank beneath the water's surface, inundating the peat deposits and allowing silts and muds to be deposited above them. Thereafter, the Hartshorne delta again became active, and a second cycle of depositional events caused the upper Hartshorne sandstone and the Upper Hartshorne peat to be deposited and again to be overlain by silt and mud. Through compaction, under the weight of subsequently deposited McAlester and younger formations, the mud became shale, and the peat metamorphosed through the coalification stages into bituminous coal. Thermal maturation and the degree of compaction were significant as the coals evolved into semianthracite in the eastern areas of the Arkoma basin and graded into high-volatile bituminous coal in the western reaches of the basin.

In the Cameron area the coal has been found to be medium- to low-volatile bituminous (vitrinite reflectance of 1.58%), ranks that are extremely favorable for coalbed-methane development. Cores in the Spiro area are characterized by vitrinite reflectances of similar or higher values. Analyses of coal in cores from

the Quinton area (west of Kinta) confirm that the coal is medium-volatile bituminous and consists of a high percentage of vitrinite with fixed carbon in the mid-70% range. Gas contents of net ash-free coal in the Cameron area have been evaluated as averaging 585 cubic feet of gas per ton (CFG/ton) from desorptions of coals near a 1,350-ft depth. Ash contents vary from 8% to >35%. Low-volatile bituminous coal produces approximately 3 thousand cubic feet of gas per ton (MCFG/ton) during coalification. With approximately 0.6 MCFG remaining with the coal, mostly in an adsorbed state, almost 2.4 MCF of methane migrated out of the coal and is either trapped in sands, shales, and other rocks, or vented to the atmosphere.

The Hartshorne sandstone has been a prolific producer throughout the Arkoma basin, and it is also potentially prospective in many of the prospect areas. Notable fields with Hartshorne sandstone reservoirs are near McAlester, Cameron, and Poteau. In the vicinity of the upper Hartshorne sandstone at some localities the coal thins and vanishes entirely directly over the main body of sand. However, as described above, the coal is thicker on the flanks of the upper Hartshorne sandstone and grades from 2 to 8 ft in thickness, for each coal member, as it moves away from the thicker sand channel. This agrees with the findings of Houseknecht and Iannacchione (1982).

The geology was validated in the area of study from a combination of other operators' offsets and logs from nearby wells, as well as from results of the U.S. Bureau of Mines' coring and desorption of coal-test wells. Also used was information from other CBM operators, coal-company cores, surface geology, interpretation of seismic lines in the area, well logs, and core analyses and sample data provided from recently drilled wells in the area.

In the CBM areas, several regional faults trend in a general northeast–southwest direction. These are typical thrust faults, with gentle to greater folding, resulting from the regional deformation. Each fault segment exhibits minor to significant rollover, with more pronounced bending at the juncture of the formation–fault interfaces. The faults generally show that the blocks were overthrust and, in some cases, relaxed back, with the resulting alignment being close to the original positioning that existed before faulting. In the vicinity of the Kinta field and Poteau, both synclinal and anticlinal structures are present, as shown in Figure 2.

During the thrusting and relaxing events, some splinter, or secondary, thrust faults, minor relaxation faults, and minor fracturing occurred. The thrusting caused isolated cases of vertical structural development that may be sufficient to minimize coalbed-dewatering requirements. Mapping the structure at the top of the Upper Hartshorne coal, using data from several area operators' drilled wells, showed the structural configuration to be essentially as postulated in earlier geologic work.

The structure in the vicinity of the wells studied is controlled by the thrust faults in and surrounding the Arkoma basin. The compressional or thrusting forces were applied in a direction from the southeast to the northwest during the Ouachita orogeny, which defined the Arkoma basin's structural orientation. This stress and resultant deformation caused cleating of the coal to form butt cleats, trending essentially northeast to east-northeast, generally parallel to the structural trends in the area.

The analysis of cores by Sam Friedman (Oklahoma Geological Survey) from the Aztec well in the SW¼ sec. 10, T. 6 N., R. 26 E., established that face cleating occurs approximately 75° to the butt cleats and therefore approximately parallel to the axis of compression. It then follows that the butt cleats parallel the axis of deformation.

This confirmed work reported by Iannacchione and Puglio (1979) using the methodology devised by Diamond (1976) for measuring cleat directions at strip mines and other surface exposures in the eastern Arkoma basin. The direction of face and butt cleating from this work established that the face cleats are essentially perpendicular to structural trends in the area and range in direction from N. 32° W. to N. 17° W. The friability of the Hartshorne coal is due to close cleat spacing and numerous shear fractures that dip 45–55°. The cleating establishes the natural permeability in the coal, which, as exhibited through injection tests in area wells, can be as much as 30 md or better. Cleat spacing is 10 per in., and some natural fracturing was also present in the Aztec sec. 10 core.

Analysis of the thrusting and faulting in the area confirms that the major horizontal stress was from southeast to northwest. Wells generally are fractured parallel to the major stress in the formation. However, the stress fields are complex and are modified by thrusting and relaxing. Also, stress has transitioned from compression to tension where strata have draped over and fallen from anticlines into synclines. Conversely, the compressional stress may have been increased in the bottom of synclines. This would indicate that the "frac" orientation would probably follow the plane of the butt cleating and be essentially southwest to northeast, moving from ridges paralleling the structural trend and progressing into synclines.

Comments by Iannacchione and Puglio (1979) characterized the area coals as gas bearing and the presence of gas at high enough levels to constitute a serious potential safety hazard for future deep mining. Recovered coal samples evaluated from recently drilled wells have confirmed the coal rank as low-volatile bituminous. Desorption tests on recently and previously drilled wells in the basin show gas contents ranging from a low of 450 to >750 CF/ton for clean coal.

Early CBM gas production in the Arkoma basin relied on natural completions or very small nitrogen injections for stimulation. More aggressive methods are now in use to liberate and produce the coalbed methane.

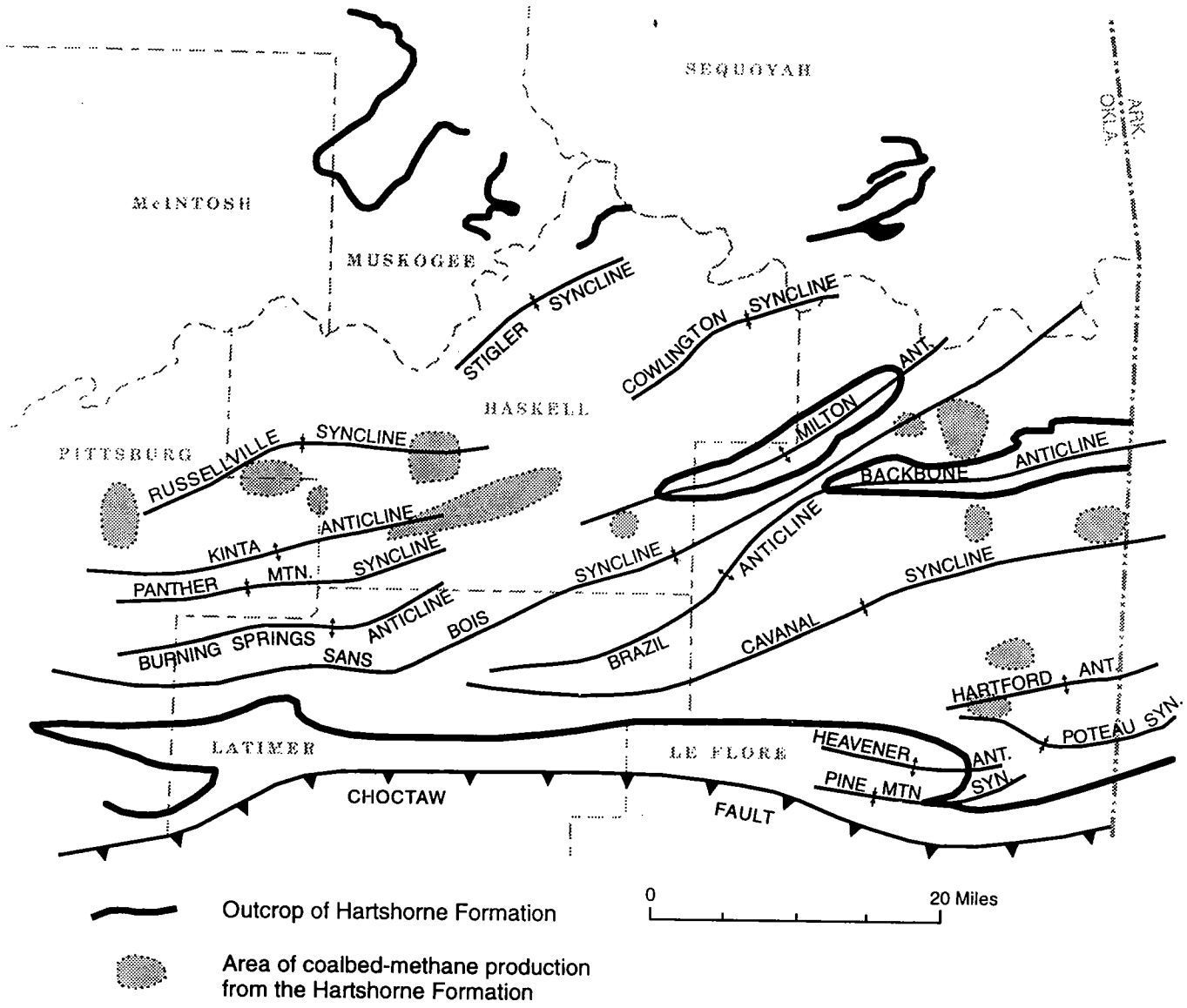

Figure 2. Map showing structural features that influence stress and faulting in the Hartshorne Formation (modified from Hemish and Suneson, 1997, fig. 8).

DRILLING METHODS

Air-drilling with small, mobile rigs is generally used for the CBM wells in the Arkoma basin. Drilling conditions are generally benign, with few problems from heaving shales, large water flows, or high-pressure formations that could cause blowouts. The drilled rock is usually competent, with few lost holes. The logs required are minimal and normally consist of gamma ray and density. For wells of 3,000 ft or less, 4½-in. casing is sufficient. The most effective method is to set the casing through the coal with 150 ft or more of "rathole" below the producing interval. The cement job favored by most operators is the "alternate casing program" in which the casing is cemented back to the surface. Care must be taken when cementing to prepare the hole sufficiently with gel and other sweeping agents to clean the hole. The use of various fluid-loss materials, ground-up coal, "cello-flake" (shredded cellophane), gels, and other substances are needed to lighten the cement and to preclude cement invasion into the coal. Concurrently, the cement should be designed to prevent cement loss into thief zones and cement bridge-off.

Cement-bond logs are run, and the casing is perforated with jet guns. There are different ideas on how dense to shoot the coal. A few operators prefer to shoot only a minimum number of holes to limit entry into the coal. This rationale is that limited entry would produce fewer coal "fines." On the contrary, I use at least eight shots per foot of 23-g shaped charges that make a 0.52-in. entry hole. This perforation density reduces friction and lowers the velocity of fluids entering the coal, which should also minimize the generation of fines and the shearing of the coal with attendant coal-slurry and pressure problems. After perforating, the coal is stimulated by using a variety of

methods. My preferred stimulation methods are discussed later in this paper in the section "Fracturing Coal for Increased Production."

Following fracture treatment, the well is washed out to bottom, and tubing, pump, and rods are run. Electricity is available in most areas for pumping. Salt water must be disposed of. The average requirement is one salt-water-disposal well for each 30–50 producing wells. Several depleted zones from earlier production exist in much of the area, as well as wet Booch and Hartshorne sands. All of these have proved to be adequate for disposal wells.

The Arkoma basin is laced with pipelines from numerous carriers, which provides competitive avenues for marketing and transporting the gas.

CALCULATION OF CBM RESERVES

High-resolution logs are available from several logging companies. The logs favored by me for coal evaluations consist of bulk density, neutron porosity, density porosity, caliper, and gamma ray. Both 5-in. and 100-in. high-resolution (HR) logs are run. The HR processing generates an expanded log that provides up to 10 definable data points per foot. A representative expanded log section from a CBM well in Le Flore County, Oklahoma, is reproduced in Figure 3. The bulk-density curve provides high-resolution data through the coal measure that may be either manually or machine digitized into analysis programs to calculate the potential recovery of methane.

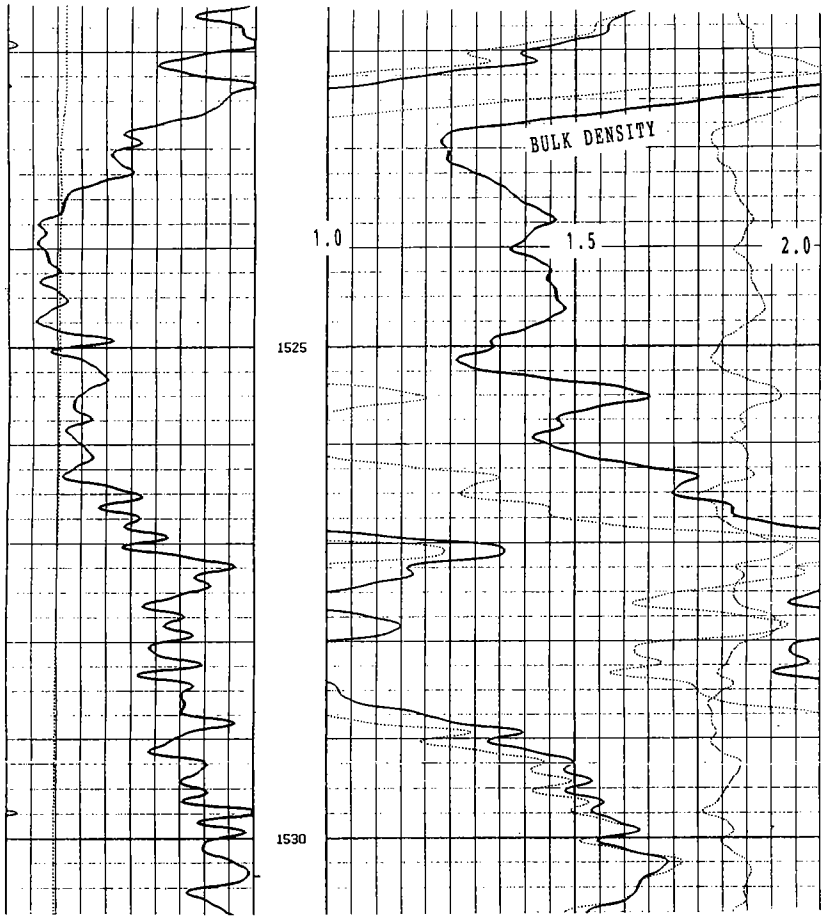

Figure 3. Density log from a CBM well in Le Flore County, Oklahoma. This is a high-resolution log, reduced from original 100-in. scale.

Coal exists in varying degrees of purity, depending on the amount of its other constituents such as clays/shales, sands, and other contaminants and minerals found with the various forms of carbon (coal). These contaminants result in differing amounts of "dry ash," which can be calculated on the basis of the purity as indicated through the specific gravity of the coal sample. Pure coal has a specific gravity of approximately 1.18 g/cm^3, and carbonaceous shale that produces 100% dry ash has a specific gravity of about 2.68 g/cm^3. The dry-ash content of the coal can be calculated by using the assumption that coal varies linearly on the continuum from 0% to 100% ash (specific gravity of 1.18 to 2.68). Therefore, the dry-ash content of the coal can be calculated by simple ratios or through the use of the following equation:

$$\text{Ash fraction} = (0.6666 \times \text{coal density}) - 0.7866.$$

If the dry-ash content of the coal is known from desorbed cores or from data provided through analysis of density logs, the ash-free component of the coal can be determined. Data for ash-free gas content can be taken from specific cores in offsets to the wellbore in question, or extrapolated from a body of data from a number of cores taken in the area, or through generic curves that represent gas content for classes of coal. The ash-free gas content, corrected for pressure (depth), can then be used to calculate the gas content of the coal under analysis in the purity level observed on the density logs.

While being a useful tool, this method of using log-obtained densities is not exact and is "prejudiced" to calculate a higher dry-ash content for higher density coals and therefore results in a lower gas-in-place content. For example, in a core analysis by Core Labs, Inc., from the Farrar No. 29-6 well, in sec. 29, T. 8 N., R. 27 E., Le Flore County, the average ash contents for two coal-core samples were as follows:

Sample no.	Depth (ft)	Ash-free gas content (SCF/ton)	Specific gravity (g/cm^3)	Ash (%)
1	1,346.8–1,351.7	575.0	1.75	32.2
2	1,359.1–1,360.9	595.9	1.48	27.6

Using the method outlined above, the coal with a

specific gravity of 1.75 would have an ash content of 38%, and the coal with a specific gravity of 1.48 an ash content of 20%. This provides a conservative cut-off value for the density that actually contributes gas but concurrently calculates a lower ash content for samples of lower density.

Iannacchione and Puglio (1979) used data from surface geology, logs, and 16 coal cores to define various Hartshorne coal characteristics. Cores were from depths of 200 to 1,500 ft and were taken between 1976 and 1978. The cores were subjected to U.S. Bureau of Mines (USBM) direct-method coal-desorption analyses. The data from these 16 desorption samples are shown on the graph reproduced in Figure 4. Regressing the data results in these equations:

$$\text{Gas content } (\text{cm}^3/\text{g}) = 6.251 \times ln_e \text{ (depth in feet)} - 27.882,$$

and

$$\text{Conversion factor} = 32.0375 \text{ ft}^3/\text{ton for 1 cm}^3/\text{g}.$$

Using these equations to calculate the ash-free gas contents and to compare the desorption tests of the coal by Core Labs, Inc., for the two recovered coal core samples from sec. 29, T. 8 N., R. 27 E., gives the following results:

$$\text{Sample 1 (1,349 ft)} = 550.2 \text{ ft}^3/\text{ton},$$

and

$$\text{Sample 2 (1,360 ft)} = 551.7 \text{ ft}^3/\text{ton}.$$

The USBM equation calculated approximately 94% of the actual gas recovered in the core measurements. Therefore, the use of the USBM equation for calculating gas in the area of Haskell County and the northern part of Le Flore County, in conjunction with the equations for calculating the dry-ash content of cores, would provide a useful tool for reserve projections but would usually trend toward the conservative side in the calculations.

KINTA AREA COALS

If you assume that the Aztec–Le Flore County cores were taken from wells with a standard pressure gradient of 0.433 psi/ft, then normalizing the USBM gas content versus depth (pressure) curve for the Kinta area pressure, by applying a localized constant of 0.96375 × 6.251, makes it possible to calculate a realistic recovery of gas from the coal seams around Kinta. Specifically, the pressure gradient in the Kinta area is 0.279 psi/ft, with a bottomhole pressure, from bomb tests, of 411 psig at 1,475 ft. When the desorption curve is adjusted for this pressure–depth relationship, an ash-free gas content of approximately 524 ft³/ton results for a well of average depth in this area.

The Hartshorne coal in Haskell County is medium-volatile bituminous. One core from the Kerr-McGee mine near Stigler, of like depth, reported approximately 550 ft³/ton from a desorption. If a well is completed in the undivided Hartshorne coal at a depth of ~1,542 ft, the gas content could be calculated from the adjusted formula of 16.34 cm³/g (524 ft³/ton). Further, if the well produced until the reservoir pressure drops to ~75 psig, the gas content would be ~5.82 cm³/g. The recovery would be 10.52 cm³/g (16.34–5.82). The recovery factor would be 10.52/16.34 or 64%. These numbers are near the expected values that have been predicted and recovered from similar coals in other basins.

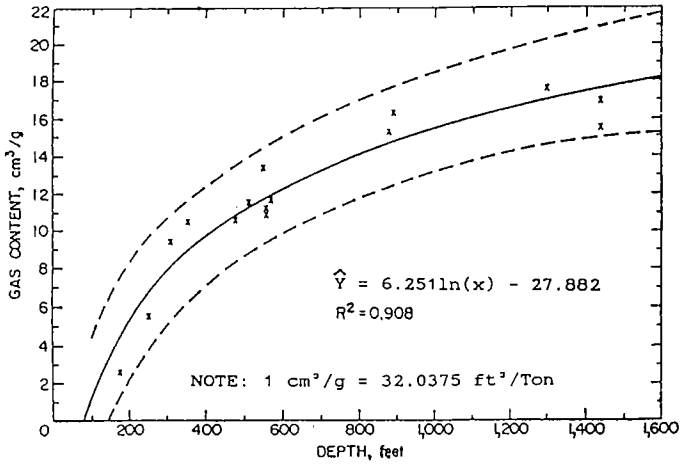

Figure 4. Desorbed gas content by U.S. Bureau of Mines for 16 Hartshorne coal cores from Haskell and Le Flore Counties (from Iannacchione and Puglio, 1979).

Desorption curves in Figures 5 and 6 are provided, which are representative of average Hartshorne coals in Le Flore and Haskell Counties.

The permeability for Kinta area wells can be determined with a tank/gravity slug-type flow in tests because of the underpressured reservoir. Permeability values of 25 md to >35 md (matrix) have been measured.

Assuming a 5.0-ft coal with 80-acre drainage, 1,825 tons of coal/acre-ft, a 10% ash content, and an average recovery of 64%, the average CBM well in the Kinta–Lequire area would recover 220.332 MMCFG. However, data obtained from more than 6 to 7 years of production from wells such as those described make it clear that many of the wells have already amassed a cumulative production of >220 MMCFG. A curve analysis for a representative group of these wells (23 adjacent wells in three 640-acre sections) indicates that the individual economic ultimate recoverable reserves (EURs) will be in the range of 264–461 MMCFG, with an average of ~350 MMCFG. This phenomenon has been noted for many of the basins producing gas with histories long enough to make accurate estimations of EURs. Actual recoveries have exceeded initial projections, based on gas-in-place (GIP) calculations, from 25% to >100%. Therefore, the experience

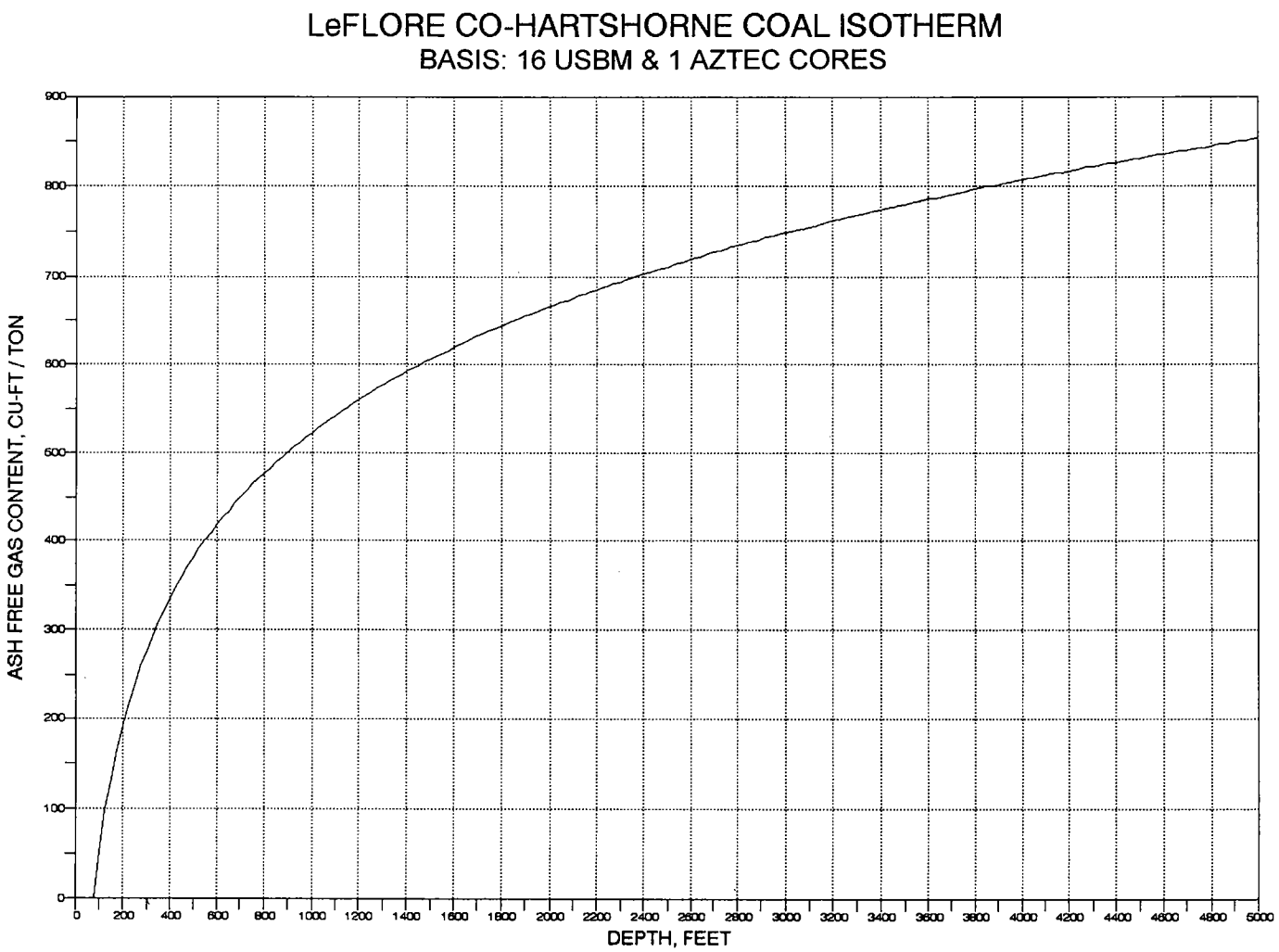

Figure 5. Hartshorne coal isotherm for Le Flore County, based on analyses of 16 cores by U.S. Bureau of Mines, and No. 1 Aztec cores. Ash-free gas content versus depth.

with the Kinta area wells of exceeding initial projections of EUR by 45% to 100% confirms what has been observed for other basins.

Current papers, such as several GRI (GTI) reports by Charles Nelson, are being disseminated that attribute this difference to several factors. More modern and accurate methods of obtaining gas content through desorption methodology are being used. Lost-gas analyses and residual-gas determinations have been improved. Cores are now being desorbed at reservoir temperature, which has also increased lost-gas values and measured-gas contents. Perhaps the second most important factor in evaluating how much gas a well will make is to consider whether the adjacent strata (carbonaceous shales and sand stringers) would also make a substantial contribution to the produced gas. Many areas in the United States are now productive from shales that contain absorbed gas and thus are able to be exploited.

The CBM wells in the Arkoma basin will be pumped and the wellhead pressure eventually lowered to 10 psig or less through compression. It is reasonable to expect average reservoir-abandonment pressures to be in the range of 30–75 psig. This results in enhanced-recovery factors that are higher than those used in the above projections. The past history of coal production in similar reservoirs suggests that the higher recovery factors may be achieved in a smaller drainage area (80 acres) than the larger areal extent that is considered normal in other basins.

POTEAU AREA COALS

The Hartshorne coal changes from northwest to southeast across the Arkoma basin. In the area around Eufaula, Oklahoma, only the undivided Hartshorne coal exists. Eastward, toward Poteau, Oklahoma, the coals split and generally are found as the Upper and Lower Hartshorne coals. In the area near Monroe, Oklahoma (southeast of Poteau), it is common to find multiple Upper Hartshorne coal stringers and, infrequently, an Upper Hartshorne coal of 4 ft or more in thickness that is productive. However, the Lower Hartshorne coal is the predominant coal member being produced in the area.

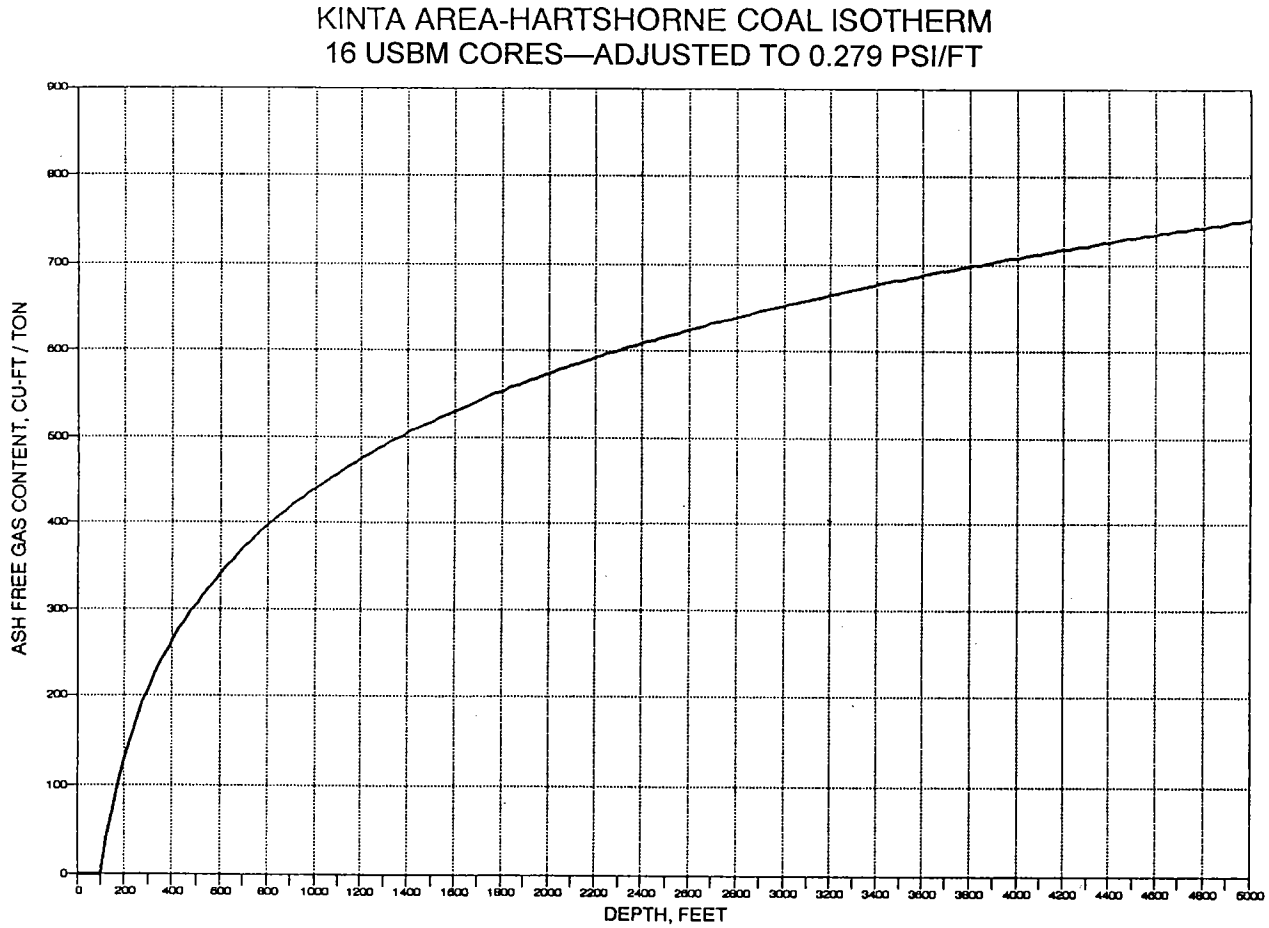

Figure 6. Hartshorne coal isotherm for Kinta area, Haskell County, based on analyses of 16 cores by U.S. Bureau of Mines, adjusted to 0.279 psi/ft. Ash-free gas content versus depth.

The coal rank becomes higher in the eastern part of the Oklahoma portion of the Arkoma basin, with the Poteau area Hartshorne coals being low-volatile bituminous. The pressure gradient is higher in this part of the basin, with normally pressured or even overpressured coals being present. These two factors combine to give higher gas contents for the Poteau area Hartshorne coals. Past desorptions by Aztec Energy and CWF have found gas contents of 450 to >700 ft^3/ton.

Fracture gradients in the Poteau–Monroe region, at similar depths to those in the Kinta–Stigler area, are generally lower. Permeability tests require pump-in equipment because of the normal/overpressured reservoirs. Permeability values of 12–25 md have been observed in recent tests. Newer gas desorptions by El Paso are now being accomplished, but no data have yet been released.

FRACTURING COAL FOR INCREASED PRODUCTION

Opinions as to the proper methods for fracturing the Hartshorne coal reservoirs are as varied as the individuals involved. The relative "greenness" of CBM drilling and production, and the motivation by fracturing companies to provide a "new and superior" answer have helped to continue the proliferation of ideas relative to what is most effective. These emotional drivers are coupled with the lack of mature knowledge of the way in which coals produce gas and what is effective or detrimental. Different regions and types of coals require different methods of treatment. My own opinions steer the balance of the discussion toward what I believe to be the most successful way to stimulate coals in Haskell and Le Flore Counties in the Arkoma basin.

My ideal "frac" is a long, vertical, wide-diameter frac channel that is packed with the largest diameter sand from frac tip to wellbore.

Chemicals that cause formation damage should be minimized. Coals contain a number of minerals and fines that react unfavorably with acid and other reactive substances. It is evident from the production restriction in a well shown in Figure 7 that the acid used severely damaged the permeability. As a rule of thumb, I suggest that you do not put anything in the reservoir that you cannot put in your eyes. That does not leave much but water as a conveying fluid to stimulate the coal by hydraulic fracturing and to transport the sand to prop the frac channel. Because of the lack

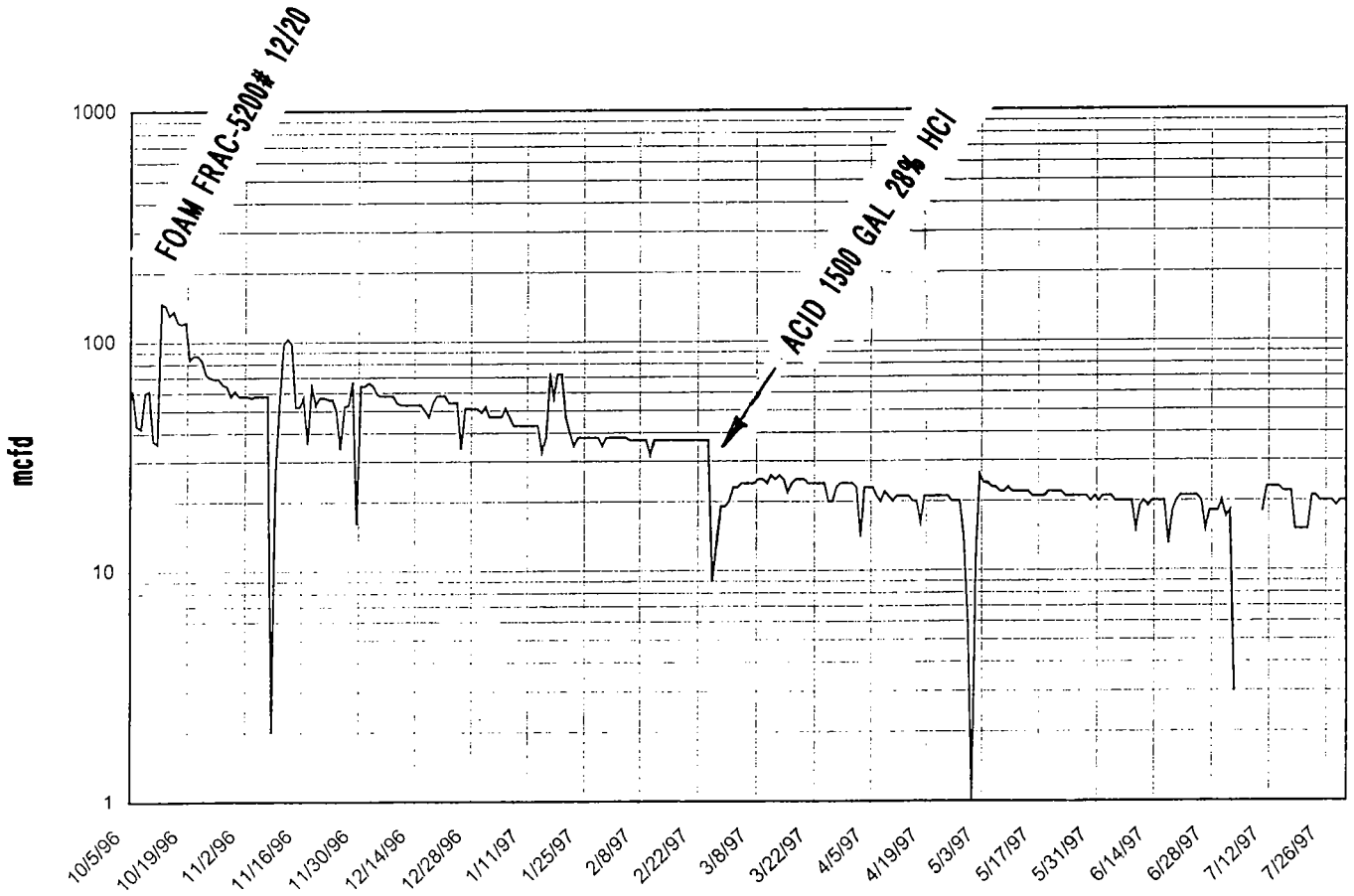

Figure 7. Graph showing detrimental effect of acid-fracturing of a Hartshorne coal at 1,258–1,266-ft depth. Acid treatment in February 1997 caused a significant drop in production.

of knowledge of what is possible with ungelled or otherwise unthickened frac fluids (water), numerous methods and fluids have been used. Stim-Lab, under contract to GRI, performed a series of important tests on Hartshorne coals to determine what effect, if any, on permeability was caused by the introduction of various agents. Detrimental substances include the following chemicals: acids, xylene–toluene, gasoline–benzene–diesel oil, condensate, strong solvents, bleach, gels, nitrogen foams, long-chain polymers, strong surfactants, and foaming agents.

My own preference is to use only ungelled or unthickened water and sand for stimulating a well. My past experience of restimulating wells that were previously treated with substances that caused formation damage gave me an insight into designing frac methods that cause minimum damage to the formation. The use of gels, foams, surfactants, acids, fluid-loss additives (including 100-mesh sand), and other "frac aids" are usually detrimental to the permeability of the frac channel. If there is a compelling engineering reason to use these substances, then do it, but know that production will be less than optimum.

The fracs proven most successful for me are straight water fracs with the largest diameter proppant that can be successfully carried and placed deep within the frac channel. The coal is hydraulic-fractured with approximately 100,000 to more than 150,000 lb of 12/20-, 16/30-, and 20/40-mesh sands, using fresh water and appropriate bacteria-killing additives in procedures designed specifically for the characteristics of the particular coal encountered.

Most importantly, the frac should be designed to match the known properties of the coal: frac gradient, permeability, friability, rank and mineral content, unusual stress patterns, and how the coal will fracture. The orientation of the fracture is dictated more by local stress fields than by depth of overburden for coals 700–1,600 ft deep. Also, multiple-stage fracs could comprise both horizontal and vertical fractures. It is possible sometimes to abort a frac that is treating horizontally by letting the formation rest for 45 minutes and then starting a new fracture. In a significant number of cases, the new fracture will break in to the vertical plane.

The economics and production projections used in this report are based on results of water–sand fracs in coals of the Arkoma basin. Recent innovations in methodology that I am using have resulted in enhanced production through redundancy of access to the formation's induced- and natural-fracture systems as well as increased connectivity with cleat permeability.

The most optimum fracture for maximum drainage is a single-stage frac with long extension that uses only 12/20-mesh sand. This frac was performed on a 790-ft-deep, single-completion, 6-ft-thick Hartshorne coal with 3,500 bbl of water and 131,082 lb of sand. The treatment-schedule graph for this frac is shown in Figure 8. The frac consisted of a step-rate pad of 650 bbl of water, ending at 35 barrels per minute (BPM). Sand was run in a "lean-frac" schedule of 0.5 to 0.85 lb/gal until approximately 600 bbl of water remained. The density was then ramped from 0.85 lb/gal to 4.0 lb/gal over 110 bbl. Following this, the density was held at 4.2 lb/gal for 290 bbl until the sand-out of the well was indicated. A progressive shutdown of the pumps was used to provide a "soft landing" as the well sanded out.

It is significant to note that 50,000 lb of 12/20-mesh sand was pumped at high densities during the ramp and then at constant levels of more than 4 lb/gal. Another important aspect of using only large (12/20) mesh sand is that when a natural fracture is encountered during the frac, it is filled with the large sand and not with finer mesh sands that do not provide as efficient a permeability channel. This large-diameter-proppant frac design has been very successful in execution and provides the maximum area of drainage with the possibility of longer persistence of a relatively clear propped frac channel with the highest permeability.

Modifications of this design could include one or more shutdowns to allow the fracture to close and then to restart the fracture treatment, thus opening new fracture channels. During many of the fracs, the Nolte-Smith plot indicates that the fracture is near maximum extension and that imminent sand-out is being approached when about 60,000 lb of sand has been pumped. This is a good time to stop and let the fracture close and, in about 30–45 minutes, start back up and break into a new fracture. These multistage, multi-winged fracs are very good conduits, as they have excellent entry into the coal and provide redundant access paths if near-wellbore plugging occurs.

The treated coal zones are expected to be productive within 10 to 20 days after the frac and might exhibit a rapid rise in production from 30 to 100 MCFGPD to a temporary peak initial-production rate of 350 MCFGPD or more if not restricted. However, allowing the well to flow freely at the higher rates (100–350 MCFGPD or more) will contribute to proppant flowback, coal-fines migration, and permeability plugging.

I prefer a more conservative approach to initial production by restricting initial-gas-production flows and holding back pressures in order to minimize high-velocity, turbulent flow and increased movement of coal fines to reverse screen-out in the proppant pack. Pressure should be lowered gradually, and in only the

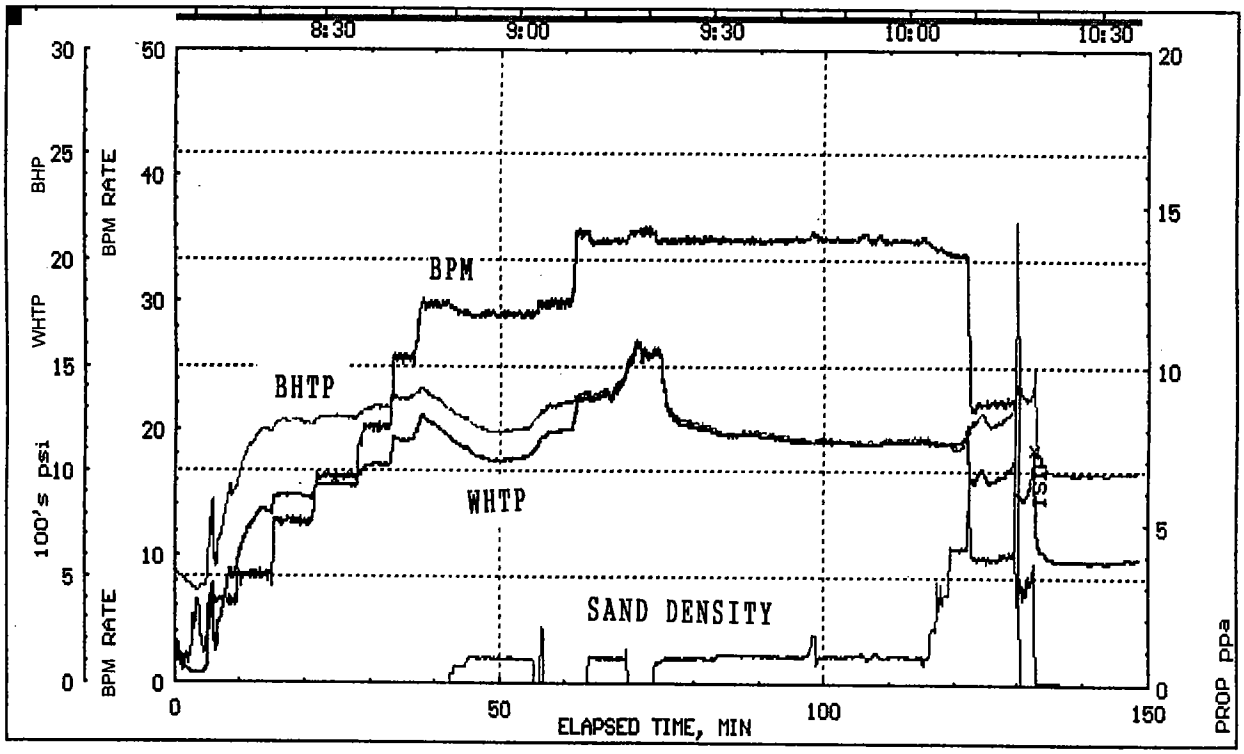

Figure 8. Graph showing data for sand-fracture treatment of Hartshorne coal bed at 790 ft with 131,000 lb of 12/20-mesh sand and 3,500 bbl of water. *BHP* = bottomhole pressure; *BHTP* = bottomhole treating pressure; *BPM* = barrels per minute; *WHTP* = wellhead treating pressure; *ISIP* = initial shut-in pressure; *PROP* = proppant.

minimum amount, to allow dewatering of the coal to proceed.

The production profile expected for the above described fracture treatment is shown in Figure 9. The treatment starts the "average" well slowly, allowing production to rise to approximately 30–50 MCFGPD under back pressure in the first 3 to 4 months, then gradually rising to 130 MCFGPD during the next 9 months, and finally peaking at 150 MCFGPD at 18 months after starting production. Production will "bell" over the top and begin a pseudo-steady-state condition when the reservoir has extended to its full drainage area, and desorption is continuing. The well will then begin a hyperbolic decline at rates of 23% to 20% per year until reaching a "constant-residual" productive rate throughout the remainder of its economic life. In like wells in the Appalachian coal fields, residual rates of production have been 25–40 MCFGPD for periods >25 years to >50 years. This residual productive rate has not been considered in the production profile just described. This same characteristic has also been found in some wells in the Arkoma basin. An abandoned well in the Kinta area had been venting approximately 50 MCFGPD for >25 years, and the recognition of this phenomenon spurred Bear Productions into beginning CBM exploration and production.

GAS QUALITY AND ANALYSIS

It is expected that wells will produce gas of like characteristics and quality as those of the several operators in the respective areas described. Test results report gas that grades from 97% to 98% methane with approximately 970–990 Btu per MCF. The gas shows low nitrogen and carbon dioxide contents of <1% each; a very small mole fraction of ethane is present.

RESERVE ECONOMICS

Table 1 provides an economic run for the "average" well described above to complement the expected decline curve that is based on experience with like wells. The cost of drilling and completing the well was placed at $95,000. Monthly lease-operating expenses were $750. The gas price was $3.00 per MCF. Compression charges were $0.25 per MCF. These costs were held level for 12 months, and then escalated exponentially at 3% per year. Economic factors follow:

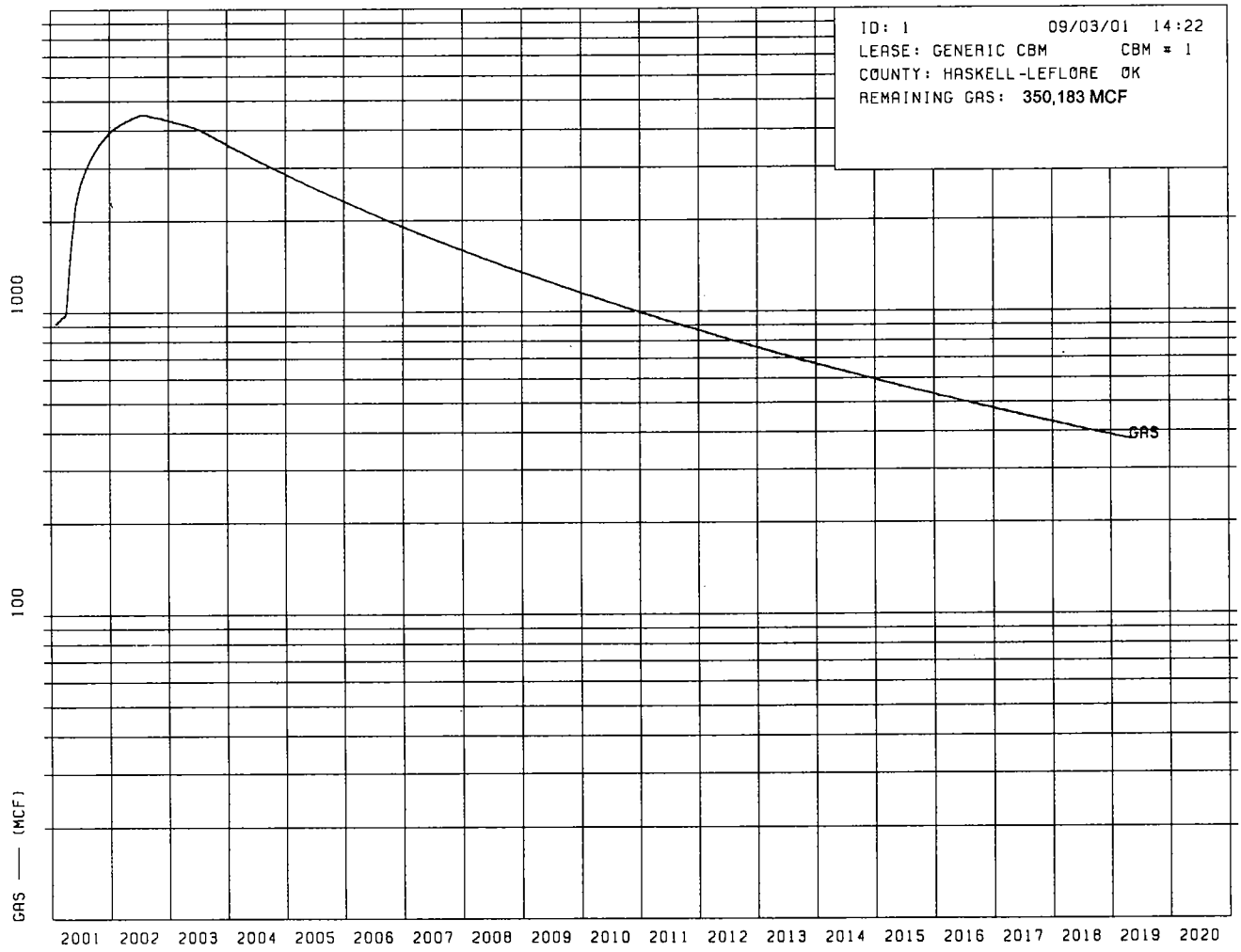

Figure 9. Graph shows an average per-well production profile, based on 23 CBM wells in a three-section pod.

Table 1. — Average Econonmic Profile Based on 23 CBM Wells in a Three-Section Pod

1500 FT PRODUCING ZONE -- ALL LEASES

YEAR	WELL CNT	GROSS PRODUCTION BBL OIL	GROSS PRODUCTION MCF GAS	NET PRODUCTION BBL OIL	NET PRODUCTION MCF GAS	PRICE OIL	PRICE GAS	SALES INCOME OIL $	SALES INCOME GAS $	SALES INCOME TOTAL $
2001	1	0	30,169	0	24,135	0.00	3.000	0	72,405	72,405
2002	1	0	51,976	0	41,581	0.00	3.041	0	126,468	126,468
2003	1	0	47,459	0	37,968	0.00	3.131	0	118,868	118,868
2004	1	0	37,949	0	30,359	0.00	3.224	0	97,891	97,891
2005	1	0	30,523	0	24,419	0.00	3.321	0	81,102	81,102
2006	1	0	24,984	0	19,987	0.00	3.421	0	68,377	68,377
2007	1	0	20,756	0	16,605	0.00	3.524	0	58,513	58,513
2008	1	0	17,466	0	13,973	0.00	3.630	0	50,718	50,718
2009	1	0	14,863	0	11,890	0.00	3.739	0	44,454	44,454
2010	1	0	12,772	0	10,218	0.00	3.851	0	39,348	39,348
2011	1	0	11,071	0	8,857	0.00	3.967	0	35,131	35,131
2012	1	0	9,671	0	7,737	0.00	4.086	0	31,611	31,611
2013	1	0	8,507	0	6,806	0.00	4.208	0	28,640	28,640
2014	1	0	7,530	0	6,024	0.00	4.335	0	26,113	26,113
2015	1	0	6,704	0	5,363	0.00	4.465	0	23,943	23,943
2019	1	0	17,781	0	14,225	0.00	4.750	0	67,560	67,560
TOT		0	350,183	0	280,146	0.00	3.467	0	971,143	971,143

YEAR	EXPENSES TAXES	EXPENSES MKTG	EXPENSES OPER	EXPENSES TOTAL	NET OPER INCOME	OTHER COSTS	NET CASH FLOW ANNUAL	NET CASH FLOW CUMULATIVE	NET CASH FLOW 10.00 PCNT DISCOUNTED
2001	7,168	6,034	9,000	22,202	50,203	95,000 C	-44,797	-44,797	-47,212
2002	12,520	10,395	9,123	32,039	94,429	0	94,429	49,632	81,493
2003	11,768	9,492	9,397	30,657	88,212	0	88,212	137,844	69,358
2004	9,691	7,590	9,679	26,960	70,931	0	70,931	208,775	50,719
2005	8,029	6,105	9,969	24,103	56,999	0	56,999	265,775	37,048
2006	6,769	4,997	10,268	22,034	46,343	0	46,343	312,118	27,381
2007	5,793	4,151	10,576	20,520	37,993	0	37,993	350,111	20,406
2008	5,021	3,493	10,893	19,408	31,310	0	31,310	381,421	15,287
2009	4,401	2,973	11,220	18,594	25,860	0	25,860	407,281	11,479
2010	3,895	2,554	11,557	18,007	21,341	0	21,341	428,622	8,612
2011	3,478	2,214	11,904	17,596	17,536	0	17,536	446,158	6,433
2012	3,129	1,934	12,261	17,324	14,286	0	14,286	460,444	4,765
2013	2,835	1,701	12,628	17,165	11,475	0	11,475	471,919	3,480
2014	2,585	1,506	13,007	17,099	9,014	0	9,014	480,933	2,486
2015	2,370	1,341	13,398	17,109	6,835	0	6,835	487,768	1,714
2019	6,688	3,556	47,630	57,874	9,686	0	9,686	497,453	2,078
TOT	96,143	70,037	212,510	378,690	592,453	95,000	497,453	497,453	295,527

PCNT DSCNT	$ VALUE
0.00	497,453
10.00	295,527
15.00	236,862
20.00	193,136
25.00	159,468
30.00	132,844
35.00	111,318
40.00	93,589
50.00	66,185
75.00	24,350
100.00	1,031

ROR: > 100.00 IROI: 5.24
PAYOUT: 1.50 EROI: 6.24

	BBL OIL	MCF GAS
ULTIMATE GROSS	0	350,183
CUM PROD GROSS	0	0
FUTURE RES GROSS	0	350,183
FUTURE RES NET	0	280,146
GROSS WELL COUNT	0.000	1.000
NET WELL COUNT	0.000	1.000

INTERESTS

YR	MO	OILINT	GASINT	WORKINT	TANGINT	INTANGINT
1	1	0.800000	0.800000	1.000000	1.000000	1.000000

PREPARED BY: WENDELL CONSULTING, LLC

EFFECTIVE DATE: 1 JANUARY 2001
LEASE ID: 1
LEASE NAME: GENERIC CBM
WELL NAME: CBM # 1
STATE: OKLAHOMA
COUNTY: HASKELL-LeFLORE
FIELD: ARKOMA HARTSHORNE CBM
OPERATOR: WENDELL CONSULTING, LLC
RES CAT: PROBABLE UNDEVELOPED NONPRODUCING
ECON LIMIT: 1904

1500 FT W/600 CU-FT/T, 80 AC, 6.0' 360,000 MCF RECOVERABLE

Recoverable reserves	350,183 MCFG
Drainage	80 acres est.
Rate of return	>100%
Payout	1.5 years
Cash on cash	6.24 to 1
10% discounted cash flow	$295,527

Much discussion has focused on whether horizontal wells are superior to vertical, hydraulic-fractured completions. A representative horizontal well was drilled on trend in close proximity to the 23 vertical wells that were discussed above; with similar geologic characteristics, this well is excellent for making comparisons. The horizontal well has been in production for more than 2 years and is considered to be a good horizontal well. The initial production was 500 MCFGPD, and the well has been on a 34% exponential decline thereafter. Replacement costs for the well at today's rates are estimated to be >$300,000. Other expenses are assumed to have been the same as for a vertical well. Figure 10 and Table 2 depict the well performance and financial analysis. The economic factors for an individual horizontal well follow for purposes of comparison with those factors for a vertical well:

Recoverable reserves	529,061 MCFG
Drainage	121 acres est.
Rate of return	>100%
Payout	1.08 years
Cash on cash	3.25 to 1
10% discounted cash flow	$461,098

Based on the assumptions given above, these numbers indicate that vertical completions deliver superior economics than horizontal completions. Another factor to consider is that most of the horizontal ex-

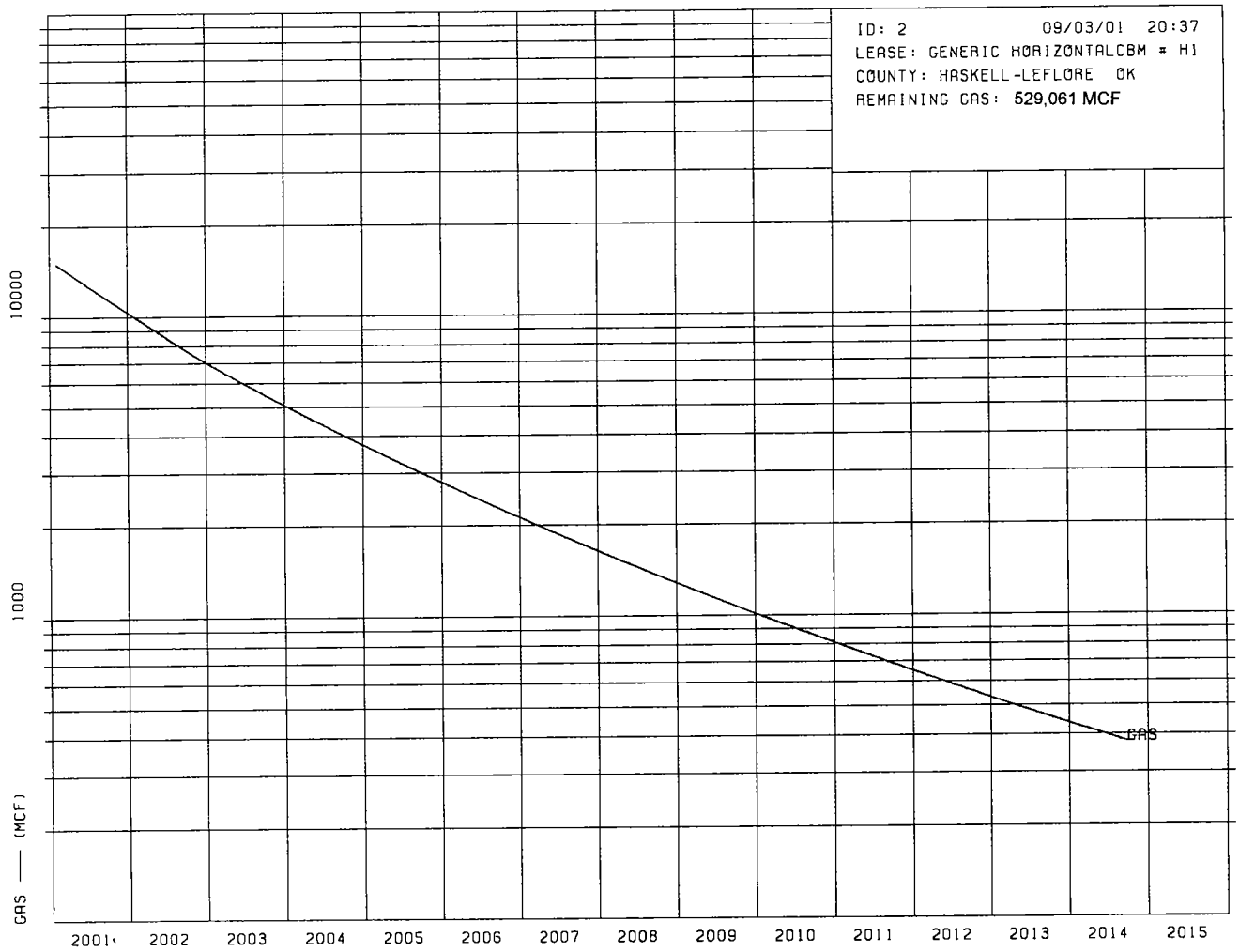

Figure 10. Actual production profile of a horizontal well that offsets 23 CBM wells.

tensions are unsupported open holes. Many of these horizontal holes have collapsed and have had to be redrilled or cleaned out, and some wells or well segments have been abandoned. At present, no effective or economic method of dewatering horizontal wells is in use. When produced water contains percolated gas, the water vapor that is carried by the gas is essentially mineral free. The water left behind becomes more concentrated with mineral solids, and deposition of scale from calcium, iron, carbonates, and sulfur compounds occurs. This allows scale buildup and degrades permeability. Several of these compounds also cause serious corrosion. Further, continual agitation by gas through water in an unsupported coal seam tends to cause the competency of the well walls to degrade, with rubble and fines being generated, or caving that can block off the wellbore.

Therefore, my preference remains with a vertically drilled, hydraulically fractured, and sand-propped well. A 3-darcy, proppant-packed fracture channel extending deep into the reservoir with two or more frac wings is in fact a horizontal well, and it would be obtained at lower risk, cost, and effort.

LESSONS LEARNED

Protect permeability. Keep wells from surging. Restrict initial production rates to minimize the movement of fines. Avoid the use of substances that cause formation damage.

Detrimental items are acids, xylene–toluene, gasoline, benzene, diesel oil, condensate, strong solvents, sodium hypochlorite (bleach), cross-linked or guar gels, long-chain polymers, foams, strong surfactants and other foam-inducing agents, and 100-mesh sand. These items should be avoided if at all possible. Remember, if you can't put it in your eyes, the coal probably will not like it either.

As in all things, the most simple and direct method is usually the best. Excellent production can be obtained by using uncomplicated and conservative procedures. The geology is readily available and understandable. Well data are accessible. Drilling methods, pipe requirements, and cement are not unnecessarily unusual in any way. Perforating by itself is normally sufficient to get into the zones with no acid or other breakdown measures being necessary. Technical consulting to determine reservoir conditions and frac de-

Table 2. — Projected Economic Profile for a Horizontal Well That Offsets 23 Vertical CBM Wells

ARKOMA BASIN CBM PROJECT
HARTSHORNE COALS
1500 FT PRODUCING ZONE -- ALL LEASES

YEAR	WELL CNT	GROSS PRODUCTION BBL OIL	GROSS PRODUCTION MCF GAS	NET PRODUCTION BBL OIL	NET PRODUCTION MCF GAS	PRICE OIL	PRICE GAS	SALES INCOME OIL $	SALES INCOME GAS $	SALES INCOME TOTAL $
2001	1	0	149,918	0	119,935	0.00	3.000	0	359,804	359,804
2002	1	0	100,924	0	80,739	0.00	3.038	0	245,299	245,299
2003	1	0	70,779	0	56,623	0.00	3.130	0	177,218	177,218
2004	1	0	51,570	0	41,256	0.00	3.224	0	133,002	133,002
2005	1	0	38,291	0	30,633	0.00	3.321	0	101,722	101,722
2006	1	0	28,912	0	23,129	0.00	3.420	0	79,113	79,113
2007	1	0	22,159	0	17,727	0.00	3.523	0	62,457	62,457
2008	1	0	17,214	0	13,771	0.00	3.629	0	49,975	49,975
2009	1	0	13,536	0	10,829	0.00	3.738	0	40,477	40,477
2010	1	0	10,762	0	8,609	0.00	3.850	0	33,148	33,148
2011	1	0	8,643	0	6,914	0.00	3.966	0	27,421	27,421
2012	1	0	7,005	0	5,604	0.00	4.085	0	22,893	22,893
2013	1	0	5,727	0	4,581	0.00	4.207	0	19,275	19,275
2014	1	0	3,621	0	2,897	0.00	4.319	0	12,509	12,509
TOT		0	529,061	0	423,249	0.00	3.223	0	1,364,312	1,364,312

YEAR	EXPENSES TAXES	EXPENSES MKTG	EXPENSES OPER	EXPENSES TOTAL	NET OPER INCOME	OTHER COSTS	NET CASH FLOW ANNUAL	NET CASH FLOW CUMULATIVE	10.00 PCNT DISCOUNTED
2001	35,621	29,984	9,000	74,604	285,200	300,000 C	-14,800	-14,800	-25,784	-25,784
2002	24,285	20,185	9,123	53,592	191,706	0	191,706	176,906	166,055	140,271
2003	17,545	14,156	9,397	41,097	136,121	0	136,121	313,027	107,143	247,414
2004	13,167	10,314	9,679	33,160	99,842	0	99,842	412,869	71,436	318,850
2005	10,070	7,658	9,969	27,698	74,024	0	74,024	486,893	48,145	366,995
2006	7,832	5,782	10,268	23,883	55,230	0	55,230	542,123	32,655	399,650
2007	6,183	4,432	10,576	21,191	41,265	0	41,265	583,388	22,181	421,830
2008	4,948	3,443	10,893	19,284	30,691	0	30,691	614,079	14,998	436,828
2009	4,007	2,707	11,220	17,935	22,542	0	22,542	636,622	10,016	446,844
2010	3,282	2,152	11,557	16,991	16,157	0	16,157	652,779	6,528	453,372
2011	2,715	1,729	11,904	16,347	11,074	0	11,074	663,853	4,069	457,441
2012	2,266	1,401	12,261	15,928	6,965	0	6,965	670,817	2,329	459,770
2013	1,908	1,145	12,628	15,682	3,593	0	3,593	674,411	1,095	460,865
2014	1,238	724	9,719	11,682	827	0	827	675,238	233	461,098
TOT	135,067	105,812	148,195	389,074	975,238	300,000	675,238	675,238	461,098	461,098

PCNT DSCNT	$ VALUE
0.00	675,238
10.00	461,098
15.00	389,844
20.00	333,174
25.00	287,115
30.00	248,985
35.00	216,921
40.00	189,590
50.00	145,484
75.00	72,781
100.00	28,459

ROR: > 100.00 IROI: 2.25
PAYOUT: 1.08 EROI: 3.25

	BBL OIL	MCF GAS
ULTIMATE GROSS	0	529,061
CUM PROD GROSS	0	0
FUTURE RES GROSS	0	529,061
FUTURE RES NET	0	423,249
GROSS WELL COUNT	0.000	1.000
NET WELL COUNT	0.000	1.000

INTERESTS

YR	MO	OILINT	GASINT	WORKINT	TANGINT	INTANGINT
1	1	0.800000	0.800000	1.000000	1.000000	1.000000

PREPARED BY: WENDELL CONSULTING, LLC

EFFECTIVE DATE: 1 JANUARY 2001
LEASE ID: 2
LEASE NAME: GENERIC HORIZONTAL CBM
WELL NAME: CBM # H1
STATE: OKLAHOMA
COUNTY: HASKELL-LeFLORE
FIELD: ARKOMA HARTSHORNE CBM
OPERATOR: WENDELL CONSULTING, LLC
RES CAT: PROBABLE UNDEVELOPED NONPRODUCING
ECON LIMIT: 1409

1500FT HORIZONTAL-6'-1800FT HORIZONTAL LEG-529 MMCF RECOVERABLE

sign is available. The best frac treatment is the simplest—water and sand—but it requires experience to achieve correct performance. Reliable independent advice is the most difficult commodity to find.

REFERENCES CITED

Diamond, W. P., 1976, Use of surface joint and photolinear data for predicting subsurface coal cleat orientation: U.S. Bureau of Mines Report of Investigations 8120, 13 p.

Friedman, S. A., 1982, Determination of reserves of methane from coal beds for use in rural communities in eastern Oklahoma: Oklahoma Geological Survey Special Publication 82-3, 32 p.

Hemish, L. A.; and Suneson, N. H., 1997, Stratigraphy and resources of the Krebs Group (Desmoinesian), south-central Arkoma basin, Oklahoma: Oklahoma Geological Survey Guidebook 30, 83 p.

Hendricks, T. A., 1937, The McAlester district, Pittsburg, Atoka, and Latimer Counties, *pt. 1 of* Geology and fuel resources of the southern part of the Oklahoma coalfield: U.S. Geological Survey Bulletin 874-A, p. 1–90.

Houseknecht, D. W.; and Iannacchione, A. T., 1982, Anticipating facies-related coal mining problems in Hartshorne Formation, Arkoma basin: American Association of Petroleum Geologists Bulletin, v. 66, p. 923–946.

Iannacchione, A. T.; and Puglio, D. G., 1979, Methane content and geology of the Hartshorne coalbed in Haskell and Le Flore Counties, Oklahoma: U.S. Bureau of Mines Report of Investigations 8407, 14 p.

McDaniel, G. A., 1968, Application of sedimentary directional features and scalar properties to hydrocarbon exploration: American Association of Petroleum Geologists Bulletin, v. 52, p. 1689–1699.

Rieke, H. H., III; and Kirr, J. N., 1984, Geologic overview, coal, and coalbed methane resources of the Arkoma basin, Arkansas and Oklahoma, *in* Rightmire, C. T.; Eddy, G. E.; and Kirr, J. N. (eds.), Coalbed methane resources of the United States: American Association of Petroleum Geologists Studies in Geology 17, p. 135–161.

Scruton, P. C., 1950, The petrography and environment of deposition of the Warner, Little Cabin, and Hartshorne sandstones in northeastern Oklahoma: American Journal of Science, v. 248, p. 408–426.

Finding New Pays in Old Plays: Recent Geochemical-Exploration Successes from Texas and Oklahoma

Dietmar Schumacher, Daniel Hitzman, and Brooks Rountree
Geo-Microbial Technologies (GMT)
Ochelata, Oklahoma

ABSTRACT.— Most oil and gas accumulations leak, predominantly vertically (with obvious exceptions in some geologic settings). This leakage can be detected and mapped by using any of a number of direct and indirect geochemical-exploration methods. The areal extent of a surface geochemical anomaly can approximate the productive limits of the reservoir(s) at depth. These characteristics of hydrocarbon microseepage expand the applications of geochemical surveys beyond prospect evaluation to include exploration for bypassed pay in producing or abandoned fields, as well as finding new pays in mature plays. How successfully this can be done depends on the geologic setting, choice of method, survey design and sample spacing, and proper integration of geochemical results with conventional geologic and seismic data.

Results of recent geochemical surveys in the Fort Worth basin of north Texas and a maturing waterflood in Payne County, Oklahoma, are reviewed. Each area was surveyed using the microbial oil survey technique (MOST) developed by Phillips Petroleum Co. and available to industry through GMT in Ochelata, Oklahoma.

In the Fort Worth basin example, geochemical evaluation of an Ordovician Ellenburger structural trap identified a minor seepage anomaly associated with the Ordovician "high" and an areally extensive microbial anomaly over a nearby structural "low." Subsequent drilling found noncommercial oil on the high but discovered a new Park Springs Conglomerate (Pennsylvanian) field in the area of the low. The Payne County example illustrates the use of repeat microbial surveys over a waterflood operation to monitor hydrocarbon migration and drainage over time.

Applications such as these require close sample spacing and are most effective when results are integrated with subsurface data, especially three-dimensional (3-D) seismic data. The need for such integration cannot be overemphasized. Seismic data will remain unsurpassed for imaging trap and reservoir geometry, but only detailed soil-gas or microbial surveys can reliably image hydrocarbon microseepage from those same reservoirs. High-resolution microseepage surveys offer a flexible, low-risk, and low-cost technology that naturally complements more traditional geologic and seismic methods. Properly integrated with 2-D and 3-D seismic techniques, their use has led to the discovery of new reserves, drilling of fewer dry or marginal wells, and optimization of the number and placement of delineation, development, or secondary wells.

INTRODUCTION

Petroleum reservoirs and their heterogeneous pressure regimes present a distinct and *dynamic* geochemical signature at the surface as light hydrocarbon gases (methane, ethane, propane, butane) escape from the reservoir and travel vertically to the surface. Geologists and geochemists describe this process as hydrocarbon microseepage. As these gases pass through the shallow-soil environment, they are partially consumed by specific microorganisms that use the gases as a source of nutrients. Similar in strategy to microorganisms that attack oil spills, these unique microbial populations are living in *dynamic equilibrium* with their hydrocarbon-microseepage environment.

New oil and gas fields have been discovered by mapping their hydrocarbon-microseepage signatures. However, the microseepage signature of a new field will immediately begin to change as the reservoir pressures are effectively altered by new wells and production practices. As the reservoir pressures change, so will the microseepage and subsequent microbial activity. A reservoir's traps, bypassed compartments, geologic heterogeneities, sedimentary facies, fluid properties, etc., all influence hydrocarbon microseepage. An operator's planned infill- and stepout-well lo-

Schumacher, Dietmar; Hitzman, Daniel; and Rountree, Brooks, 2002, Finding new pays in old plays: recent geochemical-exploration successes from Texas and Oklahoma, *in* Cardott, B. J. (ed.), Revisiting old and assessing new petroleum plays in the southern Midcontinent, 2001 symposium: Oklahoma Geological Survey Circular 107, p. 101–108.

cations and injector placements can be optimized by using hydrocarbon-microseepage results.

The latest challenge for hydrocarbon-microseepage surveys addresses the increased need of the oil and gas industry to optimize reservoir-characterization studies. Locating additional reserves between present wells and identifying additional zones of production are key components to extending the life of oil and gas fields. Recent testing of producing fields with detailed microseepage surveys reveals surprising and effective data sets that can be easily integrated with more conventional reservoir-characterization studies.

INCREASED SENSITIVITY

Reservoir deposits of oil and gas leak light hydrocarbon gases in quantities detectable at the surface. These migrating gas molecules create a *hydrocarbon-microseepage signature* that reflects a reservoir's original heterogeneities and then changes over time while the oil and gas field is being produced and exploited. Historically, microseepage signatures have helped to identify and high-grade exploration targets only. Improved survey strategies and increased sensitivity now allow for detailed reservoir characterizations by using dynamic microseepage data.

Today's elaborate conventional reservoir-characterization tools measure and test a myriad of rock and trap properties found within reservoirs. For example, innovative 3- and 4-D multi-component seismology has made remarkable advances in recent years, especially when fully integrated with available log data. But the extreme cost of these studies puts the technology out of reach for most small operators and independents. Futhermore, these conventional tools—no matter how advanced—still do not directly test for the one basic element that operators desire: *hydrocarbons*.

HETEROGENEOUS COMPONENTS

As production proceeds over the life of an oil and gas field, the reservoir's character changes with that production. Original pressures and fluids are subsequently altered by production and recovery methodologies. Subtle changes can occur that affect the heterogeneous components of the reservoir. Field operators are looking for a low-cost, rapid, and environmentally benign reservoir-characterization tool to economically enable increased production.

Recent advances in petroleum geochemistry, specifically in our understanding of the near-surface effects of hydrocarbon migration, suggest a new and very different approach for the characterization of oil and gas reservoirs (Tucker and Hitzman, 1994; Schumacher and Abrams, 1996; Quigley, 1999; Hitzman and others, 2000). Faults, fractures, and most petroleum accumulations are known to leak small but detectable amounts of hydrocarbons to the surface. Detailed geochemical and microbial surveys and research studies document that hydrocarbon microseepage from oil and gas accumulations is common and widespread, is predominantly vertical, and is dynamic (Klusman and Saeed, 1996; Jones and Burtell, 1996). These characteristics—unique to hydrocarbon microseepage—create a new suite of potential applications for surface geochemical surveys that include (1) natural-fracture and reservoir-heterogeneity detection, (2) early delineation of field limits, (3) locating bypassed petroleum, and (4) monitoring patterns of hydrocarbon drainage (Schumacher and others, 1997; Schumacher, 1999).

Results of high-resolution hydrocarbon-microseepage surveys can be used to high-grade leases with maximum efficiency. The optimum spacing and placement of both vertical and horizontal wells should be foremost in an operator's choices. Logic dictates that *reservoir heterogeneities* demand a *heterogeneous well pattern*. By tracking leaking hydrocarbons, a high-resolution surface geochemical survey will look for and identify this heterogeneous pattern (Fig. 1). Likewise, the location and extent of much costlier geophysical surveys and reservoir-stimulation projects can be optimized by using evidence of active hydrocarbons as a lead tool. For every square mile of 3-D seismic surveys saved, at least 10 mi^2 of additional hydrocarbon microbial data could be collected. The total amount of seismic data could still be programmed, but only on the best reservoirs and, furthermore, on the best parts of those reservoirs.

Several critical questions of this microseepage technology should be raised: Can a cost-effective and practical *surface* hydrocarbon-microseepage survey identify reservoir properties *at depth*? What relationship exists between surface microseepage signatures and subsurface-reservoir information (geological, production, and engineering)? What are the limitations of a hydrocarbon-microseepage survey? Examination of a recent Fort Worth basin microbial survey addresses these issues.

MICROBIAL OIL SURVEY TECHNIQUE

The microbial oil survey technique (MOST) is based on the presence of hydrocarbon microseepage above buried accumulations. Active microseepage is detected by measuring the concentrations and distributions of unique microbial populations in dynamic equilibrium with their hydrocarbon-microseepage environment. MOST soil samples are collected at a depth of 20 cm (8 in.), using shovels or augers. Collection crews usually travel by foot and determine sample sites with the help of hand-held GPS units. A two-person collection team can collect from as much as a 2-mi^2 area in one day, depending on sampling densities.

Sample patterns and densities for MOST surveys are selected to best define the hydrocarbon potential of the target area, subject to considerations of terrain and accessibility. Both reconnaissance and detailed surveys of acreage or prospects can be completed with this strategy. The integration of geological and geophysical data with microbial microseepage signatures

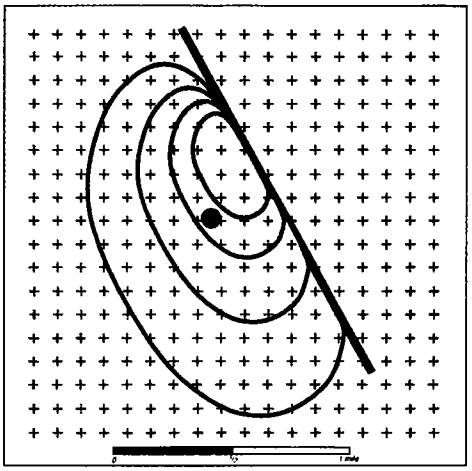

1. Hydrocarbon reservoir identified by 2D / 3D seismic *and* geochemical microseepage signatures. Geochem program using 10th mile grid pattern.

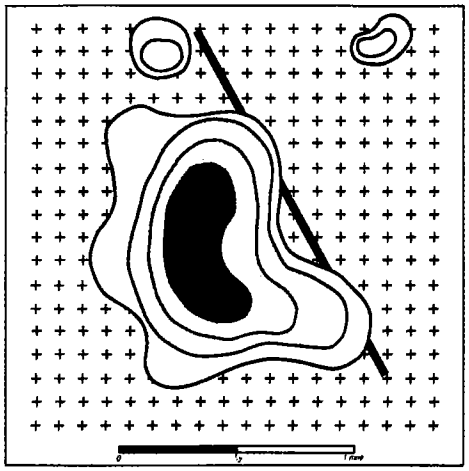

2. Microseepage signatures *prior to drilling* roughly agrees with seismic anomalies. Discovery well location plotted. Field development begins.

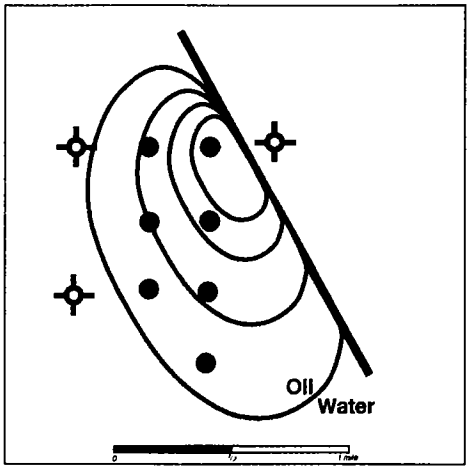

3. Field development continues. Drilling results and conventional logging identify reservoir heterogeneities. 2nd microseepage survey planned.

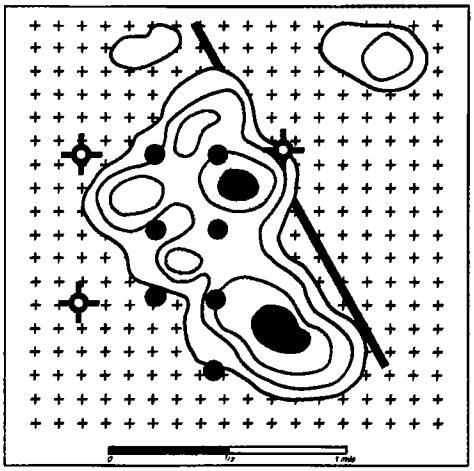

4. Follow-up microseepage survey reveals hydrocarbon-charged areas located between wells and a residual anomaly -- still undrilled -- southeast of the producing field.

Figure 1. Four-part model of dynamic hydrocarbon-microseepage signatures.

can greatly enhance both exploration and production programs.

NEW-FIELD DISCOVERY, FORT WORTH BASIN

The integration of microbial hydrocarbon-microseepage signatures and 3-D seismic data directed explorationists to a new-play concept and resulted in discovery of a Park Springs Conglomerate field in Montague County, Texas. A 3-mi^2 3-D geophysical survey identified a prospective Ellenburger structure at a depth of ~7,200 ft (Fig. 2). A reconnaissance hydrocarbon-microseepage survey (167 samples) of the area was conducted in December 1995, using the microbial oil survey technique (MOST), which was developed by Phillips Petroleum Co. and modified by Geo-Microbial Technologies, Inc. (GMT). The Ellenburger structure was found to have a positive, but small, hydrocarbon-microseepage signature. A stronger and more extensive microbial anomaly was identified over a structural trough 1 mi south.

In February 1996, additional detailed MOST samples were collected over the area of interest. The latest survey confirmed the small hydrocarbon anomaly associated with the seismic prospect, as well as the large anomaly associated with the structural trough 1 mi south (Fig. 3). A review of geologic-play analogs for north Texas suggested that the trough might contain Atokan conglomerates—a risky exploration target in the Fort Worth basin—but the primary prospect remained the Ellenburger structure and its associated smaller microseepage anomaly. The surveyed area included no producing wells prior to

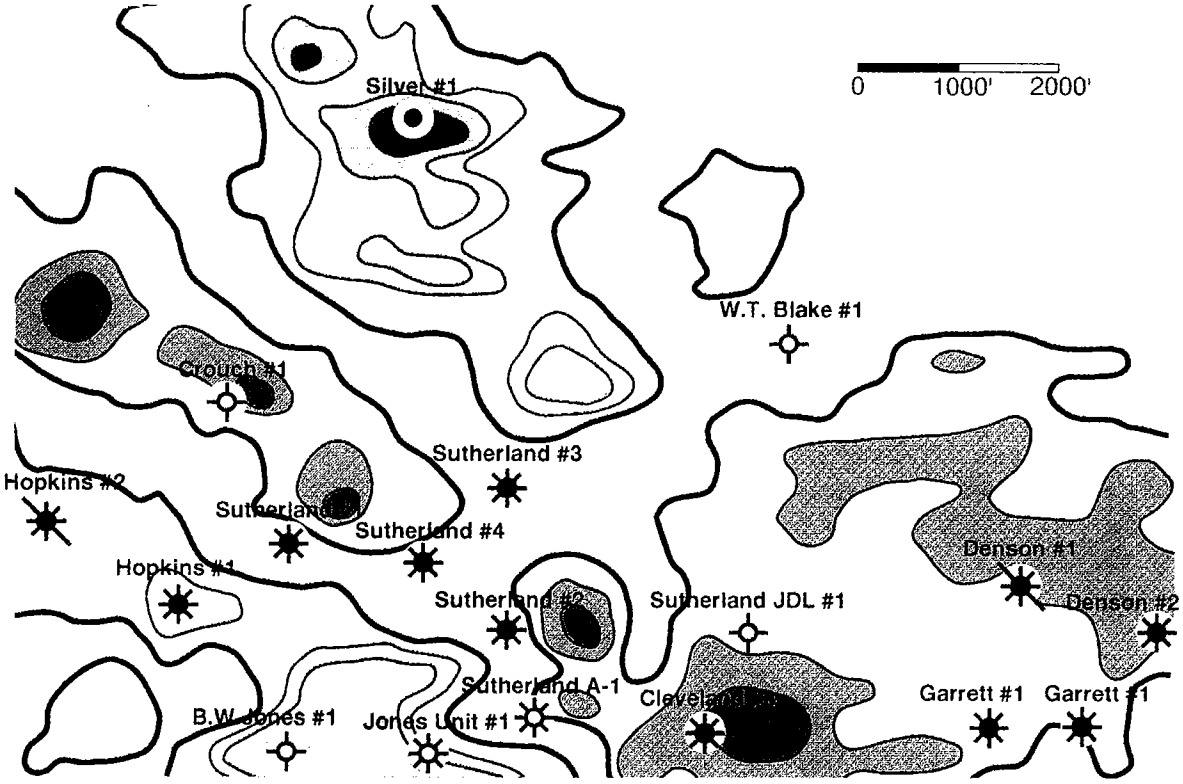

Figure 2. Ellenburger time horizon from 1995 3-D seismic survey, Montague County, Texas. Ellenburger structure highlighted with red, orange, and yellow. Conglomerate trough shown in blues. Note that all wells were drilled after the seismic and microbial surveys were completed.

this project, which represented a wildcat exploration program.

The seismic prospect was drilled at the crest of the structure in March 1996. The No. 1 Silver well encountered 6 ft of tight Salona sand in the Ellenburger section. Completion efforts recovered only marginally commercial hydrocarbons: approximately 340 barrels of oil (BO) was produced in 3 years. The operators intensified their investigation of a possible conglomerate reservoir. In October 1996, the J. G. Stone No. 1 Sutherland Unit was drilled within the microbial anomaly coincident with the trough and encountered two separate conglomerate zones, each with 10 ft of pay. Initial production from the lower zone was 500 thousand cubic feet of gas per day (MCFGPD) and 5 barrels of oil per day (BOPD). The next well found three charged conglomerate zones, including 22 ft of pay in the lower zone, and an initial production near 1,000 MCFGPD. A total of 14 producing wells have been drilled in or near the conglomerate trough. Additionally, four dry holes have been drilled inside the geophysical trough feature but were in areas outside the microbial microseepage anomalies.

Approximately 1 year after the conglomerate discovery well was drilled, a repeat microbial survey was completed in order to document changes in the microseepage signature over time of the new-field discovery (Fig. 4). In general, areas with background microbial values remained stable after 1 year's production, whereas the two producing areas experienced as much as a 50% decrease in microseepage signature. This phenomenon of apparent reduced hydrocarbon microseepage over producing fields is thought to be due to a decline in reservoir pressure as well as changes in the drive mechanism that controls microseepage.

Seismic/MOST Survey Parameters

The Montague County 3-D seismic program consisted of a vibroseis survey. Parameters include 7 source lines, 336 source points, source-point intervals of 220 ft, source-line intervals of 1,540 ft, 9 receiver lines, 396 receiver stations, geophone-group intervals of 220 ft, and receiver-line intervals of 1,320 ft. A 110- × 110-ft bin size was utilized. There were approximately 94 source points and 110 receiver stations per square mile. The sampling rate was 2 ms, and the record length was 3 s.

The reconnaissance MOST survey was designed to evaluate the Ellenburger structure found by seismic methods at a depth of 7,200 ft in the northern part of the survey area. The first MOST survey consisted of 63 samples. The Ellenburger structure was associated with a positive, but small, microbial signature. A group of higher microbial values was aligned with what appeared to be a trough oriented northwest–southeast through the survey area south of the structure. A second microbial survey with 104 infill samples was completed to further delineate the microseepage anomalies.

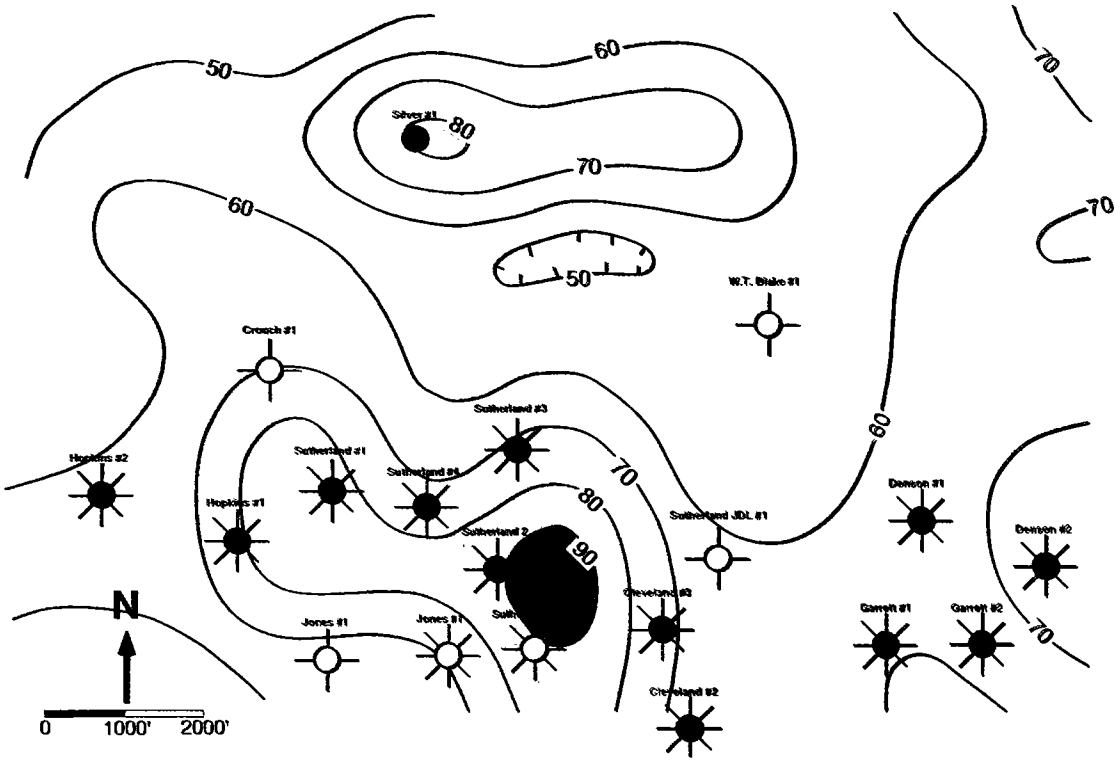

Figure 3. Microbial microseepage signatures completed after the seismic survey. Contour values are concentrations of MOST microbial samples. Red, orange, and yellow are the anomalous hydrocarbon-indicating microbial signatures. All wells were drilled after the microseepage survey was completed.

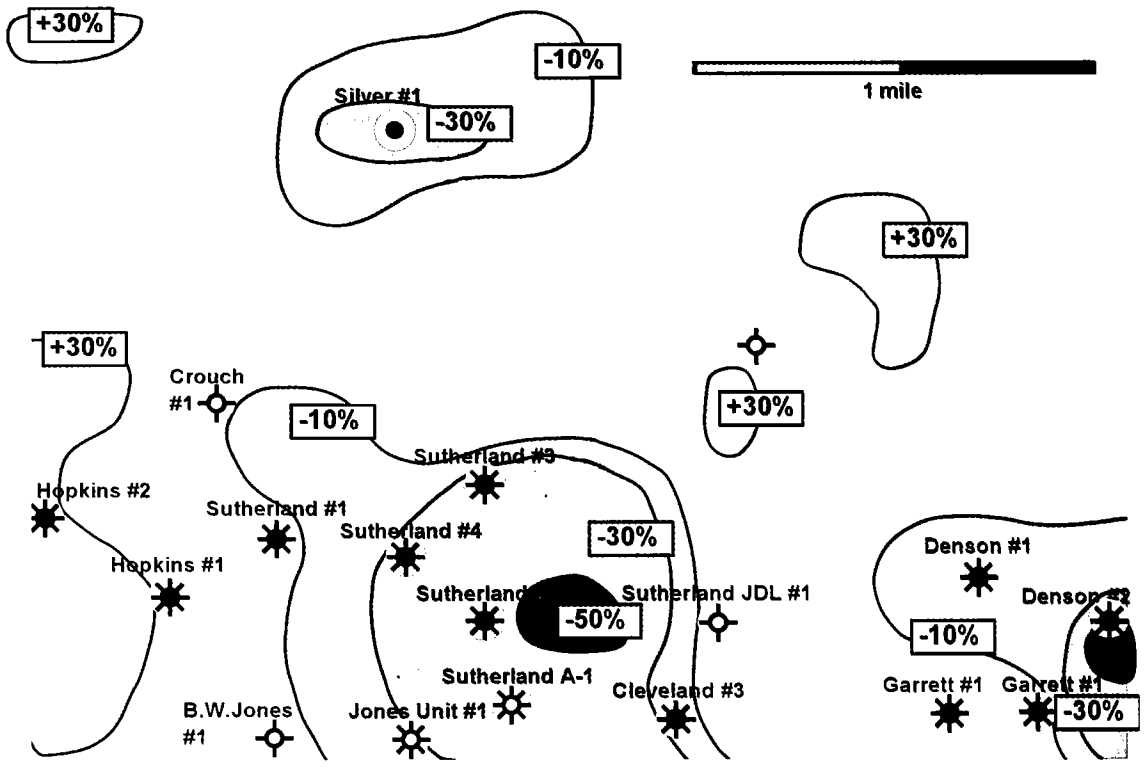

Figure 4. Repeat MOST survey completed 1 year after the first wells were discovered. Contour values show the change from the discovery MOST contours of Figure 3. Blue, green, and light blue highlight the greatest decrease in values, which occur in the areas of greatest production. All wells were drilled before the MOST survey was completed.

The operator, J. G. Stone Oil Co., Victoria, Texas, focused initially on the Ellenburger structure as their primary prospect target. This structure was clearly identified by the 3-D seismic survey. The Salona sand is a fine-grained quartz sand approximately 30–70 ft below the top of the Ellenburger in this area of Montague and Wise Counties. The rule of thumb for this part of the Fort Worth basin is that 50 ft of closure on the Ellenburger means 100,000 BO. Seismic data showed almost 100 ft of closure for the No. 1 Silver location. Success also depends on porosity and permeability; unfortunately, the Silver well was tight.

As indicated by the strongest microbial microseepage anomalies, a second prospective target was identified as Atokan conglomerates in a stratigraphic trap south of the Ellenburger structure. Exploration for these zones has been difficult in the past because production can be achieved only where the charged conglomerates pinch out against higher areas. Like river sands and conglomerates of today, the best Atokan conglomerate accumulations occur in low areas. These conglomerates were derived from the Muenster–Red River arch complex to the north and were transported into the basin through a series of prograding, high-constructive deltas (Lovick and others, 1982). Atokan conglomerates are commonly found as point-bar deposits, distributary-mouth-bar deposits, distributary-channel-fill deposits, meander-channel-fill deposits, and crevasse-splay deposits of primarily coarse, quartzose sands. Permeabilities average 4 to 10 md. A single well can produce >1 billion cubic feet of gas (BCFG).

Drilling Results

The 7,200-ft Ellenburger test, the No. 1 Silver, was completed first but proved to be tight and marginally productive. The well has only produced 337 BO and some gas in 3 years. However, the large trough area filled with Atokan conglomerates has proved to be a more attractive target. Several operators have joined the effort of drilling the conglomerate zone after the J. G. Stone Oil Co.'s successful No. 1 Sutherland Unit discovery well. A total of 14 wells have penetrated the Park Springs Conglomerate field to depths of approximately 5,800 ft. Four dry holes were drilled in the survey area. All four are in areas with low or background microbial values, even though the seismic data suggest conglomerate deposition in or near the trough. By May 1999 the estimated total field production was approximately 1.5 BCFG and 34,000 BO.

Microseepage Changes Over Time

A repeat MOST survey was completed over 152 of the original 167 sample sites approximately 1 year after the conglomerate discovery well was drilled. Some of the wells had been producing for less than a year. The same collection crew was utilized, and the same conditions were encountered in the field. All laboratory procedures were also duplicated.

Figure 4 shows a map of the percentage change in microbial values from February 1996 to October 1997. Most striking is the mirror image of microbial value reduction—some as high as 50% in the heart of the conglomerate producing area—from that of the initial pre-drilling microbial anomalies. In general, the survey's microseepage background areas remained the same after 1 year. Small parts of the repeat survey increased as much as 30% in value, but these are mostly in nonproductive background areas. The microseepage signatures of the pre-drilling anomalous MOST map is almost identical to the anomalous microseepage *reduction* map created after 1 year's production.

Similar in strategy to 4-D geophysical evaluations, time-lapse microbial evaluations anticipate reduced microbial populations above parts of a reservoir in direct communication with the producing wells. This phenomenon of apparent reduced hydrocarbon microseepage over producing fields is thought to be due to a decline in reservoir pressure as well as to changes in the drive mechanism controlling microseepage. When a well is brought into production, the drive changes from a vertically migrating buoyancy force to horizontal gas streaming to low-pressure sinks created around producing wells. When this occurs, microseepage ends, and microbial populations decline rapidly. This change in drive mechanism and microbial-population densities can be used to help define reservoir drainage directions, radii, and heterogeneities around existing wells in producing fields. Conversely, in areas where the reservoir is being repressured, as in a waterflood, microseepage is reestablished. Microbial counts will increase at the surface, reflecting the increased hydrocarbon microseepage coming from the portion of the reservoir in direct contact with the waterflood.

Without seismic or integrated geologic data, the stand-alone microseepage data are limited to identification of hydrocarbon "hot spots." No direct evidence as to a prospect's depth can be derived from surface microseepage data alone. However, there is evidence that deeper untapped reservoirs do create surface microseepage signatures in areas of shallower mature production.

VASSAR WATERFLOOD CASE STUDY

First in 1994, and then again in 1999, 441 shallow soil samples were collected every 100 yards, covering a total area of 1.25 mi^2, of Sullivan and Co.'s Southeast Vassar Vertz Sand Unit in Payne County, Oklahoma. The Vassar Unit consists of 21 active production wells, 7 active injection wells, 3 inactive injection wells, and 8 dry holes (Fig. 5). Microseepage-signature patterns, as measured by microbial populations, were mapped and compared to (1) well locations and waterflood sweep patterns, (2) sand-unit thicknesses, and (3) injection and production rates. This comparison demonstrated a correlation between microbial microseepage patterns and reservoir-production parameters.

There exists a dynamic microseepage system within the waterflood pattern. At the time of the first survey in 1994 (Fig. 5), the most recent and prolific producing wells in the northern part of the reservoir displayed

positive hydrocarbon-microseepage signatures. The older producing wells farther south showed stronger microseepage patterns adjacent to and between present producing-well locations, thus identifying possible infill locations. The oldest reservoir well locations, which are now abandoned injection wells, demonstrate possible re-pressuring with elevated microseepage measurements. The newest Vassar producing well in the southeastern part of the waterflood was successfully predicted to be a producer, although undrilled locations just north of the new well site were targeted as preferred locations by their microseepage signature. The 1999 data set (Fig. 6) shows an expected across-the-board reduction in microseepage signatures as the Vassar waterflood matures and production rates continue to decline. The large background area in the northwestern part of the survey area remained stable and low for both surveys.

FUTURE INTEGRATION NEEDED

Finding deeper reservoirs within a producing area has always been difficult for microseepage surveys. Anomalous values might have a deeper source or might reflect a residual signature from shallower production. More recent extensive microbial surveys completed in the Texas and Oklahoma Panhandles have targeted deeper producing targets, such as Morrow channels. These new prospects—primarily stratigraphic traps—can be found below the shallower Hugoton field wells by using 3-D seismic techniques. But not all the seismic targets are charged with hydrocarbons, and some are so subtle that their seismic image is undefined. By utilizing a MOST sample density of every 10th mile, collected in a grid, 1 mi^2 is covered by 121 samples. More than 400 sections have been evaluated by using a combination of seismic and microbial data. Seismic prospects of commercial value are both confirmed and denied by this MOST reconnaissance density. Without the integration of seismic and microbial data, the ability to look deeper in mature areas is greatly reduced.

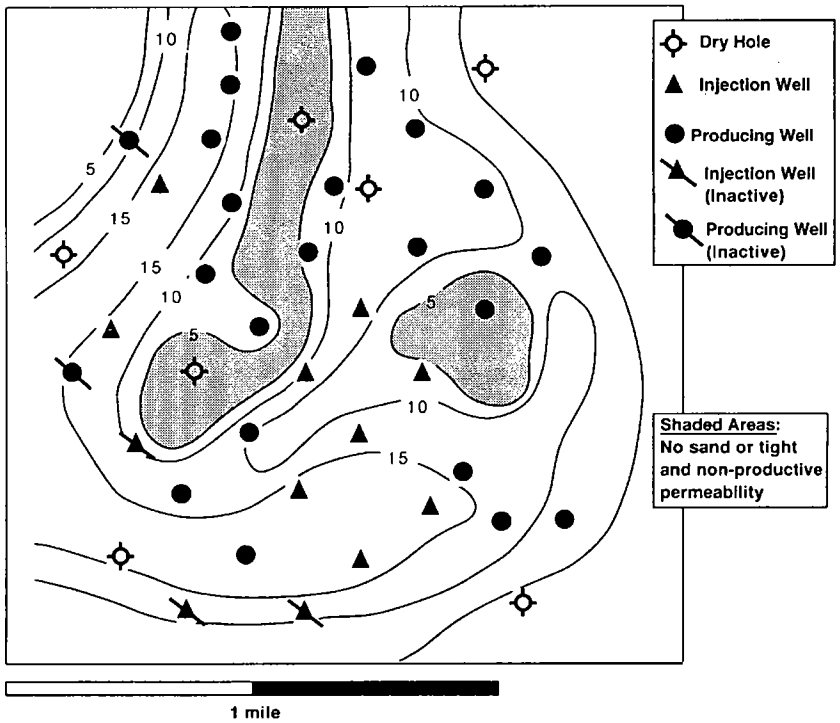

Figure 5. Net isopach of Vertz sand and production map, 1993–99, Vassar Vertz Unit, Payne County, Oklahoma.

REFERENCES CITED

Hitzman, D. C.; Tucker, J. D.; and Rountree, B. A., 2000, Microbial reservoir characterization of Hobart field, Kiowa County, Oklahoma, *in* Johnson, K. S. (ed.), Platform carbonates in the southern Midcontinent, 1996 symposium: Oklahoma Geological Survey Circular 101, p. 129–130.

Jones, V. T., III; and Burtell, S. G., 1996, Hydrocarbon flux variations in natural and anthropogenic seeps, *in* Schumacher, Dietmar; and Abrams, M. A. (eds.), Hydrocarbon migration and its near-surface expression: American Association of Petroleum Geologists Memoir 66, p. 203–221.

Klusman, R. W.; and Saeed, M. A., 1996, Comparison of light hydrocarbon microseepage mechanisms, *in* Schumacher, Dietmar; and Abrams, M. A. (eds.), Hydrocarbon migration and its near-surface expression: American Association of Petroleum Geologists Memoir 66, p. 157–168.

Lovick, G. P.; Mazzine, C. G.; and Kotila, D. A., 1982, Atokan clastics—depositional environments in a foreland basin: Dallas Geological Society, p. 193–210.

Quigley, D. C., 1999, Decrease in natural marine hydrocarbon microseepage near Coal Oil Point, California, associated with offshore oil production: Geology, v. 27, p. 1047–1050.

Schumacher, Dietmar, 1999, Surface geochemical exploration for petroleum, *in* Beaumont, E. A.; and Foster, N. H. (eds.), Exploring for oil and gas traps, *pt. 3 of* Handbook of petroleum geology: American Association of Petroleum Geologists, Tulsa, Treatise of Petroleum Geology, p. 18-1–18-27.

Schumacher, Dietmar; and Abrams, M. A. (eds.), 1996, Hydrocarbon migration and its near-surface expression: American Association of Petroleum Geologists Memoir 66, 445 p.

Schumacher, Dietmar; Hitzman, D. C.; Tucker, J. D.; and Rountree, B. A., 1997, Applying high-resolution surface geochemistry to assess reservoir compartmentalization and monitor hydrocarbon drainage, *in* Kruizeng, R. J.; and Downey, M. W. (eds.), Applications of emerging technologies: unconventional methods in exploration for oil and gas, V: Southern Methodist University Press, Dallas, p. 309–322.

Tucker, J. D.; and Hitzman, D. C., 1994, Detailed microbial surveys help improve reservoir characterization: Oil and Gas Journal, v. 92, no. 23, p. 65–68.

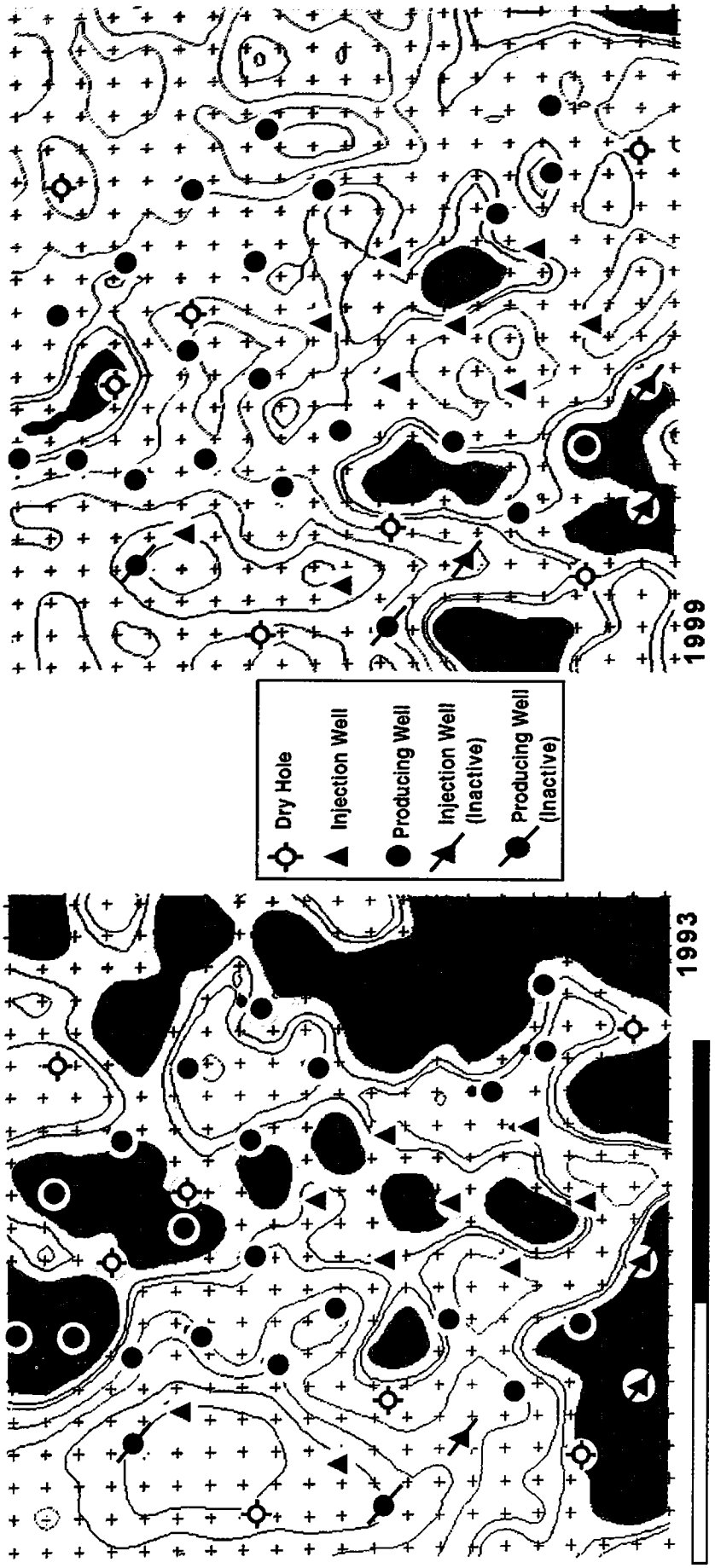

Figure 6. Tracking waterflood production with microseepage, Vassar Vertz Unit. Warm colors (yellow, orange, and red) indicate areas of higher production, and cool colors (green and blue) indicate areas of lower production.

Interpreting Seismic Data from the Wichita Frontal Fault Zone with the Help of Ray-Trace Modeling

Jan M. Dodson, Roger A. Young, and Kevin J. Smart
University of Oklahoma
Norman, Oklahoma

Ray-trace modeling calculates seismic raypaths that obey Snell's law as they travel through layers of known velocity. Snell's law states that when a sound wave reflects from a surface, the angle of incidence equals the angle of reflection. The velocities of the layers above and below the surface determine (1) the angle of the reflection, (2) traveltimes through the layers, and (3) the amplitude of the reflection. If the velocities are the same, there will be no reflection.

Rays reflecting from a surface at 90° are called normal-incidence rays, which travel the same path down to the reflector and back up to the surface. Seismic data are processed and presented to interpreters as a stacked section. Many theoretical assumptions underlie the concept of the stacked section. Of primary importance for this study is the assumption that a stacked section represents normal-incidence raypaths. Reflections on a stacked seismic section of undeformed, horizontally layered rocks are assumed to come from directly below their surface location. In areas of structurally complex geology, reflections can be recorded at large horizontal distances from the reflection points. Seismic migration is the process that attempts to move reflections from below their recorded locations to their true subsurface locations. Migrated events typically move updip to become steeper and shorter.

The Wichita frontal fault zone (WFFZ) is part of a linear trend in southern Oklahoma that extends from the Arbuckle Mountains in south-central Oklahoma through the Wichita Mountains to the buried Amarillo Mountains in the Texas Panhandle. Intense subsurface deformation exists along the WFFZ. Oil- and gas-well data document intense subsurface deformation, including overturned beds and crystalline basement rocks thrust over Paleozoic sedimentary rocks. High-resolution, two-dimensional seismic data do not show correctly positioned and well-focused structures. Correct migrations of seismic data are vital to accurate interpretations, but they cannot be achieved without well-defined velocity models. Velocity models are in turn based on interpretations of the data. Seismic ray-tracing can confirm or disprove an interpretation.

A synthetic, zero-offset seismic data set paralleling an actual seismic line was created with ray-tracing software by building a cross section (Fig. 1) using all available data, including well data and seismic data. Raypaths were calculated and analyzed to determine where reflections occurred in the subsurface and where they were recorded at the surface. Arrival times and reflection amplitudes were used to produce synthetic traces for comparison to actual seismic data.

Although synthetic data cannot be quantitatively compared to the actual data, qualitative comparisons can be made. In areas of complex deformation, geologists and geophysicists tend to interpret linear dipping events as faults. This study suggests an alternate interpretation. If the geological model is accurate, the velocity contrast across the fault cannot produce a significant reflection event. Ray-tracing confirms that the fault does not generate an extensive coherent event. There is no difference in velocity along most of the length of the fault to create a reflection. The time and location of the steeply dipping event on SEI 5223 (Fig. 2) correspond relatively well with the time and location of a reflection from the overturned limb of the anticline on the synthetic data set shown in Figure 3. We can conclude that the steeply dipping event on SEI 5223 is actually the reflection from the overturned limb of the anticline.

Insights from ray-trace modeling might provide information (such as improved acquisition and processing parameters) that will help produce enhanced seismic images of complex subsurface structures. Extending this study into three dimensions will improve our understanding of seismic-reflection data from structurally complex areas.

Dodson, J. M.; Young, R. A.; and Smart, K. J., 2002, Interpreting seismic data from the Wichita frontal fault zone with the help of ray-trace modeling, *in* Cardott, B. J. (ed.), Revisiting old and assessing new petroleum plays in the southern Midcontinent, 2001 symposium: Oklahoma Geological Survey Circular 107, p. 109–111.

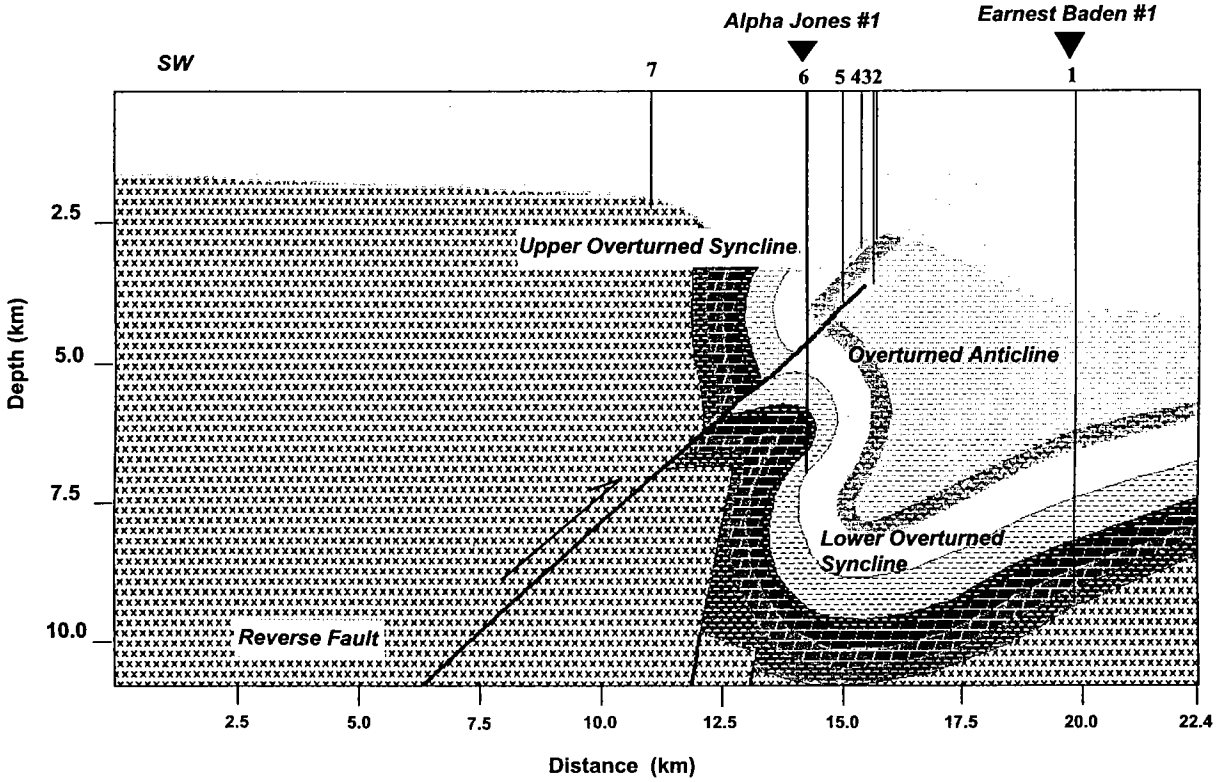

Figure 1. Cross section for ray-tracing (created in GX2® software), based on well logs. The overturned folds and reverse fault are constrained by dipmeter data from the No. 1 Alpha Jones well. Gray-scale patterns represent different interval velocities. The lower half of the fault shows layers of the same velocity on each side of the boundary. No reflection will occur at this interface.

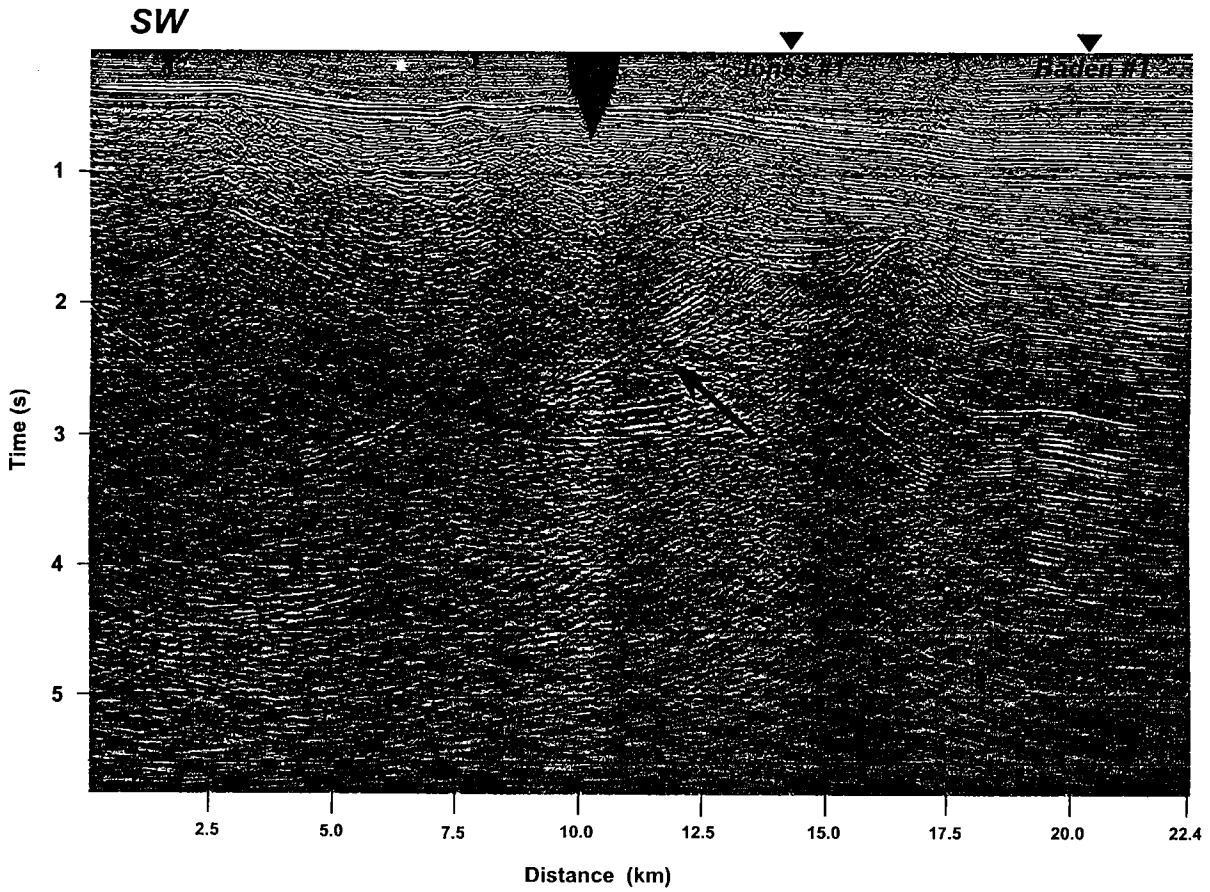

Figure 2. Variable-intensity display of SEI 5223 post-stack time-migration ellipse highlights a linear dipping reflection.

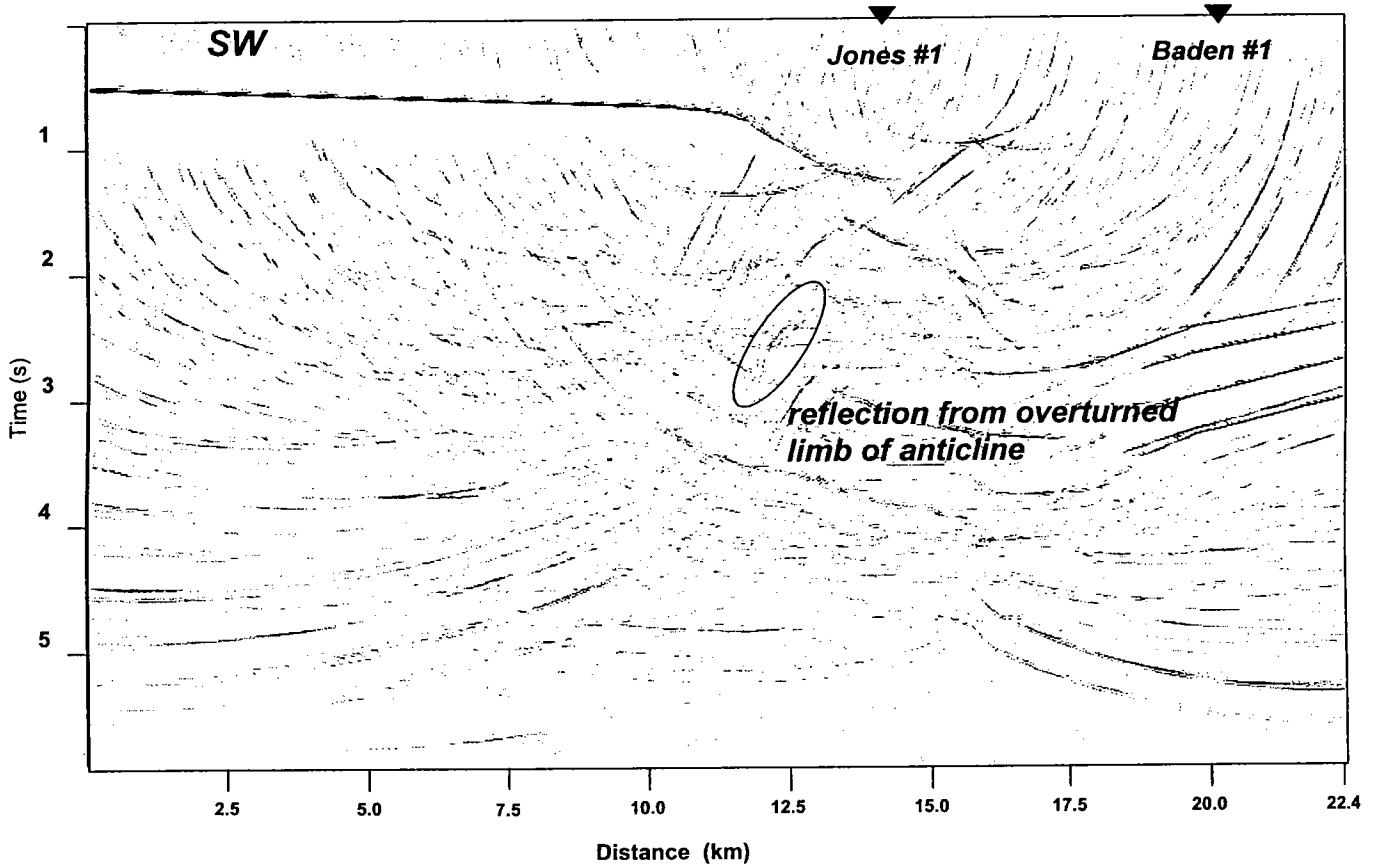

Figure 3. Variable-area display of migrated synthetic seismic data. Note the approximate time and horizontal location of the ellipse highlighting the reflection from the overturned limb of the anticline. Reflection events were positively identified in the ray-tracing process.

Size-Frequency Effects and Reservoir Structure

Evgeni M. Chesnokov
University of Oklahoma
Norman, Oklahoma

John H. Queen
Conoco, Inc.
Ponca City, Oklahoma

Yuri A. Kukharenko
Russian Academy of Sciences
Moscow, Russia

John M. Hooper
Conoco, Inc.
Ponca City, Oklahoma

Irina O. Bayuk and Alexandr A. Vikhorev
Russian Academy of Sciences
Moscow, Russia

ABSTRACT.—This report is designed to aid in further development of a recent theory for the calculation of effective physical parameters to explain the behavior of experimental characteristics of wave fields at different scales in order to predict the properties of reservoir structures. The most important of these physical parameters are (1) mineralogical composition and the concentration of pores and cracks (fractures); (2) elastic, electrical, and thermal properties of a rock's mineral content; and (3) distribution of minerals and cracks with respect to space and shape.

The results of our research have allowed us to (1) solve the problem of construction of macroscopic equations and obtain the exact expressions of effective tensors of elastic modules for various distribution functions of fractures, including size, aspect ratio, and space statistics; (2) develop software that can include 10 different methods of calculating the effective elastic and transport properties and determining their correlation; (3) identify the features that allow us to distinguish gas- and oil-saturated fractures; (4) calculate Green's function, the mass operator in dynamic cases, which leads to determination of dynamic elastic constants, thus permitting us to estimate the frequency dependence of multiscale fractured media; and (5) investigate the stress dependence of elastic and transport characteristics of fractured media.

INTRODUCTION

The experimental data obtained from seismology, deep-sounding seismic exploration, and rock-sample investigations demonstrate the existence of anisotropy in the physical properties of the Earth's lithosphere. Anisotropy of elastic properties is related to the inner structure of the media, such as preferred mineral orientation, fissility, thin layers, and stress in porous cracked (fractured) media (Chesnokov, 1977; Nikitin and Chesnokov, 1984).

A recently developed theory of the calculation of effective physical parameters, such as elastic, electrical, and thermal (Chesnokov and others, 1995, 1998; Chesnokov and Zatsepin, 1991), has presented new information about the structure and composition of the Earth's lithosphere. To calculate these parameters, it is necessary to accept a satisfactory model of a medium. The real structure of the lithosphere is very complicated, so as a rule, when carrying out geophysical modeling, we must use average characteristics of a medium to simplify the problem. It is convenient in this case to use effective characteristics of inhomogeneous media that give the properties of equivalent homogeneous media. The use of effective parameters makes it possible to predict the macroscopic properties of a medium when the physical and geometric characteristics of its phases are known. It is necessary to stress that a knowledge of the effective physical properties of media under stress is helpful in solving different application problems, as follows:

Chesnokov, E. M.; Queen, J. H.; Kukharenko, Y. A.; Hooper, J. M.; Bayuk, I. O.; and Vikhorev, A. A., 2002, Size-frequency effects and reservoir structure, *in* Cardott, B. J. (ed.), Revisiting old and assessing new petroleum plays in the southern Midcontinent, 2001 symposium: Oklahoma Geological Survey Circular 107, p. 113–122.

1. *Rock-sample investigations under stress and temperature.* The comparison of theoretical and experimental data for these properties allows one to predict the properties of rock mass in deep layers of the Earth and even to estimate the values of stress in some cases.

2. *Estimating reservoir structure.* Seismic parameters obtained, for example, from vertical-seismic-profiling (VSP) data make it possible to distinguish rocks saturated with liquids and gases. Also, electrical, thermal, and permeability parameters allow us to distinguish subsurface oil- and water-bearing rocks.

The purpose of this report is to assist the further development of the theory of the calculation of effective physical parameters (elastic, electrical, and thermal) to explain the behavior of experimental characteristics of wave fields at different scales (from rock samples to large areas) in order to predict the properties of reservoir structures.

METHODS OF CALCULATING EFFECTIVE PHYSICAL PARAMETERS OF SOLIDS

Current Status

Physical parameters of rocks are governed by different factors. The most important of these are (1) mineralogical composition and the concentration of pores and cracks; (2) elastic, electrical, and thermal properties of the mineral content of each rock sample; and (3) distribution of minerals and cracks with respect to space and shape.

Up to the mid-1970s, almost all mathematical approaches for the calculation of average modules of elasticity for polycrystalline rocks were based on the Voight-Reuss-Hill approximation (see review in Chesnokov, 1977). The principal deficiency of this method is related to the statement that the average and effective values of characteristics of physical properties are the same. This statement is not correct, however, because fluctuations of stress and strain in real media are not equal to zero. This means that the average and effective parameters are equal to each other in unusual cases only.

The calculations of effective parameters for porous fractured media are based mainly on the Eshelby method (Eshelby, 1957) or its modifications. The principal deficiencies of these approaches are as follows:

1. These methods usually consider the interaction between matrix and inclusions, which means that inclusions cannot "see" each other (e.g., no interactions between them);

2. Independence of coordinates (effective homogeneous media) and frequencies, which ignores the spatial distribution of inclusions;

3. Investigation of only the simplest shapes of inclusions (spheroid or elliptical as a rule);

4. The approaches considered do not include the calculation of effective physical parameters for porous cracked media under stress;

5. The influence of chemical processes on elastic and transport properties of porous fractured media is ignored.

Aims of This Work

1. To develop a mathematical method that allows us to consider the problems that are impossible to take into account in using other approaches. We suggest the Feynman diagram mathematical technique (FDMT) as the most powerful for the calculation of effective elastic and transport characteristics of microinhomogeneous media in static and dynamic cases;

2. To carry out a comparative analysis of all known methods, using FDMT to choose the most simple and effective;

3. To develop the software for calculating elastic and transport characteristics of porous cracked anisotropic media;

4. To derive the formulas for estimating the influence of size and shape of inhomogeneities on effective physical parameters of fractured media, and, based on these results, to develop new algorithms and software that allow us to analyze the influence of these factors on elastic and transport properties of studied media;

5. To develop software for calculating attenuation from the scattering of fluctuations of elastic parameters;

6. To find the relationship between elastic and transport characteristics of porous fractured media.

SUGGESTED APPROACH FOR CALCULATION OF EFFECTIVE PHYSICAL PARAMETERS OF ANISOTROPIC MEDIA WITH INCLUSIONS

Static Case

As a basic model of a porous cracked medium, we assume a linearly elastic (mostly anisotropic) matrix with some system of distributed penny-shaped or ellipsoidal inclusions (voids, saturated cracks). The distribution function of inclusions with respect to orientation angle and aspect ratio is considered to be a function of applied stress. The approach for the calculation, C, is based on the solution of the problem of averaging Green's tensor in an inhomogeneous medium with a fluctuating elastic tensor, $\mathbf{C_{ijkl}(r)}$. We follow this approach, using a new method for geophysical investigations of the solid Earth called the *diagram technique* (Chesnokov and others, 1995, 1998), which was developed in the context of the quantum-field theory.

The main idea of this method is concerned with calculations of effective physical parameters for media with random distribution of inclusions. Mathemati-

cally, this means that we have to proceed from equations with random parameters to average equations.

Basic Equations

Let us consider the static equation of linear theory elasticity without initial stress (Mura, 1991; Shermergor, 1977):

$$Lu = -f, \tag{1}$$

where: $L_{ik}(x) = \partial_j C_{ijkl} \partial_l$, C_{ijkl} is the symmetric tensor of elasticity, and f is the stress source. The solution to this equation can be written in the form:

$$u_i(x) = \int G_{ik}(x, x_1) f_k(x_1)\, dx_1, \tag{2}$$

where: G is Green's function of static equation (1) relating the value, u, in a point, x, with the value, f, in a point, x_1. Green's function, G, satisfies the equation (Shermergor, 1977; Mura, 1991):

$$L_{ik}(x) G_{kj}(x) = -\delta_{ij} \delta(x - x_1). \tag{3}$$

Here, δ_{ij} is the Kroneker symbol, and $\delta(x - x_1)$ is the Dirac delta-function.

We will consider a microinhomogeneous medium with a random distribution of inclusions (crystals, pores, cracks). The elastic tensor, **C**, of such a medium is a random function over coordinates and can be presented in the form:

$$C_{ijkl}(x) = \left\langle C_{ijkl}(x) \right\rangle + C'_{ijkl}(x), \tag{4}$$

where: $\langle \mathbf{C(x)} \rangle$ is the average value of $C(x)$, and $C'(x)$ is the fluctuation. According to the common definition (Mura, 1991; Shermergor, 1977):

$$\left\langle C_{ijkl} \right\rangle = \frac{1}{V} \int C_{ijkl}(x) dV;$$
and
$$\left\langle C'_{ijkl} \right\rangle = \frac{1}{V} \int C'_{ijkl}(x) dV \equiv 0. \tag{5}$$

Here, a volume, V, consists of a great number of inclusions, but less than $(\lambda)^3$, where λ characterizes a macroscopic scale of a consideration (e.g., length of an elastic wave). Using expression (4), we can write:

$$L_{ik}(x) = \left\langle L_{ik}(x) \right\rangle + L'_{ik}(x), \tag{6}$$

where:

$$\left\langle L_{ik}(x) \right\rangle = \partial_j \left\langle C_{ijkl}(x) \right\rangle \partial_l;$$
and
$$L'_{ik}(x) = \partial_j C'_{ijkl}(x) \partial_l. \tag{7}$$

It can be shown that Green's function, G, satisfies the integral equation

$$G_{ik}(x, x_1) = G^0_{ik}(x, x_1) + \int G^0_{il}(x, x_2) L'_{lp}(x_2) G_{pk}(x_2, x_1)\, dx_2. \tag{8}$$

This equation is suitable for transformation from a microinhomogeneous to an effective medium, which is described by the exact average Green's function, $\langle \mathbf{G} \rangle$. This function, $\langle \mathbf{G} \rangle$, performs a link between average field, $\langle \mathbf{u} \rangle$, and source, **f**:

$$\left\langle u_i(x) \right\rangle = \int \left\langle G_{ik}(x, x_1) \right\rangle f_k(x_1)\, dx_1. \tag{9}$$

The exact average Green's function, $\langle \mathbf{G} \rangle$, involves contributions of fluctuations $\mathbf{C'(x)}$ of an elastic tensor $\mathbf{C^*(x)}$ of any order. For calculations of $\langle \mathbf{G} \rangle$ it is convenient to use the diagram technique (Chesnokov and others, 1995). The final expression for the averaged Green's function (Dyson equation) can be written in the form:

$$\left\langle G_{ij}(r, r_1) \right\rangle = G^0_{ij}(r, r_1) + \sum_{kl} \int G^0_{ik}(r, r_2) M_{km}(r_2, r_3) \left\langle G_{mj}(r_3, r_1) \right\rangle dr_2\, dr_3 \tag{10}$$

where: r_1 is the radius-vector of the point of source, and r is the radius-vector of the point of observation; G^0_{ij} is the zero Green's function, which reflects the properties of the matrix without fractures.

Although equation (10) is obtained by the summing of a perturbation series over fluctuations of the elastic tensor, C', this equation represents the exact equation for the average Green's function, $\langle G \rangle$. The situation here is like that in the ordinary theory of integral equations: the value C' is replaced by $\varepsilon C'$, where $\varepsilon << 1$ is a small parameter, and by summing the perturbation series over the degrees of ε we obtain the solution, which can be analytically continued up to $\varepsilon = 1$. Of course, as in the many-body problem, the analytical solution of the Dyson equation cannot be found in a general case. But the significance of this equation is in the possibility of building the solution not for Green's function but for the reciprocal value, which is the mass operator, M_{ik}. This is important, because Green's function is a slowly decreasing oscillating function of the coordinate difference. The Fourier image has a singularity—i.e., has poles near real axes—and does not allow us to apply the perturbation theory because the perturbation series slowly converges in this case. At the same time the mass operator is rapidly decreasing over the coordinate difference, and the Fourier image is a smooth function, which can be expanded in the perturbation series. In addition, in contrast to the matrix method (Mura, 1991; Shermergor,

1977), the diagram technique allows one to partly sum up the terms of the infinite perturbation series and express the M_{ik} in a series form by the exact average of Green's function, $\langle G \rangle$ (not over the zero Green's function, G^0), and hence automatically get the self-consistent system of equations for $\langle G \rangle$.

In accordance with definition (5), we understand the averaging in equation (10) as averaging over volume, $V(a^3 << V << \lambda^3)$. As a result of this definition, all averaged values may be dependent on coordinates only in a macroscopic scale ($\lambda >> a$).

Where wavelength (λ) is comparable or less than a size (a) of randomly distributed inhomogeneities, we must use the averaging in equation (8) over an ensemble of realizations. In this case the Dyson equation (8) is valid for any relationship between (λ) and (a). In accordance with the ergodic hypothesis, both methods of averaging coincide where $\lambda >> a$ and the mass operator, as a function of coordinate difference, decreases on a scale of $r^{corr} << \lambda$.

Local Approximation

In order to go from the Dyson equation to equations of the macroscopic theory of elasticity of effective media, we need to take into account that the correlation radius of fluctuations, r^{corr}, is small in comparison to the scale of our consideration—for example, to the wavelength, λ. In this local approximation the mass operator, M, is equal to zero where $|r_2 - r_1| >> r^{corr}$, and is not zero where $|r_2 - r_1| \le r^{corr}$. Taking this into account, the Dyson equation (10) can be written in the form:

$$\left\langle G_{ij}(r, r_1)\right\rangle = G^0_{ij}(r, r_1) + \int G^0_{ik}(r, r_2) M^*_{kl}(r_2)\left\langle G_{lj}(r_2, r_1)\right\rangle dr_2 \tag{11}$$

where: $$M^*_{kl}(r_2) = \int dr_1 M_{kl}(r_1, r_2). \tag{12}$$

After some algebraic transformations, tensor $M^*_{kl}(r)$ can be presented in the form:

$$M^*_{kl}(r) = \partial_m C^*_{klmn}\partial_n - \partial_m\left\langle C_{klmn}\right\rangle\partial_n \tag{13}$$

where: C^*_{klmn} is the tensor of effective modules of elasticity for media with inclusions.

General Singular Approximation Method

Basic Relationships

The purpose of this report is to show the method of calculation of M^* or C^*. In the literature (Mavko and others, 1993; Mura, 1991; Shermergor, 1977) various approximations are used. The reason for using different approximations relates to the impossibility of getting the analytical solution to many body problems. In our case it is important to point out that the approximation is accomplished by the mass operator, M'_{ik}—i.e., in the kernel of the Dyson equation (not in Green's function). This means that the different approximation of the mass operator leads to different forms of the Dyson equation but not to the perturbation theory. The problem of the choice of the mass-operator approximation for studies of experimental data can be solved by determining the minimum free-energy function or by comparison with the considered experiment, which means the solution of the inverse problem. Taking all of this into account, we need to develop a mathematical approach that allows us to calculate M'_{ik} in a quite simple way, and at the same time it should be rather effective in order to take into account various physical effects.

After some algebraic transformations, we can obtain the basic formulas for calculating elastic characteristics of media with inclusions (Bayuk and Chesnokov, 1998):

$$C^* = \left\langle C(I - gC')\right\rangle^{-1}\left\langle (I - gC')^{-1}\right\rangle^{-1} \tag{14}$$

where: I is the fourth-rank unit tensor and $g_{ijkl} = \int_V G^0_{ijkl}(r)\,dr$ (Bayuk and Chesnokov, 1998).

Expression (14) is the basic equation of the general singular approximation (GSA) (Shermergor, 1977; Fokin, 1996; Bayuk and Chesnokov, 1998) and contains the algebraic (not integral) operations that allow us to carry out complete summation of series (8). A more detailed justification for the GSA method can be found in Bayuk and Chesnokov (1998).

The developed method has several advantages:

1. It coincides with correlation approximation (Lifshits and Rozentsveig, 1946) where the contrast of properties between matrix and inclusions is small;
2. It coincides with the virial approximation where the volume of concentration is small;
3. The corresponding choice of the so-called comparison body allows us to find the "upper" and "lower" Hashin-Shtrickman boundaries; to coincide with self-consistent approximation; and to bring us to the Willis (1977) formula, which is obtained by using the variational principles;
4. In contrast with the variational principles, this method allows us to calculate the deviations, which are connected with the rejection terms and consequently give an estimation of the accuracy of the method.

As can be shown (Chesnokov and others, 1995; Bayuk and Chesnokov, 1998), the elastic constant **C*** in equation (14) is the function of six groups of the parameters, which define the structure of the studied medium, namely:

$$C^*_{ijkl} = F(\Omega_i, R_i, \chi_i, a_i, x_i, M) \tag{15}$$

where:
Ω_i is the distribution function (DF) of inclusions over angles; R_i is the distribution function (DF) of inclusions over crystallographic axes (in the case of anisotropic inclusions); χ_i is the DF of inclusions over aspect ratio in the case of elliptical inclusions; a_i is the DF of inclusions over size; x_i is the DF of centers of inclusions over coordinate (space statistics); and M reflects the existence of liquid, gas, and brine inclusions simultaneously in the studied medium.

On the basis of this approach, we can analyze elastic and transport characteristics of various types of media such as (1) microinhomogeneous (low-porosity isotropic or anisotropic) media with different types of distributed fractures; (2) laminated media with isotropic (anisotropic), periodic (randomly) distributed layers with various types of fractures; and (3) microinhomogeneous (laminated) media under stress and temperature.

Comparison of Numerical and Experimental Data

To substantiate the validity of the GSA method, we compared theoretical results with experimental data. Figure 1 shows longitudinal velocities in a sample of water-saturated artificial sandstone (Rathore and others, 1995) with aligned cracks and with an aspect ratio of 0.00364. The crack density is 0.1. The velocities are measured in the plane normal to the crack plane. Bulk and shear moduli of the wet sandstone polycrystals (so-called matrix) are 7.78 GPa and 3.32 GPa, respectively; the density is 1.711 g/cm^3.

The numerical results obtained by different theoretical methods (Castaneda and Willis, 1995; Eshelby, 1957; Hudson, 1981; Nishizawa, 1982; Thomsen, 1995; Brown and Korringa, 1975) are also shown in Figure 1. As shown, our method agrees best with experimental data (Bayuk and Chesnokov, 1998).

How Can We Discriminate between Gas and Liquid Inclusions?

The GSA method can be used to find the parameters sensitive to the type of fluid in inclusions. We consider a clay matrix with bulk and shear elastic modules, K = 26.83 GPa and μ = 16.77 GPa, and a density of 2.6 g/cm^3. The cracks are modeled as aligned ellipsoids with an aspect ratio of 0.03, being typical of clay reservoirs (Xu and White, 1996). The effective elastic tensor, C^*, is calculated by equation (10) for gas, water, and oil inclusions. Because this equation is derived by assuming that the components are elastic, we take the bulk modulus of low-viscous oil equal to 0.8 GPa (Dortman, 1992). The azimuthal dependencies of longitudinal- and shear-wave velocities are calculated for the plane perpendicular to the crack plane by using the Christoffel equation. Figure 2 plots the ratio of the longitudinal-wave velocity to the faster shear-wave velocity versus the angle of propagation. The angular dependence of the ratio is monotonic for gas inclusions but exhibits peculiarity in the case of liquid inclusions. The observed peculiarity is explained by the fact that differently polarized shear waves intersect at a certain angle.

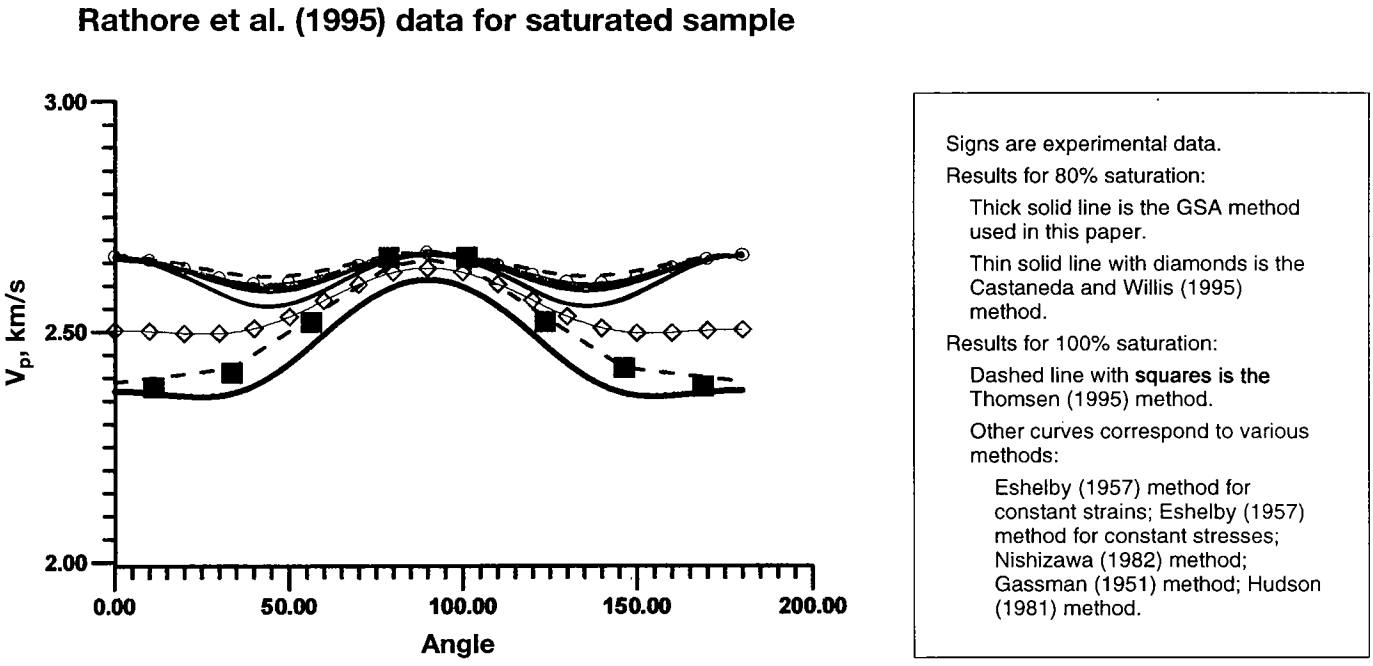

Figure 1. Comparison of measured (black squares) and calculated longitudinal-wave (*P*-wave) velocities for wet artificial sandstone in the plane normal to the crack plane. Saturation used in calculation is shown.

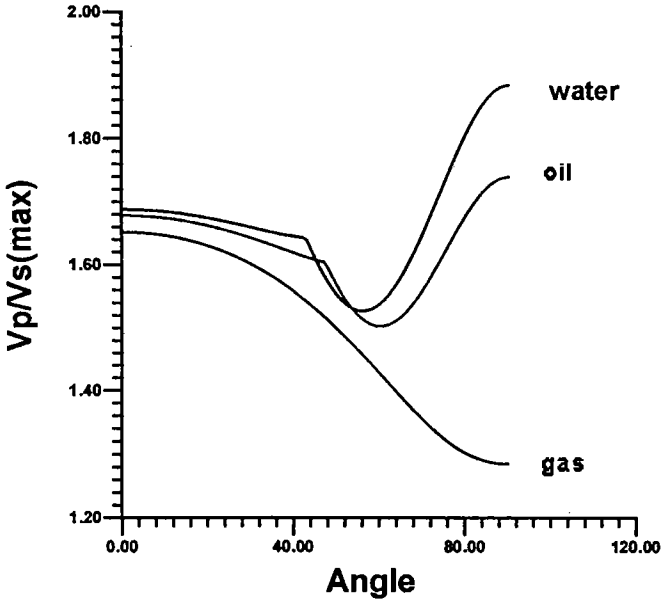

Figure 2. Ratio of longitudinal-wave velocity (V_p) and shear-wave velocity (V_s) for a clay reservoir model for wave propagation in the plane normal to the crack plane.

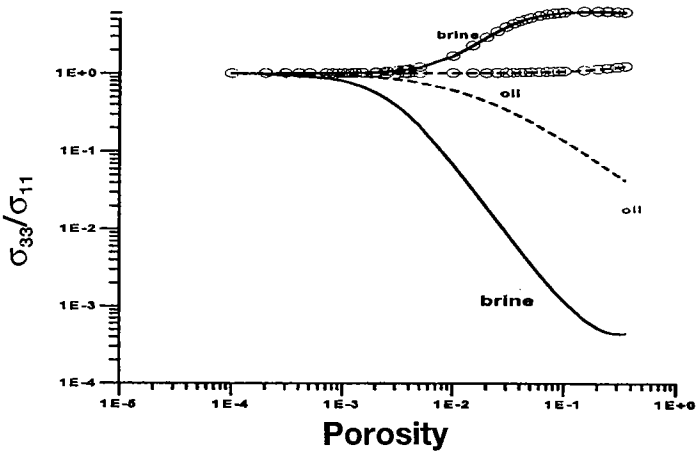

Figure 3. Clay reservoir model: clay matrix and ellipsoidal aligned cracks with the 0.03 aspect ratio (disks; solid lines) and the 3 aspect ratio (channels; lines with circles). Results were obtained with the help of the GSA method. Electrical conductivity of the matrix, brine, and oil were chosen to be 10^{-4}, 30, and 10^{-12} S/m, respectively. The figure shows the ratio of conductivity normal to the crack plane to that in the crack plane. The plane X_1X_2 is the crack plane (plane of isotropy), in which the crack cross sections are circular. The plane X_1X_2 is the plane of disk-shaped cracks. The axes of channels are parallel to the X_3 axis. As can be seen, the dependence is monotonic in the case of oil with the constant sign of the second derivative, whereas the second derivative of the dependence may change its sign in the case of brine inclusions. We have extended the formulas of the Eshelby (1957) and Nishizawa (1982) methods to the case of transport properties and have performed these calculations by using these methods. We found that appropriate results can be obtained only by the GSA method.

We abandoned the use of these methods for prediction of fluid type. We also calculated the effective electrical properties for a medium with inclusions whose shapes are disks and channels. The aspect ratio of the disks is 0.01, and that of channels is 3. The electrical conductivities of the matrix, brine, and oil are chosen as 0.0001, 0.5, and 10^{-12} S/m, respectively. Figure 3 shows the ratio of maximal and minimal values of electrical conductivity versus porosity.

Correlation between Elastic and Transport Properties

We simultaneously calculated the longitudinal-wave (P-wave) velocities and the conductivity of a clay reservoir, depending on the porosity of oil and brine inclusions. The crack aspect ratio was 0.03 (typical of clay). To estimate the effect of matrix friability, k, on conductivity, we used two greatly different values for friability: 0.5 (Fig. 4a) and 10^{-6} (Fig. 4b).

The values for the conductivity of clay, brine, and oil were 10^{-4}, 30, and 10^{-12} S/m, respectively. In calculations, we varied only the volume concentration of inclusions, and their aspect ratio was kept constant. The results demonstrate that a variation in the matrix friability greatly affects the values of conductivity, whereas the values of elastic velocities change only slightly. The calculations also show that conductivity values are also strongly dependent on friability values. To predict permeability, we have to solve an inverse problem. Using elastic data, we find the aspect ratio of cracks. The connectivity of inclusions (the matrix friability) should be obtained from the electrical data. To find these parameters, we can also use the elastic and electrical data simultaneously. Knowing the aspect ratio and matrix friability, and using equation (10), we can calculate an effective permeability. Figure 5 plots the values for P-wave velocity versus permeability for a clay reservoir model with a matrix friability of 0.5.

To estimate the permeability of inclusion material, we determined the permeability of "pure" fluid from the permeability of limestone, assuming that the permeability of the host matrix is 10^{-40} m^2 and using the GSA method. The fluid permeability was estimated at $7 \cdot 10^{-10}$ m^2. The permeability of sedimentary rocks calculated with the use of the accepted values agrees well with the set of experimental data (Volarovich, 1988).

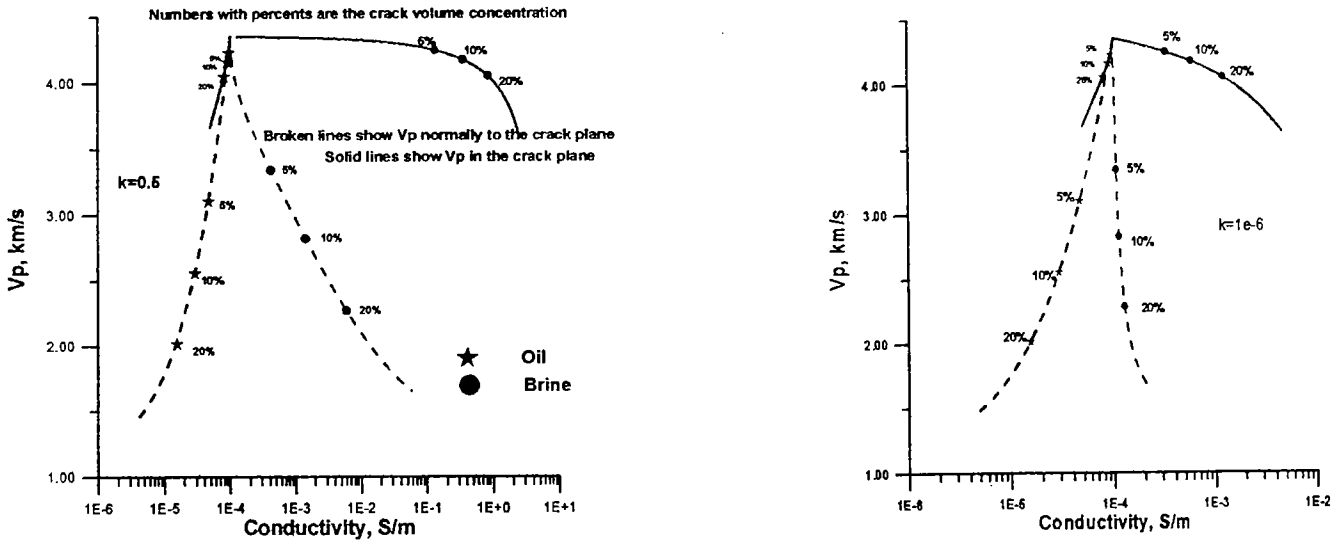

Figure 4. Clay reservoir model, consisting of a clay isotropic matrix (bulk modulus, $K = 26.83$ GPa; shear modulus, $\mu = 16.77$ GPa; density, $\rho = 2.00$ g/cm^3; and conductivity $\sigma = 10^{-4}$ S/m) and aligned ellipsoidal inclusions with the 0.03 aspect ratio typical of clay reservoirs. The numerical results were obtained by using the GSA method. Results obtained for the crack concentration, varying from 0 to 0.5, and constant aspect ratio. The oil parameters are $K = 1.39$ GPa, $\rho = 0.80$ g/cm^3, and $\sigma = 10^{-12}$ S/m. Brine parameters are $K = 2.2$ GPa, $\rho = 1.00$ g/cm^3, and $\sigma = 30$ S/m. Calculations are performed for different values of matrix friability: (a) $k = 0.5$, and (b) $k = 10^{-6}$ (see GSA method formulas).

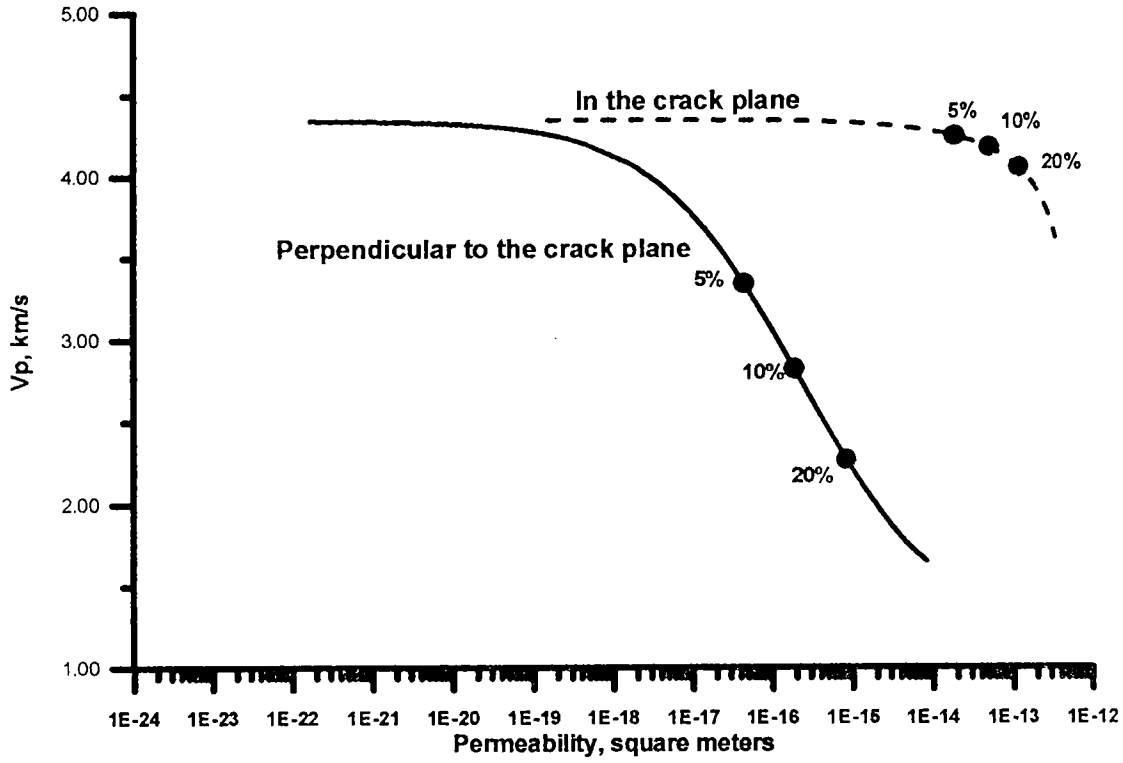

Figure 5. Clay reservoir model, consisting of a clay isotropic matrix (bulk modulus, $K = 26.83$ GPa; shear modulus, $\mu = 16.77$ GPa; density, $\rho = 2.60$ g/cm^3; and permeability, $P = 10^{-40}$ m^2) and aligned ellipsoidal inclusions with the 0.03 aspect ratio typical of clay reservoirs. The numerical results were obtained by using the GSA method. Results obtained for the crack concentration, varying from 0 to 0.5, and constant aspect ratio. Cracks are assumed to be filled with brine, with $K = 2.2$ GPa, $\rho = 1$ g/cm^3, and $P = 7 \bullet 10^{-10}$ m^2. Solid lines show P-wave velocity (V_p) versus permeability in the direction normal to the crack plane, and broken lines present this dependence in the crack plane. Calculations are performed for matrix friability.

As the conclusion of this part of the report, we can say:

1. The GSA method provides the best agreement with experimental elastic data in comparison with other mathematical approaches. The GSA method can be used to find the correlation between elastic waves (longitudinal and shear) and transport (electrical conductivity and permeability) properties of porous cracked anisotropic media.

2. It is shown that such a correlation of the properties allows us to discriminate the type of inclusions (liquid or gas) and the sort of liquid (oil or brine) in inclusions.

3. Using such a correlation, it is also possible to predict the permeability of porous cracked media. For this prediction, it is necessary to solve the inverse problem to find the crack aspect ratio and the matrix friability by using experimental data on elasticity and electrical conductivity.

All this means that the GSA method is quite powerful for the computation of the effective physical properties of porous cracked anisotropic media.

Dynamic Case

Dyson Equation

Here, we consider the frequency dependence of elastic constants. As in the static case, we will consider randomly distributed fractures. The Dyson equation for this case has the form:

$$G_{ik}(t-t_1x,x_1)=G^0_{ik}(t-t_1x,x_1)+\int G^0_{il}(t,t_2,x,x_1)L'_{lp}(x_2)G^0_{pk}(t,t_1,x,x_1)\,dx_2\,dt_2 \quad (16)$$

where:

$$M^*_{ik}(t,t_1,x)=\int dy M_{ik}(t,t_1,x,y) \quad (17)$$

is the mass operator in the dynamic case.

It can be shown that equation (17) can be presented in the form:

$$M^*_{ik}(t,t_1,x)=\nabla_m\left[C^*_{imkn}(t,t_1)-\langle C_{imkn}\rangle\delta(t,t_1)\right]\nabla_n. \quad (18)$$

This expression is the basic expression for calculating the dynamic tensor for elastic constants—i.e., estimating its frequency dependence.

The final expression of C^*_{ijkl} as a function of frequency can be written in a form using a correlation approximation (Chesnokov and others, 1998):

$$C^*_{ijkl}(\omega)=\langle C_{ijkl}\rangle+\frac{1}{(2\pi)^3}\int G^0_{mn,pq}(\omega,k)B^{pqkl}_{ijmn}(k)\,dk. \quad (19)$$

Here, in the isotropic case:

$$B^{ijmn}_{pqkl}(k)=\int dx e^{ik(x-x_1)}B^{ijmn}_{pqkl}(x-x_1)$$

$$G^0_{mn,pq}(\omega,k)=ik_pik_qG^0_{mn}(\omega,k), \quad (20)$$

$$G^0_{mj}(\omega,k)=\frac{\delta_{ij}-\nu_i\nu_j}{\langle\mu\rangle k^2-\rho\omega^2}+\frac{\nu_i\nu_j}{\langle\lambda+2\mu\rangle k^2-\rho\omega^2}.$$

Using this expression, we can calculate the frequency dependence of elastic constants.

Influence of Shape and Size of Inhomogeneities on Frequency Dependencies of Elastic Constants

This part of the results allows us to estimate the influence of size and shape of fractures on the dynamic effective characteristics of an elastic medium. This is essentially to point out that the existence of the spatial distribution of inclusions (far order) leads to the strong influence of size and shape of inclusions on effective dynamic elastic constants and completely suppresses the weak correlation of sizes of inclusions with the length of a propagating wave. Taking into account the paired correlation function of spherical inclusions of the radius, **a**, the configuration of which is determined by the structural factor, $S(k)$, an equation can be written in the form:

$$C^*_{ijkl}(\omega)=\langle C_{ijkl}\rangle-\frac{n^2g^{(1)}|S(k_0)|^2\bullet|\chi(k_0)|^2}{\langle\mu\rangle k_0^2-\rho\omega^2}\bullet\left[C^I_{ijkl}k^0_pk^0_qC^I_{pqkl}-\frac{\langle\lambda+2\mu\rangle}{\langle\lambda+2\mu\rangle k_0^2-\rho\omega^2}C^I_{ijkl}k^0_mk^0_nk^0_pk^0_qC^I_{pqkl}\right]$$

$$B^{pqmn}_{ijkl}(k)=|S(k)|^2\bullet|\chi(k)|^2\bullet C^I_{ijkl}C^I_{pqmn}g(k) \quad (21)$$

and, using equations (21) and (22), we can write:

$$C^*_{ijkl}(\omega)=\langle C_{ijkl}\rangle-\frac{n^2g^{(1)}|S(k_0)|^2\bullet|\chi(k_0)|^2}{\langle\mu\rangle k_0^2-\rho\omega^2}\bullet\left[C^I_{ijkl}k^0_pk^0_qC^I_{pqkl}-\frac{\langle\lambda+2\mu\rangle}{\langle\lambda+2\mu\rangle k_0^2-\rho\omega^2}C^I_{ijkl}k^0_mk^0_nk^0_pk^0_qC^I_{pqkl}\right] \quad (22)$$

Expression (22) gives the complete description of the effective dynamic elastic constants and their de-

pendence on the size and shape of inclusions. The functions $S(k_0)$ and $\chi(k_0)$ are defined by the same expressions as in the static case. The existence of space statistics reveals the fact that the values of functions $S(k_0)$ and $\chi(k_0)$ depend on the argument k_0, which defines the order in homogeneous locations (but not the wavelengths of P and S elastic waves). These formulas work in a static case as well, where $\omega = 0$.

ADDITIONAL REMARKS

Taking into account the foregoing approach, we plan to develop new software for calculations of various static and dynamic effects such as (1) scattering, including multiple scattering; and (2) taking into account the fluctuation of densities.

In addition, the developed method allows us to study the inverse problem of determining the statistical structure of inhomogeneous media. From the results of the solution to this problem we can expect (1) estimation of the type of symmetry from experimental data of the studied medium, and (2) estimation of porous cracked statistical parameters using V_p and V_s in a considered medium.

The influence of stress on static and dynamic properties of inhomogeneous media is our next problem to consider, as follows.

Nikitin and Chesnokov (1984) considered the stress effect on the elastic parameters of a homogeneous anisotropic medium without random inclusions. It was shown that the initial stress effect on the elastic moduli is determined by the sixth-rank tensor expressed via the derivatives of the free energy with respect to the strain tensor. Specifically, the equation for the elastic modulus tensor, which depends on the deviator of initial stresses, has the form:

$$C_{ijkl} = C^0_{ijkl}(p) + B_{ijklmn} t^0_{mn} \tag{23}$$

where: $C^0_{ijkl}(p)$ is the elastic modulus tensor of a medium without initial stresses, B_{ijklmn} is the sixth-rank tensor generated by the initial stresses, and t^0_{mn} is the deviator of initial stress.

The tensor, **B**, was used to study the effect of initial stresses on a medium without inclusions (pores and cracks).

The next goal is to extend these results to a porous cracked medium. It will be shown that the effect of the initial stress on the parameters of the porous cracked medium is described by the same sixth-rank tensor.

Using the Feynman diagram technique, we derived the Dyson equation for the average Green's function of a porous cracked medium. The kernel of the equation, the mass operator, M_{ij}, is a function of the derived sixth-rank tensor, B_{ijklmn}. It was found that for a porous cracked medium the variation in the effective elastic modulus tensor, C^*_{ijkl}, caused by initial stresses, is expressed in terms of the functional derivative of the mass operator with respect to the elastic modulus tensor of the matrix (top part):

$$\gamma_{ijklmn} = \frac{\partial M_{ij}}{\partial C_{ijkl}} \tag{24}$$

where: C_{ijkl} is the elastic modulus tensor of the matrix (medium without pores and cracks). In turn, the top part is represented by the averaged Green's function of the medium without initial stresses and is calculated with the help of the diagram technique.

As a result, we obtain an effective sixth-rank tensor, B^*_{ijklmn}, in determining the contribution of initial stresses to the effective elastic modules of a porous cracked medium. This tensor, **B***, consists of two terms associated with the matrix effect and the effect of the microinhomogeneous medium structure, depending on the initial stresses,

$$B^*_{ijklmn} = B_{ijklmn} + \gamma_{ijklmn}. \tag{25}$$

Analytical and numerical methods for calculating **B*** for different distribution functions of inclusions will be developed. We will use the distribution functions over six groups of parameters: (1) aspect ratio, (2) orientation of inclusion axes in space, (3) the center of mass of inclusions (spatial statistics), (4) spatial orientation of crystallographic axes of inclusions, (5) inclusion size, and (6) multiphase composition of the medium studied. All these parameters determine the medium structure and depend on initial stresses. Thus, the effect of initial stresses on the aforesaid distribution functions will be considered.

CONCLUSIONS

The developed approach delineated in this report allows us to:

1. Solve the problem of construction of macroscopic equations and obtain the exact expressions of effective tensors of elastic modules for various distribution functions of fractures, including size, aspect ratio, and space statistics;

2. Develop software that can include 10 various methods of calculating the effective elastic and transport properties and determining their correlation;

3. Determine the features that allow us to distinguish gas- and oil-saturated fractures;

4. Calculate Green's function, the mass operator in dynamic cases, which leads to determination of dynamic elastic constants, thus allowing us to estimate the frequency dependence of multiscale fractured media;

5. Investigate the stress dependence of elastic and transport characteristics of fractured media.

REFERENCES CITED

Bayuk, I. O.; and Chesnokov, E. M., 1998, Correlations between elastic and transport properties of porous cracked anisotropic media: Physical Chemistry of the Earth, v. 23, p. 361–366.

Brown, R.; and Korringa, J., 1975, On the dependence of the elastic properties of a porous rock on the compressibility of the pore fluid: Geophysics, v. 40, p. 608–616.

Castaneda, P.; and Willis, J., 1995, The effect of spatial distribution on the effective behavior of composite materials and cracked media: Journal of Mechanics of Physical Solids, v. 43, p. 1919–1951.

Chesnokov, E. M., 1977, Elastic anisotropy of the upper mantle: Nauka, Moscow, 144 p. [in Russian].

Chesnokov, E. M.; and Zatsepin, S. V., 1991, Effect of applied stress on effective elastic anisotropy in cracked solids: Geophysical Journal International, v. 107, p. 563–569.

Chesnokov, E. M.; Kukharenko, Y. A.; and Kukharenko, P. Y., 1995, Diagram technique method for calculation of effective physical parameters of microinhomogeneous media: SPIE v. 2571, Mathematical Methods in Geophysical Imaging III, San Diego, p. 2–12.

_____ 1998, Frequency dependence of physical parameters of microinhomogeneous media: Space Statistics, Revue de l'Institut Français du Pétrole, v. 53, p. 729–734.

Dortman, N. B. (ed.), 1992, Petrophysics, 1–3: Nedra, Moscow, v. 1, 391 p. [in Russian].

Eshelby, J. D., 1957, The determination of the elastic field of an ellipsoidal inclusion, and related problems: Proceedings of Royal Society of London, Series A, Mathematical and Physical Sciences, v. 241, p. 376–396.

Fokin, A. G., 1996, Macroscopic conductivity of random inhomogeneous media: Physics–Uspekhi, v. 39, p. 1009–1032.

Gassman, F., 1951, Über die Elastizität Poroser Medien: Vier: Der Natur Gesellschaft, v. 96, p. 1–23.

Hudson, J., 1981, Wave speed and attenuation of elastic waves in material containing cracks: Mathematical Proceedings of Camb. Society, v. 88, p. 371–384.

_____1991, Overall properties of heterogeneous materials: Geophysical Journal International, v. 107, p. 505–512.

Lifshits, I. M.; and Rozentsveig, L. N., 1946, About theory of elastic properties of polycrystals: Journal of Experimental and Theoretical Physics, v. 16, p. 967–978.

Mavko , G.; Mukerji, T.; and Dvorkin, J., 1993, Rock physics formulas: Stanford, 323 p.

Mura, T., 1991, Micromechanics of defects in solids: Kluver Academic Publishers, Dordrechts, London, 298 p.

Nikitin, L. V.; and Chesnokov, E. M., 1984, Wave propagation in stress induced media: Geophysical Journal of Royal Astronomical Society, v. 76, p. 129–133.

Nishizawa, O., 1982, Seismic velocity anisotropy in a medium containing oriented cracks—transversely isotropic case: Journal of Physics of the Earth, v. 3, p. 331–348.

Rathore, J. S.; Fjaer, E.; Holt, R. M.; and Renie, L., 1995, *P*- and *S*-wave anisotropy of synthetic sandstone with controlled crack geometry: Geophysical Prospecting, v. 43, p. 711–728.

Shermergor, T. D., 1977, Theory of elasticity of inhomogeneous media, Moscow: Nauka, 400 p. [in Russian].

Thomsen, L., 1995, Elastic anisotropy due to aligned cracks in porous rocks: Geophysical Prospecting, v. 43, p. 805–829.

Volarovich, M. P. (ed.), 1988, Physical properties of minerals and rocks at high thermodynamic parameters: Nedra, Moscow, 367 p. [in Russian].

Willis, J. R., 1977, Bounds and self-consistent estimates for the overall properties of anisotropic composites: Journal of Mechanics of Physical Solids, v. 25, p. 185–202.

Xu, S.; and White, R. E., 1996, Modeling transport properties of anisotropic shaly formations: Society of Exploration Geophysicists Workshop, Dallas, Expanded Abstract PP 3.11.

Understanding Regional Chimneyhill Correlations and Their Impact on Reservoir Predictability

Kurt Rottmann
Consultant Geologist
Oklahoma City, Oklahoma

ABSTRACT.—The Hunton Group consists of a series of shallow-water carbonates deposited between the Ordovician Sylvan Shale and the Devonian–Mississippian Woodford Shale. Because of this unique stratigraphic relationship, the Hunton Group is easily recognized in the subsurface from open-hole logs. However, individual subgroups and formations within the Hunton Group are often miscorrelated, owing to the lack of recognizable regional time-stratigraphic markers. Detailed correlation of Hunton strata has revealed the Prices Falls Member of the Clarita Formation to be an important and reliable time-stratigraphic marker. This marker is important because it serves to separate the productive beds of the overlying Fitzhugh Member from the underlying Cochrane and Keel Formations, which are not nearly as productive.

The Fitzhugh Member of the Clarita Formation, which is part of the Chimneyhill Subgroup, is generally an organo-detrital carbonate deposited over a broad, flat platform as sheets of carbonate debris. However, an abrupt east–west stratal buildup of this member is characterized by individual beds that become very thick. It is within these beds that dolomite commonly forms, probably by the ground-water-mixing model proposed by Badiozamani in 1973. These dolomite beds have reservoir properties that make them some of the most prolific reservoirs of the Hunton Group. It was commonly thought that these dolomites were random and uncorrelatable, but it is now apparent that regional correlations of these beds are possible, especially after recognition of the time-stratigraphic Prices Falls Member. It is this ability to predict the extension of correlative porous and permeable dolomite beds of the Fitzhugh Member that makes this member an attractive target for exploration and development.

INTRODUCTION

The Hunton Group represents a series of subgroups and formations that contain an abundance of attractive economic oil- and gas-producing reservoirs in Oklahoma. Perhaps the most important productive unit is the Fitzhugh Member of the Clarita Formation, which is part of the Chimneyhill Subgroup (Fig. 1). This member is a primary target in much of west-central, central, and east-central Oklahoma. The purpose of this paper is to try and distinguish this member from other, less attractive formations of the Hunton Group by establishing its relationship with the underlying Prices Falls Member, also of the Clarita Formation. Once the Prices Falls has been correlated, the remaining organo-detrital limestones above it (and below the shaly and marly beds of the overlying Henryhouse Formation) would constitute the Fitzhugh Member. Once the Fitzhugh Member has been identified, it is possible to correlate zones within it. These zones can be areally mapped, enabling the predictability of and exploration for potential reserves from this interval.

This paper also serves as an addendum to the Oklahoma Geological Survey's recent play-based workshop on the Hunton (Rottmann and others, 2000; Rottmann, 2001). One of the objectives of the cross sections published for that workshop was to demonstrate the regional correlation and relationship between the Prices Falls and Fitzhugh Members in the area described above. This paper ties the outcrop description of the Prices Falls to those cross sections by the publication of a tie section (Fig. 2, cross section C–C′). This paper uses figures from Rottmann and others (2000), so it might be useful for the reader to obtain that publication, as those illustrations referred to will not be reprinted here.

CHIMNEYHILL SUBGROUP

The Chimneyhill Subgroup was named from outcrop exposures near Chimneyhill Creek by Reeds (1911, p. 258). He gave these beds formation rank and designated three units on the basis of lithologic variations. These included the pink-crinodal, glauconitic, and oolitic members. Amsden (1967) formally raised

Rottmann, Kurt, 2002, Understanding regional Chimneyhill correlations and their impact on reservoir predictability, *in* Cardott, B. J. (ed.), Revisiting old and assessing new petroleum plays in the southern Midcontinent, 2001 symposium: Oklahoma Geological Survey Circular 107, p. 123–128.

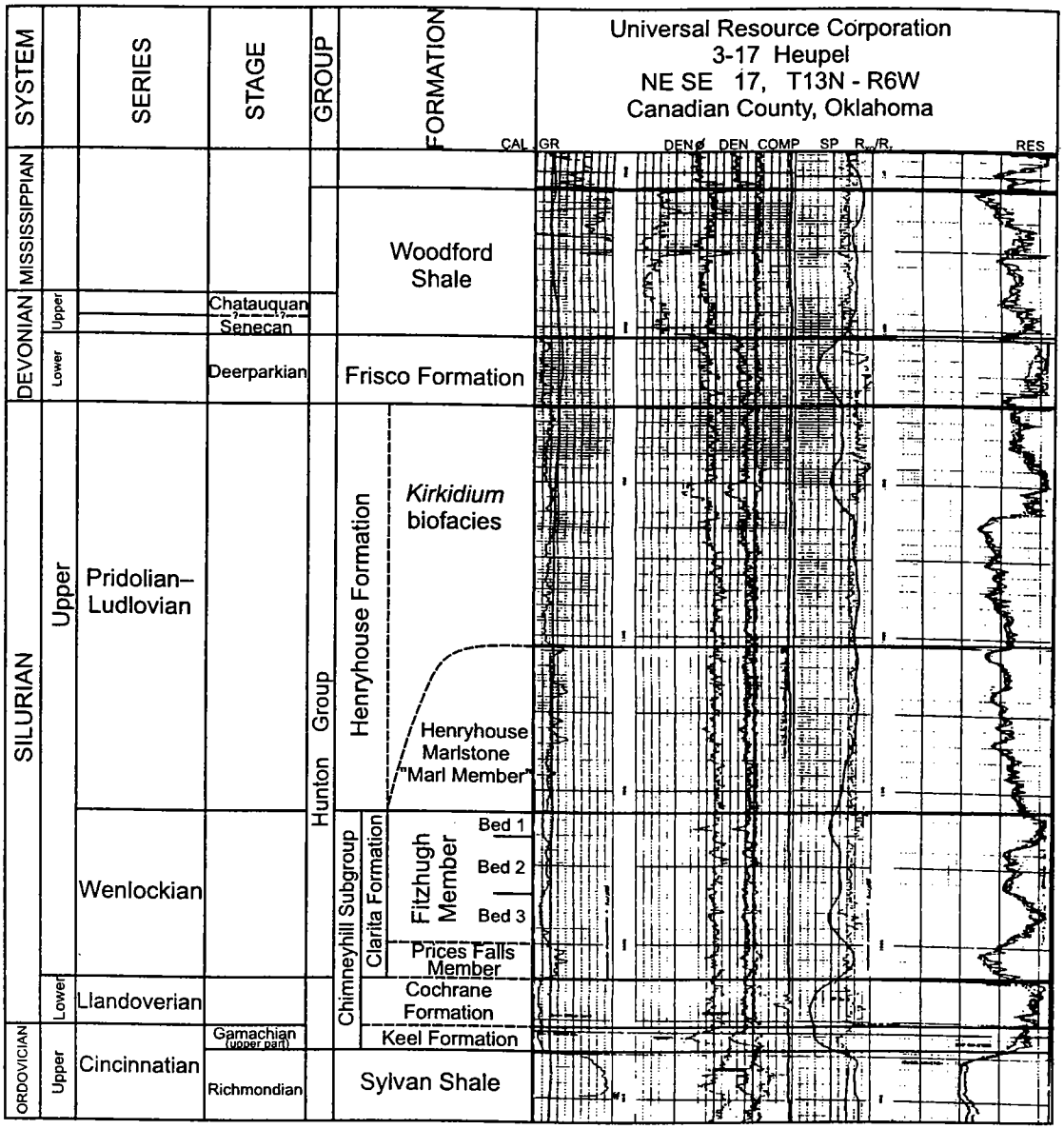

Figure 1. Type log showing the Hunton Group formations and members for an area of central Oklahoma. Characteristic electric-log signatures are shown. *CAL* = caliper; *GR* = gamma ray; *DENϕ* = density porosity; *DEN COMP* = density compensated; *SP* = spontaneous potential; R_{xo}/R_t = ratio of resistivity of flushed zone to resistivity of uninvaded zone, or true resistivity; *RES* = resistivity. From Rottmann and others (2000, fig. 21).

these three members to formation rank, naming them, in descending order, the Clarita, Cochrane, and Keel Formations. He also raised the Chimneyhill to subgroup rank. Figure 1, a type log, illustrates the formations and members of the Hunton in central Oklahoma. As can be seen, the Chimneyhill Subgroup consists of the same three formations described by Reeds, Amsden, and others from the outcrops of southern Oklahoma.

In west-central, central, and east-central Oklahoma the primary producing formation is the Clarita Formation. The Frisco Formation, and to some extent the Henryhouse Formation, are not as prolific as the Clarita. The Cochrane and Keel also are productive but are relatively insignificant.

The Clarita Formation of the Chimneyhill Subgroup is divided into two lithologically diverse units, the Prices Falls Member and the overlying Fitzhugh Member. The lower member is a persistent, low-calcium shale whose type locality is at Prices Falls in the central part of the Arbuckle Mountains (Amsden, 1980). The upper Fitzhugh Member consists of an organodetrital limestone or dolomite that is noted for its thin, even-bedded character (Amsden, 1960, pl. 3, figs. 1,2). The lithologic difference between these two members is distinct and, according to Amsden, can be recognized throughout the Arbuckle Mountains and Criner Hills. A more detailed description of these members can be found in Amsden (1980) and Rottmann and others (2000).

CORRELATION OF THE PRICES FALLS MEMBER FROM SURFACE TO SUBSURFACE

Figure 3 is a gamma-ray profile of the Hunton Group along the exposed outcrop on the north side of U.S. Highway 77 near Turner Falls, southern Oklahoma (Stanley, 2001). The exact location of this outcrop is described as the west side of U.S. Highway 77, ~0.25 mi south of the intersection with Interstate Highway 35 (I-35), Murray County. This outcrop is ~2 mi north of the type section of the Prices Falls Member (Stanley, 2001, stop 7, p. 56). The gamma-ray response for interval 7 (~10 ft above the Sylvan Shale) represents the Prices Falls Member. This interval is ~2 ft thick and is composed of argillaceous mudstone.

This outcrop is ~0.25 mi south of the Washita Valley fault (see Rottmann and others, 2000, pl. 3) on the upthrown side of the fault block. The fault has a vertical displacement >3,000 ft. To the north, on the downthrown side of the fault, a number of wells have penetrated the Hunton. Cross section C–C′ (Fig. 2) correlates the gamma-ray profile of the outcrop Hunton with the subsurface Hunton in this immediate vicinity. Notice the almost exact correlation for the Chimneyhill Subgroup as a whole, and the Prices Falls Member in particular, along the extent of the cross section. This section therefore can be used as the basis for correlation of the Prices Falls Member of the outcrop in the Arbuckle Mountains with equivalent beds in the subsurface of the Anadarko basin. Thus, the intent of this paper to tie the outcrop of the Prices Falls interval to cross section B–B′ of Rottmann and others (2000, pl. 4) has been accomplished by cross section C–C′ (Fig. 2), as can be seen in the correlation from right (outcrop) to left (subsurface).

IMPORTANCE OF THE SUBSURFACE CORRELATION OF THE PRICES FALLS MEMBER

As pointed out in the Hunton play–based workshop (Rottmann and others, 2000), the source area for many of the clastics of the Hunton Group was probably from the south or southeast. These clastics settled out in a northward direction, resulting in a gradation from shales (southern parts of Oklahoma) to marls to shaly limestones (northern parts of Oklahoma). The Prices Falls is one such example of this facies gradation. The Gulf Oil Corp. No. 2 Wheeney well (Fig. 2, cross section C–C′) shows a decreased gamma-ray value for the Prices Falls in comparison to the remaining wells of the cross section. The Wheeney well is also the tie well for this cross section and regional cross section B–B′ (Rottmann and others, 2000, pl. 4). Notice that along cross section B–B′ the Prices Falls can be correlated from well 1 (the No. 2 Wheeney) through well 10 (a distance >130 mi). The Prices Falls changes gradually to a marlstone or shaly limestone from south to north. The thickness of the Prices Falls also increases dramatically. The reasons for this thickness increase to the north, away from the depocenter of the Anadarko basin, are described in detail in Rottmann and others (2000).

Cross sections A–A′, H–H′, N–N′, and O–O′ in Rottmann and others (2000) were prepared, in part, to show the detailed correlation of the Clarita Formation, including the differentiation between the Prices Falls Member and the overlying Fitzhugh Member. These cross sections break the Fitzhugh down into beds 1, 2, and 3. It is these beds in which the productive dolomites for many of the reservoirs in west-central, central, and east-central Oklahoma are found. Regional correlation and recognition of the Prices Falls Member are therefore necessary to distinguish the beds of the productive Fitzhugh Member from strata of lesser productive capacity.

REFERENCES CITED

Amsden, T. W., 1960, Stratigraphy and paleontology of the Hunton Group in the Arbuckle Mountain region. Part VI, Hunton stratigraphy: Oklahoma Geological Survey Bulletin 84, 311 p.

_____ 1967, Chimneyhill limestone sequence (Silurian), Hunton Group, Oklahoma, revised: American Association of Petroleum Geologists Bulletin, v. 51, p. 942–945.

_____ 1980, Hunton Group (Late Ordovician, Silurian, and Early Devonian) in the Arkoma basin of Oklahoma: Oklahoma Geological Survey Bulletin 129, 136 p.

Badiozamani, K., 1973, The dorag dolomitization model—application to the Middle Ordovician of Wisconsin: Journal of Sedimentary Petrology, v. 43, p. 965–984.

Reeds, C. A., 1911, The Hunton Formation of Oklahoma: American Journal of Science, v. 182, p. 256–268.

Rottmann, Kurt, 2001, Correlation of Hunton electric logs to Hunton cores and samples: Oklahoma Geological Survey Open-File Report 1-2001, 432 p. plus 20 index p. [Prepared as a supplement to Oklahoma Geological Survey Special Publication 2000-2.]

Rottmann, Kurt; Beaumont, E. A.; Northcutt, R. A.; Al-Shaieb, Zuhair; Puckette, Jim; and Blubaugh, Paul, 2000, Hunton play in Oklahoma (including northeast Texas Panhandle): Oklahoma Geological Survey Special Publication 2000-2, 131 p.

Stanley, T. M., 2001, Stratigraphy and facies relationships of the Hunton Group, northern Arbuckle Mountains and Lawrence uplift, Oklahoma: Oklahoma Geological Survey Guidebook 33, 73 p.

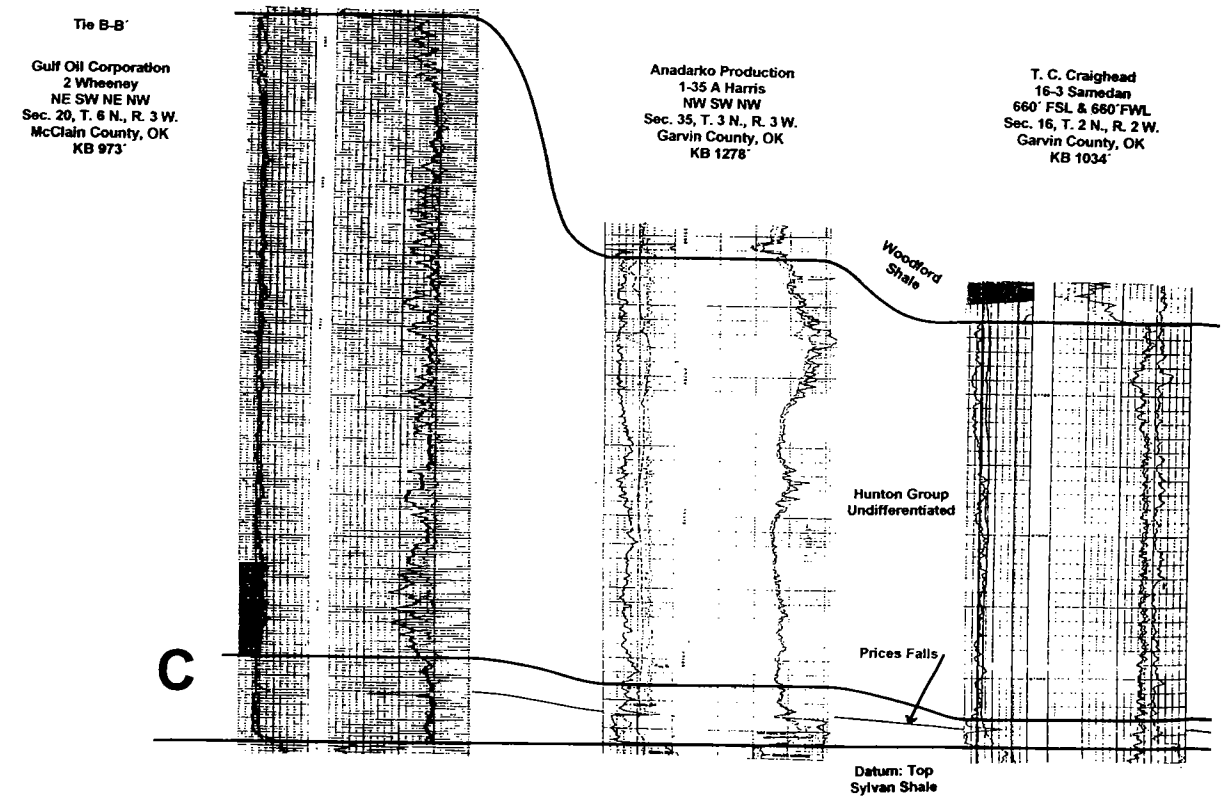

Figure 2 *(above and facing page).* Stratigraphic cross section C–C′, illustrating regional correlation of the Chimneyhill Subgroup, and the Prices Falls Member specifically, for areas of Murray, Garvin, and McClain Counties, Oklahoma.

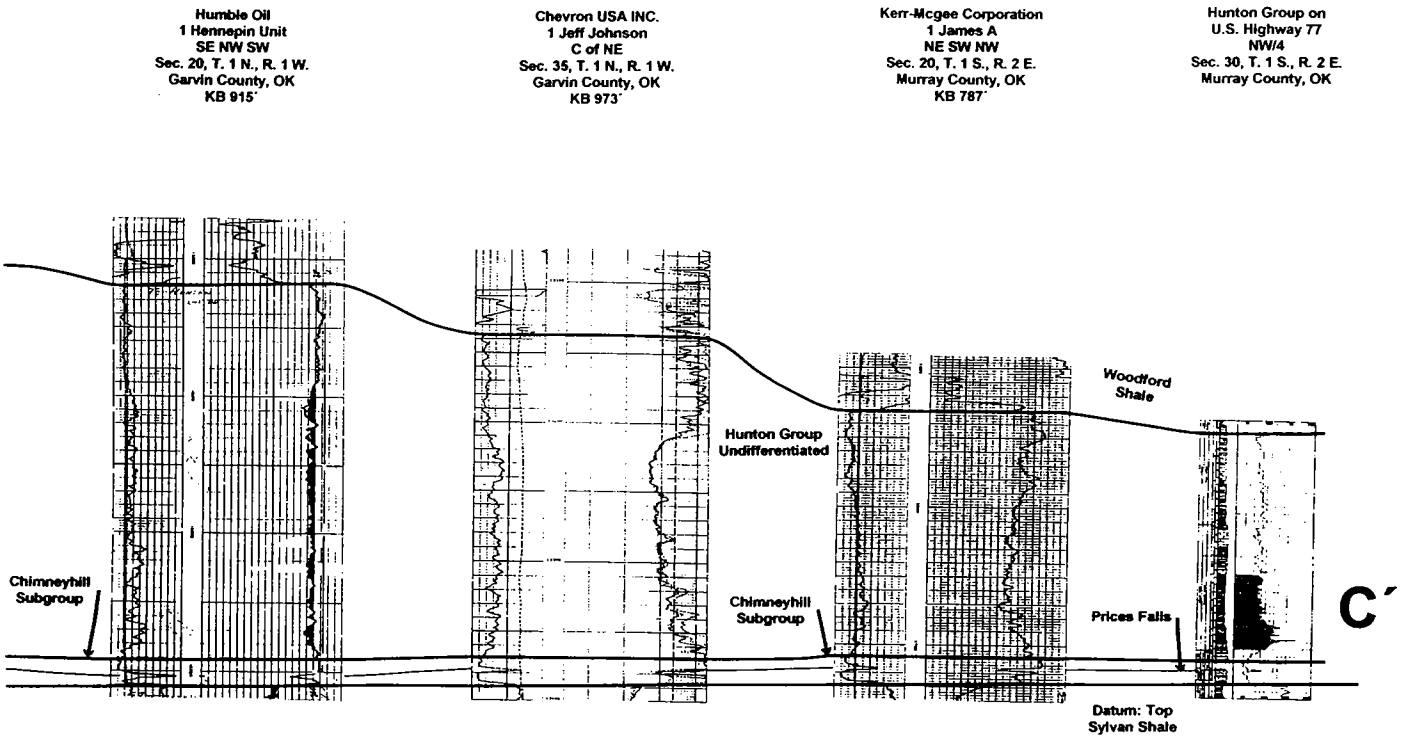
Humble Oil
1 Hennepin Unit
SE NW SW
Sec. 20, T. 1 N., R. 1 W.
Garvin County, OK
KB 915'
Chevron USA INC.
1 Jeff Johnson
C of NE
Sec. 35, T. 1 N., R. 1 W.
Garvin County, OK
KB 973'
Kerr-Mcgee Corporation
1 James A
NE SW NW
Sec. 20, T. 1 S., R. 2 E.
Murray County, OK
KB 787'
Hunton Group on
U.S. Highway 77
NW/4
Sec. 30, T. 1 S., R. 2 E.
Murray County, OK
Woodford Shale
Hunton Group Undifferentiated
Chimneyhill Subgroup
Chimneyhill Subgroup
Prices Falls
C'
Datum: Top Sylvan Shale

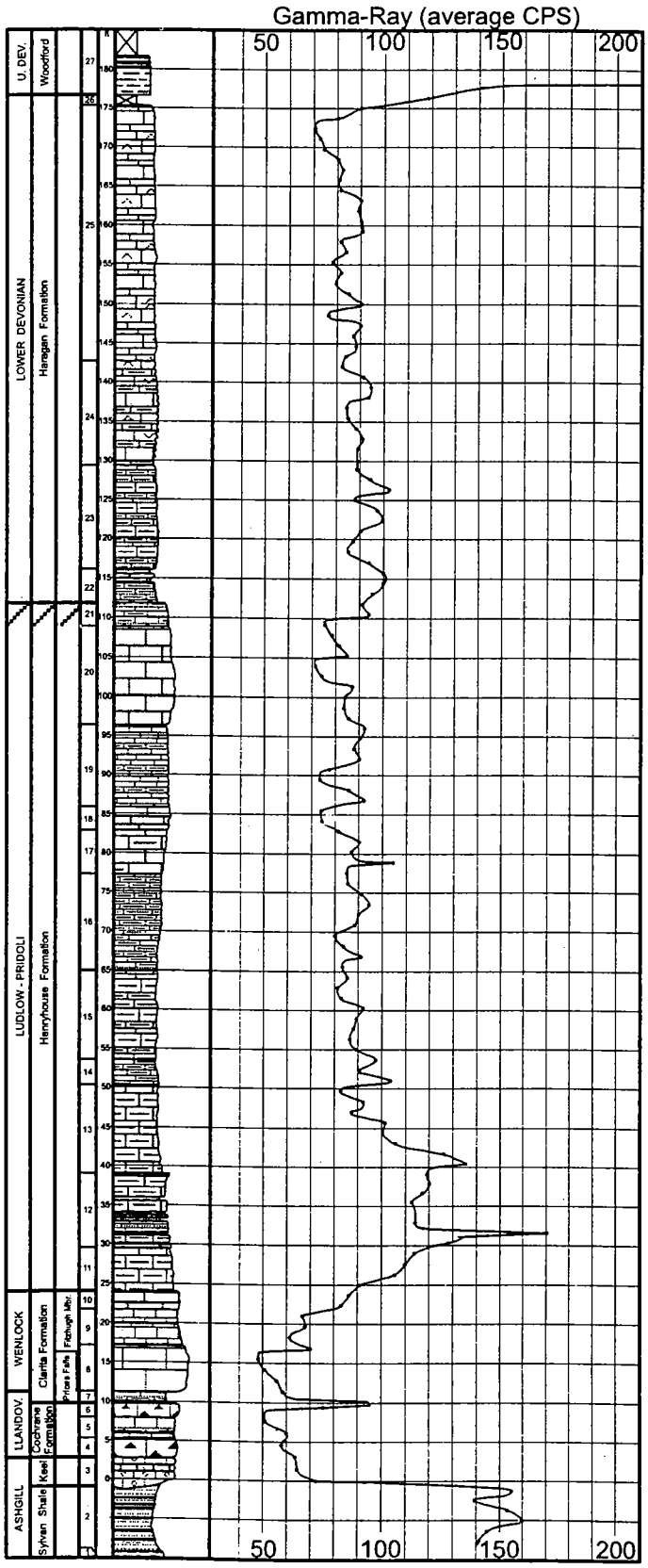

Figure 3. Gamma-ray profile of Hunton Group exposed along north side of U.S. Highway 77 near Turner Falls, Murray County, Oklahoma. From Stanley (2001, fig. 50).

Bypassed Gas Production in a Recently Discovered Hartshorne Gas Reservoir and Recognition of Important Reservoir Facies, Arkoma Basin, Oklahoma

Richard D. Andrews
Oklahoma Geological Survey
Norman, Oklahoma

ABSTRACT.—Cabaniss NW field is a Hartshorne sandstone gas reservoir discovered in 1974. The first production was obtained in 1979, and a total of ~1.8 billion cubic feet of gas (BCF) was produced over a 16-year period from mostly marine delta-front facies. In 1994 a major channel sandstone was identified in a development well that had production capabilities far greater than any previous Hartshorne well. During the 7-year period from 1994 to 2000 an additional 4.3 BCF was produced, mostly from the newly recognized channel facies. This incremental gas production is more than twice the amount produced prior to discovery of the channel facies.

The purpose of this study is to show how development drilling can be enhanced by using well logs to interpret depositional environments and identify principal reservoir facies. This field study in its entirety is included in a 1998 Oklahoma Geological Survey Special Publication of the Hartshorne play in southeastern Oklahoma (Andrews and others, 1998). For the current report it has been condensed and updated through April 2001. This field is particularly suitable for a study like this because most wells have modern logs and good production records, and the log signatures of basic depositional environments are generally very clear. All well logs were evaluated, and facies were assigned as either channel or marine (delta front) entirely on the basis of well-log signatures. In this field, all channel deposits have sharp basal contacts with shale, and blocky to fining-upward textural log profiles, whereas the marine deposits have coarsening-upward log profiles usually with sharp upper contacts. Channel deposits containing little sandstone can be more interpretive and are described later in this report.

Results of this field study indicated that the greatest gas production comes from wells completed in reservoirs having channel sandstone (reactivated distributary channels). The smallest production is attributed to wells completed in sandstone deposited in a marine delta-front environment adjacent to the channel deposits. As an example, channel wells in Cabaniss NW field produce 0.5 to >1.0 BCF—about 4 times the rate in comparison to wells completed in the marine facies. Additionally, it was determined that channels in Cabaniss NW field are older, though stratigraphically higher, than the regionally incised channel deposits east of the field.

The biggest problem for many operators seems to be recognizing depositional environments from wireline logs, and using this information to support development drilling. Although this technique is not new, recognition of channel environments from marine deposits, even in the absence of significant sandstone, is sometimes possible using gamma-ray, resistivity, and porosity logs. The application of this interpretive technique could have prevented the drilling of many marginal gas wells and focused attention much earlier on the channel facies as the primary reservoir in this field.

INTRODUCTION

Cabaniss NW field was discovered in 1974 by KWB Oil Co. and is located primarily in northwestern Pittsburg County in southeastern Oklahoma (Fig. 1). Drilled in the SE¼ sec. 18, T. 6 N., R. 12 E., the discovery well was completed in Hartshorne marine delta-front deposits consisting of 11 ft of net (≥8% porosity) sandstone and initially produced only 62,000 cubic feet of gas per day (MCFGPD). The recognition of depositional environments and the utilization of this information for subsequent development drilling were not practiced during most of the field's history. Since discovery of Hartshorne gas in Cabaniss NW field, about 6.1 billion cubic feet of gas (BCFG) was produced from 21 wells at depths of about 3,300 ft. However, about 75% of this gas was recovered after

Andrews, R. D., 2002, Bypassed gas production in a recently discovered Hartshorne gas reservoir and recognition of important reservoir facies, Arkoma basin, Oklahoma, *in* Cardott, B. J. (ed.), Revisiting old and assessing new petroleum plays in the southern Midcontinent, 2001 symposium: Oklahoma Geological Survey Circular 107, p. 129–136.

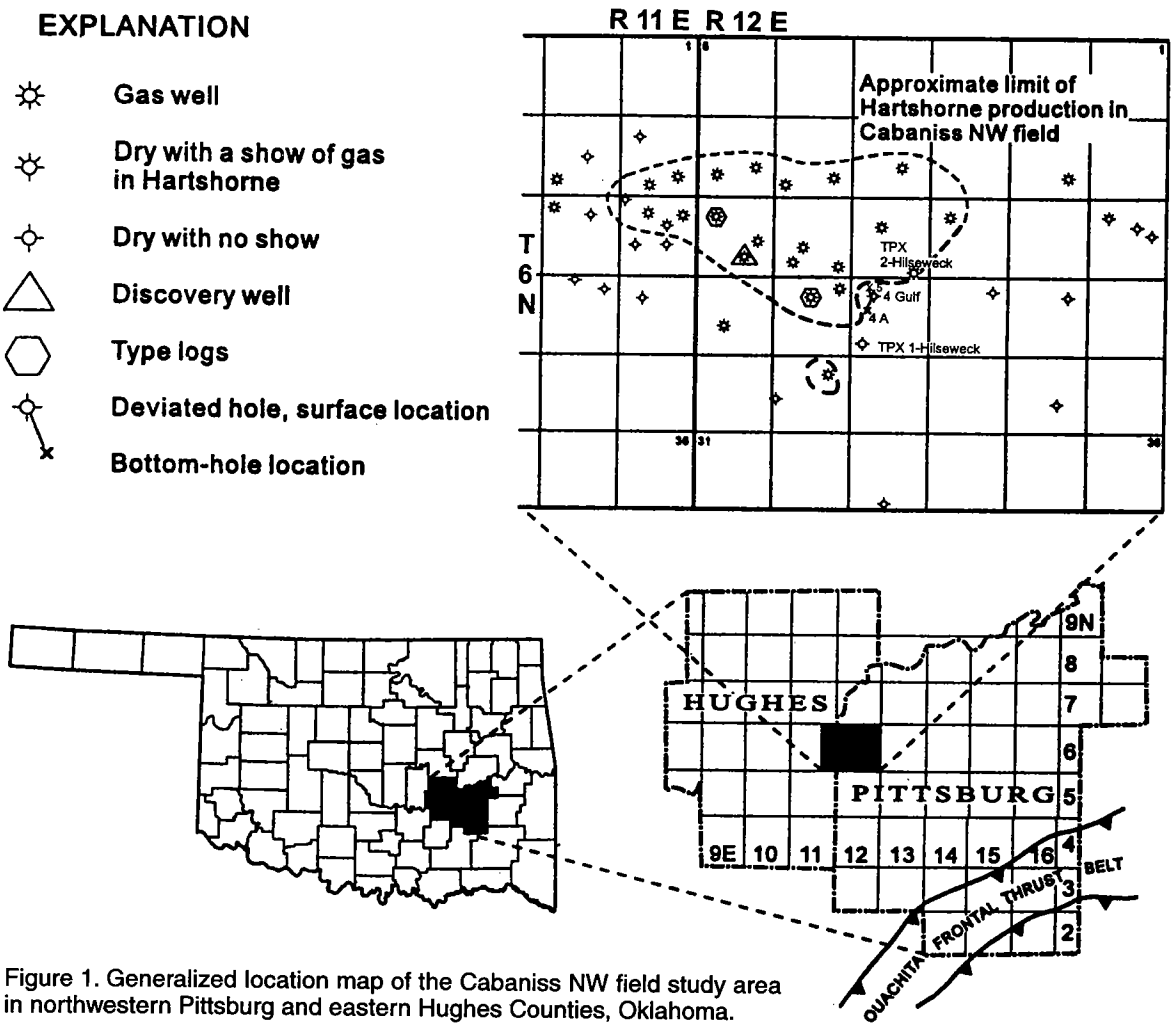

Figure 1. Generalized location map of the Cabaniss NW field study area in northwestern Pittsburg and eastern Hughes Counties, Oklahoma.

1994 (~4.3 BCF) from only eight wells when thicker, more porous channel sandstone was discovered in the south-central part of the field. During the previous 16 years (starting in 1979), gas production came mostly from thin, tight marine delta-front deposits, even though one well penetrated channel-margin strata in 1976. Although the principal field operators were experienced and competent in field operations, they had little experience in facies identification from well logs, which delayed development of the best part of the field until just recently. As late as September 1998 and January 1999, facies recognition was still not fully understood by the operators, and traditional sandstone-isopach-mapping practices prevailed in drilling for thicker sandstone trends regardless of facies. The results of these two wells were predictably poor, and the primary reservoir (channel sandstone) was not found. The most recent well drilled in Cabaniss NW field was the TPX No. 1 Hilseweck (SW¼ sec. 21, T. 6 N., R. 12 E.; see Fig. 1). Drilled in May 2001, the well encountered a relatively thick channel-sandstone sequence, as predicted by facies mapping, but the well was abandoned because the sandstone was wet.

STRATIGRAPHY

Two logs that are representative of Hartshorne stratigraphy in Cabaniss NW field, together with stratigraphic nomenclature, are shown in Figure 2. The log traces for the No. 2-18 Blevins well (type log on left) are characteristic of channel deposits in the field. In this well the sandstone has a sharp basal contact with shale and an overall fining-upward textural profile, as determined from the gamma-ray- and resistivity-log traces. The cross-plot porosity is about 12–14%, and the photoelectric (PE) log clearly deviates to the left of the shale baseline and has a value of 2–3, indicating sandstone. Curiously, the spontaneous-potential (SP) log shows an upward-increasing deflection, which is contrary to what is implied with all other log traces in the Blevins well. Therefore, the SP log is generally not a reliable indicator of depositional environments or textural patterns and should not be used by itself for this purpose. Its value is primarily in the detection of permeability.

The log of the well on the right in Figure 2, the No. 3-20 Hilseweck, is characteristic of marine delta-front deposits having an upward-coarsening textural profile. Additionally, a thin distributary channel may overlie

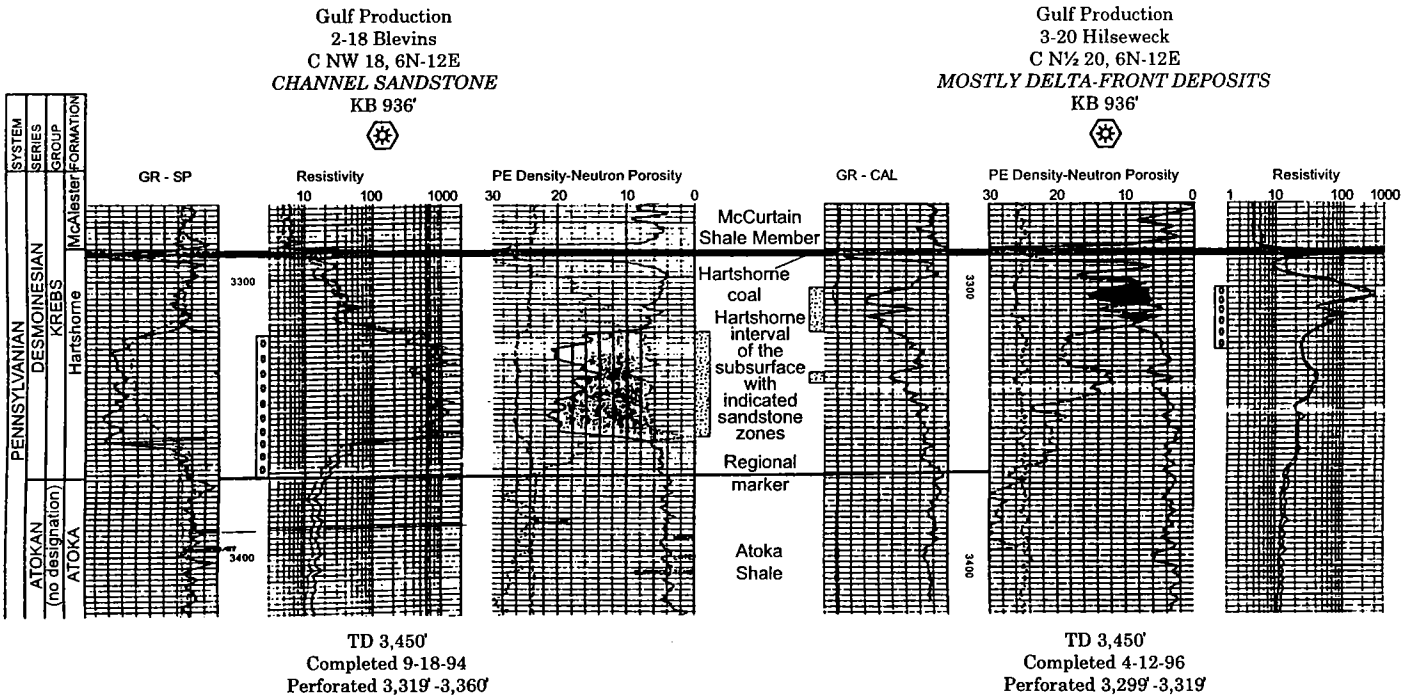

Figure 2. Type logs of the Hartshorne interval in the Cabaniss NW field. Two logs are presented that show typical log signatures of channel and nonchannel Hartshorne sandstones. The stratigraphic section and nomenclature above and beneath the Hartshorne are also shown. *GR* = gamma ray; *SP* = spontaneous potential; *PE* = photoelectric; *CAL* = caliper.

this marine sequence (uppermost sandstone bed). This stratigraphic assemblage is indicative of a progradational deltaic sequence, which is interpreted as the main depositional environment of the Hartshorne Formation in this area. Thicker channel deposits in this field appear to have cut down into the delta front in response to sea-level changes, causing stream reactivation. The marine deposits generally exhibit the best porosity and the cleanest sandstone at the very top of the depositional cycle, whereas optimum sandstone development in the fluvial channels is lower in the same stratigraphic section. The porosity in the marine sandstone is typically less than 8–10%, and the logs indicate that the sandstone is very shaly. In many places, marine sandstone directly underlies the Hartshorne coal; where this is the case, some question exists regarding the contribution of coalbed methane to the total amount of gas recovered from the sandstone.

STRUCTURE

Cabaniss NW field lies just north of the western extent of the Talawanda syncline (Fig. 3). The structure map depicts the top of the Hartshorne Formation (Hartshorne coal). The main purpose of this map is to show that no significant faulting affects production in this field: it is purely a stratigraphic trap.

SANDSTONE DISTRIBUTION

Figure 4 shows the distribution of gross sandstone as it might have been mapped prior to 1981, before many of the gas wells were drilled. The amount of gross sandstone was determined from the 50% sand–shale line from gamma-ray logs and includes total sandstone thickness in the Hartshorne Formation, regardless of porosity or facies. Two sandstone trends are mapped separately in this figure: undifferentiated Hartshorne sandstone that is productive within the field (trending east–west), and a regionally extensive incised-channel complex trending northeast–southwest. Sandstone in the regional incised channel is much lower stratigraphically and has cut down completely through the Hartshorne Formation into the underlying Atoka shale. Many geologists fail to recognize this point and interpret the Cabaniss sands as a western offshoot of the regional incised channel, which is incorrect.

Figure 5 is the most current gross-sandstone interpretation, which incorporates data from all wells drilled through April 2001. The geometry of the Cabaniss sandstone has changed significantly because of the delineation of the channel facies after 1994, and also because of a key well in the NW¼ sec. 21, T. 6 N., R. 12 E. (Fig. 6, center well). This well, the Gulf No. 4 Hilseweck, was plugged and abandoned in January 1997 after finding no porous sandstone in the Hartshorne. A month later, Gulf sidetracked their well to a bottom-hole location (BHL) only ~850 ft to the southwest but similarly found no sandstone. An analysis of the well logs, however, revealed important information to the author. The sidetracked well (No. 4-A Hilseweck, Fig. 6, right well) appeared to have crossed a facies boundary from marine strata in the vertical well (the No. 4 Hilseweck) to an abandoned-channel facies in the sidetracked well. This

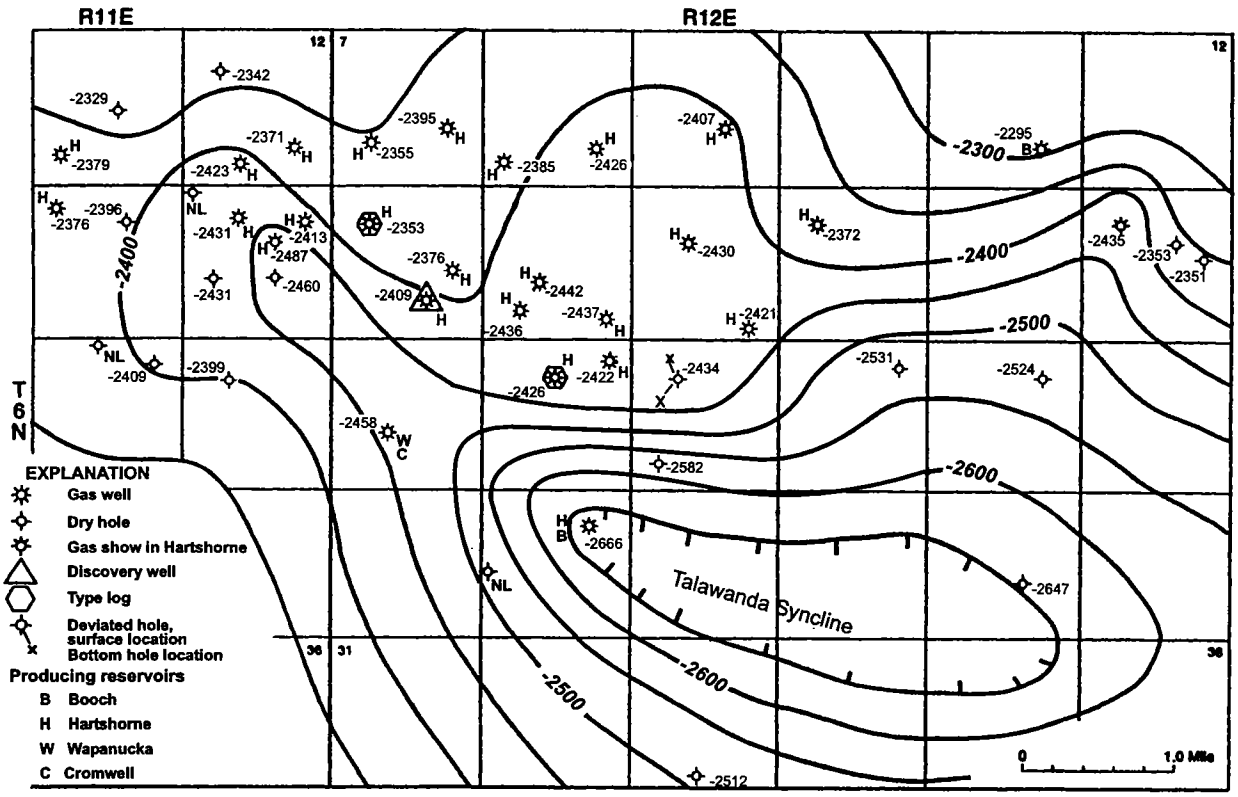

Figure 3. Structure map depicting the top of the Hartshorne Formation, Cabaniss NW field study area. Contour interval, 50 ft. Datum is mean sea level.

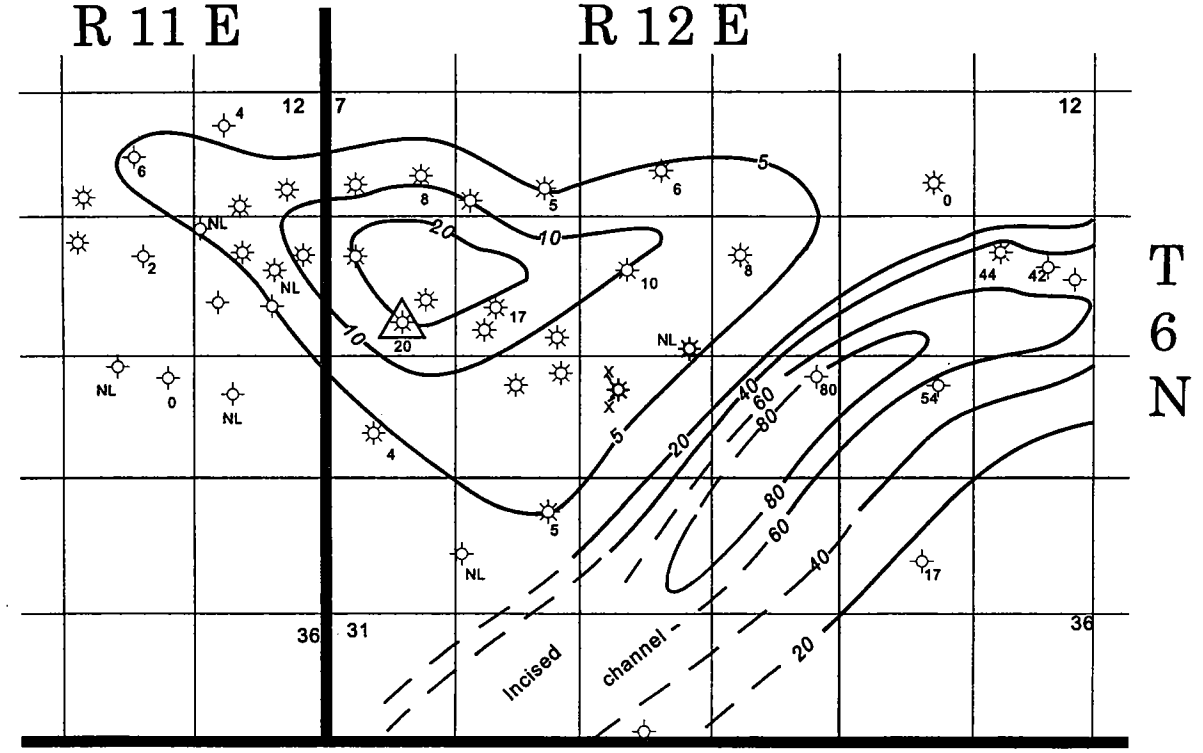

Figure 4. Gross-sandstone isopach map of the Hartshorne Formation in Cabaniss NW field as interpreted from wells drilled before 1981. Gross sandstone includes all sandstone regardless of porosity or facies. Contours in feet. *NL* = no log.

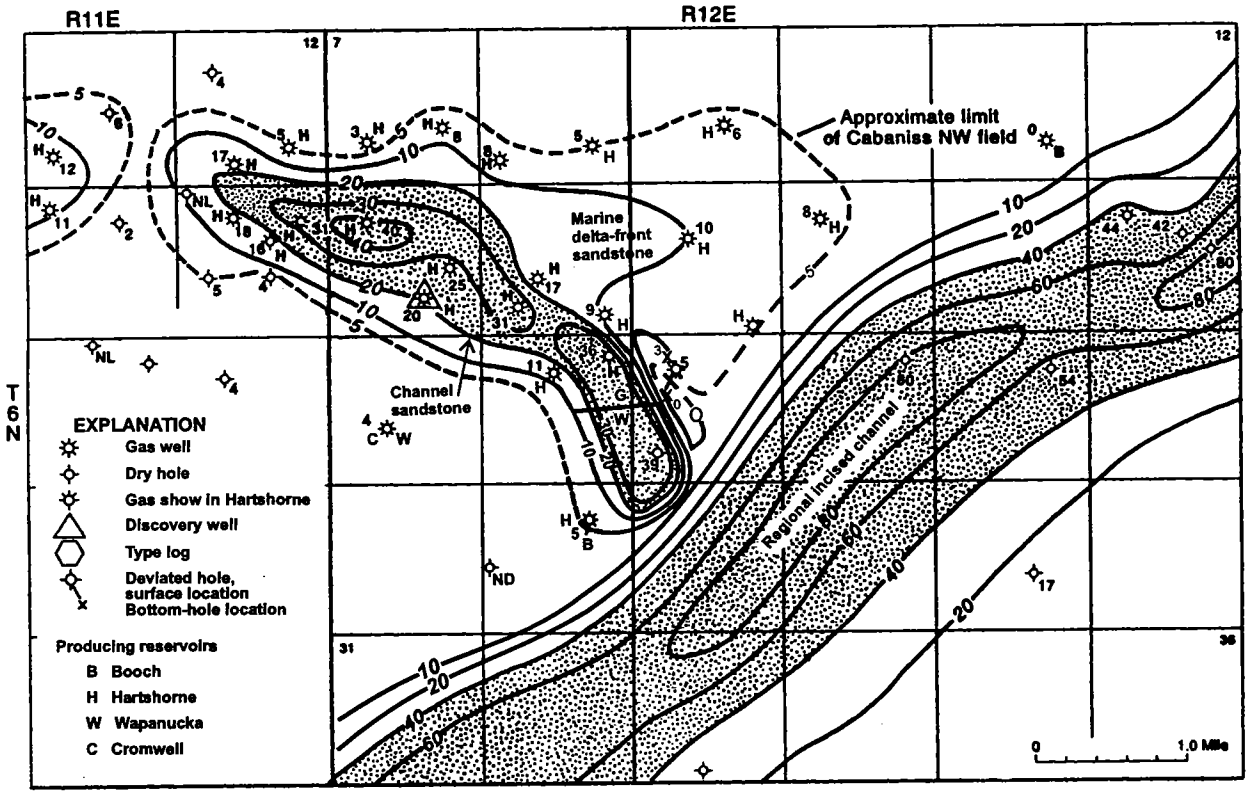

Figure 5. Gross-sandstone isopach map of the Hartshorne Formation in Cabaniss NW field as interpreted from all wells drilled through April 2001. Gross sandstone includes all sandstone regardless of porosity or facies. Contours in feet.

means that the channel extends to the south of the vertical Hilseweck well, not to the north. As shown in Figure 5, the Cabaniss channel is interpreted to extend in a southeasterly direction across the eastern part of sec. 20 and the southwestern part of sec. 21 before being truncated by a much younger and regionally extensive incised-channel complex. Because the reactivated channel facies in Cabaniss NW field is only about 0.5 to 0.75 mi wide, the thickest sandstone within the channel is likely to be only a few hundred feet laterally from the abandoned-channel facies, which consists mostly of shale deposited within the channel after it was abandoned. The term *clay plug* is often used in reference to this facies, which commonly occurs in a part of the channel having higher flow velocities and little deposition but is directly adjacent to the sand bar.

DEPOSITIONAL MODEL AND RECENT DRILLING

The interpretation of the Hartshorne facies in the study area is shown in Figure 7. The main northeast–southwest-trending channel is one of several falling-stage, incised channels that characterize the Hartshorne play in the Arkoma basin. Thinner channels such as those in the Cabaniss NW field (see left type log, Fig. 2) are generally younger and stratigraphically higher in the Hartshorne section and were formed by reactivation of distributary channels (see right type log, upper sandstone unit with highest porosity, Fig. 2). North and south of the Cabaniss channel are regionally extensive marine delta-front sands that are generally thin and tight.

Prior to acceptance of this model, two wells were drilled late in the development history of the field. Both locations were based on sandstone-thickness changes between the Gulf Nos. 4-A and 4 Hilseweck wells without consideration of facies. As shown in Figure 5, the thickness of sandstone increases from 0 ft in the No. 4-A Hilseweck (no sand, abandoned-channel facies) to ~5 ft in the No. 4 Hilseweck (marine facies) over a lateral distance of only ~850 ft. Therefore, thicker sandstone appears to trend farther north.

In late 1998, Gulf sidetracked the No. 4 Hilseweck (sec. 21), this time to the north, and drilled the No. 5 Hilseweck to total depth in the NE¼NW¼NW¼ sec. 21, ~800 ft north-northwest of the No. 4 Hilseweck well. And in early 1999, Tilford Pinson Exploration (TPX) drilled the No. 2 Hilseweck in the SW¼SE¼SE¼ sec. 16, T. 6 N., R. 12 E., which is ~0.6 mi northeast of the No. 4 Hilseweck of sec. 21. Both these wells encountered relatively thin, tight sandstone in a marine Hartshorne section, as predicted in the facies model of Figure 7; the Gulf well was plugged and abandoned, whereas the TPX well was completed for a very small amount of gas (170 MCFGPD). No channel facies was identified in either of these wells.

The relationship of the Gulf wells is shown in Figure 6. In the original vertical No. 4 Hilseweck (just east of the C NW¼ sec. 21, T. 6 N., R. 12 E.), the Hartshorne

Formation is ~70 ft thick, and the dirty sandstone at the bottom of the section has a coarsening-upward textural profile typical of the marine facies. This is similar to other marine Hartshorne sections in the field. The sidetracked hole to the south is represented by the No. 4-A Hilseweck and is shown to the right of the vertical well in Figure 6. Although this well encountered little or no sandstone in the Hartshorne section, a thin sandy "spike" at the very base of the Hartshorne Formation produces a distinct, sharp basal contact with the underlying shale. This log signature is characteristic of an abandoned channel and is clearly different than the log response that characterizes marine rocks. In the No. 4-A Hilseweck sidetracked hole, the Hartshorne is ~80 ft thick, and even when considering wellbore angle, it is still thicker than the marine Hartshorne section shown for the vertical well. The well log on the left in Figure 6 is from the No. 5 Hilseweck, which was also sidetracked from the No. 4 well but has a BHL ~800 ft to the north-northwest. The Hartshorne Formation in the No. 5 well is only ~65 ft thick and contains a marine Hartshorne section with little or no sandstone. The No. 2 Hilseweck well drilled by TPX in sec. 16 did not log the Hartshorne section, but sample descriptions indicated that a shaly marine Hartshorne interval similar to the other marine sections was also encountered.

The most recent development well in Cabaniss NW field was drilled by TPX in late May 2001. The information obtained from this well, the TPX No. 1 Hilseweck, bore out the geologic concept proposed in this paper; the well is in the NE¼SW¼SW¼ sec. 21, T. 6 N., R. 12 E. (see Figs. 5, 7). As predicted, the well encountered a relatively thick channel-sandstone sequence with 15 ft of net sandstone (porosity >8%) and ~39 ft of gross sandstone. However, the sandstone was wet, and the well was abandoned.

GAS PRODUCTION

Through 2000, cumulative gas production from the Hartshorne Formation was 6.1 BCF from 21 wells. This averages 0.29 BCF/well. However, ~4.3 BCF was produced from only eight channel wells, for an average of ~0.54 BCF/well. This is 4.5 times higher than the cumulative gas production of an average marine Hartshorne reservoir (~0.12 BCF).

The total cumulative gas production from all Hartshorne gas wells in Cabaniss NW field is shown in Figure 8. Values are in millions of cubic feet. The channel outline is shown so that production from the marine versus channel reservoirs can be clearly distinguished. Figure 9 is a plot of annual and cumulative gas production. It is clear from the rapid upward trend on the graph that the thicker, more porous channel reservoirs contributed almost three-fourths of total current gas production over a 6-year period, starting in 1994. This incremental gas production was es-

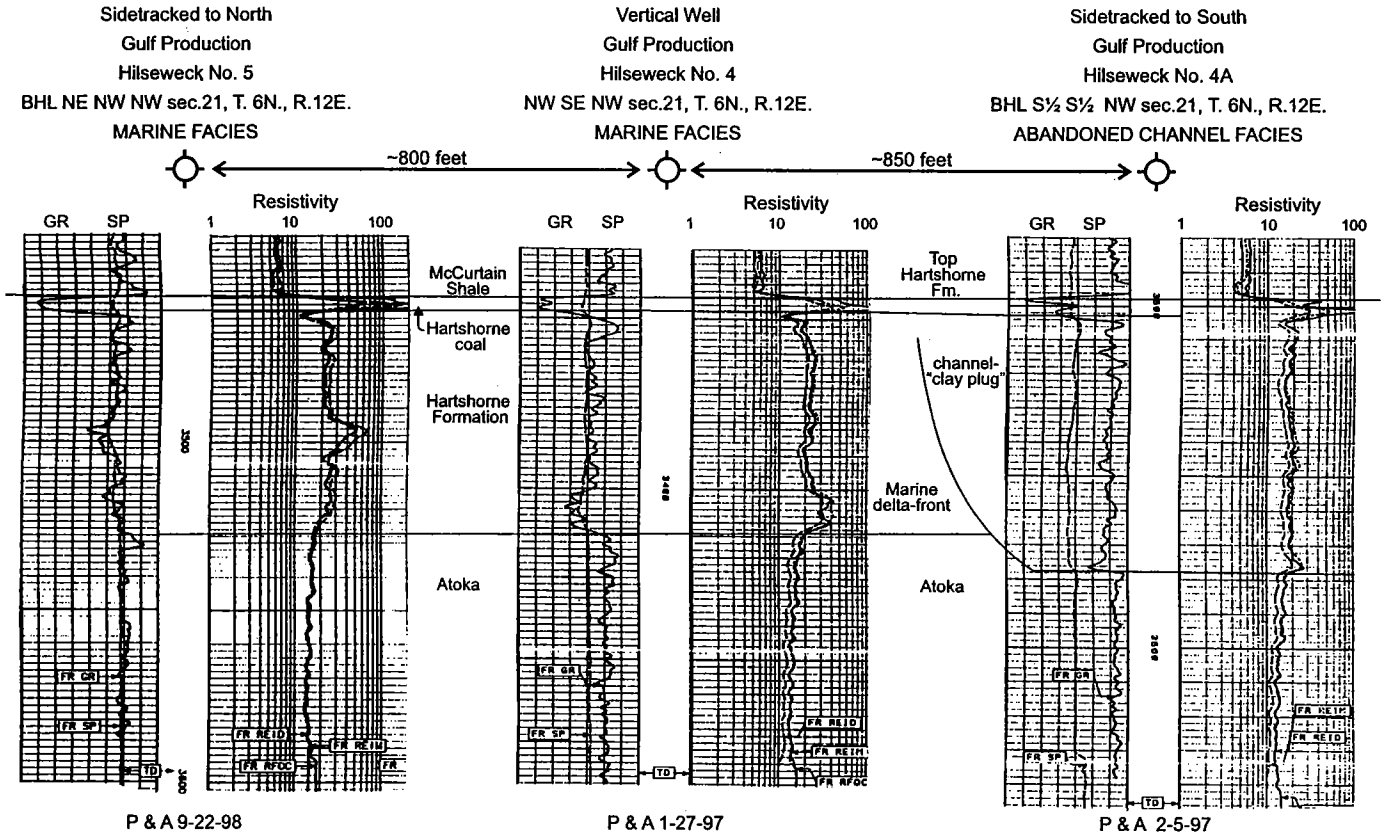

Figure 6. Log character and facies determinations of the Hartshorne Formation in the Gulf No. 4-21 Hilseweck well (center) and two sidetracked wells, Cabaniss NW field. *BHL* = bottom-hole location.

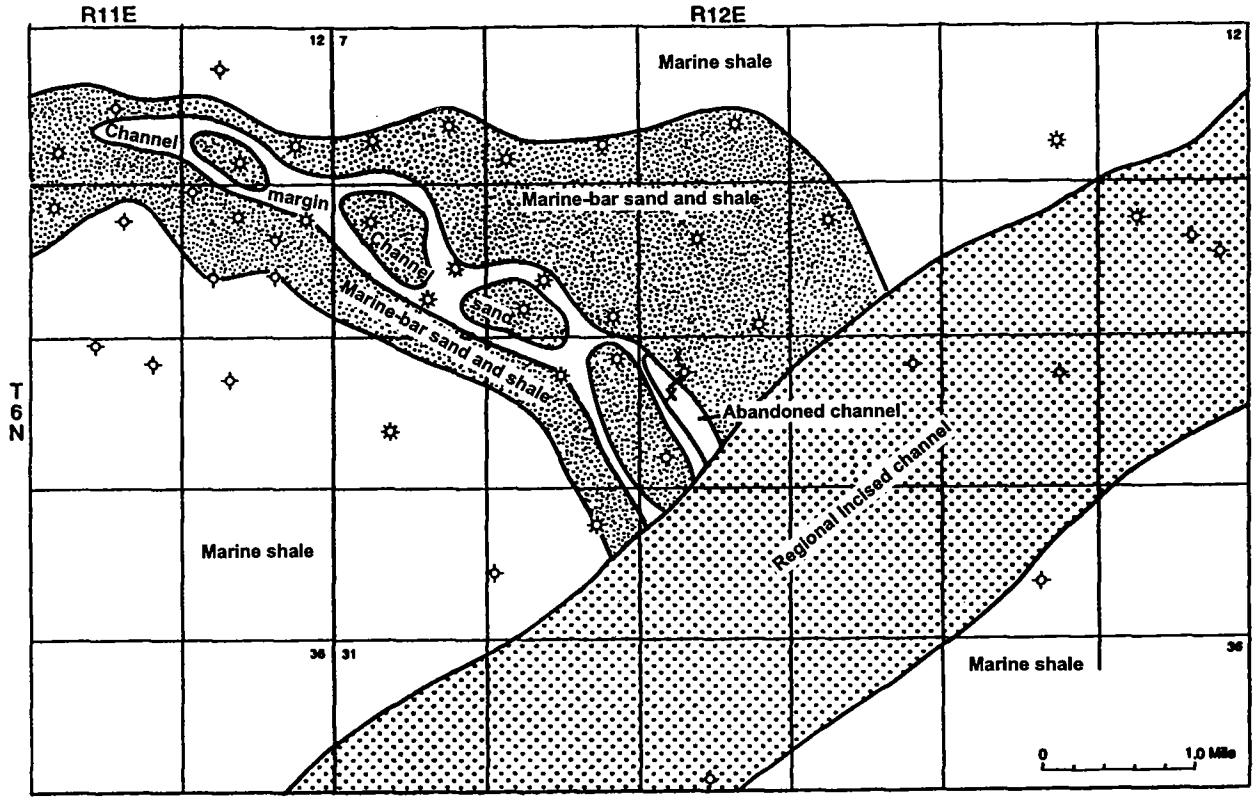

Figure 7. Depositional-facies map of the Hartshorne Formation in the Cabaniss NW field study area.

sentially bypassed for 20 years following discovery of the field in 1974.

SUMMARY AND CONCLUSIONS

Well logs can be used to interpret basic depositional environments in many geologic circumstances. In Cabaniss NW field, two basic depositional origins of sandstone can be easily interpreted from gamma-ray and resistivity well logs: channel and marine delta front (distributary-mouth bar). Sandstone in the marine sequences is generally <10 ft thick and is shaly and tight, with a coarsening-upward textural profile. In these types of reservoirs, gas production ranges from practically nothing to almost 0.3 BCF and averages ~0.12 BCF (there are 13 "marine" wells). Because the delta-front sandstones generally underlie the Hartshorne coal (about 2–4 ft thick), an unknown amount of coalbed methane may have contributed to overall cumulative gas production. Gas production from channel reservoirs is much larger in comparison to their marine counterparts. Channel wells produced 0.34 to >1 BCF and averaged ~0.56 BCF/well (there are eight "channel" wells). The channel sandstones are distinctive in having a sharp lower contact with shale and a blocky to fining-upward textural profile. The channel sequences are usually thicker than the marine depos-

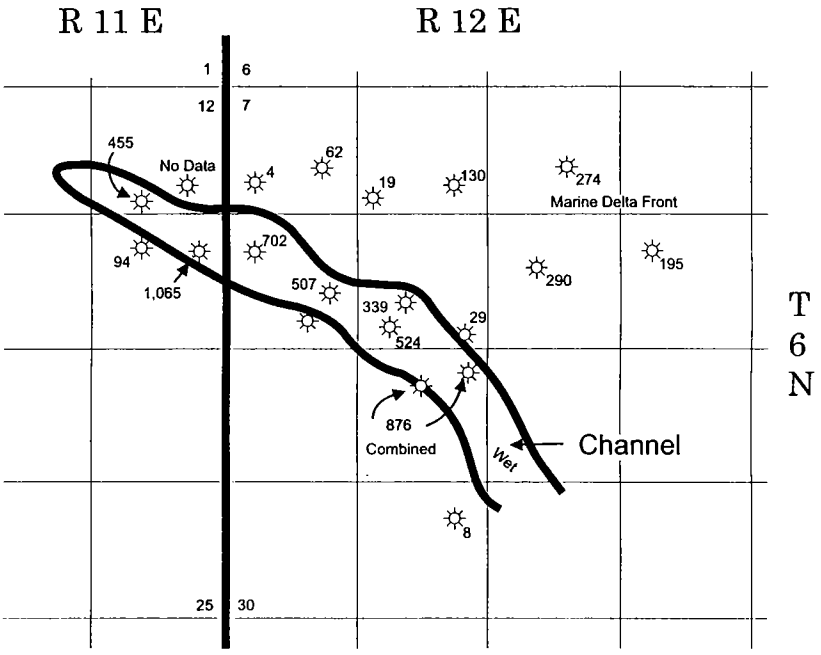

Figure 8 *(right)*. Gas production from wells in Cabaniss NW field. Values are in millions of cubic feet. The areal extent of the Cabaniss channel is shown to compare production from channel- versus marine-sandstone reservoirs. Production is current through December 2000.

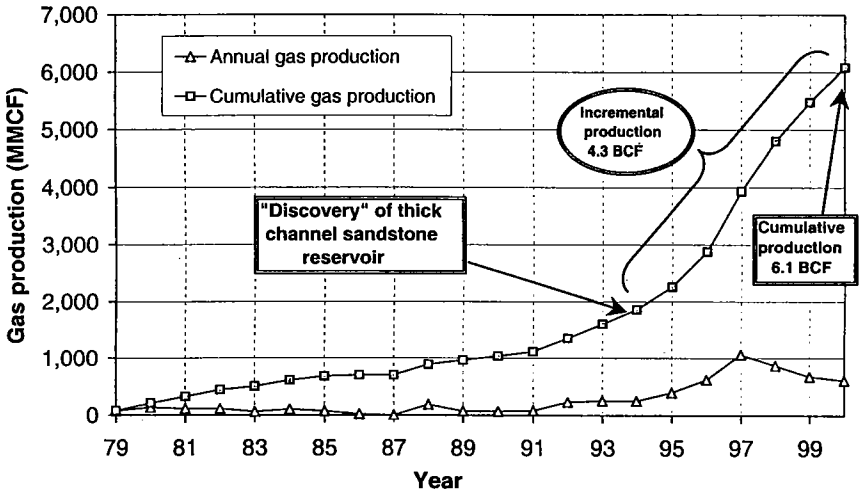

Figure 9. Plot of annual and cumulative Hartshorne gas production in Cabaniss NW field. Production is current through December 2000.

its: 20–40 ft in comparison to <10 ft for the marine deposits.

The recognition of reservoir facies could have prevented the drilling of many dry or marginal gas wells in the northern part of the field during the early development of the field in the mid- to late 1970s. Recent drilling during the mid- to late 1990s focused on the channel facies, although it seemed as if the principal operators were not adept at interpreting these facies from well logs and continued to drill wells in areas that predictably have marine strata, despite adequate well data to avoid such mistakes. The most recent well drilled in Cabaniss NW field (May 2000) is the TPX No. 1 Hilseweck. The location of this well in the SW¼ sec. 21, T. 6 N., R. 12 E., was determined from the sandstone isopach map and facies model of Figures 5 and 7, respectively. The well encountered a relatively thick channel-sandstone sequence as predicted but was abandoned because the sandstone was wet.

REFERENCE CITED

Andrews, R. D.; Cardott, B. J.; and Storm, Taylor, 1998, The Hartshorne play in southeastern Oklahoma: regional and detailed sandstone reservoir analysis and coalbed-methane resources: Oklahoma Geological Survey Special Publication 98-7, 90 p.

Case Study: AVO Analysis in a High-Impedance Atoka Sandstone (Pennsylvanian), Northern Arkoma Basin, McIntosh County, Oklahoma

Mohamed A. Eissa
Tanta University, Egypt, and
University of Oklahoma
Norman, Oklahoma

John P. Castagna
University of Oklahoma
Norman, Oklahoma

ABSTRACT.—Amplitude variation with offset (AVO) analysis can be used to detect and delineate gas-bearing fluvial–deltaic Atokan sandstone stratigraphic traps. These class I high-impedance gas-sand reservoirs are recognized by a characteristic phase change with increasing offset, a positive AVO intercept, and a negative AVO gradient.

INTRODUCTION

The variation of reflection coefficients with source-to-receiver spacing in multi-offset seismic data is known to contain information about lithology and pore-fluid content of subsurface rocks (e.g., Ostrander, 1984). However, such analysis is particularly challenging for thin, high-impedance reservoirs (Rutherford and Williams, 1989). In such instances, a key component of amplitude variation with offset (AVO) analysis is a methodology for response calibration so that fluid properties can be interpreted vertically and laterally away from a borehole with a high degree of confidence (e.g., Hong and others, 1993). The use of AVO as a direct hydrocarbon indicator in clastic rocks is based on differences in the response of the compressional-wave (*P*-wave) velocity (V_p) and the shear-wave (*S*-wave) velocity (V_s) of a reservoir rock to the introduction of gas into the pore spaces. *P*-waves are sensitive to changes in pore fluids. The introduction of only a small amount of gas into the pore spaces of a rock can greatly reduce the *P*-wave velocity. In contrast, the *S*-wave velocity is only weakly dependent on pore-fluid content. Thus, the introduction of hydrocarbons decreases the V_p/V_s ratio. This decrease, upon the introduction of gas into the pore space, changes the relative amplitudes of the reflections from the top and the base of the reservoir as a function of the angle of incidence. For thin beds (i.e., less than one-fourth wavelength), interference between reflections from the top and the base of a reservoir may obscure the AVO response (Ostrander, 1984).

The objective of this study was to determine if AVO analysis could be used to identify and delineate thin, high-impedance Atokan gas sands in the northern Arkoma basin.

LOCATION

The area of study lies on the shelf area of the northern Arkoma basin, in McIntosh County, Oklahoma (Fig. 1). The target reservoir is the Pennsylvanian Atoka sand. Figure 2 shows the general stratigraphic column of the Oklahoma portion of the Arkoma basin. The geologic setting is described in the Appendix and is described more fully by Montgomery (1989) and Flawn (1985).

WELL DATA

Well logs from the No. 1-15 Wright well (Fig. 3) were available for this study. These include the gamma-ray, deep- and shallow-resistivity, and porosity logs (neutron, density, and sonic). The target reservoir is fluvial Pennsylvanian lower Atoka sand at depths of 2,585–2,695 ft. The perforated interval (2,610–2,638 ft) showed initial production of 88 thousand cubic feet of gas per day (MCFGPD). The main reservoir package is 110 ft thick (2,585–2,695 ft) and consists of sand, shaly sand, and shale. We assume that most production comes from the thin, clean sand body (2,611–2,618 ft) within the package. The pay interval shows an average porosity of 10%. The neutron–density cross-plot shows that the pay-interval log responses exhibit gas effects (Fig. 4). Other sand bodies at 2,350 ft (45 ft thick) and 2,495 ft (30 ft thick) show gas.

SEISMIC DATA

A seismic survey was taken along a 3.5-mi two-dimensional (2-D) line oriented north–south about 1,300 ft from the No. 1-15 Wright well. Acquisition and processing parameters are listed in Tables 1 and 2.

Special processing for AVO included parabolic ra-

Eissa, M. A.; and Castagna, J. P., 2002, Case study: AVO analysis in a high-impedance Atoka sandstone (Pennsylvanian), northern Arkoma basin, McIntosh County, Oklahoma, *in* Cardott, B. J. (ed.), Revisiting old and assessing new petroleum plays in the southern Midcontinent, 2001 symposium: Oklahoma Geological Survey Circular 107, p. 137–151.

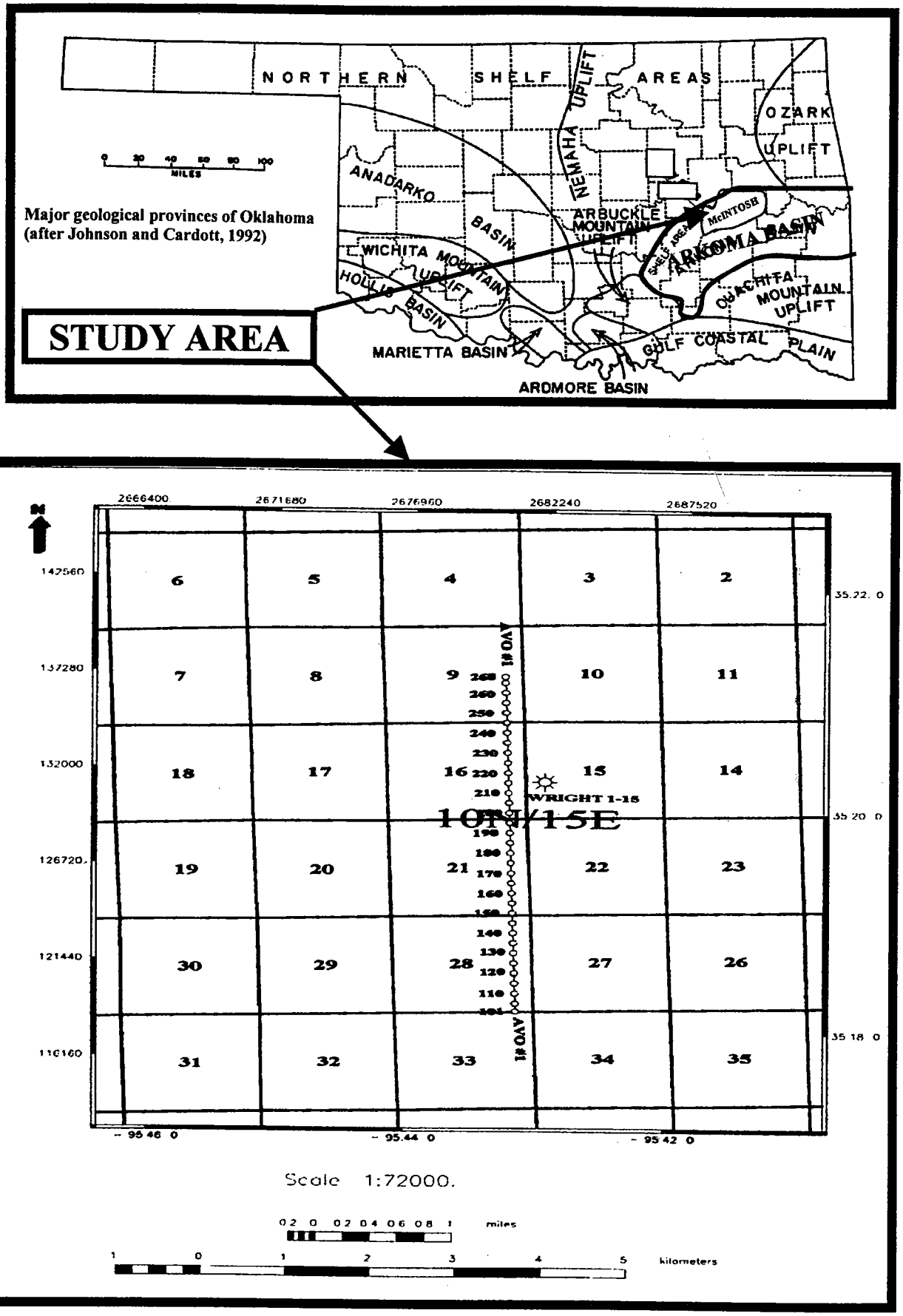

Figure 1. Location map of the study area.

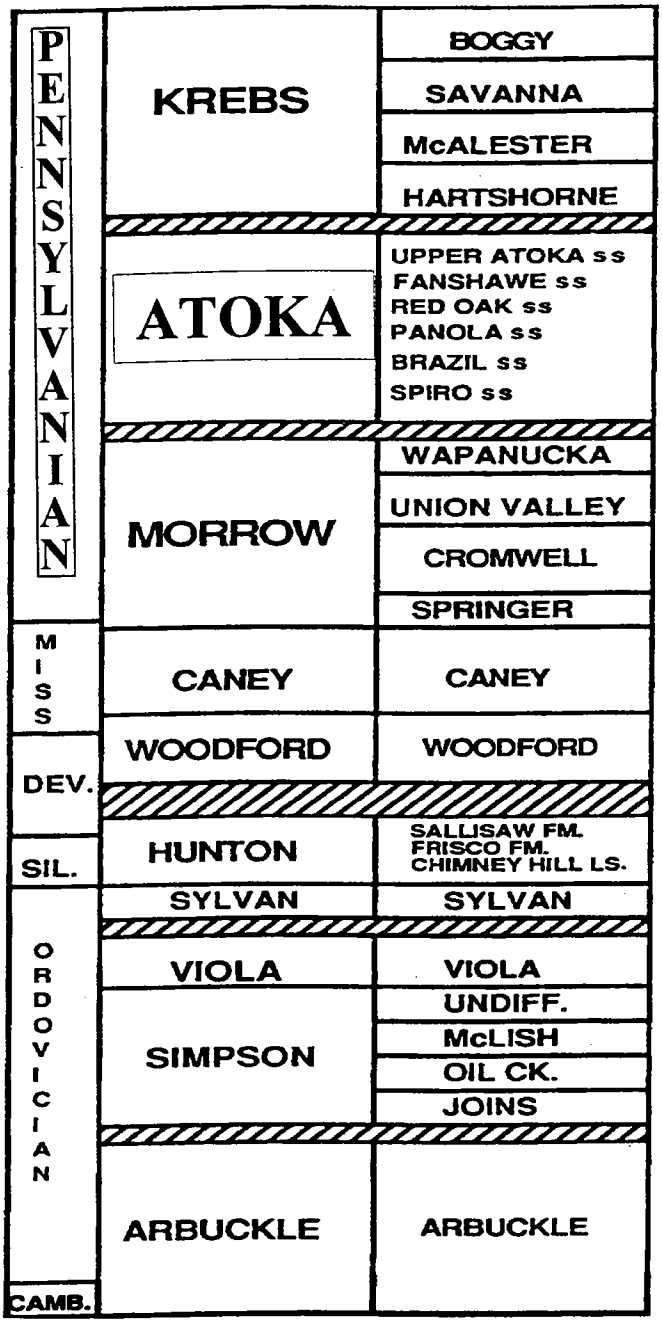

Figure 2. Generalized stratigraphic column and subsurface nomenclature (right column) of the Oklahoma portion of the Arkoma basin (modified from Hendrick, 1992).

don filtering (Hampson-Russell invest procedure, 10–80 Hz and time shifts from +80 to –80 ms were passed) of supergathers consisting of 10 summed common-depth-point (CDP) gathers. Figure 5 shows real-data gathers before and after radon filtering, and the subtracted-noise model.

SEISMIC MODELING

Primaries-only, ray-trace synthetic seismograms using sonic and density logs from the No. 1-15 Wright well were generated, using the extracted wavelet at the well location (Fig. 6). Synthetic gathers were normal-moveout (NMO) corrected and calculated at the same offset as the real data (from 0 to 3,800 ft) with no correction for spreading, transmission loss, attenuation, or geophone-array response. *S*-wave velocity was estimated using the mudrock equation for brine-saturated rocks (Castagna and others, 1985). Figure 7 shows the brine model, which shows an amplitude decrease with increasing offset at the target horizon. In the gas model, Poisson's ratio for the target reservoirs was changed to 0.1 in two ways: in gas model 1, changing V_s and keeping V_p fixed as measured (Fig. 8); and in gas model 2, changing V_p and keeping V_s fixed (Fig. 9). The top and the base of the 110-ft sand package are distinctly recognizable in the synthetics. In the brine model, target reservoirs show no AVO anomaly. In gas model 1 (Fig. 8), however, the top of the main reservoir (480 ms two-way traveltime, or TWT) shows a strong peak in the near offset traces, which decrease its amplitude with an increase of offset and lead to a change in polarity (at about 20°) and an increase of the trough amplitude in the far offset traces. The base of the reservoir is expressed in a trough at 497 ms TWT in the near offset, which has the reverse AVO behavior as the top. Notice similar AVO anomalies for sand bodies at 430 ms and 470 ms. The near and far offsets of the real data are more similar to the AVO response of gas model 2 (Fig. 9). This suggests that the sonic logs are measuring *P*-wave velocities that are higher than those to which the seismic data are responding. The AVO response of the real data exhibit typical AVO behavior for class I sands with a phase change with offset according to the Rutherford and Williams (1989) classification. Near-stack and far-stack sections (Fig. 10) exhibit clearly anomalous AVO responses between CDPs 215 and 226 at 480 ms TWT.

AVO INVERSION

AVO inversion was performed by using an iterative and linearized algorithm that allows fixed constraints (Hampson-Russell AVO inversion algorithm). This requires a starting model with a known number of layers for V_p, V_s, density, and thickness. AVO inversion was performed using the brine model, gas model 1, and gas model 2 as starting models. The maximum values of parameters to change are as follows: V_p, 5,000 ft/s; density, 1.0 g/cm^3; layer thickness, 100 ft; V_s, 5,000 ft/s. The model consists of 63 layers.

Brine-Sand Starting Model

Figure 11 shows the AVO inversion for near offsets, allowing only V_p, density, and thickness to change. The starting model is the brine model, using the original well-log data. The V_p and density values after inversion (thick black curves) show only minor changes. Figure 12 shows the AVO inversion for all offsets, allowing only V_s to change and using the near-trace inversion results, with V_s predicted from trend curves

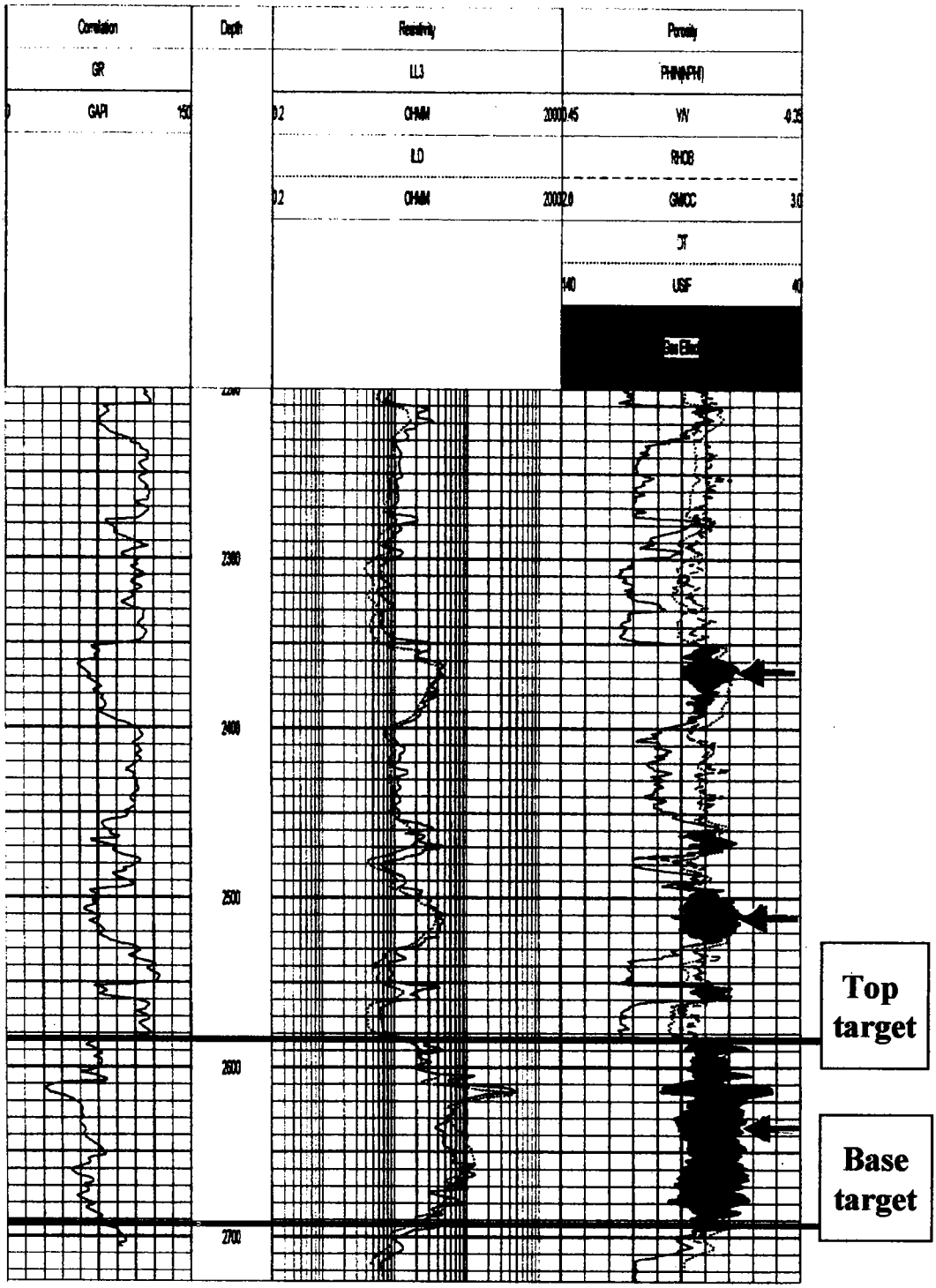

Figure 3. Well logs for target reservoirs within the Atoka interval in the No. 1-15 Wright well. Gas-bearing sands are indicated by arrows.

as the starting model. Note that V_s, after inversion (thick black curve), has slightly decreased in the lower part of the main gas intervals at 485 to 495 ms TWT. An abnormal increase of V_s is observed at 463 ms TWT (2,495 ft), which indicates an abnormal decrease in the Poisson's ratio curve (0.12), presumably caused by the presence of gas. The Poisson's ratio curve slightly increases at the bottom of the main gas interval and exhibits a major decrease at 463 ms TWT (2,495 ft).

Gas-Sand Starting Model 1

AVO inversion was performed by using gas model 1 as the starting model (Fig. 13). V_p and density reflect only minor changes after inversion for the near trace. These were used as the starting model for the

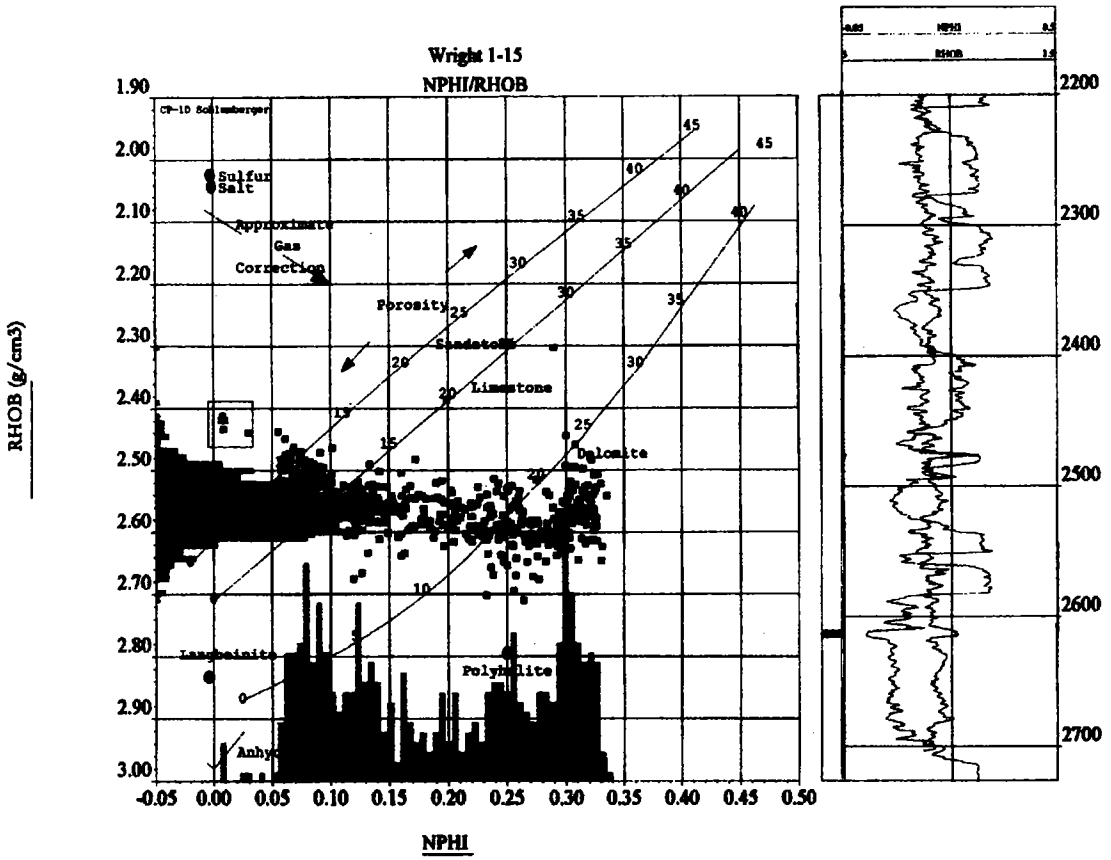

Figure 4. Neutron–density cross-plot, showing lithology, porosity, and gas effect for the Atoka interval in the No. 1-15 Wright well. *NPHI* = porosity derived from neutron log; *RHOB* = bulk density derived from density log.

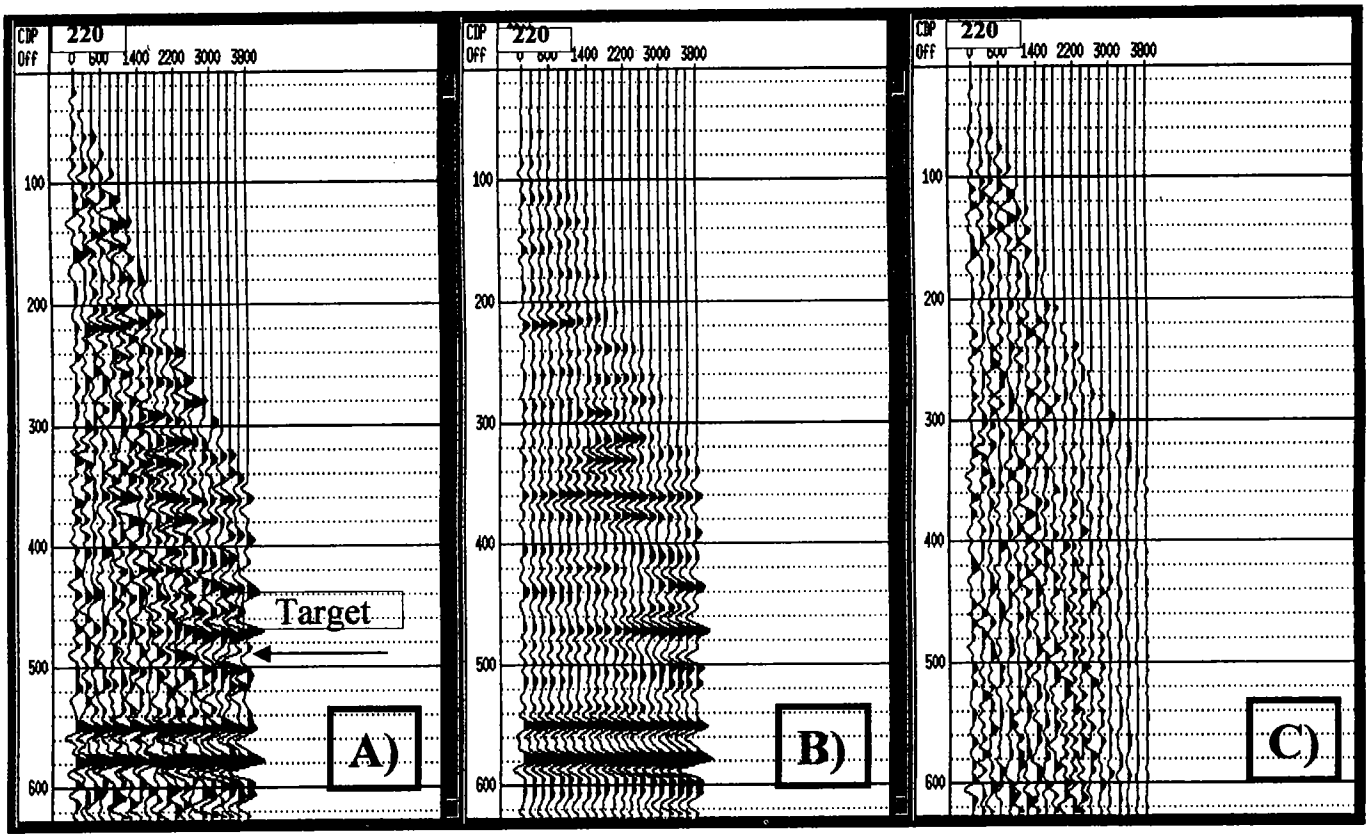

Figure 5. Real data: (A) before applying the radon filter, (B) after applying the radon filter, and (C) the subtracted-noise model.

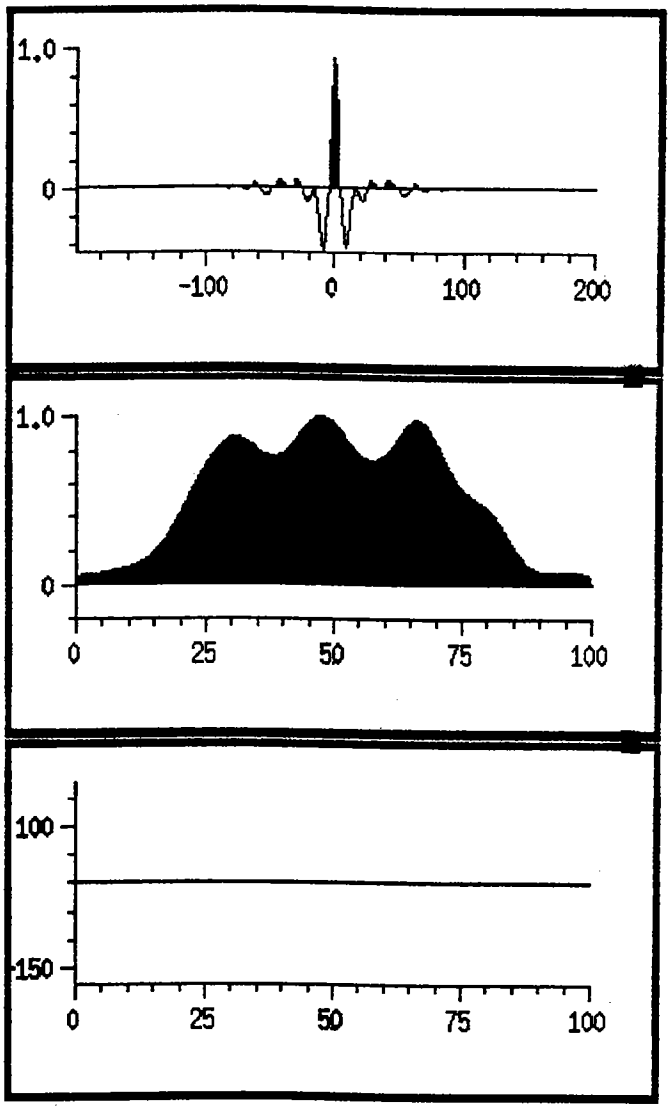

Figure 6. Extracted wavelet used in synthetic modeling.

full gather, allowing only V_s to change (Fig. 14). V_s in the lower part of the main gas interval was decreased. No significant changes were evident in the top of the main reservoir. Note an abrupt increase of V_s at 463 ms TWT (2,495 ft). Poisson's ratio increases for the bottom part of the main gas interval. A major decrease in Poisson's ratio occurs at 463 ms (2,495 ft). An inverted Poisson's ratio curve indicates no gas at 440 ms (2,350 ft) and at 457 ms (2,460 ft).

Gas-Sand Starting Model 2

First, after allowing V_p, density, and layer thickness to change (Fig. 15), the inverted V_p and density were shifted 9 ft upward, with an increase in the lower part of the main reservoir. Figure 16 shows the AVO inversion for the full gathers, using the near-trace inversion results as the starting model and allowing only V_s to change. Inverted V_s decreases in the lower part of the main gas intervals. Poisson's ratio increases at the base of the main reservoir and does not change

Table 1. — Acquisition Parameters

Energy-source type	Dynamite
Source interval	110 ft
Source size	1 lb per shot
Source depth	5 ft
Recording instrument	Bison
Record length	2 s
Sample rate	2 ms
Geophone type	20D (10 Hz)
Group interval	110 ft
Geophone layout	12 over 110 ft

at the top of this reservoir. A Poisson's ratio drop to 0.1 at 463 ms TWT (2,495 ft) indicates gas. Poisson's ratio indicates no gas in the other two intervals at 440 ms (2,350 ft) and 457 ms (2,460 ft).

Both gas models confirm the presence of gas at the top of the main reservoir at 480 ms TWT (2,590 ft). Another gas interval was detected by the inversion at 463 ms (2,495 ft). A gas interval at 440 ms (2,350 ft) was not apparent after the inversion.

SUMMARY AND CONCLUSION

A lower Atoka (Pennsylvanian) high-impedance sand package has been shown to exhibit a class I AVO anomaly with a phase reversal. This suggests that AVO analysis may be a useful tool for detecting and delineating high-impedance gas sands in the northern Arkoma basin. AVO inversion indicates the presence of gas in this lower Atoka sand.

ACKNOWLEDGMENT

The authors express their sincere thanks to Mr. Jerry Wilson, manager of Pathfinder LLC, for providing data and financial support.

REFERENCES CITED

Castagna, J. P.; Batzle M. L.; and Eastwood R. L., 1985, Relationship between compressional-wave and shear-wave velocities in clastic silicate rocks: Geophysics, v. 50, p. 571–581.

Flawn, P. T., 1985, Foreland basins and cratonic rocks north and west of Ouachita system, *in* Fallin, J. A. (ed.), The Ouachita system: oil and gas developments along the overthrust trend: Petroleum Information, Denver, Petroleum Frontiers, v. 2, no. 3, p. 41–49.

Hendrick, S. J., 1992, Vitrinite reflectance and deep Arbuckle maturation at Wilburton field, Latimer County, Oklahoma, *in* Johnson, K. S.; and Cardott, B. J. (eds.), Source rocks in the southern Midcontinent, 1990 symposium: Oklahoma Geological Survey Circular 93, p. 176–184.

Hong, M. R.; Castagna, J. P.; and Sicking, C. I., 1993, A model-based analysis of AVO in Sacramento Valley, *in* Backus, M. M., Offset-dependent reflectivity and the

theory and practice of AVO analysis: Society of Exploration Geophysicists, Tulsa, p. 230–237.
Johnson, K. S.; and Cardott, B. J., 1992, Geologic framework and hydrocarbon source rocks of Oklahoma, *in* Johnson, K. S.; and Cardott, B. J. (eds.), Source rocks in the southern Midcontinent, 1990 symposium: Oklahoma Geological Survey Circular 93, p. 21–37.
Montgomery, S. L., 1989, New depths, new possibilities, *pt. 1 of* Cain, D. L. (ed.), Drilling the deep Arkoma basin: Petroleum Information, Denver, Petroleum Frontiers, v. 6, p. 1–44.
Ostrander, W. J., 1984, Plane wave reflection coefficients for gas sands at nonnormal angles of incidence: Geophysics, v. 49, p. 1637–1648.
Rutherford, S. R.; and Williams, R. H., 1989, Amplitude-versus-offset variation in gas sands: Geophysics, v. 54, p. 680–688.

APPENDIX

The Arkoma basin is an arcuate foreland trough stretching some 250 mi across southeastern Oklahoma into central Arkansas. From Late Cambrian to Early Pennsylvanian (basal Atokan) time, the area now occupied by the basin was part of an Atlantic-type margin (shallow shelf) marking the southern edge of the Paleo–North American continent.

A basic transgressive sequence, with significant interruptions, progressed from basal Cambrian sands (Reagan) to a thick carbonate series (Arbuckle Group) to a mixture of carbonate, sand, and shale (Simpson, Viola, Sylvan, Hunton), and finally to an episode of mainly shale deposition (Woodford, Caney). The entire sequence ended in a brief period (latest Chesterian–basal Atokan) of shallow-water sand and lime sedimentation (Cromwell, Union Valley, Wapanucka, Spiro), which presumably reflects regression associated with the earliest stage of foreland basin formation. Subsequent subsidence during the Early to Middle Pennsylvanian was extremely rapid.

In direct response to the major Ouachita collisional event, a thick "flysch" wedge (Atokan, lower Desmoinesian, in the southern basin area) resulted, and then, with progressive shoaling of the basin, the southward progradation of major delta complexes (Hartshorne, Savanna, Boggy Formations) and accompanying coal swamps occurred.

In southeastern Oklahoma, the total basin fill varies from ~5,000 ft near the northern shelf edge to 20,000 ft or more near the Choctaw fault, the first major fault of the frontal Ouachita system with continuous surface expression. Atokan sediments, representing the main stage of foreland basin subsidence, increase in thickness from a few hundred feet on the flanks of the Ozark uplift to more than 10,000 ft in the vicinity of the Choctaw fault, a distance of some 25–30 mi (Montgomery, 1989).

Many folds and faults in the Arkoma basin were produced by horizontal compressive forces related to the Ouachita orogeny. The compressive forces were directed north and northwest and decreased in intensity away from the Ouachita Mountains region. Nonetheless, anticlines and synclines are tightly folded and terminated by the thrust faults near the southern margin of the basin. Gas produced from the structures is typically dry, being approximately 95% methane (Flawn, 1985).

Table 2. — Sequence of Digital Processing

Gain correction:	
Type	Exponential
Relative amplitude scaling	
Elevation and drift correction:	
Datum	700 ft above sea level
Replacement velocity	10,500 ft/s
Refraction statics	Hand and automatic
Deconvolution (surface consistent):	
Design gate	0.08–1.2 at 0 ft offset 0.74–1.5 at 6,930 ft offset
Operator length	128 ms
Prewhitening	0.1%
Bandpass	10/20–110/120 Hz
CDP sort	
Velocity analysis	
NMO correction	
Automatic residual static	Window 0.1–0.9 s
Zero phase spectral amplitude balancing	
Trim statics	
F-X Deconvolution	
Migration	

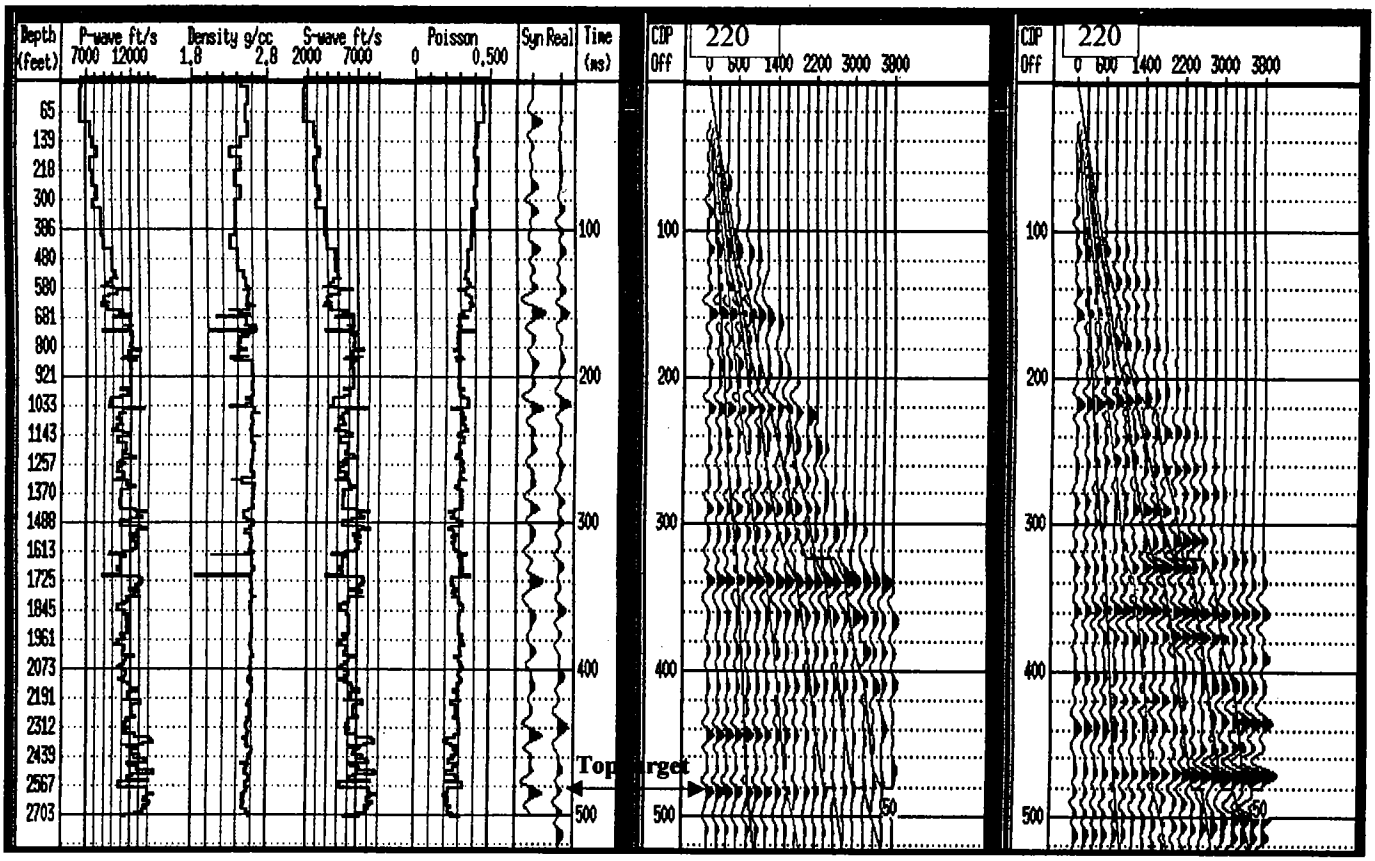

Figure 7. AVO brine synthetic-seismogram model of the No. 1-15 Wright well.

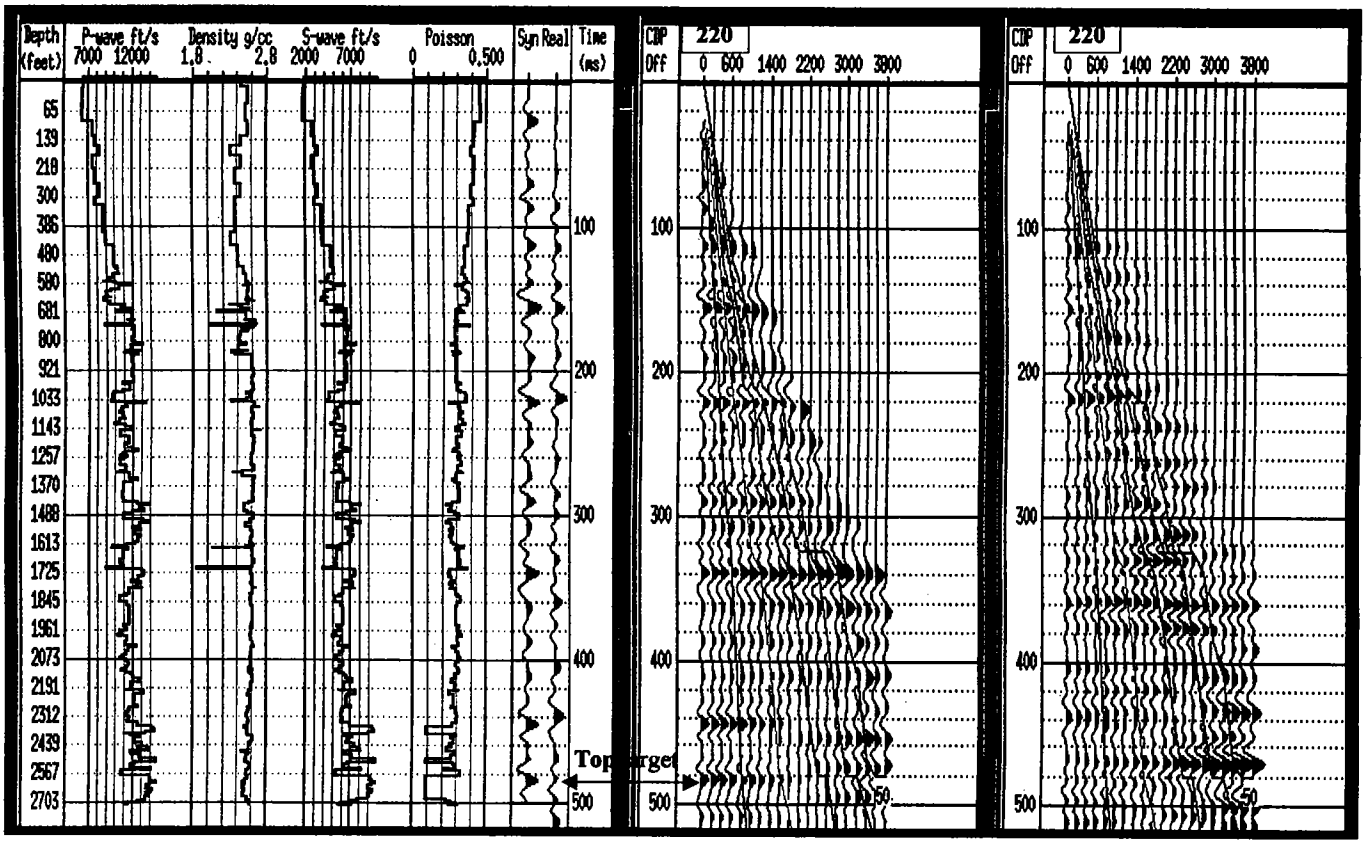

Figure 8. AVO gas synthetic-seismogram model 1 for the No. 1-15 Wright well, allowing V_S to change in the gas interval.

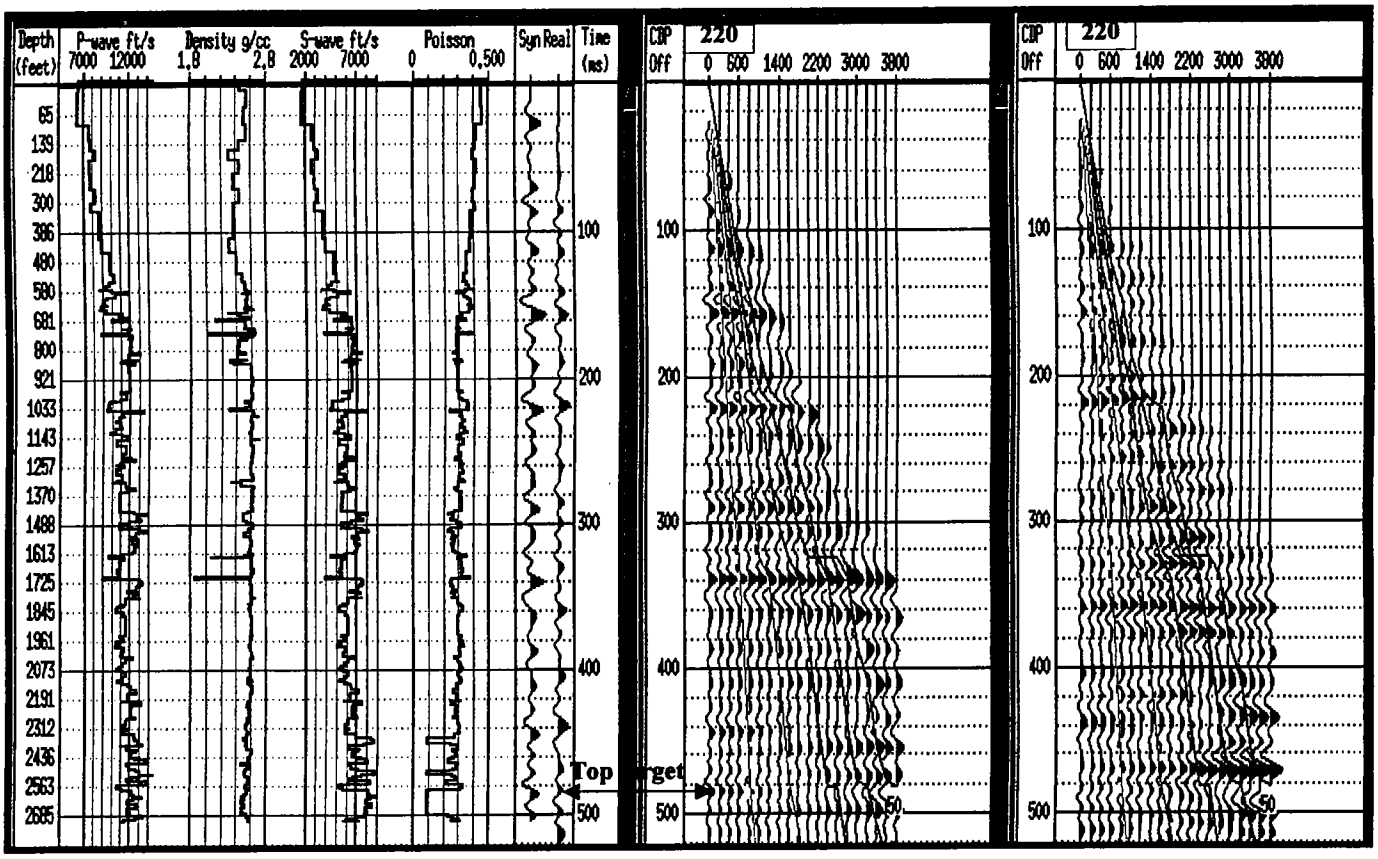

Figure 9. AVO gas synthetic-seismogram model 2 for the No. 1-15 Wright well, allowing V_p to change in the gas interval.

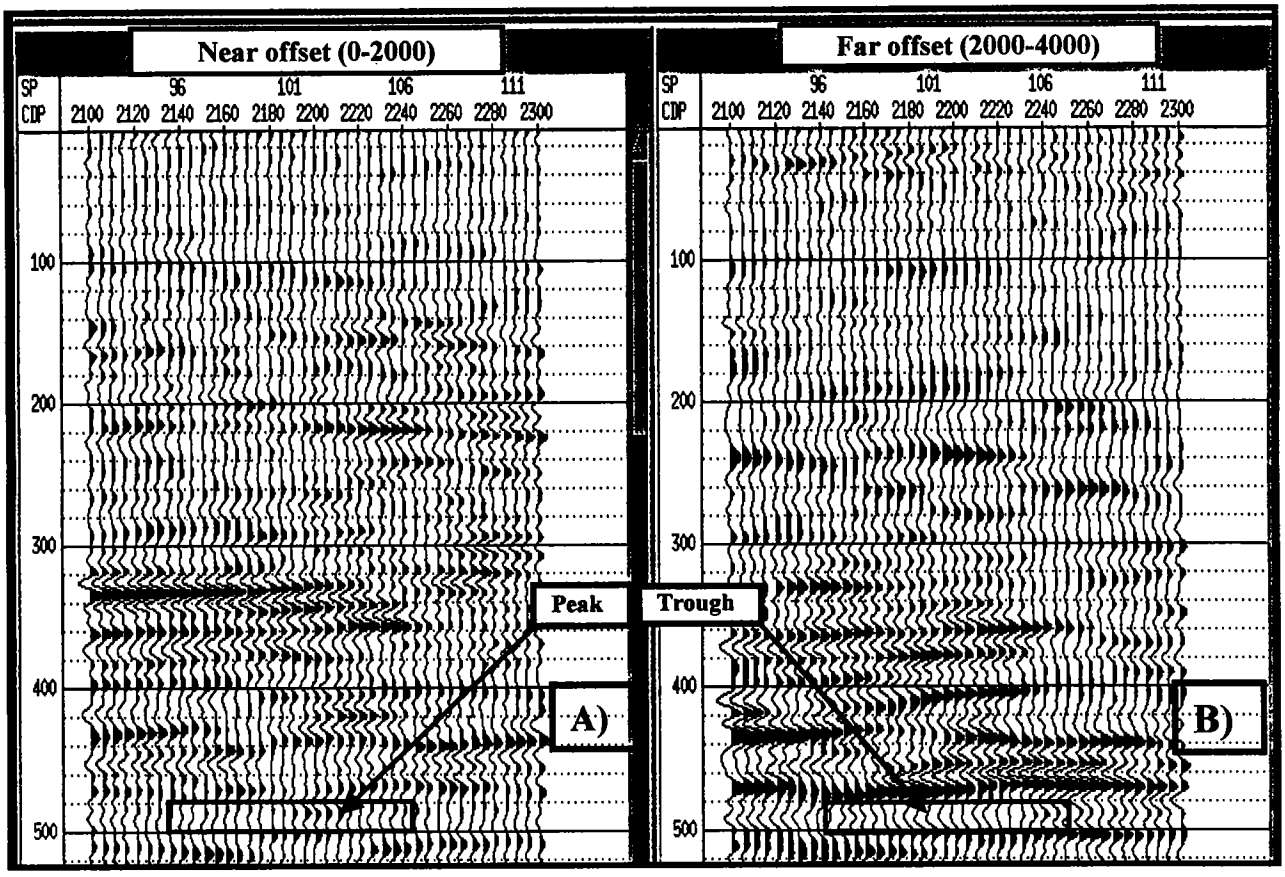

Figure 10. (A) Near-offset stacking, and (B) far-offset stacking, showing the AVO anomaly for the target reservoir.

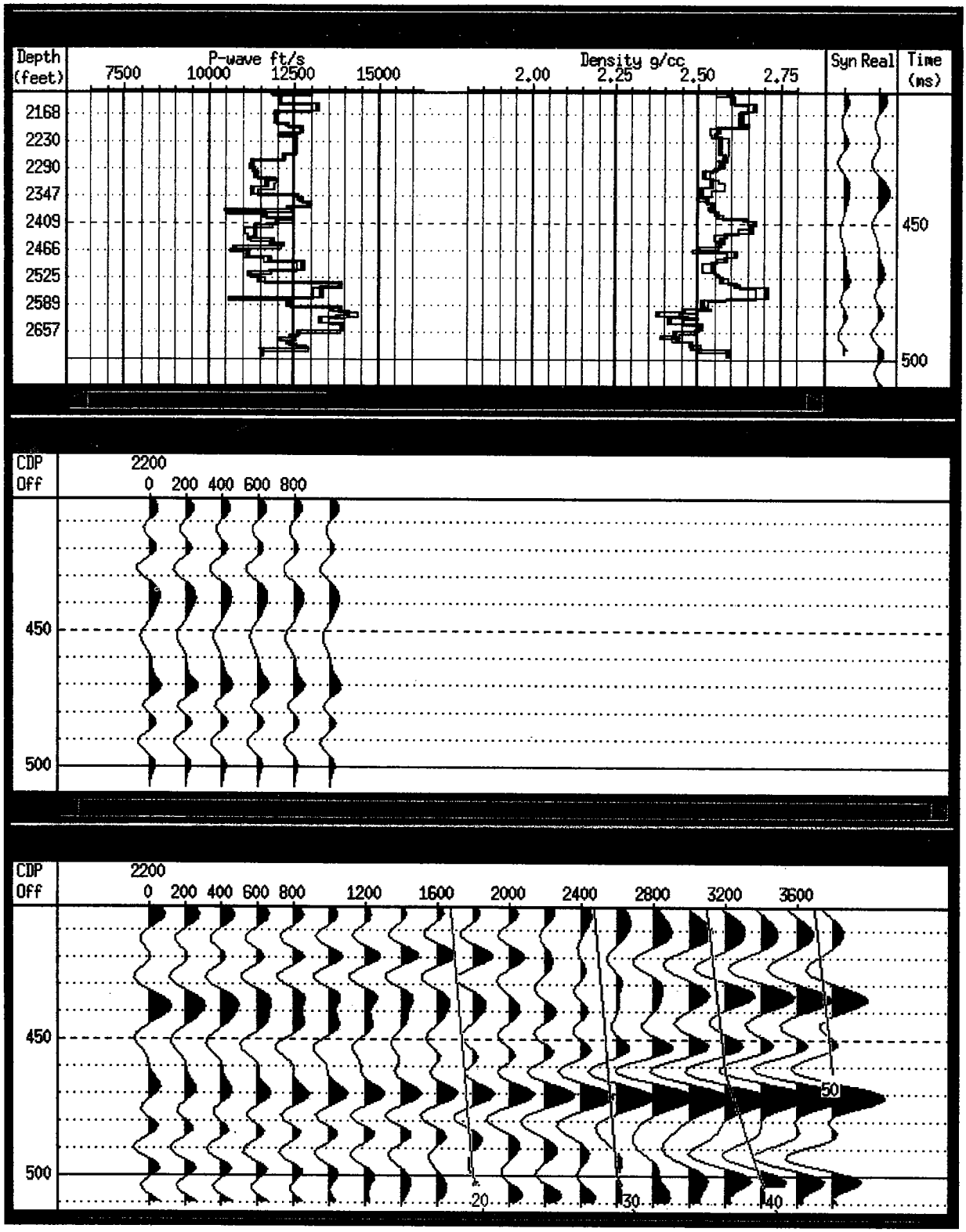

Figure 11. AVO inversion for near offset, allowing V_p, density, and layer thickness to change and using the original log with V_s from the mudrock trend model as the starting model.

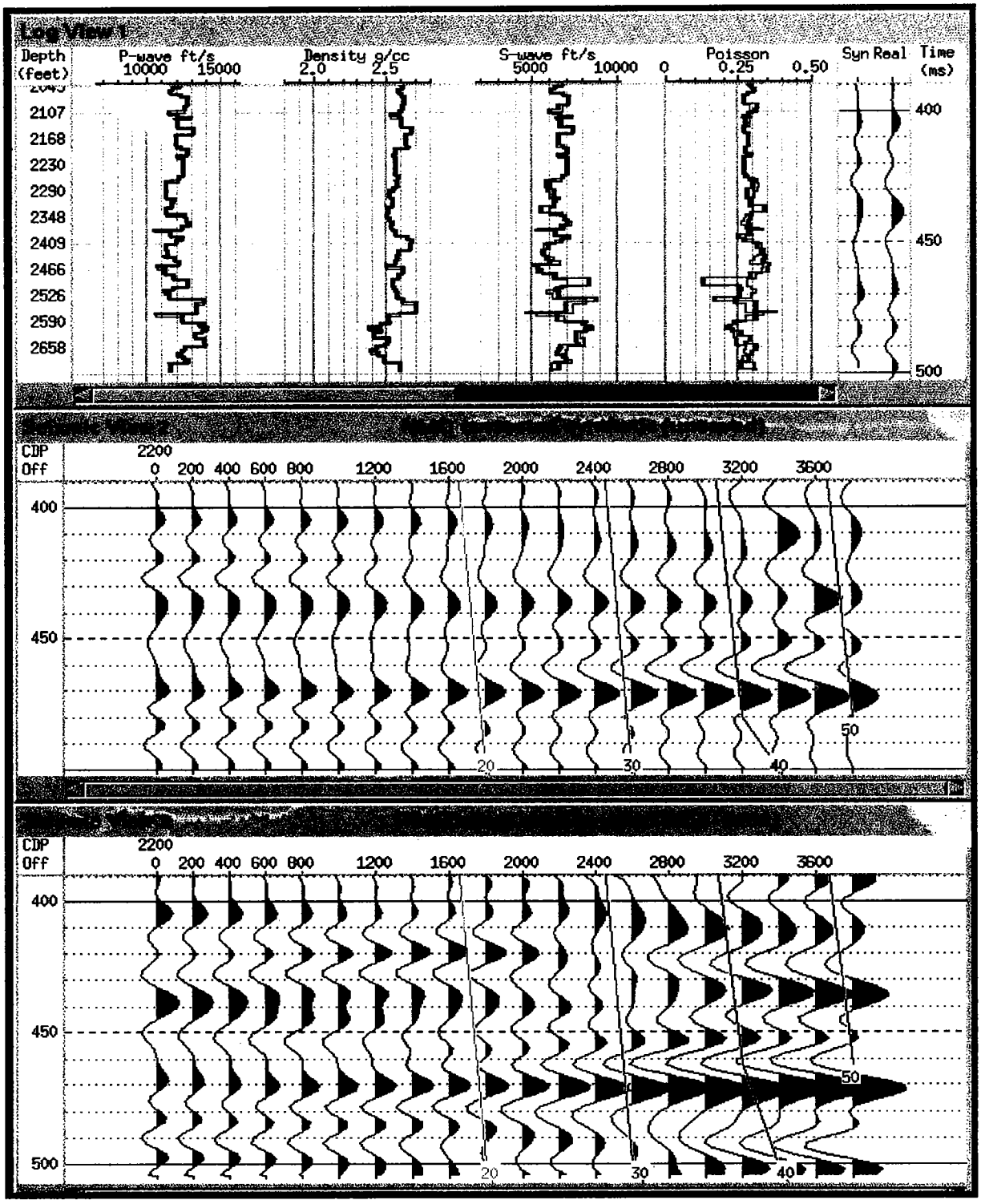

Figure 12. AVO inversion for near and far offset, allowing V_S to change and using the original log model as the starting model.

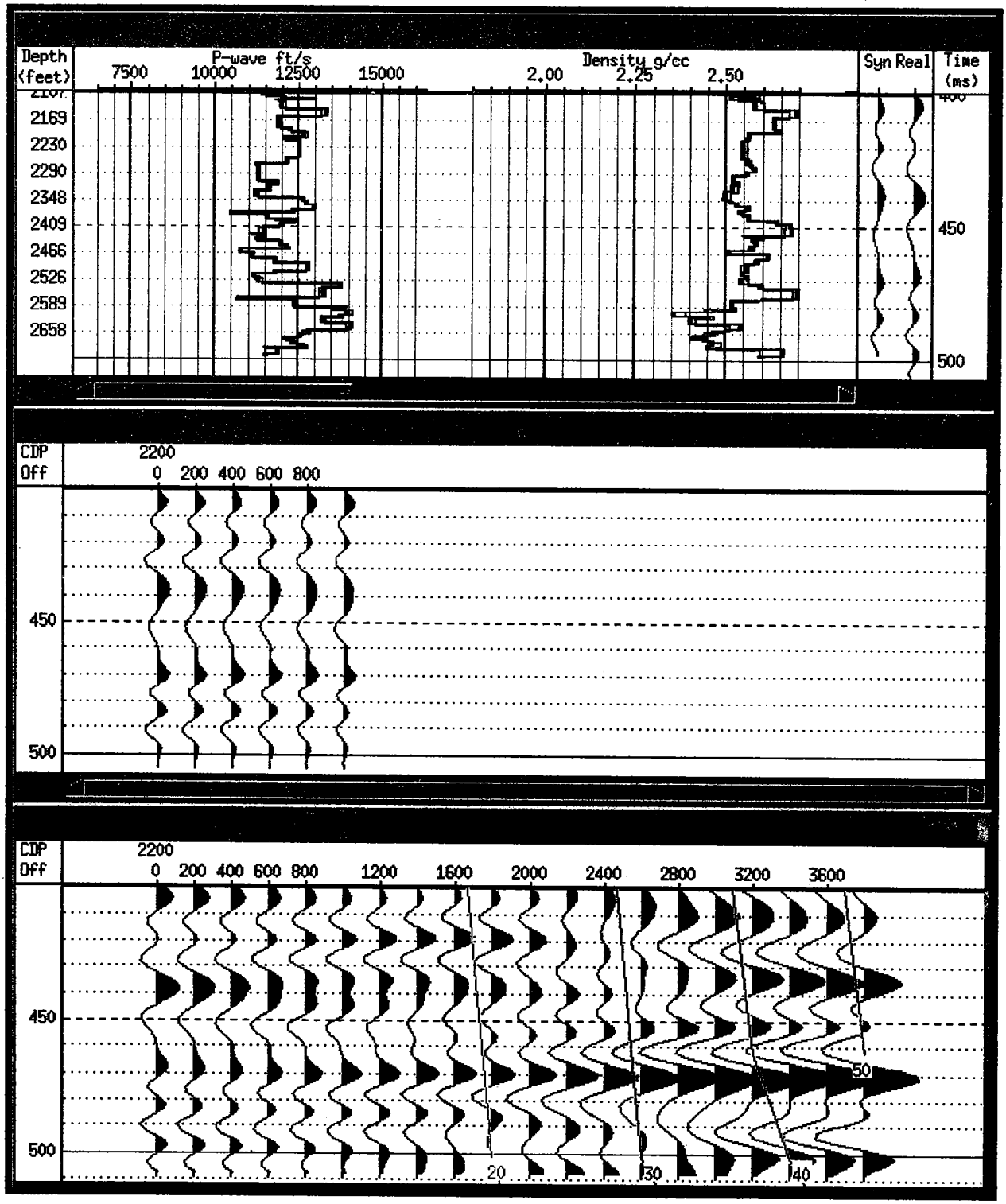

Figure 13. AVO inversion for near offset, allowing V_p, density, and layer thickness to change and using gas model 1 as the starting model.

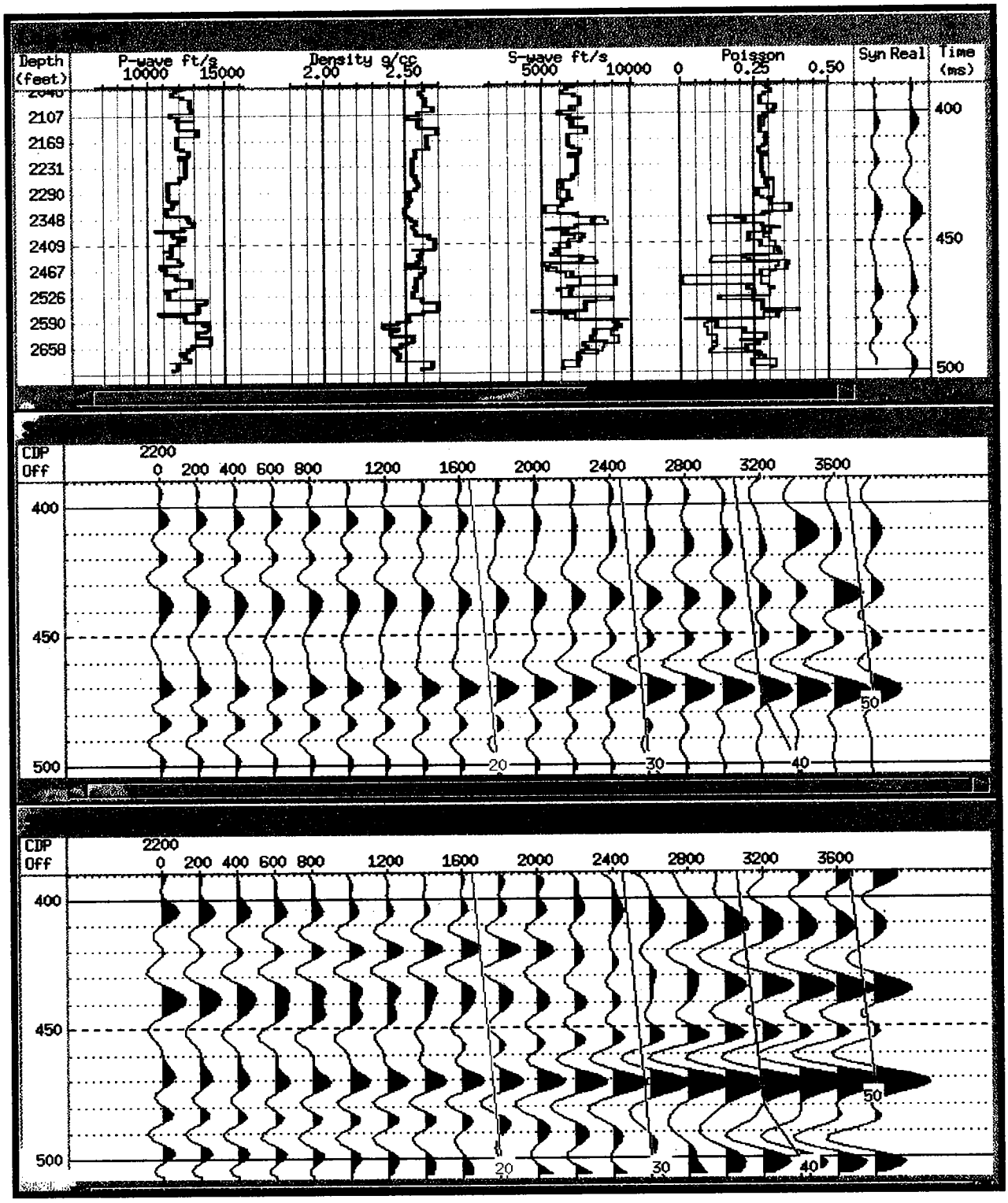

Figure 14. AVO inversion for near and far offset, allowing V_S to change and using gas model 1 as the starting model.

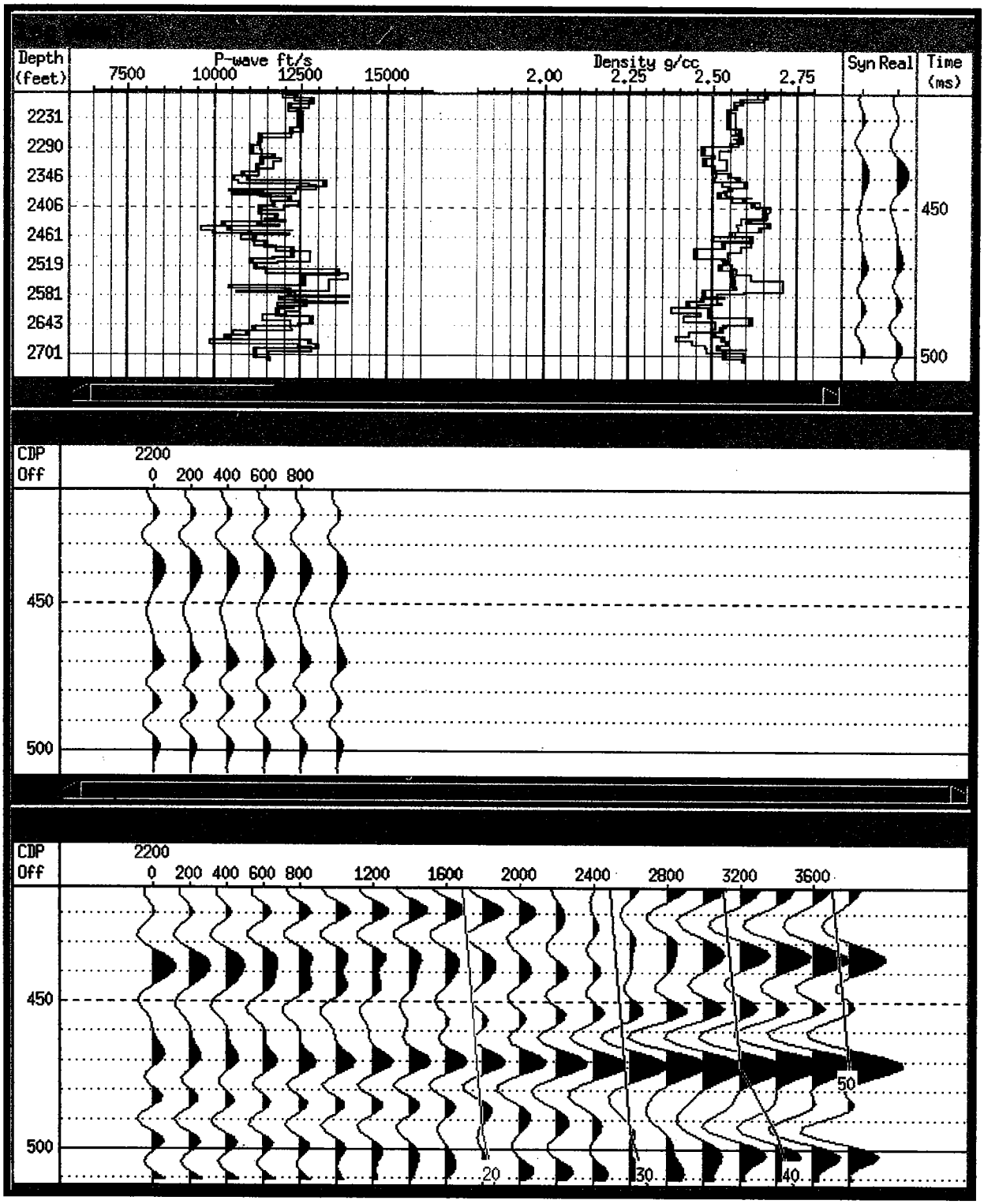

Figure 15. AVO inversion for near offset, allowing V_p, density, and layer thickness to change and using gas model 2 as the starting model.

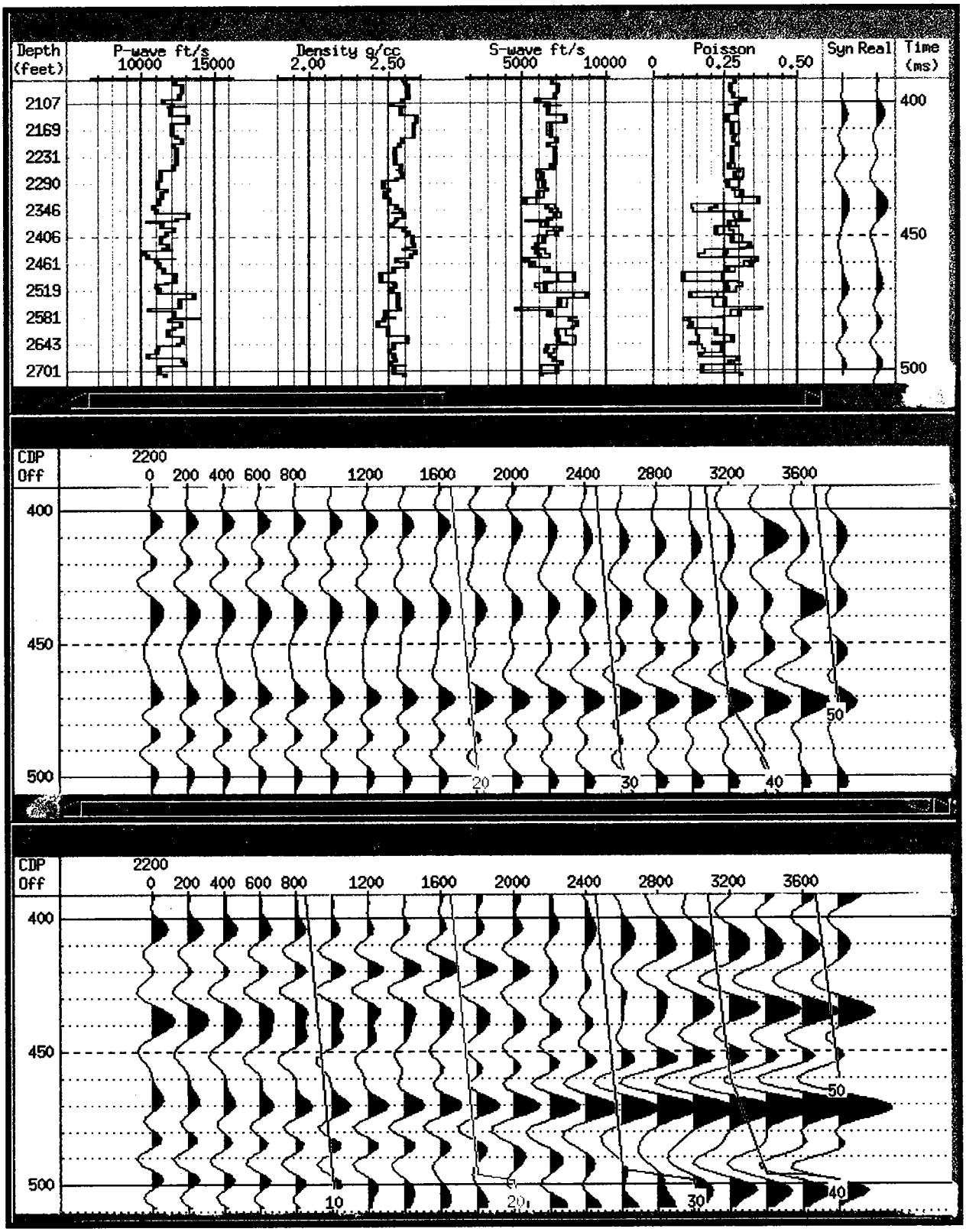

Figure 16. AVO inversion for near and far offset, allowing V_S to change and using gas model 2 as the starting model.

Seal Characterization and Fluid-Inclusion Stratigraphy of the Anadarko Basin

Zuhair Al-Shaieb, James O. Puckette, and Amy Close
Oklahoma State University
Stillwater, Oklahoma

ABSTRACT.—The Anadarko basin of western Oklahoma and the Texas Panhandle contains >30,000 ft of Paleozoic sedimentary rocks. These rocks embrace a tiered system of shallow-normal, overpressured, and deep-normal pressure domains. A hierarchy of seals separates pressure tiers and compartmentalizes the basin.

The pressure architecture of the basin includes an overpressured and completely sealed compartment called the megacompartment complex (MCC), which is composed mainly of Mississippian and Pennsylvanian rocks. First-order seals separate the primary pressure tiers and isolate the MCC. Second-order seals separate stratigraphic intervals, and third-order seals separate individual compartments and contribute to reservoir heterogeneity.

The seals are rich in fluid inclusions, which provide insight into seal genesis and burial history. Early silica-cement phases formed protoseals that preceded oil generation. These seals evolved with burial and began to confine overpressures caused by hydrocarbon generation and thermal expansion. Once the seals were in place, overpressures were generated by the thermal transformation of liquid petroleum into gas.

Capillary-pressure measurements indicate that seals in the Anadarko basin have a high sealing capacity and were capable of confining overpressures across geologic time.

INTRODUCTION

The Anadarko basin, in western Oklahoma and the Texas Panhandle, is an asymmetric, fault-bounded, elongate depositional and tectonic basin that contains >30,000 ft of Paleozoic sedimentary rocks (Fig. 1). Pressure measurements indicate that this thick column of rocks contains a tiered pressure system consisting of shallow-normal, overpressured, and deep-normal pressure domains. A hierarchy of seals separates pressure tiers and compartmentalizes the basin. These seals evolved during the rapid-subsidence phase of the basin and contain diagenetic- and capillary-pressure components.

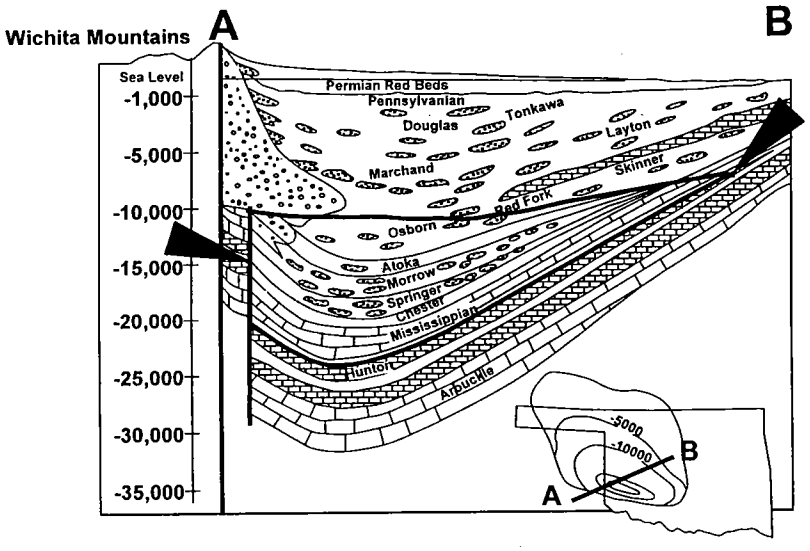

Figure 1. Generalized schematic cross section of the Anadarko basin, showing boundaries (heavy lines) of the megacompartment complex (MCC). Location of Anadarko basin is shown on inset map. Depths are in feet. From Al-Shaieb and others (1994a).

Inclusion data support the hypothesis that liquid-to-gas transformation was a primary source of overpressuring in the basin. Hydrocarbon generation and transformation sharply decreased and ultimately ceased as a result of cooling following the Laramide uplift. Therefore, seals that maintained their integrity across geologic time confined the overpressure that presently exists in the basin.

PRESSURE ARCHITECTURE OF THE ANADARKO BASIN

Al-Shaieb and others (1994a,b, 1999) described the pressure architecture of the Anadarko basin and established the presence of an overpressured and completely sealed basin-scale compartment called the megacompartment complex (MCC) (Fig. 1). The MCC is composed primarily

Al-Shaieb, Zuhair; Puckette, J. O.; and Close, Amy, 2002, Seal characterization and fluid-inclusion stratigraphy of the Anadarko basin, *in* Cardott, B. J. (ed.), Revisiting old and assessing new petroleum plays in the southern Midcontinent, 2001 symposium: Oklahoma Geological Survey Circular 107, p. 153–161.

of rocks of the Mississippian and Pennsylvanian Systems (Fig. 2). Its interior consists of a network of totally isolated, smaller compartments that are separated by seals.

A compartment hierarchy, based on size and distribution, was developed to classify compartments (Fig. 3). Level 1 is a regional feature that includes most of the overpressured rocks in the basin. Level 2 is a field- or district-size feature, with relatively uniform pressures, that is confined within a stratigraphic interval. Level 3 is the smallest in size and consists of reservoir-size compartments. The size and geometry of these compartments are strongly linked to their depositional setting and facies (Al-Shaieb and others, 1994b).

Compartments are delineated by their distinct pressure values and/or fluid compositions. The intricate internal structure of the MCC is a result of the evolution of this complex of seals and compartments. Isolated, overpressured satellite compartments, which occur outside the MCC, are found in the Simpson and Hunton Groups.

CLASSIFICATION OF SEALS

Seals in the Anadarko basin were classified according to the size of the compartments they confine (Fig. 4). First-order seals are regional-size, separate overpressured and normally pressured domains and isolate the MCC. The MCC is bounded on the base by a first-order seal that corresponds to the Devonian–Mississippian Woodford Shale in the central and western parts of the basin and/or the Mississippian Caney Shale in the eastern part. Another first-order seal occurs at the top of the MCC and separates the shallow-normal-pressure tier from the overpressured MCC. A third first-order seal forms the southern boundary of the MCC. This vertical seal is associated with the Wichita frontal fault zone and is composed of highly cemented Pennsylvanian conglomerates.

Second-order seals divide the MCC into smaller compartments that conform to stratigraphic intervals. These seals typically coincide with shale that represents late-stage transgressive-systems-tract deposition and might correspond to maximum flooding surfaces. Second-order seals in the Anadarko basin are evident on pressure–depth profiles as the boundaries between pressure "steps." The pressures at each step are similar and represent measurements from the same stratigraphic horizon. The adjacent steps are formed by pressure measurements from overlying and underlying stratigraphic horizons.

Third-order seals subdivide reservoirs within stratigraphic intervals. These seals are flow barriers that contribute to reservoir heterogeneity.

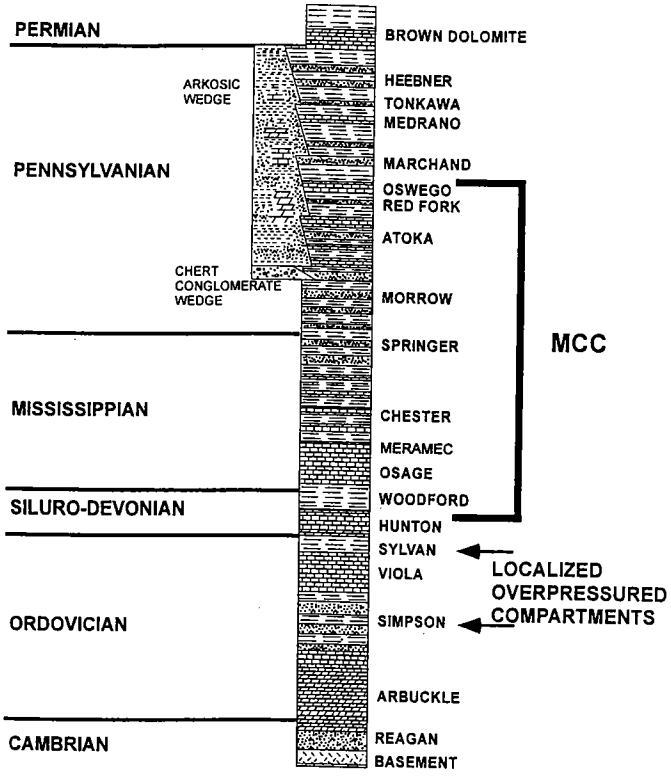

Figure 2. Generalized stratigraphic column of the Anadarko basin, showing the rock units that contain the MCC and local overpressured "satellite" compartments.

DIAGENETIC BANDING

Many seal rocks display unique diagenetic banding that formed as a result of the interplay of stress-induced mineral reactions, pore-fluid interactions, mass transport, and precipitation (Al-Shaieb and others, 1994c, 1999). This diagenetic signature is present in rocks that were buried deeply enough to enter the "seal window." In the Anadarko basin, the seal window occurs at about 6,000 to 10,000 ft. Rocks from shallower intervals lack these banding features. The origin of diagenetic bands has been simulated by using reaction-transport models developed by Dewers and Ortoleva (1988, 1990).

Within the MCC, diagenetic banding is manifested as silica-cement bands that consist of zones of en-

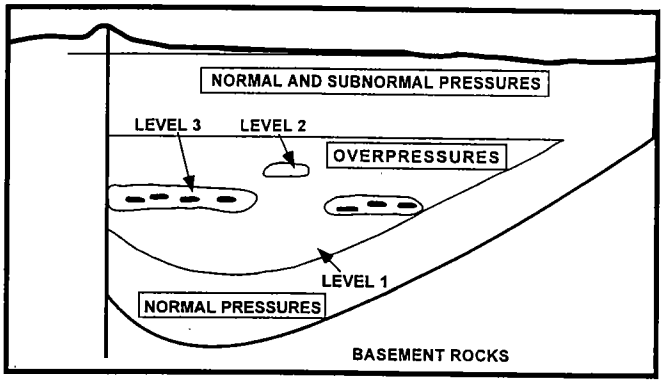

Figure 3. Classification of pressure compartments. Level 1 coincides with the MCC. Level 2 represents large field- or district-size features with similar reservoir pressures. Level 3 represents small field- to reservoir-size compartments.

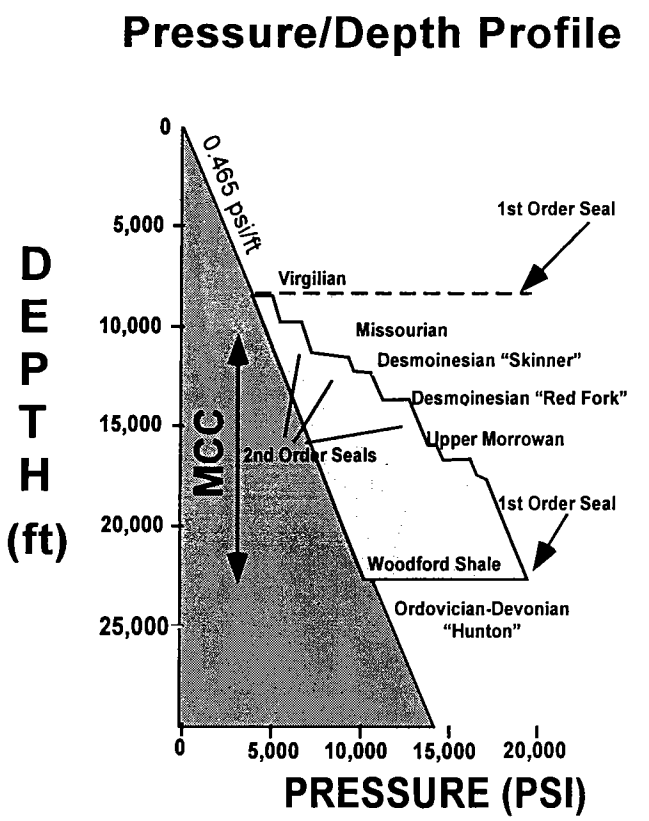

Figure 4. Pressure evidence of first-order and second-order seals seen on a pressure–depth profile from the western Anadarko basin. First-order seals at the base and top of the MCC isolate it from adjacent normal-pressure tiers. Second-order seals within the MCC separate stratigraphic units and create the "steps" evident on the profile.

hanced quartz overgrowths alternating with bands that contain intergranular porosity. Some of the silica seemed to be derived from pressure solution of quartz grains in the adjacent band. Other silica apparently was transported in from another source. Porous regions commonly contain thicker clay coatings on grains, suggesting clay inhibition of quartz cementation. Silica bands occurred relatively early in the diagenetic history (5,600 ft at 65°C) and reflect mechanochemical processes associated with burial compaction, dissolution, and precipitation (Al-Shaieb and others, 1994c; Ortoleva and others, 1995).

Some shale and siltstone in seal zones contain distinct diagenetic bands. Comparative analysis of cores and outcrops reveals that these bands are noticeably absent in clay-rich rocks that were never buried deeply enough to become overpressured. Pennsylvanian and Mississippian shales that entered the seal window exhibit two types of banding. In the Pennsylvanian (Desmoinesian) Pink limestone–Red Fork sandstone interval, diagenetic bands of silica and chlorite appear to have formed independently of depositional features. On the other hand, silica banding in the Devonian–Mississippian Woodford Shale usually occurs as an enhancement or modification of existing sedimentary features (Al-Shaieb and others, 1994c).

Satellite pressure compartments occurring outside the MCC have a significant diagenetic component to their seals. Satellite compartments in the Ordovician Simpson Group contain alternating permeable and cemented sandstone beds. The compositionally homogeneous Bromide sandstone contains silica bands that were apparently generated by local dissolution and precipitation. Sandstone with a thin, nonpervasive clay grain coating compacted and became a silica source as penetrating grain contacts liberated silica. Adjacent intervals received imported silica and evolved into silica-cemented bands. Clay coating inhibited silica precipitation and preserved primary porosity in porous bands.

A second type of banding in the Bromide sandstone is composed of carbonate that precipitated after the silica bands were formed. Carbonate-cemented bands consist of calcite or dolomite that alternate with porous bands of silica-cemented sandstone. Carbonate and silica bands occur on similar scales. They occur on a millimeter scale within a thin interval and as thicker (centimeter-scale) homogeneous bands. The earliest diagenetic calcite cements apparently were derived from compactional dissolution of carbonates within or adjacent to the sandstone. Potential sources include limestone beds and fossil-rich zones within the sandstone as well as overlying Bromide and Viola carbonates. Detailed descriptions of these bands are found in Al-Shaieb and others (1994c, 1999) and Tigert and Al-Shaieb (1990).

BURIAL HISTORY AND SEAL GENESIS

A burial-history curve, modified from Schmoker (1986), depicts relative subsidence and depositional rates for the Anadarko basin (Fig. 5). The basin underwent modest subsidence rates and sediment accumulation until the Pennsylvanian orogenies, when ~20,000 ft of sediment accumulated in ~40 million years. The rapid subsidence and burial associated with these orogenies generated geochemical disequilibrium that contributed to dissolution and re-precipitation. These processes are reflected by cementation episodes (Q-1, C-1, Q-2, and C-2) described by Al-Shaieb and others (1994c). Homogenization temperatures of fluid inclusions from these cement phases were used to establish their timing.

The first episode (Q-1) coincides with the generation of early silica cement that precipitated at temperatures of 70°–100°C. The second episode consists of calcite cement (C-1) containing aqueous inclusions that formed at about 80°–110°C. The third episode (C-2) is higher temperature calcite (95°–140°C) that contains petroleum-bearing aqueous inclusions. The fourth episode is higher temperature (110°–120°C) silica cement (Q-2) that contains petroleum (Al-Shaieb and others, 1994c).

Fluid inclusions from silica and carbonate cements in the large lateral seal zone along the southern mar-

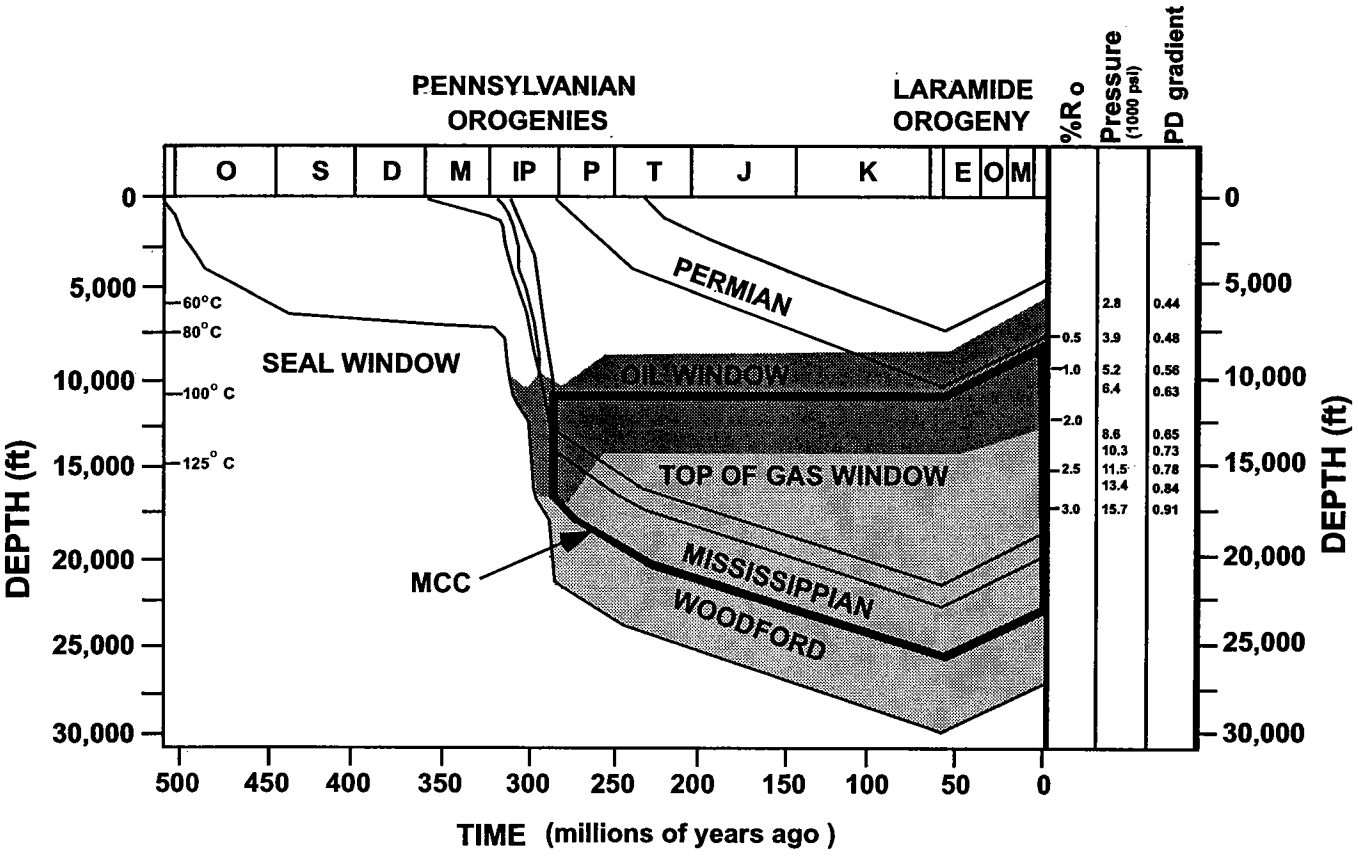

Figure 5. Burial-history curve for the Anadarko basin (modified from Schmoker, 1986). Seal genesis occurred primarily during the rapid-subsidence phase associated with the Pennsylvanian orogenies. The interrelationship between values of vitrinite reflectance (%R_o), reservoir pressure, pressure–depth (PD) gradient, and depth is shown. Temperature values represent homogenization temperatures from cement phases.

gin of the MCC were used to interpret the origin of this feature. Here, silica cement formed at ~170°C, whereas carbonate precipitated at temperatures of ~124°C. These temperatures are similar to those recorded for cements associated with petroleum migration and indicate a heated, basinal fluid source. It is proposed that warm, pressurized fluids migrated from the basin center toward the hydrostatically pressured Wichita frontal fault zone. Cement precipitated in the rocks with lower pressure that are adjacent to the fault zone, and a large seal zone some 6,000–8,000 ft thick and 4–6 mi wide resulted. This seal effectively confines extremely high (near lithostatic) pressures in Morrowan chert-conglomerate reservoirs a few miles north of the frontal fault zone.

LONGEVITY OF SEALS

The deep Anadarko basin reached maximum burial depth in the Mesozoic Era (66 mya) and has undergone uplift since the Laramide orogeny (Schmoker, 1986) (Fig. 5). As a result of this uplift and cooling, the generation of hydrocarbons and overpressures ceased. Hubert (1995) demonstrated that oil-to-gas transformation provided a viable mechanism for generating overpressures, and that deep Pennsylvanian (Morrowan) reservoirs reached a transformation ratio of 0.8. Vitrinite-reflectance data indicate that kerogen has remaining gas-generating capacity in the deep basin (Walker, 1986; Hubert, 1995). Because post-Laramide uplift and cooling froze gas generation and transformation, overpressures are ancient (>10 my minimum; Hubert, 1995), and seals must be capable of confining pressure across geologic time.

SEAL CAPACITY

Capillary-pressure curves were used to determine sealing capacity and evaluate pore structure. Sealing capacity was defined in terms of (1) the height of a hydrocarbon (gas) column (Hpd) the rock will hold without leaking, and (2) displacement pressure (Pdma). Pdma is the pressure required to displace the wetting phase fluid (water) in a rock with a non-wetting phase (gas). As pore-throat aperture decreases, Pdma generally increases. Similarly, the height of the gas column the rock will hold is inversely proportional to porosity and permeability. Low-porosity and low-permeability rocks with small pore-throat apertures will confine larger columns of gas before the gas displaces the water and leaks.

Capillary-pressure measurements were taken in diagenetic bands from seal zones. These were compared to capillary measurements from reservoir and

seal zones in other geologic provinces. Low-porosity (<5%), low-permeability (<0.001-md) sandstones from the Gulf Coast had displacement pressures up to 2,454 psi, and the greatest gas-column heights (Hch) of ~550 ft (Al-Shaieb and others, 2000). In comparison, a thin diagenetic band from the Pink limestone–Red Fork interval (Fig. 6) has displacement pressures >10,520 psi and gas columns >4,700 ft. The porosity in these bands was below instrument-measurement capabilities. In contrast, very fine grained sandstone with ~20% porosity and ~9-md permeability had displacement pressures of ~200 psi and gas-column heights of <10 ft.

The sealing capacity of diagenetic bands illustrates the confining capability of seal zones. Because seal zones are composed of multiple bands, these low-porosity, low-permeability rocks have become capable of confining the high reservoir pressures evident in the Anadarko basin.

FLUID-INCLUSION STRATIGRAPHY

Seal cements are enriched in fluid inclusions that contain a history of migrating fluid compositions (Hall and others, 1997). Inclusion contents reflect changing temperature and fluid types as cements precipitated. They also record changes in composition resulting from deep burial or exhumation.

Fluid-inclusion stratigraphy involves the complete analysis of volatiles trapped in inclusions, using quadrupole mass analyzers (Hall and others, 1997). The procedure records the presence and relative abundance of ionized volatile fragments released from inclusions when they are crushed. Results are shown as millivolt responses and are displayed on a series of parallel tracks that represent different ionic species or species ratios (Fig. 7). This format allows for the simultaneous comparison of results and easy recognition of positive and inverse relationships between species.

A composite vertical profile of fluid inclusions was constructed from rock samples from Roger Mills and Ellis Counties, Oklahoma. This profile was designed to establish the fluid-inclusion stratigraphy in the deep basin (Fig. 7). The profile extends from the normally pressured reservoirs downward through the MCC and across the basal seal into normally pressured rocks below. The sampled section included whole-rock samples from cores of Pennsylvanian, Mississippian, Devonian, Silurian, and Ordovician units, and ranged in depth from 7,900 to 16,360 ft.

Mass-spectrometry analyses of inclusion volatiles from the shallow-normal-pressure tier indicated low gas and liquid hydrocarbon concentrations in comparison to deeper samples. Fluorescence of inclusions in healed microfractures suggests that these inclusions contain low- to moderate-gravity petroleum. Once the onset of overpressuring is encountered, a transitional increase in methane is evident (Fig. 7, ~9,000 ft, track 1). Inclusions in this zone appear to contain high-gravity petroleum. The vapor phase within these inclusions is large, suggesting a fairly volatile petroleum phase. Within the MCC, a continuously high methane response was recorded. This supports the hypothesis that the transformation of liquid petroleum to gas (methane) provided the increased fluid volume that generated overpressure within the MCC. A high methane response continued through the MCC. Liquid-range species were still present and became more noticeable in the argillaceous Mississippian carbonates. Hydrogen sulfide concentration also increased in the Mississippian. Fluorescence indicates that Mississippian inclusions contain moderate- to high-gravity petroleum. The vapor phase in these inclusions is relatively large, suggesting a volatile petroleum phase. The response across the Woodford Shale (basal seal) indicates high concentrations of methane and C_4 to C_8 species (Fig. 7, 16,000 ft). Because the Woodford is a source rock, it is uncertain if these responses reflect trapped migrating petroleum or internally generated hydrocarbon species.

Hunton rocks below the basal seal of the MCC continued to display a high methane response. Higher molecular species were present, but in reduced numbers. Responses for both gas- and liquid-range hydrocarbons were extreme in the upper part of the Simpson Group section in an interval of shale and carbonate that may represent a seal zone. Abundant non-fluorescent gas inclusions and pyrobitumen (Fig. 8) were present in the Simpson units. Pyrobitumen coats grain surfaces in macro- and microporosity in dolomite and lines the walls of gas-filled inclusions. These inclusions and reservoirs initially contained liquid petroleum that was thermally altered after entrapment. Methane continued to be the dominant species in the lower part of the Simpson Group and in the Arbuckle Group. Pale blue fluorescent gas-condensate inclusions were present in healed microfractures in quartz detrital grains in the Simpson. These inclusions also have a large vapor phase and contain pyrobitumen.

INTERPRETATION

Fluid-inclusion analyses indicate that rock units within and below the MCC followed similar diagenetic paths. Silica cement was generated initially, beginning at about 6,000 to 7,000 ft. This cement precipitated prior to the generation of hydrocarbons and formed a protoseal. As compaction increased with burial, carbonate (C-1) was mobilized and precipitated in areas with amenable pore-fluid chemistry. During this phase, fluid flow was relatively unrestricted, and heated basinal fluids moved from the subsiding basin center toward the lower pressures along the margins of the basin. Accompanying these brines were organic acids and hydrocarbons generated during source-rock maturation. These acids attacked labile grains in reservoirs and generated secondary porosity. As the local pore-fluid chemistry changed in response to H^+ ion consumption, carbonate began to precipitate, and petroleum was trapped in inclusions.

Anadarko Basin

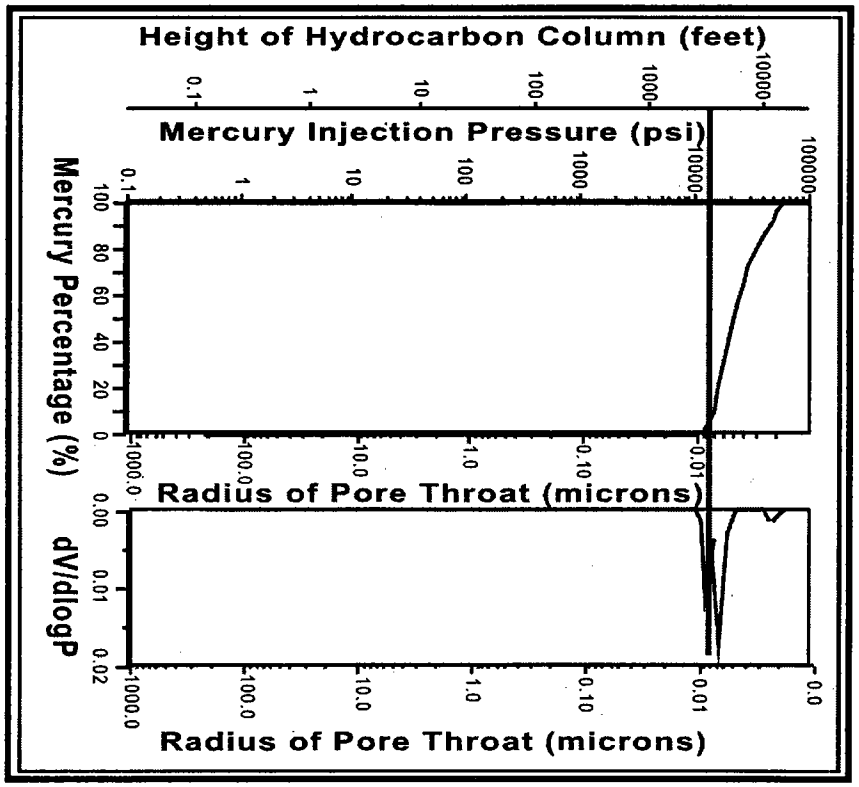

Banded Seal

Pdma=10,520psi

Hpd= 4725 ft

Moderc= 0.002 μm

Medianrc = 0.004 μm

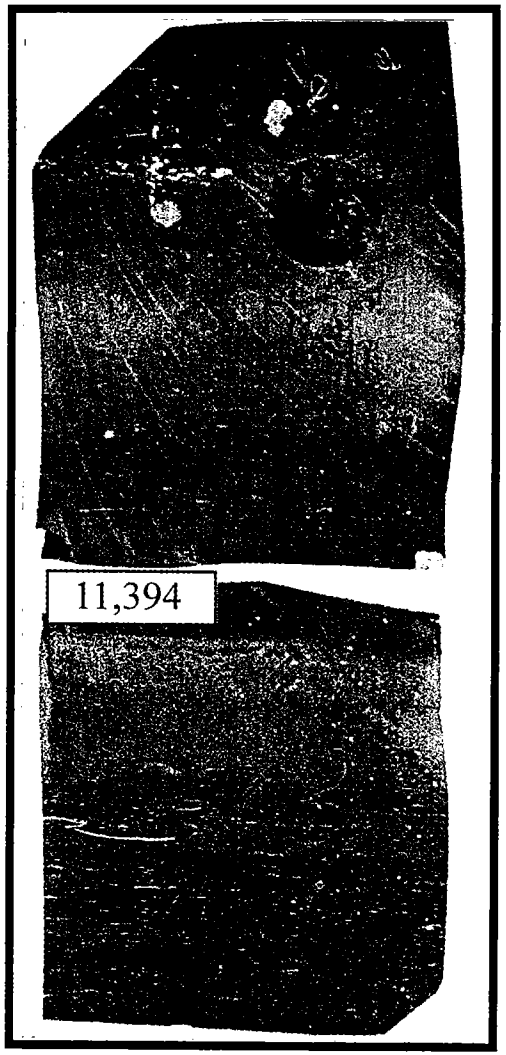

Figure 6. Capillary-pressure measurements of a diagenetic cement band from the Pink limestone–upper Red Fork seal interval in Roger Mills County, Oklahoma. Displacement pressure (Pdma) exceeds 10,520 psi. Gas-column height (Hpd) held by this seal exceeds 4,700 ft. Modal pore-throat-aperture size is 0.002 μm, whereas median aperture size is 0.004 μm.

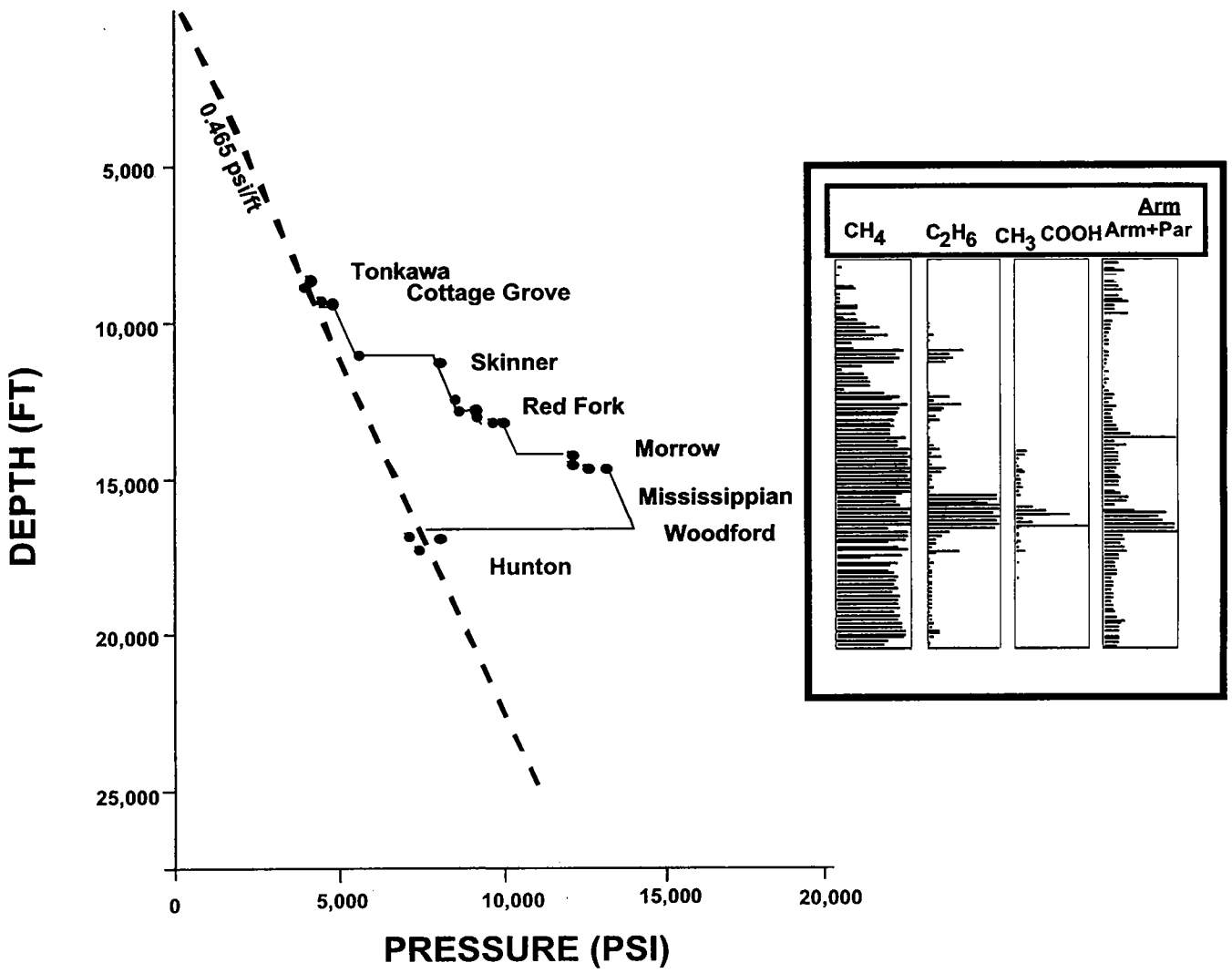

Figure 7. Fluid-inclusion contents (inset) correlated to a pressure–depth profile from Roger Mills and Ellis Counties, Oklahoma. An increase in methane (CH_4 track) coincides with the top of overpressure and a decrease in aromatics (Arm/Arm + Par). Methanogenesis resulted from the thermal transformation of liquid petroleum to gas and is evident in all rocks buried deeply enough to enter the seal window. Increases in all species in the Woodford may reflect its sealing and/or source-rock capabilities.

Fluid migration within rock units was relatively unrestricted until the rock units entered the seal window. At this time, reservoirs with diagenetic protoseals had their seals enhanced by the precipitation of additional cement. With continued burial and the thermal transformation of liquids to gas, sealing was likely completed by capillary pressure. The seal along the southern boundary of the MCC evolved during this stage. The Pennsylvanian (Morrowan) clastic wedge provided a flow path of least resistance as high-temperature fluids migrated from the subsiding basin center toward the normally pressured fault zone (Fig. 9). Normal pressure was maintained near the fault by continuing displacement that destroyed cement integrity within the faults. Cement precipitated in the vicinity of the lower pressured fault zone. This seal accumulated as subsiding rocks entered the seal window and fault-focused flow continued. Once the seal was in place, the additional transformation of liquid petroleum into gas generated increased volume and the extreme overpressures in the deep Morrow reservoirs.

The pressure differential between the fault and the MCC developed as a result of burial, thermal expansion, and hydrocarbon maturation below the seal window. Rocks in the Pennsylvanian clastic wedge that were not buried sufficiently to enter this window did not develop fault-focused flow and were not cemented. This is evident in the normally pressured tier above the MCC, where a number of porous reservoirs are present up to and within the fault zone.

Deep, normally pressured rocks below the MCC entered the seal window but either failed to seal or ruptured. Burial-history curves indicate that Hunton, Simpson, and Arbuckle rocks were well within the seal window during the Desmoinesian. However, a combination of factors likely prevented them from becoming extensively compartmentalized and overpressured. The first factor was lithology. The Hunton and

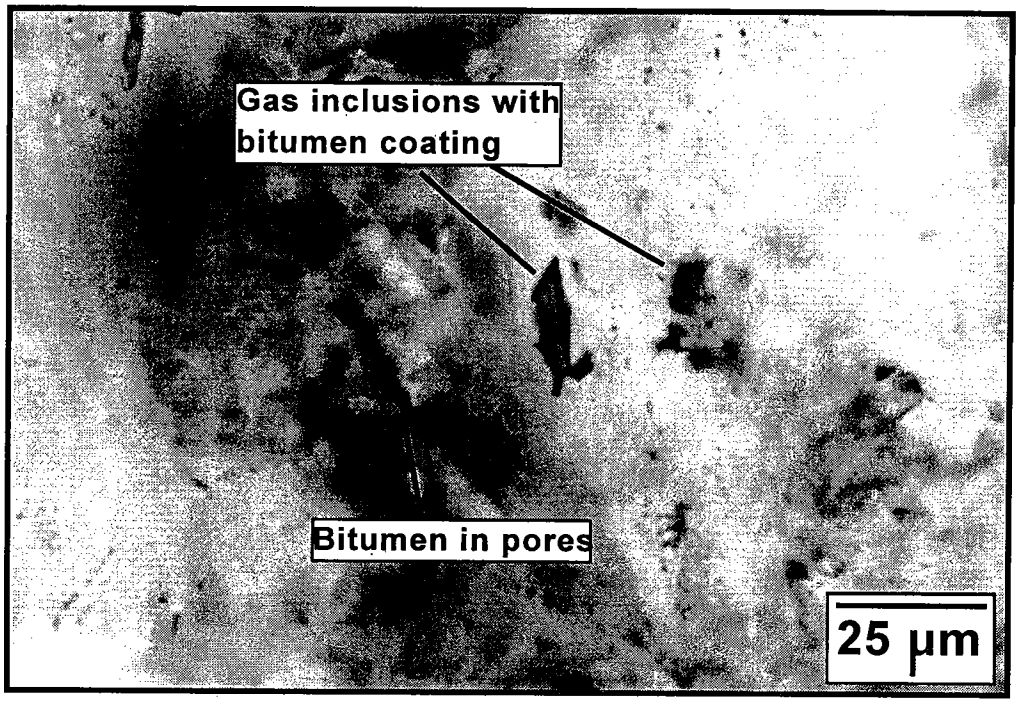

Figure 8. Photograph of fluid inclusion in sandstone from the lower Paleozoic Simpson Group that contains gas and pyrobitumen derived from the thermal alteration of oil. Thermal transformation of liquid petroleum to gas was a viable mechanism for the generation of overpressures in the Anadarko basin. Sample depth is 14,414 ft.

Arbuckle Groups contain laterally extensive carbonates that were subjected to several episodes of meteoric diagenesis, dolomitization, and karstification. As a result, widespread porosity networks evolved (Matthews and Al-Shaieb, 1993; Al-Shaieb and others, 1999) that provided conduits for the dissipation of overpressures generated during burial. Simpson sandstones are also laterally continuous, porous units, and they apparently dissipated overpressures. Isolated satellite compartments developed within these units, and overpressuring is restricted to the satellites. A second factor was the outcrop of the lower Paleozoic units during the Pennsylvanian Period. Hunton, Simpson, and Arbuckle rocks were exposed along the Nemaha and Arbuckle uplifts during the Desmoinesian Epoch. These outcrops may have provided a release for abnormal pore pressure generated in the deeper part of the basin. Pressure dissipation in the lower Paleozoic prevented fault-focused flow that generated the fault-bounding seal of the MCC. As a result, porous reservoirs are found within the lower Paleozoic section up to and within the fault zone.

Lithologic, pressure, and fluid-inclusion data from the Anadarko basin suggest that all reservoirs in the rock column below the shallow-normal-pressure tier have similar burial histories. However, the basin developed a tiered pressure system in which deep-normal pressure is found below highly overpressured reservoirs of the MCC. Furthermore, these deep, normally pressured reservoirs typically contain a water column beneath dry-gas accumulations. In contrast, most reservoirs within the overpressured MCC produce gas and/or petroleum liquids with minor volumes of water. The spatial arrangement of distinct level 3 compartments within the MCC indicates that it behaves like a large seal rock with isolated porous compartments. In contrast, the normally pressured gas accumulations below the MCC have similar pressures (within stratigraphic intervals), suggesting that they are hydraulically connected to a common reservoir. Isolated, overpressured satellite compartments developed in this normal pressure domain, but they are limited in number and size.

SUMMARY AND CONCLUSIONS

The Anadarko basin is a tiered pressure system. First-order seals separate the primary pressure tiers and isolate the MCC. Second-order seals separate stratigraphic intervals and coincide with maximal flooding. Third-order seals separate individual compartments and contribute to reservoir heterogeneity. Seals are rich in fluid inclusions that provide valuable insight into seal genesis and burial history. Early silica-cement phases formed protoseals that preceded oil generation. These seals evolved with burial and began to confine overpressures caused by hydrocarbon generation and thermal expansion. In the deep Anadarko basin, fluid flow was focused toward the Wichita frontal fault zone. As a result, a seal evolved along the fault zone that confines pressure in the MCC. Pressure dissipation in normally pressured tiers above and below the MCC prevented fault-focused mi-

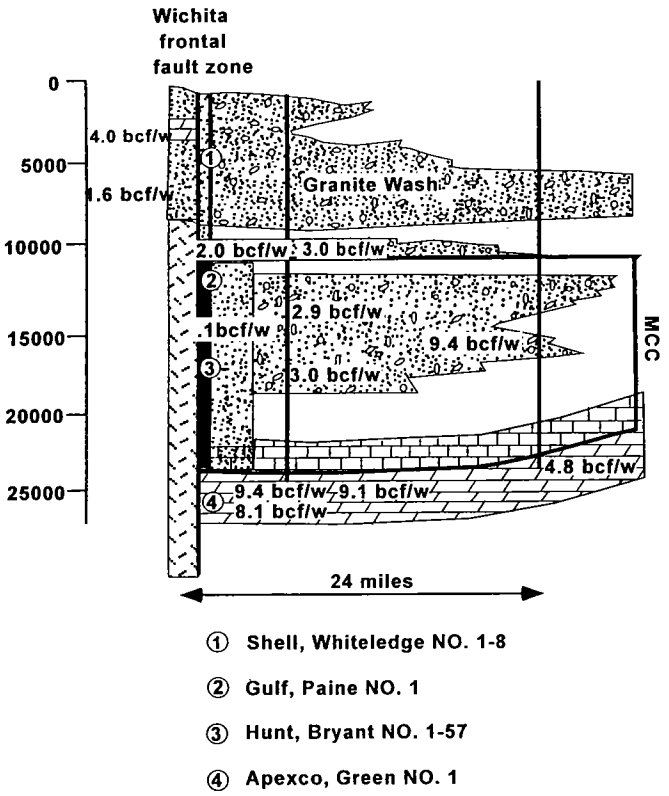

Figure 9. Schematic cross section of the Wichita frontal fault zone, where the southern lateral seal of the MCC formed by fault-focused flow. Depths are in feet. The highly cemented nature of seal rocks is reflected by low values of gas production (wells 2 and 3: 0.1 BCFG/well). Wells above and below the MCC (1 and 4) produced large volumes of gas (1.6 to 4.0 and 8.0+ BCFG, respectively), indicating that rocks in and adjacent to the fault zone were not cemented. Homogenization temperature (T_h) of silica is 170°C, and T_h of carbonate is 124°C.

gration and sealing. Once seals were in place, overpressures were generated by the thermal transformation of liquid petroleum into gas. Methanogenesis continued until the Laramide orogeny, when uplift and cooling slowed and eventually disrupted the process. Capillary-pressure measurements indicate that seals in the Anadarko basin have a high sealing capacity and were capable of confining overpressures across geologic time.

ACKNOWLEDGMENTS

We thank James Howard and Phillips Petroleum Co. for providing capillary-pressure measurements used in this study. We thank the Gas Technology Institute (GTI) for providing generous financial support of research on compartmentalized and overpressured basins. We also thank Ken Rechlin, Melanie McPhail, and Julie Turrentine for their help and support in the preparation of this manuscript.

REFERENCES CITED

Al-Shaieb, Zuhair; Puckette, James; and Abdalla, A., 1994a, Megacompartment complex in the Anadarko basin: a completely sealed overpressured phenomenon, *in* Ortoleva, P. (ed.), Basin compartments and seals: American Association of Petroleum Geologists Memoir 61, p. 55–68.

Al-Shaieb, Zuhair; Puckette, James; Abdalla, A.; and Ely, P., 1994b, Three levels of compartmentation within the overpressured interval of the Anadarko basin, *in* Ortoleva, P. (ed.), Basin compartments and seals: American Association of Petroleum Geologists Memoir 61, p. 69–83.

Al-Shaieb, Zuhair; Puckette, James; Abdalla, A.; Tigert, V.; and Ortoleva, P., 1994c, The banded character of pressure seals, *in* Ortoleva, P. (ed.), Basement compartments and seals: American Association of Petroleum Geologists Memoir 61, p. 351–368.

Al-Shaieb, Zuhair; Puckette, James; and Deyhim, P., 1999, Compartmentalization of the overpressured interval in the Anadarko basin, *in* Merriam, D. F. (ed.), Geoscience for the 21st Century: American Association of Petroleum Geologists, 1999 Midcontinent Section Transactions, Kansas Geological Survey Open-File Report 99-28, p. 63–70.

Al-Shaieb, Zuhair; Puckette, James; Patchett, J.; Deyhim, P.; Li, H.; Close, Amy; and Birkenfeld, R., 2000, Identification and characterization of reservoirs and seals in the Vicksburg Formation, TCB field, Kleberg County, Texas: Search and Discovery, AAPG/Datapages Inc. electronic journal, http:www.searchanddiscovery.net/.

Dewers, T.; and Ortoleva, P., 1988, The role of geochemical self-organization in the migration and trapping of hydrocarbons: Applied Geochemistry, v. 3, p. 287–316.

_____1990, A coupled reaction/transport/mechanical model of intergranular pressure solution, stylolites, and differential compaction and cementation in clean sandstones: Geochimica et Cosmochimica Acta, v. 54, pt. 2, p. 1609–1625.

Hall, D.; Shentwu, W.; Sterner, M.; and Wagner, P., 1997, Using fluid inclusions to explore for oil and gas: Hart's Petroleum Engineer International, Nov. 9, p. 29–34.

Hubert, L. B., 1995, Pressure regimes, burial history and source rock maturation of the Pennsylvanian Morrow Formation in the western Anadarko basin and the Hugoton embayment, Kansas, Oklahoma and Texas: University of Wyoming unpublished M.S. thesis, 123 p.

Matthews, F. D.; and Al-Shaieb, Zuhair, 1993, Paleokarstic features and reservoir characteristics of the Hunton Group in central and western Oklahoma, *in* Johnson, K. S.; and Campbell, J. A. (eds.), Petroleum-reservoir geology in the southern Midcontinent, 1991 symposium: Oklahoma Geological Survey Circular 95, p. 140–162.

Ortoleva, P.; Al-Shaieb, Zuhair; and Puckette, James, 1995, Genesis and dynamics of basin compartments and seals: American Journal of Science, v. 295, April, p. 345–427.

Schmoker, J. W., 1986, Oil generation in the Anadarko basin, Oklahoma and Texas: modeling using Lopatin's method: Oklahoma Geological Survey Special Publication 86-3, 40 p.

Tigert, V.; and Al-Shaeib, Zuhair, 1990, Pressure seals: their diagenetic banding patterns: Elsevier Earth-Science Reviews, v. 29, p. 227–240.

Walker, P. E., 1986, A regional study of the diagenetic and geochemical character of the Pennsylvanian Morrow Formation, Anadarko basin, Oklahoma: Oklahoma State University unpublished M.S. thesis, 156 p.

Influence of Fracturing-Fluid Rheology on the Productivity of Stimulated Oil and Gas Reservoirs

Naval Goel and Subhash N. Shah
University of Oklahoma
Norman, Oklahoma

ABSTRACT.—The objective of hydraulic-fracturing treatment is to increase productivity of oil and gas reservoirs by creating a proppant-packed fracture having higher conductivity than that of the reservoir. The permeability of the proppant pack in a fracture can be 10,000 times that of the reservoir. The proppant is placed in the fracture with a fluid that must have adequate rheology to keep it in suspension across the perforated interval of the reservoir. An understanding of fluid rheology is, therefore, important to optimize productivity of stimulated oil and gas reservoirs. This influence of fluid rheology has been studied in the present work.

The study was performed by stimulation treatments of two reservoirs as examples. The first treatment was evaluated with a two-dimensional fracture model, and the second with a three-dimensional model in a commercial fracturing simulator. In both stimulation treatments, fracturing-fluid viscosity was varied while maintaining constant all other stimulation and reservoir parameters. The results of these simulations are discussed in the present work. The observations of the theoretical models were then compared with the images obtained from a large-scale physical model of a fracture at the University of Oklahoma. These comparisons provide useful implications for characterization of the fluids used in the fracturing treatments of oil and gas wells.

INTRODUCTION

Hydraulic fracturing is a treatment that creates a fracture in an oil and gas reservoir and places proppant in the created void (Economides and Nolte, 2000). The proppant keeps the fracture open and provides a highly conductive path, which allows oil and gas to flow readily to the borehole. The fracturing treatment is performed by pumping a viscous fluid at a high enough pressure to initiate and propagate a fracture in the formation. The fluid also keeps the proppant in suspension during its flow from surface equipment to the fractured formation.

The success of the stimulation treatment of a reservoir depends on the final geometry of the propped fracture. The fracture geometry is determined from the final distribution of the proppant placed across the perforated interval of the reservoir. For increased productivity of the stimulated reservoir, the proppant should remain suspended in the fracturing fluid across the perforated interval. The placement of the proppant is governed by the fracturing fluid's ability to keep particles in suspension. Currently, the suspension capability of a fracturing fluid is described by its viscosity (API RP 39, 1998). Therefore, an understanding of fracturing-fluid viscosity is important to optimize the productivity of stimulated oil and gas reservoirs.

The purpose of this study was to investigate the influence of fluid viscosity on the dimensions of the fracture created during the fracturing treatment and on the productivity of the stimulated reservoir. The ultimate objective of this study was to identify the minimum fluid rheology above which a fluid would satisfactorily suspend proppant (Goel and Shah, 2001) and thus provide optimum production of oil and gas from a hydraulically fractured reservoir.

This investigation was performed using the fracture models of today (Gidley and others, 1989). The study was performed by the stimulation treatment of two different reservoirs as examples. The first treatment was evaluated with a two-dimensional (2-D) fracture model (Geertsma and de Klerk, 1969), and the second treatment was evaluated with a three-dimensional (3-D) model of a commercially available fracture simulator (FRACPRO 99, 2000). In both simulated treatments the fluid viscosity was varied while maintaining constant all other stimulation and reservoir parameters. The results of this investigation and their implications are discussed as follows.

BACKGROUND OF MODELS

2-D Fracture Model

The influence of fluid rheology on fracturing treatment was first studied using a 2-D model called the Geertsma–deKlerk (GdK) model.

Goel, Naval; and Shah, S. N., 2002, Influence of fracturing-fluid rheology on the productivity of stimulated oil and gas reservoirs, *in* Cardott, B. J. (ed.), Revisiting old and assessing new petroleum plays in the southern Midcontinent, 2001 symposium: Oklahoma Geological Survey Circular 107, p. 163–171.

The GdK model assumes fracture height to be constant but fracture width and length to change during the fracturing treatment. The width is expressed as a function of fracture length. This model assumes that the fracture face near the wellbore has a rectangular shape in the vertical plane and that the fracture has an elliptical shape in the horizontal plane (Geertsma and de Klerk, 1969).

3-D Fracture Model

The effect of viscosity on reservoir performance was also studied using a 3-D commercial simulator called FRACPRO™.

The 3-D model of FRACPRO 99 was not described in the users' manual of the simulator (FRACPRO, 2000), so its characteristic features are not known. The manual indicated that the simulator model considered spatial variations in reservoir stress, rock modulus, pressure, and flow distribution but did not calculate the variations at specific points within the fracture. It further considered the non-Newtonian effects of the fracturing fluid, hindered settling rates, and settled bank buildup. These features of the 3-D simulator model described in the FRACPRO 99 manual are similar to those considered for the 2-D fracture model.

Fracturing-Fluid-Viscosity Model

For the evaluations performed using the two fracture models, the fracturing fluid was assumed to exhibit non-Newtonian characteristics and that a power-law model described its viscosity (API RP 39, 1998).

The power-law model is given by

$$\mu_a = k\left(\dot{\gamma}\right)^{n-1} \quad (1)$$

where μ_a is apparent viscosity of the non-Newtonian fluid at a shear rate of $\dot{\gamma}$. The power-law model has two parameters: k, consistency index, and n, flow-behavior index. Equation 1 shows that at a given shear rate, the fluid viscosity can be varied by changing either of the two parameters, k or n.

RESULTS AND DISCUSSION

Evaluation Using the 2-D GdK Model

The influence of fluid rheology on fracturing treatment was first studied using the GdK model.

The petrophysical properties of the reservoir and design parameters of the stimulation treatment are summarized in Table 1. The fracturing-fluid viscosity was varied by changing separately the power-law index, n, and the consistency index, k. The values of n were varied from 0.5 to 1, and those of k from 0.005 to 0.03 $lbf\,sec^n/ft^2$. The results of the influence of viscosity are shown in Figures 1 and 2.

Figure 1 shows the fluid viscosity at 100 sec^{-1} as a function of the productivity ratio of the stimulated to non-stimulated reservoir, J_f/J_o. The figure shows that the productivity ratio dropped from 10 to about 7 as the fluid viscosity was increased from 40 to 400 cp.

Table 1. — Reservoir and Treatment Parameters for Evaluations with 2-D GdK Model

Static reservoir pressure, P_r	1,800 psi
Reservoir permeability, k	0.1 md
Reservoir porosity, ϕ	8%
Depth to producing formation	4,025 ft
Young's modulus, E	3.5 x 10^6 psi
Poisson's ratio, v	0.3
Vertical-stress gradient, S_v	1.15 psi/ft
Well spacing, A_c	80 acres
Wellbore radius, r_w	2.5 in.
Producing-formation height, h	50 ft
Fracturing fluid	VERSAGEL 1300
Fracturing-fluid type	30 lb/Mgal HPG
Fluid rheological model	$\mu = k\left(\dot{\gamma}\right)^{n-1}$
Base case:	
Power-law exponent, n	0.62
Consistency index, k	0.009 lbf sec^n/ft^2
Fluid volume, V_{fluid}	40,000 gal
Pad volume, V_{pad}	10,000 gal
Fluid pump rate, Q	15 bbl/min
Fluid-loss coefficient, C	0.00147 ft/$min^{1/2}$
Spurt loss, V_{sp}	0.0 gal/ft^2
Proppant size and type	20/40 mesh sand
Average proppant concentration	3 ppg
Closure stress on proppant bed	2,000 psi
Maximum wellhead pressure	4,500 psi
Static bottomhole temperature	100°F

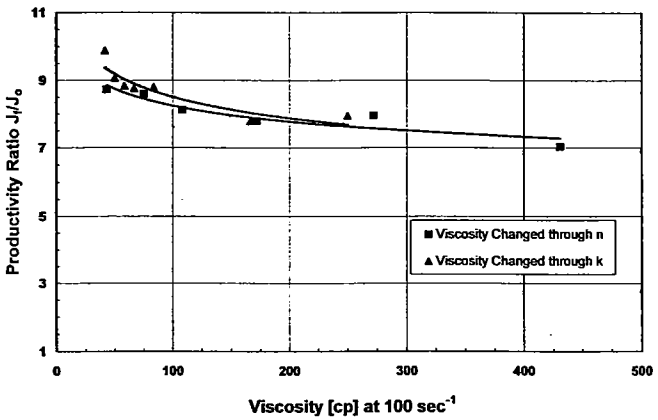

Figure 1. Effect of fluid viscosity on productivity ratio, using the 2-D GdK model.

This decrease in the productivity ratio with an increase in viscosity was due to a decrease in the fracture dimensions, as shown in Figure 2. This figure depicts a decrease in fracture length and propped height with an increase in fluid viscosity.

This observation is contrary to what one would expect. As fluid viscosity increases, the proppant-suspension characteristics of a fracturing fluid would improve, and so the propped length of the fracture should increase. However, the expected behavior is not seen in Figures 1 and 2. The 2-D GdK model, hence, does not accurately depict the effect of fluid viscosity on fracture dimensions. This inaccurate depiction also means that this model cannot provide a critical viscosity value above which the fluid would exhibit transport of proppant through a fracture. This value can be used prior to a fracturing treatment to evaluate whether a fracturing fluid would perform satisfactorily during the treatment.

Figures 1 and 2 show that the effects of changing n and k are dissimilar. At similar viscosities, the productivity ratio and the fracture dimensions are dissimilar because of the selection of different parameters of the power-law model. This difference highlights the importance of understanding the influence of each characteristic of the fluid on the stimulation treatment.

Table 2. — Reservoir Parameters for FRACPRO Simulation

Reservoir parameter	Parameter value
Permeability	5,933 to 6,008 ft — 0.01 md 6,008 to 6,152 ft — 0 md 6,152 to 6,227 ft — 0.01 md
Porosity	7.5%
Formation type	0 to 6,375 ft — sandstone Beyond 6,375 ft — shale
Reservoir temperature	170°F
Reservoir pore pressure	2,010 psi
Average pressure in fracture	5,350 psi
Pore-fluid compressibility	0.0005 psi^{-1}
Leakoff-fluid permeability ratio (K_p/K_l)	10.0
Leakoff-fluid viscosity	1 cp (cold) 0.5 cp (hot)
Pore-fluid viscosity	0.02 cp (cold) 0.01 cp (hot)

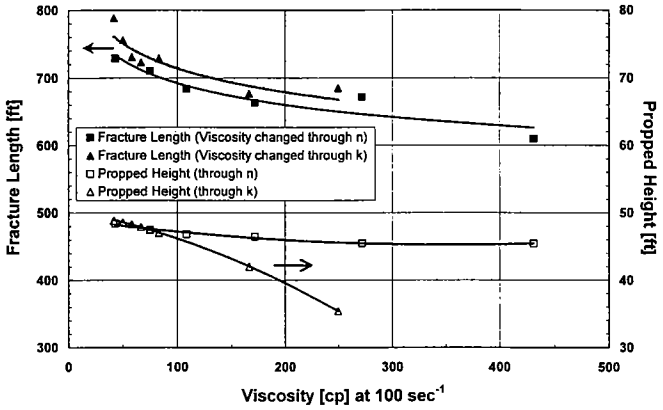

Figure 2. Effect of fluid viscosity on fracture dimensions, using the 2-D GdK model.

Evaluation Using the 3-D Simulator

The fracture design was applied to a reservoir whose parameters were taken from the tutorial example described in the simulator manual (FRACPRO 99, 2000).

The example reservoir for the simulations was the Sawyer 144A No. 5 well from Sutton County in west-central Texas (FRACPRO 99, 2000). The well was stimulated in the middle and upper Canyon sands (Pennsylvanian). The simulation runs described in the present study were performed on the middle sand only. These runs were made by varying the fracturing-fluid-viscosity parameters in the simulator while keeping all other reservoir and treatment parameters identical to those in the tutorial example.

The parameters that were input into the simulator are summarized in Tables 2 through 6, and the results of the simulation runs are shown in Figures 3 through 5. Table 2 lists the petrophysical and reservoir-fluid properties, Table 3 the well-completion parameters, Table 4 the formation-stress profile, and Table 5 the fracturing-treatment schedule. Table 6 lists the miscellaneous options selected in the FRACPRO program for the simulation runs.

The fracturing treatment was performed with a borate–cross-linked 35-lb/Mgal guar gel. This gel was listed in the FRACPRO fluid library as HL_BOR_G35_1, manufactured by Halliburton as BoraGel. The fluid for the pad and the slurry stages of the treatment were maintained identically. The fluid-viscosity data given in the simulator library are summarized in Table 7, which lists the viscosity data as the power-law-model parameters at several temperatures at an initial time and after 4 hours. For the simulation runs, the FRACPRO linearly interpolated the fluid-library data to the reservoir-temperature conditions.

The fluid-library data were first used to perform an initial simulation run; this run was named base case 1. The fracturing-fluid-viscosity data were then manipulated by changing either the consistency index, k, or the power-law index, n, to simulate several fracturing treatments. These runs were performed by varying the individual power-law-model parameters as a percentage of the base case while keeping all other reservoir and fracturing parameters in the simulations similar. The fluid formulations thus generated and their viscosity data are summarized in Table 8. These fluid formulations simulated fluid viscosities from 50 to 300 cp at 100 sec^{-1}.

The results of the fracturing-simulation runs for

Table 3. — Well-Completion and Tubular-Configuration Parameters for FRACPRO Simulation

Well parameter	Parameter value
Annulus segment 0 to 5,609 ft	Casing ID 4.892 in. Tubing OD 2.6 in., and ID 2 in.
Casing segment up to 6,186 ft	Casing ID 4.892 in.
Perforated interval bottom	6,186 ft
Number of perforations	200
Perforation diameter	0.33 in.
Perforation intervals	One
Wellbore orientation	Vertical
Wellbore fluid	Slick water

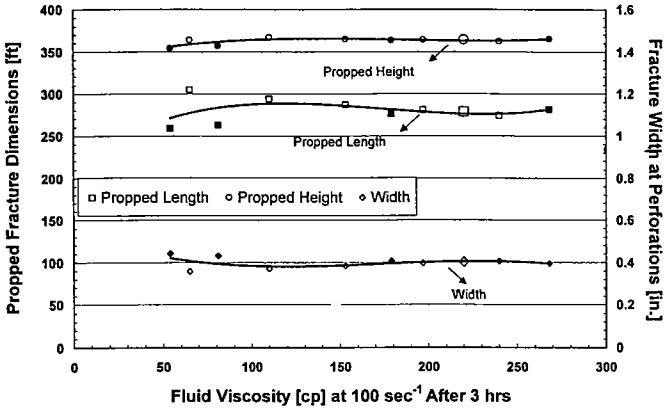

Figure 3. Effect of fluid viscosity on fracture dimensions, using the FRACPRO model.

all 10 cases were then incorporated into the reservoir-simulation mode of the FRACPRO simulator package. The reservoir simulator was then used to study stimulated-reservoir production performance over a period of 10 years. The reservoir and economic parameters for the reservoir-simulation runs are given in Table 9.

The results of the fracture-simulation runs are shown in Figures 3 and 4, and those of the reservoir-simulation runs in Figure 5. Figure 3 shows the effect of fluid viscosity on the fracture dimensions and also shows changes in the viscosity through adjustments in the n values as filled marker points, and those through adjustments in the k values as unfilled points. The fracture dimensions obtained with base case 1 fluid are shown by larger size markers.

Figure 3 displays small changes in propped height and length of the fracture, and fracture width at perforations, when the fluid viscosity was changed from 50 to 250 cp. The small change in the fracture dimensions indicates only slight dependence of fracture geometry on fracturing-fluid viscosity. This result implies an insignificant contribution of the fluid rheology on the stimulation treatment of a reservoir. It is, however, not true, as discussed below.

Table 4. — Formation-Stress Profile for FRACPRO Simulation

No.	Depth (ft)	Stress (psi)	Young's modulus (psi)	Poisson's ratio
1	0	4,100	$5 * 10^6$	0.2
2	5,695	4,400	$5 * 10^6$	0.2
3	5,805	4,650	$5 * 10^6$	0.2
4	5,917	4,250	$5 * 10^6$	0.2
5	6,023	4,950	$5 * 10^6$	0.2
6	6,060	4,250	$5 * 10^6$	0.2
7	6,230	4,900	$5 * 10^6$	0.2
8	6,255	5,200	$5 * 10^6$	0.2
9	6,277	4,900	$5 * 10^6$	0.2
10	6,325	5,150	$5 * 10^6$	0.2
11	6,375	5,350	$5 * 10^6$	0.2
12	6,470	5,450	$7.5 * 10^6$	0.22

Figure 3 indicates only a small difference in fracture dimensions, whether the fluid viscosities were manipulated with either n or k. Thus, there is no difference in the viscosity with either of the power-law-model parameters. But when the simulation results are plotted as proppant concentration in the fracture, a different picture evolves.

Figure 4 shows the proppant concentration in the fracture (lb/ft^2) for the three cases (1, 6, and 8) described in Table 8. This figure shows, first, the proppant distribution obtained with the base-case fluid, followed by that for cases 6 and 8. Base case 1 describes the stimulation with a 220-cp-viscosity fluid, case 6 with 110 cp, and case 8 with 81 cp. The right track of each case displays the proppant concentration after each of the 11 stages of the fracturing treatment. The left track presents the permeability and stress profile as a function of formation depth.

The proppant concentration in Figure 4 is a ratio of the weight of the proppant placed in the fracture to the fracture-face area, and was calculated from the product of the fracture length and height.

Figure 4A shows that the proppant concentrations were higher in the upper half of the fracture for the base-case fluid of 220-cp viscosity. The figure also depicts the increased proppant concentration near the wellbore, because the higher concentration slurries were pumped in the later stages of the treatment. Since the concentration of proppant was higher in the upper half of each stage, it is safe to conclude that this fluid successfully transported proppant through the fracture and that the stimulation treatment was successful with the base-case fluid. On the basis of similar arguments, the performance of case 6 fluid formulation having 110-cp viscosity after 3 hours, as

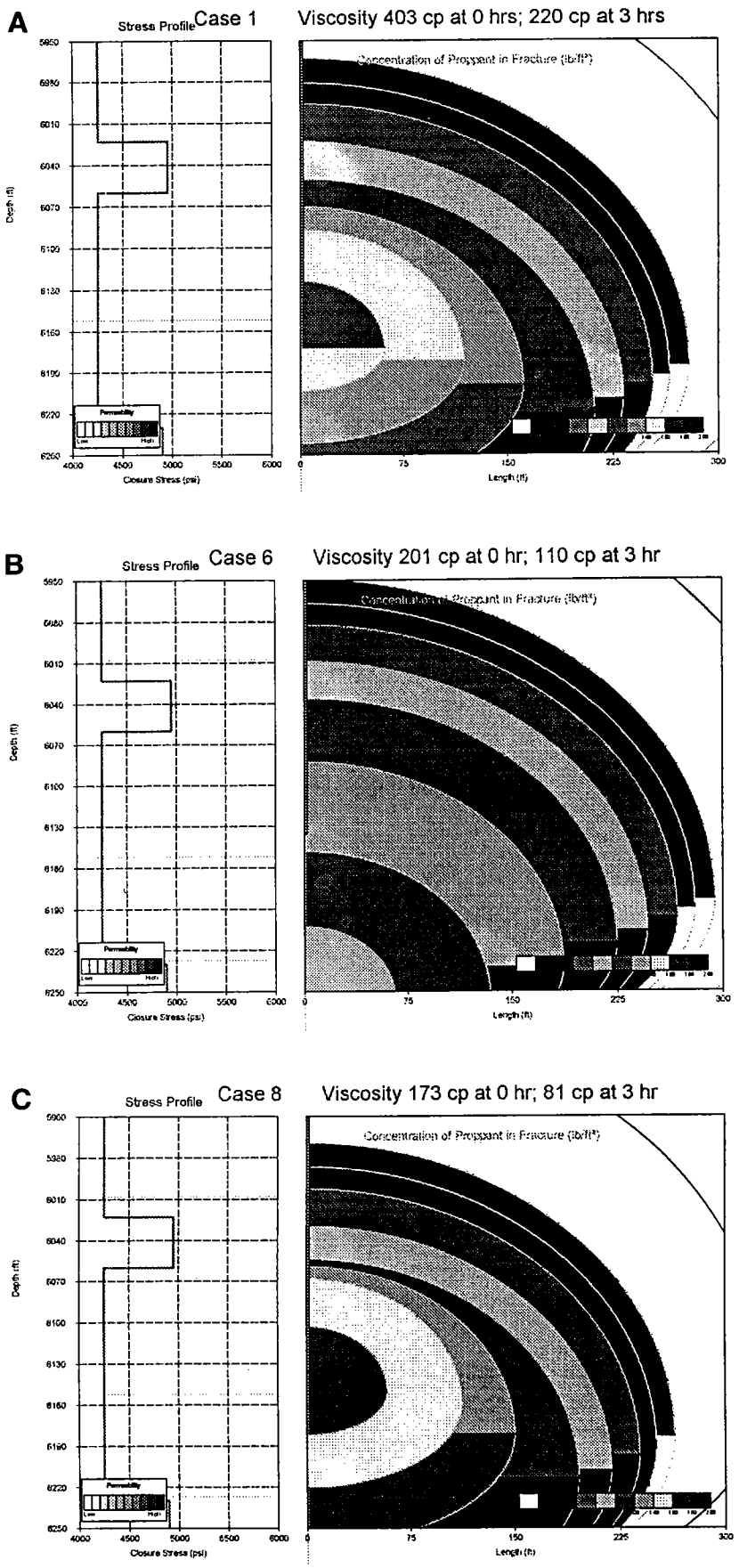

Figure 4. Effect of fluid viscosity on proppant concentration for cases 1, 6, and 8.

shown in Figure 4B, cannot be called successful. It shows that the sand settled down in the fracture because the proppant concentrations were higher in the bottom of the fracture than those in front of the perforations, 6,086 to 6,186 ft. The concentrations were lower than those obtained in the base case. These observations suggest unsatisfactory performance of the case 6 fluid. The poor stimulation treatment for case 6 would be attributed to the lower viscosity of this fluid in comparison to that of the base case. A further reduction in fluid viscosity, however, depicts contrasting behavior. Figure 4C shows the proppant concentration in the fracture when case 8 fluid with 81-cp viscosity was used to stimulate the formation. The figure shows that the proppant concentration was uniform in the upper and lower halves of the fracture and that the proppant was well distributed in the fracture. Thus it can be seen in Figure 4 that the proppant transport and suspension with case 8 fluid were as good as those of the base case, and were better than those with case 6 fluid, even though fluid viscosity in case 8 was the lowest of the three cases.

The dissimilar performances of the three cases are difficult to explain on the basis of fluid viscosity alone. The difference between the fluid formulations of cases 6 and 8 was that in case 6 the consistency index of the fluid was 50% of the base-case value, whereas in case 8 the power-law index of the fluid was 50% of the base-case value. The unsatisfactory performance of case 6 fluid indicates a greater dependence on the consistency index of the 3-D model used in the FRACPRO simulator.

A higher proppant concentration in the fracture means higher fracture conductivity and higher permeability of the stimulated formation. Thus, the productivity index of the reservoir stimulated with the fluid formulations of the base case and case 8 would be higher than that obtained with the case 6 fluid.

Figure 5 shows the effect of fluid viscosity on the performance of the reservoir. The figure displays a negligible difference in cumulative gas production in 10 years, or in the net present value of the stimulated formation when the fluid viscosity was changed from 50 to 250 cp. For a similar change in viscosity, there was negligible improvement in the pro-

Table 5. — Fracturing-Treatment Schedule for FRACPRO Simulation

No.	Slurry rate (bpm)	Proppant concentration (ppg)	Stage length (min)	Proppant type
1	27	0	23	—
2	27	1	3	Brady sand 20/40 mesh
3	27	2	2.5	— do —
4	27	3	4	— do —
5	27	4	3.5	— do —
6	27	5	5	— do —
7	27	6	4.5	— do —
8	27	7	4.8	— do —
9	27	8	2	— do —
10	27	0	3.5	—
11	0	0	40	Shut-in

Table 6. — Miscellaneous Options Selected for FRACPRO Simulation Runs

1	Run from job-design data
2	FRACPRO 3-D model
3	No temperature modeling
4	Proppant convection
5	Allow fracture growth at shut-in
6	Model wellbore and perforation
7	FRACPRO fluid path tubular configuration
8	Run fracture and wellbore models
9	General iteration
10	Vertical fracture
11	General reservoir
12	Ignore back-stress effects
13	Calculate *C*-total from permeability
14	Producing bottomhole pressure 2,614 psi
15	Calculate fluid volume from stage length
16	Simulator start time 0, end time 100 min with time step of 0.5

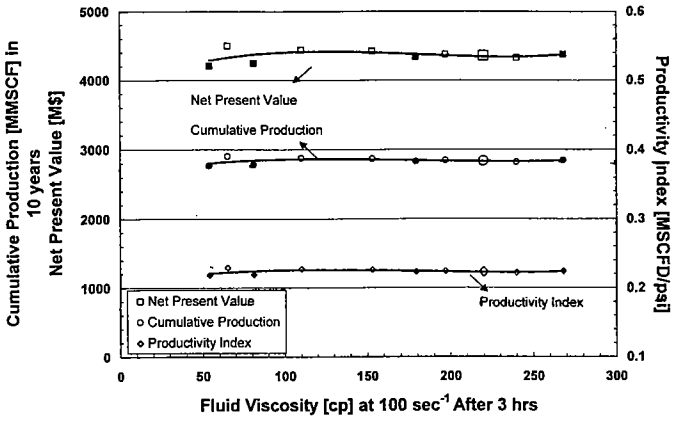

Figure 5. Effect of fluid viscosity on stimulated-reservoir performance.

ductivity index of the stimulated formation. Thus, Figure 5 suggests no impact of fluid viscosity on the performance of the stimulated reservoir.

Implications of the Study

The fracture-design simulations performed with the FRACPRO simulator and the GdK model indicate that viscosity is not a critical parameter during a hydraulic-fracturing treatment. Figure 4, however, shows the role of fluid rheology on stimulation treatment, because the proppant distribution in the fracture was observed to be dissimilar in the three cases, which differed only in the rheological parameters of the fluids used for the stimulation. Thus, the proppant distribution seen in Figure 4 cannot be explained through fluid viscosity. Therefore, the 3-D commercial simulator was as unsuccessful as the 2-D model for evaluating a fracturing fluid and identifying a critical viscosity above which the fluid would satisfactorily transport proppant through a fracture in a stimulation treatment.

Several case histories on hydraulic-fracturing treatments have shown that fluid viscosity plays a significant role in the creation of a fracture in a reservoir (Johnson and Cleary, 1991). Viscosity was observed to be an important parameter to transport proppant effectively in the near-wellbore region (Aud and others, 1994), a critical region for stimulating reservoir productivity. The importance of fluid viscosity is evident in the field but is absent in the fracture models available today. This implies that the fracture models are incapable of correctly describing the hydraulic-fracturing operation.

Therefore, only experimental investigation can evaluate the fluid rheology for satisfactory proppant transport through a fracture. Thus, experimental evaluation offers an opportunity to understand the relationship between fluid rheology and proppant transport and to identify the rheological property that can differentiate a successful stimulation from an unsuccessful one without actually performing the fracturing treatment.

Experimental Investigation

The experimental investigation was performed by evaluating the proppant-suspension characteristics of two fracturing fluids. This characterization was performed using the field-scale test facility at the University of Oklahoma.

In the experimental investigation, a fracture was assumed to have parallel faces. Hence, the fracture was simulated with a slot model, whose dimensions

Table 7. — Fluid-Viscosity Data for BoraGel from FRACPRO Fluid Library

Temp.	Power-law exponent n		Consistency index k $lb_f\ sec^n/ft^2$	
(°F)	Time = 0 hr	Time = 4 hr	Time = 0 hr	Time = 4 hr
75	0.32	0.40	0.323	0.0999
100	0.33	0.41	0.274	0.0837
125	0.34	0.43	0.226	0.0681
150	0.35	0.44	0.185	0.0548
175	0.37	0.46	0.149	0.0435
200	0.39	0.48	0.117	0.0336
225	0.42	0.51	0.0874	0.0249

were such that it represented a real fracture. The parallel walls of the slot model were separated at a gap equal to the width of the fracture created during a stimulation treatment. The slot height and length were selected to simulate fluid flow through the model under laminar-flow conditions as in a flow through a fracture. Moreover, the slot model was long enough to allow fluid to reside in the slot for a sufficient period to enable the proppant-suspension behavior of the fluid to be satisfactorily evaluated.

The slot model was 12 ft long, 20 in. high, and 0.25 in. wide. It was made of Plexiglas, so it allowed direct visual observations of the proppant distribution. This model was used to investigate the significance of fluid viscosity on the proppant transport through a fracture. The investigation was performed with borate–cross-linked 35-lb/Mgal guar gel, which was also used in the evaluation with the 3-D FRACPRO fracture simulator.

The cross-linked guar gels were prepared using two borate–cross-linked concentrations: 0.25 and 0.45 lb/Mgal of guar solution. The gel prepared at 0.25-lb/Mgal concentration had an initial viscosity of 200 cp at 100 sec^{-1} and 135 cp at the end of the 3-hour API viscosity test (API RP 39, 1998). Similarly, the gel prepared at 0.45-lb/Mgal concentration had an initial viscosity of 260 cp, which stabilized to 150 cp after 3 hours. These values suggested that the two gels had viscosities very close to each other, and so their proppant-transport behavior should also be similar. It was, however, not so. Figures 6 and 7 describe the sand-suspension behavior of the two gels.

Figure 6 shows a settled bed formed in the transparent slot model when a 2-ppg slurry was pumped with the gel prepared at 0.25-lb/Mgal cross-linker concentration. This bed was formed as soon as the slurry was introduced into the slot. The figure further illustrates that the bed was formed below the inlet opening of the slot. This meant that the proppant concentration and the fracture conductivity would be poor in front of the perforated interval. A lack of proppant particles across the perforation would undermine the success of the stimulation treatment, because these particles keep the fracture open and provide a highly conductive path for the reservoir fluids. The performance of the guar gel prepared at 0.25-lb/Mgal concentration would therefore be unsatisfactory.

On the other hand, the performance of the gel prepared at 0.45-lb/Mgal cross-linker concentration was satisfactory, as shown in Figure 7. The figure shows the proppant uniformly distributed across the height and length of the slot, showing no settled bed. This fracturing gel, therefore, was able to transport sand particles successfully through the fracture model.

Figures 6 and 7 show that the gel prepared at 0.45-lb/Mgal cross-linker concentration performed better

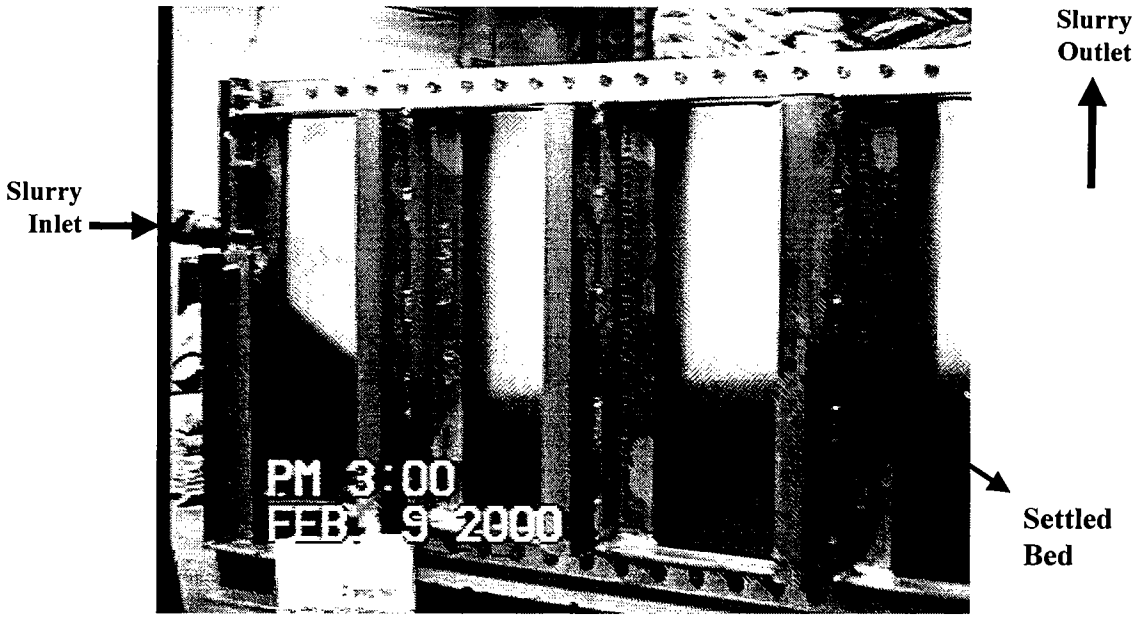

Figure 6. Proppant transport in transparent slot with 0.25-lb/Mgal borate–cross-linked guar gel.

than the gel at 0.25-lb/Mgal, even though both had similar viscosity values. Thus, fluids having similar viscosities do not necessarily exhibit identical proppant-transport characteristics. The fluid evaluations performed with the fracture-simulator models showed that the fluid having lower viscosity exhibited better proppant distribution in the fracture.

The lack of correlation between proppant transport and viscosity implies that some other fluid property, instead of viscosity, may better describe the particle-suspension behavior of the fracturing fluids. This fluid property cannot be identified with the fracture simulators available today, because these models utilize only viscosity-based correlations to describe proppant settling. The new fluid property has been identified with an experimental investigation of the proppant-transport characteristics of fracturing fluids (Goel and Shah, 2001).

Thus, further research is needed to describe proppant-suspension characteristics accurately during a hydraulic-fracturing treatment.

Table 8. — Summary of Viscosity Data at 170°F for Different Simulation Runs

Cases		Power-law exponent n at 0 hr	Power-law exponent n at 4 hr	Consistency index k $lb_f\ sec^n/ft^2$ at 0 hr	Consistency index k $lb_f\ sec^n/ft^2$ at 4 hr	Viscosity cp at 100 sec^{-1} after 3 hr
1	Base	0.366	0.456	0.156	0.04576	220
2	1.1 n	0.403	0.502	0.156	0.04576	268
3	0.9 n	0.33	0.41	0.156	0.04576	179
4	1.1 k	0.366	0.456	0.1716	0.05	240
5	0.9 k	0.366	0.456	0.1404	0.0412	197
6	0.5 k	0.366	0.456	0.078	0.0229	110
7	0.7 k	0.366	0.456	0.109	0.032	153
8	0.5 n	0.183	0.228	0.156	0.04576	81
9	0.3 n	0.11	0.137	0.156	0.04576	54
10	0.3 k	0.366	0.456	0.0468	0.01373	65

SUMMARY AND CONCLUSIONS

The investigation using the 2-D fracture model showed practically no influence of fluid viscosity on fracture dimensions. Similarly, evaluations with the 3-D fracture model also depicted poor dependence of fracturing-fluid viscosity on the created fracture dimensions and stimulated-reservoir production performance. The 3-D model, however, exhibited the influence of fluid viscosity on proppant concentration in the fracture.

The experimental investigation illustrated that fracturing fluids having similar viscosities might not exhibit identical proppant suspension in a fracture.

This study shows the importance of understanding the influence of each parameter of the fracturing fluid on stimulation treatment and reservoir productivity. Finally, there appears to be a poor correlation between the viscosity of a fluid and its proppant-suspension characteristics.

REFERENCES CITED

API RP 39, 1998, API recommended practices for standard procedures for evaluation of hydraulic fracturing fluids [3rd edition]: American Petroleum Institute, Washington, DC, 25 p.

Aud, W. W.; Wright, T. B.; Cipolla, C. L.; Harkrider, J. D.; and Hansen, J. T., 1994, The effect of viscosity on near-wellbore tortuosity and premature screenouts: Paper SPE 28492, presented at 1994 Society of Petroleum Engineers

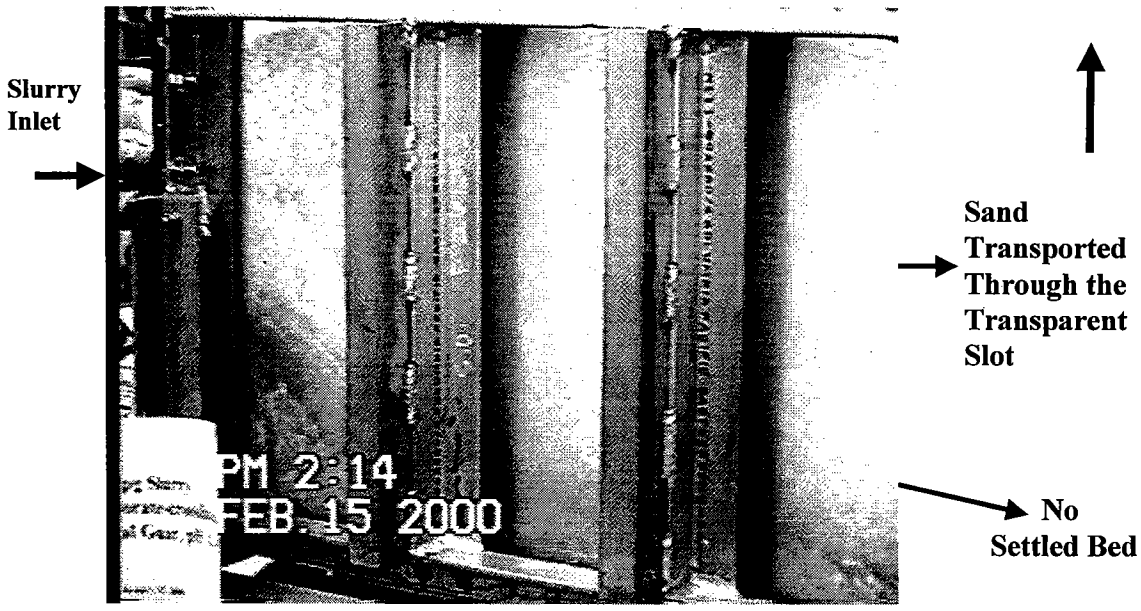

Figure 7. Proppant transport in transparent slot with 0.45-lb/Mgal borate–cross-linked guar gel.

Table 9. — Input Parameters for the Reservoir-Simulation Runs

Input parameter	Parameter value
Depth to middle of pay	6,136 ft
Gross pay thickness	200 ft
Net pay thickness	100 ft
X–Y extent of the reservoir	1,000 ft by 2,500 ft
Gas price	$3/MSCF
Price escalation	3% per year
Discount rate	15%
Operating cost	$5,000 per month
Cost-escalation factor	5% per year
Initial investment	$650,000
Stimulation cost	$85,000
Total production period	10 years

Technical Conference and Exhibition, New Orleans, 13 p.
Economides, M. J.; and Nolte, K. S. (eds.), 2000, Reservoir stimulation: John Wiley, Chichester, England.
FRACPRO 99, 2000, Users manual: Resources Engineering Systems, Acton, Massachusetts, 514 p.
Geertsma, J.; and de Klerk, F., 1969, A rapid method of predicting width and extent of hydraulically induced fractures: Journal of Petroleum Technology, December, p. 1571–1581 (Transactions of AIME, v. 246).
Gidley, J. L.; Holditch, S. A.; Nierode, D. E.; and Veatch, R. W., 1989, Recent advances in hydraulic fracturing: Society of Petroleum Engineers Monograph 12, 452 p.
Goel, Naval; and Shah, S. N., 2001, A rheological criterion for fracturing fluids to transport proppant during a stimulation treatment: Paper SPE 71663, presented at 2001 Society of Petroleum Engineers Technical Conference and Exhibition, New Orleans, 18 p.
Johnson, E.; and Cleary, M. P., 1991, Implications of recent laboratory experimental results for hydraulic fractures: Paper SPE 21846, presented at 1991 Society of Petroleum Engineers Rocky Mountain Regional Meeting and Low Permeability Reservoirs Symposium, Denver, 16 p.

Enhanced Oil Recovery with Downhole-Vibration Stimulation, Osage County, Oklahoma

Robert V. Westermark
Seismic Recovery LLC
Tulsa, Oklahoma

J. Ford Brett
Oil & Gas Consultants International, Inc.
Tulsa, Oklahoma

ABSTRACT.—This paper provides details of the test of downhole vibration for oil-production stimulation in Osage County, northeastern Oklahoma. This project has been supported by a grant from the U.S. Department of Energy (DOE). Seismic Recovery LLC, Phillips Petroleum Co., and Calumet Oil Co. will test downhole vibration as a potential technology for enhanced oil recovery in a Pennsylvanian sandstone.

Russian literature reported success in shallow reservoirs with a high water content, using surface equipment to generate vibro-seismic stimulation. Downhole-vibration-stimulation technology will be applied to the North Burbank Unit (NBU), a major field in Osage County, which is characterized by wells with low oil cuts and substantial water production.

Even when a well has a high water cut, there is still much oil trapped in the formation. The vibrational energy imparted to the reservoir is thought to facilitate the movement of oil in one or more ways, either by diminishing the capillary forces of adhesion between the rock and the oil, or by causing the droplets of trapped oil to cluster into "oil streams" that flow with the waterflood. However, other theories abound.

A new well will be drilled and cored within the NBU and will be used as the vibration-stimulation well. The vibration core-testing system patented by Phillips will be used to measure the effect of vibration on the flow of oil and water in cores. Preliminary tests have indicated that optimum flow enhancement occurs at a discrete frequency, generally in the 50- to 300-Hz range.

The installation of the downhole-vibration device was planned for the third quarter of 2001. The operating parameters for the vibration tool will be based on the Phillips' test results. Offset wells will be instrumented to monitor the vibrations emitted. Injection and production wells will be monitored for changes. The vibration stimulation is planned to run 3 months, and then its impact will be assessed and reported. This information will be disseminated through technical papers, workshops provided to Osage County production operators, and to other appropriate Midcontinent technology-transfer venues.

INTRODUCTION

Though wells in waterflooded fields are abandoned because production is uneconomical owing to high water cuts, significant amounts of oil can be trapped in a reservoir. Vibration stimulation may be a method for improving oil production and increasing ultimate economic recovery in these situations. The vibration force introduced to the reservoir is thought to facilitate the movement of oil in one or more ways: by diminishing capillary forces, hence reducing adhesion between the rock and fluids; or causing oil droplets to cluster into "streams" that flow with the waterflood.

Historical Background of Vibration Stimulation

The interest in elastic-wave-vibration stimulation (as opposed to nonelastic vibration, such as explosions) goes back to the 1950s. This interest is well documented by Beresnev and Johnson (1994), who reported on the full spectrum of investigative work in both the USSR and the U.S.A. They reviewed the efforts of more than a hundred researchers who had probed the effects of man-made vibrations from the ultrasound range of 5 MHz to the barely audible, low end of 1 Hz. The effects of earthquakes on oil production were also included in this paper. Westermark and others (2001) included a comprehensive update of current vibration-related stimulation technologies from around the world when they presented the initial plans for the Osage County project.

Research Reported in the United States

Los Alamos National Laboratory

A joint industry project, funded by DOE's Office of Basic Energy Science, Division of Advanced Energy Projects, to study the fundamentals of vibration stimu-

Westermark, R. V.; and Brett, J. F., 2002, Enhanced oil recovery with downhole-vibration stimulation, Osage County, Oklahoma, *in* Cardott, B. J. (ed.), Revisiting old and assessing new petroleum plays in the southern Midcontinent, 2001 symposium: Oklahoma Geological Survey Circular 107, p. 173–177.

lation was initiated by Peter M. Roberts at Los Alamos in 1995. This startup project evolved into a current project called "Seismic Stimulation for Enhanced Production of Oil Reservoirs."

The laboratory experimental portion of this project has utilized a core test cell with a magnetostrictive actuator applying mechanical-stress excitation to sandstone core samples during single-phase and two-phase fluid flow. Results indicate that mechanical-stress excitation at 100 Hz and lower can strongly influence two-phase fluid-flow behavior in the Berea sandstone (Mississippian) under both steady-state and simulated-flood conditions (Sharma and Roberts, 1998). Recently, Roberts (2001) presented the updated details of the Los Alamos core studies, which can be found at the project's homepage: http://www.ees4.lanl.gov/stimulation.

The project is currently monitoring industry-supported field-stimulation tests in California's Central Valley. Initial tests have shown an increase in oil cut that is directly correlative with the stimulation treatment.

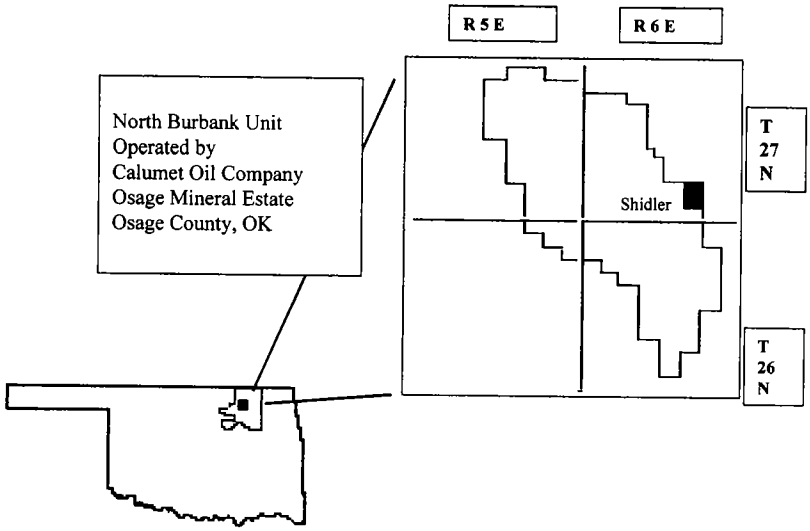

Figure 1. Map showing location of North Burbank Unit field, Osage County, Oklahoma. Black rectangle is town of Shidler.

DOWNHOLE-VIBRATION-STIMULATION PROJECT, NORTH BURBANK UNIT FIELD

Project Team

Oil and Gas Consultants International and Phillips Petroleum Co. had followed the research of reservoir-vibration stimulation by Los Alamos National Laboratory. With the DOE solicitation for project proposals, the opportunity presented itself to collaborate in an effort to apply this novel technology to the nearby, nearly watered-out Osage County oil fields. When the Osage Tribe was approached, they issued a warm endorsement of this proposal in Resolution 30-490 of the Osage Tribal Council in August 1999. Calumet Oil Co. was contacted about conducting a pilot test in the North Burbank Unit (NBU), the largest field in Osage County. Figure 1 shows the location of the NBU field in Osage County, northeastern Oklahoma.

Downhole-Vibration Tool

Backward-Whirl Vibrator: A Unique Orbital Vibrator Design

Backward whirl has been studied for the past 20 years in the oil-well-drilling industry. These intense vibrations have been known to be harmful to man-made diamond drill bits. While the motion is certainly harmful for bits, the patented tool to be used on this project attempts to exploit this phenomenon. To control the frequency and intensity of the created vibrations, the tool is built with a self-contained housing. Backward whirl occurs when a smaller cylinder rotates inside a housing, as seen in Figure 2.

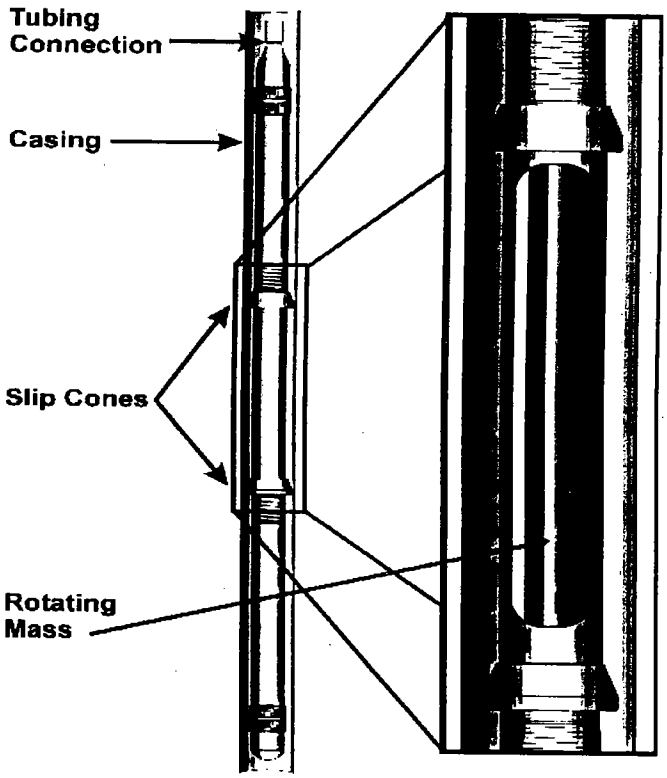

Figure 2. Schematic drawing of 7-in. downhole-vibration tool, anchored with a dual set of mechanical slip cones.

Field-Test Protocol in a Mature Waterflood

Field Selection

The test is to be performed in the NBU field in Osage County. Table 1 lists the average values of the field's parameters. Discovered in 1922, this is now a mature waterflooded field, which produces ~1,200 barrels of oil per day (BOPD) and >160,000 barrels of

Table 1. — Average Reservoir Properties for North Burbank Unit, Osage County, Oklahoma

Parameter	Value	Units
Area	36.5	Square miles
Average thickness	53.3	Feet
Acre-feet	128,000	Acre-feet
Depth	2,850	Feet
Stock-tank oil gravity	39	API gravity
Reservoir-volume factor	1.2	(Dimensionless)
Original reservoir pressure	1,200	PSIA
Original gas/oil ratio	380	Cubic feet/barrel
Temperature	120	Degrees Fahrenheit
Viscosity	3.3	Centipoise
Produced water salinity	85,000	Parts per million
Average porosity	16.8	Percentage
Connate-water saturation	26	Percentage
Average permeability	50–100	Millidarcies

water per day (BWPD). The Burbank reservoir is a Middle Pennsylvanian sandstone commonly present in the western half of Osage County.

Test-Area Selection

The criteria for selecting the location for the pilot-test area and the vibration-stimulation well were (1) an area that has had a consistent waterflood pattern for at least 2 years and produces into one tank battery, (2) an area with good total pay thickness (>40 ft), and (3) an area characterized by low initial-production rates (<500 BOPD after being shot with nitroglycerin).

Drilling and Coring of Vibration-Stimulation Well

The vibration-test well will be drilled, cored, and cased through the Burbank sandstone. After logging, 7-in. casing will be set and cemented.

Core Testing

The goal of laboratory vibration tests is to identify the cause and effect of how particular vibration frequencies and intensities influence hydrocarbon recovery for specific reservoir rocks. Phillips Petroleum Co.'s "coreflood" apparatus was used in this project to assess effects of vibration on fluid flow.

Figure 3 is a partial schematic diagram of the apparatus. The system consists of a biaxial core holder with hydraulic rams on both ends of the sample, fluid reservoirs, pumps, pressure transducers, mass-balance and volumetric-balance fluid-production measurement devices, and vibration-measurement and -control devices. Vibration is applied to a core in the same direction as fluid flow, using a magnetostrictive actuator that supplies cyclical compressive stress. This stress, which is superimposed on the static longitudinal stress, is in the form of a sine wave. The frequency of operation varies from about 8 to 2,000 Hz. A dynamic-force transducer is mounted along the load path between the core and the vibration actuator, and the output is read from an oscilloscope. Dynamic force supplied during vibration is adjusted to achieve target vibration intensities at test-vibration frequencies.

Typical Vibration-Test Sequence.—The permeability of the core plug to brine is measured to establish baseline permeability without vibration. Subsequently, permeability is measured while applying a range of vibration frequencies and intensities to determine whether permeability enhancement occurs under particular vibration conditions. The core is then oil-flooded to a residual-water-saturation condition.

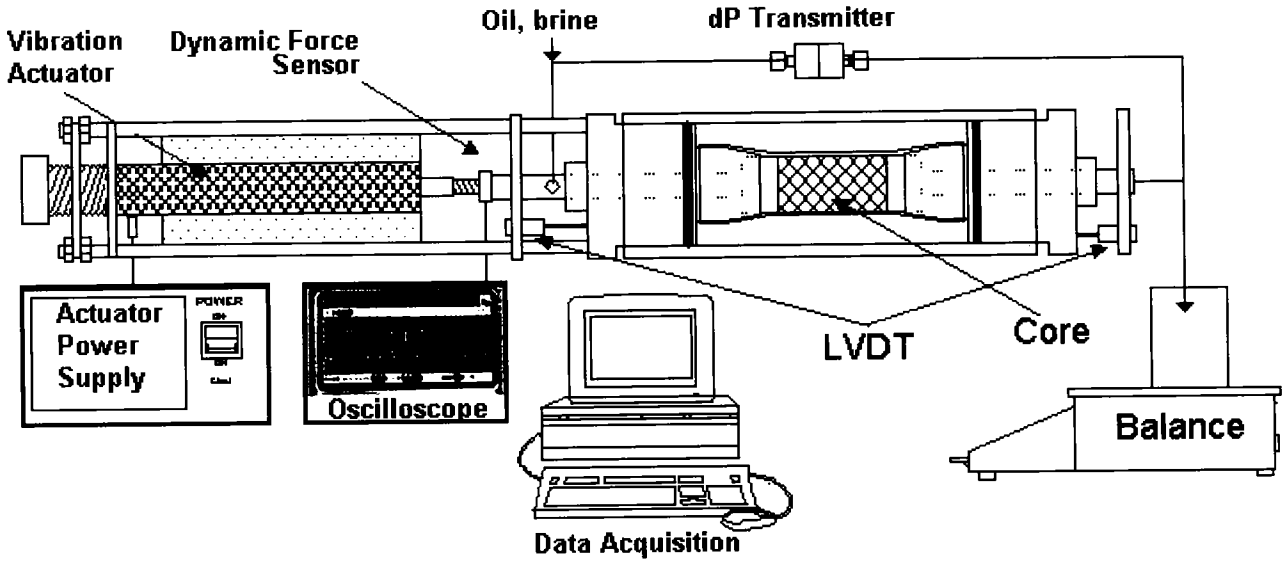

Figure 3. Sonic-core-test cell, with axial magnetostrictive source. *LVDT* = low-voltage displacement transducer.

After an aging period, the core is waterflooded without vibration to document oil production versus pore volumes of water injected.

Another waterflood test is conducted with vibration on the same or a similar core. Options include vibrating continuously throughout the waterflood, vibrating continuously after water breakthrough occurs and water cuts are high, or vibrating intermittently by turning vibration on and off several times during a test.

In-house laboratory tests have shown that the permeability of many brine-saturated cores can be increased by 10% or more by imposing particular vibration frequencies and intensities. For example, Figure 4 shows absolute permeability enhancement as a function of vibration intensity and frequency for a Berea sandstone (Mississippian) core plug. Highly water-wet samples tested thus far show about the same waterflood-production response with and without vibration. Subtle enhanced waterflood performance has been seen when testing cores that are not highly water wet.

One such example is shown in Figure 5 from a test on an intermediate-wet to oil-wet core from the NBU field. Two types of vibration tests were conducted: one with continuous vibration, and a second test in which the vibration was intermittently turned on and off (intermittent vibration). Waterfloods with vibration provided slightly higher oil recoveries than those without vibration, whereas recovery versus time with intermittent vibration somewhat outperformed the continuous-vibration test.

Designing, Building, and Testing the Downhole-Vibration Tool

For this field test, the downhole-vibration tool (DHVT) will be run at a depth of ~2,800 ft, placing it across the Burbank sandstone. Because of the mechanical nature of this backward-whirl orbital vibrator, it was desirable to employ commercially available rotating systems. A rod rotating system was chosen for its simple, field-proven operation and for ease in adapting from a progressive cavity-pump installation to the downhole-vibrator application.

The final determination for the desired frequencies and intensities to be generated by this tool will be based on results from the lab tests. With the whirling orbital vibrator, the output frequency is a function of the rotating speed times a multiplying ratio. This mechanical aspect allows for optimizing vibration intensity over a select range of frequencies for the available horsepower. The DHVT will be mechanically attached to the casing (much like a production packer) and placed opposite the reservoir to maximize the energy transmitted to the formation.

The DHVT will be operated with a computer-controlled, variable-speed, 50-hp electric motor. The motor controls will be able to slowly increase frequencies and intensities of the DHVT, hold the system at that level of output, and step it back down in a predetermined manner. The motor has safety devices at the surface to shut down the automated stimulation cycle should it draw current levels outside of tightly controlled limits. The history of the vibration-tool operation will be recorded and time stamped to allow for cross-referencing both fluid-response data and all geophone recordings (both downhole and surface listening devices).

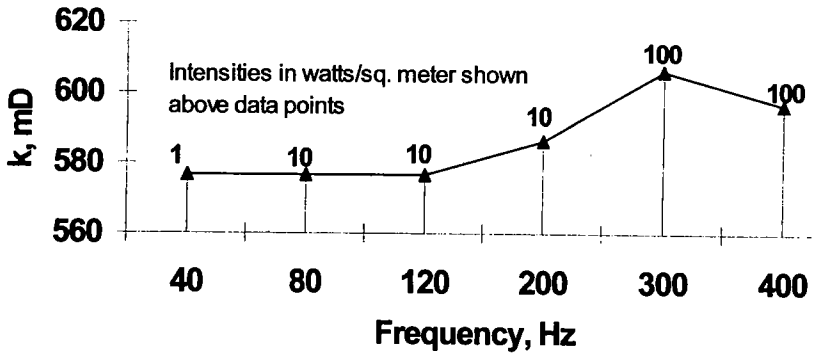

Figure 4. Brine permeability enhancement with vibration, Berea sandstone (Mississippian) core.

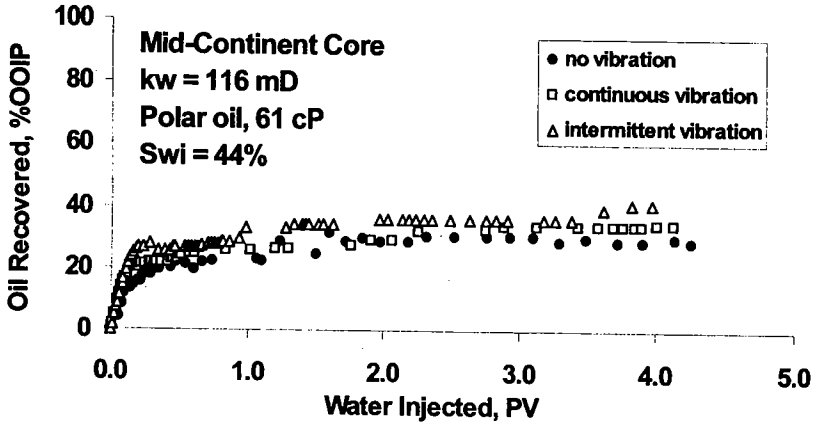

Figure 5. Waterflood results for a North Burbank Unit reservoir core without and with vibration stimulation. *OOIP* = original oil in place; *kw* = permeability to water; *Swi* = initial water saturation; *PV* = pore volume.

Installing Downhole- and Surface-Monitoring Equipment

Vibration-detection tools (geophones) will be installed in selected wells at various distances from the vibration-stimulation well. To allow the sensitive geophones to detect and identify the generated vibrations, the selected well will remain inactive while monitoring is being conducted. Equipment and personnel from Lawrence Livermore National Laboratory in conjunction with Los Alamos National Laboratory will be used to measure and record the strength of vibrations within the reservoir. These data will be recorded and time-stamped to allow for cross-referencing with the tool's operation.

Prior to attempting vibration stimulation, surface monitoring of produced and injected fluids within the pilot area will continue as normal production operations for the selected pilot wells. Pilot production wells will be placed on a continuously rotating production-testing schedule to determine water and oil rates for individual wells. A real-time record of the performance of pilot injection wells will also be kept. This will produce a high-quality baseline for production and injection data in advance of initiating the vibration-stimulation field test.

Performing Three-Month Vibration-Stimulation Test

Initially, the vibration-test well will be stimulated and the offset wells closely monitored for changes in fluid characteristics and produced or injected volumes and pressures. Simultaneously, the listening devices will be recording any discrete seismic signals that are identified as occurring above ambient noise. The acoustic response will be rapid (measured in seconds), owing to the close distances between the wells.

Initially, the well will be vibrated continuously at discrete frequencies in the 50- to 200-Hz range. Should the geophones detect a dominant or a resonant frequency, modification to operations or to the tool itself will be made to generate that frequency, if possible. This may require a reconfiguration of the tool to produce higher amplitude vibrations at a narrower frequency range.

Assessing Vibration Effects on Oil Production

A technical assessment of the field test will be the focus of the project's final report. Project success will obviously be tied to economical increases in oil production from the field test.

The question of the economics for this particular test will be straightforward. Using an estimate for manufacturing costs, the reliability of this version of the tool, its maintenance requirements both at the surface and downhole, and its power consumption will determine the capital investment required and the operating expense incurred. These costs will be compared to the changes in the water/oil ratio, the oil sold during the field test, and the possible reduction in injection-energy requirements.

Transferring Vibration-Stimulation Technology

Reports covering the project will be submitted to the DOE and the Osage Tribal Council. Technical papers and presentations will be prepared and delivered. Preliminary conversations with the Petroleum Technology Transfer Council (PTTC) have explored offering workshops through the South Mid-Continent Region to introduce this technology to the Osage County operators. A 1-day short course will be offered at the 13th Society of Petroleum Engineers/DOE Improved Oil Recovery Symposium in April 2002 in Tulsa, Oklahoma. Researchers and practitioners of vibration-stimulation technology from throughout the world have been invited to present their current efforts to provide the industry with a concise and intense review of the state of the art in vibration-stimulation activities, successes, challenges, and areas of opportunity.

ACKNOWLEDGMENTS

This work was prepared with the support of the U.S. Department of Energy under Award No. DE–FG26-00BC 15191. However, any opinions, findings, conclusions, or recommendations expressed herein are those of the authors and do not necessarily reflect the views of the DOE.

The authors extend their appreciation to Rhonda Lindsey and Virginia Weyland, NETL, NPTO, Tulsa, for their guidance and encouragement in this project. Peter Roberts, Los Alamos National Laboratory, and Ernie Majors, Lawrence Berkeley National Laboratory, have facilitated the increased application of this technology and are commended for their efforts. The project is indebted to the Osage Tribal Council for the hearty endorsement of Principal Chief Charles O. Tillman. In addition, we thank Phillips Petroleum Co. and Calumet Oil Co. for their support of this project.

REFERENCES CITED

Beresnev, I. A.; and Johnson, P. A., 1994, Elastic-wave stimulation of oil production: a review of methods and results: Geophysics, v. 59, p. 1000.

Roberts, P. M., 2001, Seismic stimulation for enhanced production of oil reservoirs: Natural Gas and Oil Technical Partnership Project Reports, Los Alamos National Laboratory, homepage: http://www.ees4.lanl.gov/stimulation.

Sharma, A. J.; and Roberts, P. M., 1998, Seismic stimulation of oil production in mature reservoirs [abstract]: American Association of Petroleum Geologists Annual Convention, Extended Abstracts, v. 2, p. 591.

Westermark, R. V.; Brett, J. F.; and Maloney, D. R., 2001, Enhanced oil recovery with downhole vibration stimulation: Society of Petroleum Engineers, SPE Paper 67303, Production Operations Symposium, Oklahoma City [CD-ROM publication].

Hunton Transition Zone in Oklahoma: A Case Study in West Carney Field, Lincoln County

David Chernicky and Scott Schad
New Dominion, LLC
Tulsa, Oklahoma

ABSTRACT.—West Carney field in T. 15 N., R. 2 E., and T. 16 N., R. 2 E., Lincoln County, Oklahoma, produces from the Hunton Group, utilizing dewatering techniques similarly used in coalbed-methane production. In a high-water-saturation, bimodal-porosity carbonate reservoir, virgin-state hydrostatic pressure exerts adequate confining pressure on the primary porosity network to limit the amount of gas expansion, and thus oil production, into the wellbore. The secondary-porosity network delivers a steady influx of water to the wellbore from more distal areas of the reservoir greater than the radius of deliverability of oil and gas from the primary (lower) porosity, so the predominant phase of production is salt water.

To dewater the Hunton, operators perforate and fracture the entire zone before installing submersible pumps. Aggressive water production begins the dewatering process, and the reservoir pressure starts dropping as the oil cut and gas/oil ratio increase. Declining reservoir pressure triggers a gas-expansion drive in hydrocarbons formerly trapped in place by poor reservoir quality and excessive hydrostatic pressure, causing them to migrate to the wellbore. Maximum oil production occurs when reservoir pressure is decreased to approximately 50% of original static bottomhole pressure. At this point the operator converts many of the wells to beam pumps, and the reservoir behaves more conventionally. Oil production peaks first, followed by a peak in gas production. Water production continues to decline, while the hydrocarbon phases exhibit characteristics similar to a classical depletion-drive reservoir.

This study focuses on a small area of West Carney field (4,800 acres) that experienced sporadic drilling over a period of 30 years. Out of 31 previous penetrations of the Hunton Group, five reported conventional Hunton completions that yielded a total of just 37,552 barrels of oil and 482,901,000 cubic feet of gas. An aggressive dewatering campaign over 2 years fostered the drilling or reentry of 28 new Hunton producers, resulting in proven recoverable reserves of 2.2 million barrels of oil and 16.2 billion cubic feet of high-Btu gas. Total reserves are expected to increase as field development continues.

Chernicky, David; and Schad, Scott, 2002, Hunton transition zone in Oklahoma: a case study in West Carney field, Lincoln County, *in* Cardott, B. J. (ed.), Revisiting old and assessing new petroleum plays in the southern Midcontinent, 2001 symposium: Oklahoma Geological Survey Circular 107, p. 179.

Three-Dimensional Applications in South-Central Oklahoma: Imaging and Exploiting Complex Structure in Knox, Chitwood, Bradley, and Cement Fields

Larry Lunardi
Chesapeake Energy Corporation
Oklahoma City, Oklahoma

ABSTRACT.—The availability of recent speculative and proprietary three-dimensional (3-D) data across parts of the southern and central Oklahoma fold-and-thrust province has provided a significant new exploration tool for the continued development of the oil and gas potential of this historic producing province.

This potential is directly associated with the structural and stratigraphic complexities inherent in a region characterized by multiple episodes of extensional, compressional, and wrench tectonics, now juxtaposed in the subsurface. The intersecting and overlapping fault patterns derived from this tectonic history present a particular challenge for subsurface and 2-D seismic interpretation as well as a significant opportunity for 3-D imaging to accurately portray untested or underdeveloped fault blocks.

Chesapeake Energy Corp. is currently utilizing >700 mi^2 of recent 3-D imaging in and around this area to develop an extensive acreage position acquired over the past 10 years. This data volume has proven crucial for the identification and positioning of both exploratory and development wells throughout this core area, and provides the basis for an aggressive ongoing drilling program.

Lunardi, Larry, 2002, Three-dimensional applications in south-central Oklahoma: imaging and exploiting complex structure in Knox, Chitwood, Bradley, and Cement fields, *in* Cardott, B. J. (ed.), Revisiting old and assessing new petroleum plays in the southern Midcontinent, 2001 symposium: Oklahoma Geological Survey Circular 107, p. 180.

Application of Microbially Enhanced Coalbed Methane to Stimulate Coal-Gas Production

Andrew R. Scott
Altuda Geological Consulting
San Antonio, Texas

ABSTRACT.—Naturally occurring secondary biogenic gases represent a significant fraction of coalbed-methane resources worldwide. Coal gases in the Powder River basin are entirely secondary biogenic, whereas gases in the Black Warrior and San Juan basins contain a significant secondary biogenic component. For example, an estimated 2 trillion cubic feet (TCF) of secondary biogenic gases has already been produced from the San Juan basin. If only one-hundredth of 1% (1/10,000) of U.S. coal resources were converted into methane through microbial processes, coal-gas reserves would increase by 23 TCF, approximately 10% of current reserves. Therefore, bioconversion of coal into methane has the potential to impact gas reserves significantly in the United States and worldwide.

Microbially enhanced coalbed methane (MECoM) imitates and enhances the natural process of secondary biogenic-gas generation in coal beds that occur in basins worldwide. MECoM involves the introduction of anaerobic bacterial consortia, consisting of hydrolyzers, acetogens and methanogens, and/or nutrients, into coalbed-methane wells. Coalbed-methane production can increase through generation of additional methane, removal of pore-plugging coal waxes, and/or permeability enhancement as cleat-aperture width is enlarged during biogasification. Under appropriate conditions, bacteria are capable of generating significant quantities of methane over relatively short time periods in the subsurface. Biogenic-gas generation from municipal waste sites and biogenic-gas generation from coal-cutting canisters are examples of real-time gas generation.

Coal surface area and biogasification-reaction rates in the subsurface might potentially limit gas generation, indicating that permeability enhancement might be the most significant benefit of MECoM. Additional research, including microbial sampling of deeply buried bituminous coals to identify genetically unique consortia, is required to evaluate MECoM fully and to determine if the process will improve coalbed-methane producibility. If economically feasible, MECoM can generate methane in coal beds that currently have limited coalbed-methane potential and thereby provide cheap, environmentally clean energy for many parts of the world.

Scott, A. R., 2002, Application of microbially enhanced coalbed methane to stimulate coal-gas production, *in* Cardott, B. J. (ed.), Revisiting old and assessing new petroleum plays in the southern Midcontinent, 2001 symposium: Oklahoma Geological Survey Circular 107, p. 181.

Integration of All Existing Data for Optimal Modeling of an Old Oil Field, Thus Creating Development Sites Hitherto Overlooked

Bert A. Weimer
Weimer Consulting
Norman, Oklahoma

ABSTRACT.—Today's modern search for oil and gas all too often looks to exotic methods. In old fields, such as the Panhandle field in Texas, only local firms, producers, or leaseholders have any interest in additional development. Even these firms often conclude that no additional development potential exists.

The reality is that a comprehensive study of all existing data resources often results in new and definitive findings that might generate new development sites. The beauty of this type of analytical review is that the data already exist and can be obtained at little or no capital cost. To achieve the desired results of obtaining new insights from old data, one needs to research the subject area on a large scale and dispose of the "offset" mentality so common in well-developed fields.

This form of study focused on the Panhandle field in Texas. As a mature hydrocarbon play, this field is not often looked upon as a source of new development. The main value of reanalyzing a large and heavily drilled field such as this is that large amounts of hydrocarbons are proven in the area and that extensive data exist from years of drilling. The study involved using any and all data available for the field and included old magnetic surveys, gravity maps, scout tickets, electric logs, cores, drill samples, and any other data that could be found. Also included were new and less specific data, such as published basement tectonic research, surface topographic maps, Landsat photos, chemical analyses of produced hydrocarbons, regional seismic research, and other forms of published research that might cover the overall Panhandle region.

The results of this Panhandle study generated a new understanding of the driving mechanism of structural development. This result also yielded new understandings of the methods of sediment deposition and hydrocarbon emplacement. With a new and enlightened view of the established producing field, areas of potential development were found. Among the results of the investigation were several overlooked drill sites and a surprise explanation for an area of nonproduction that has yielded numerous dry holes. These are no-risk development sites in one of the world's largest producing fields. Prospects such as these might be revealed in other areas from a cheap, inquisitive review of antiquated data requiring little capital investment and yielding great economic opportunities.

Weimer, B. A., 2002, Integration of all existing data for optimal modeling of an old oil field, thus creating development sites hitherto overlooked, *in* Cardott, B. J. (ed.), Revisiting old and assessing new petroleum plays in the southern Midcontinent, 2001 symposium: Oklahoma Geological Survey Circular 107, p. 182.

Surface and Subsurface Evidence Indicative of Possible Significant Oil and Gas Accumulations beneath the Arbuckle Mountains, Southern Oklahoma

R. P. Wilkinson
Consulting Petroleum Geologist
Ardmore, Oklahoma

ABSTRACT.—Reverse faulting near the edge of a stratigraphic boundary can create a false image of a strike-slip fault. The Washita Valley fault might be an excellent example of such a fault. If, in fact, the Washita Valley fault is a reverse fault and not a strike-slip fault, the Arbuckle Mountains might overlie some unexplored oil and gas prospects in a subthrust zone parallel to the Washita Valley fault surface.

The Washita Valley fault is adjacent to two of the most prolific oil and gas fields in southern Oklahoma. The Eola field, at the northwest end of the Washita Valley fault, has produced ~76 million barrels of oil (MMBO) from ~90 wells. This calculates to be ~855,000 BO per 40-acre well. The Cumberland field, at the southeast end of the Washita Valley fault, has produced ~72 MMBO from ~82 wells. This calculates to be ~850,000 BO per 10-acre well. Therefore, a structural trend that has not yet been fully explored might exist between two prolific oil fields.

One way to determine the difference between a reverse fault and a strike-slip fault is to examine the direction of the force that produced the fault. The force required to produce a strike-slip fault is parallel to the fault surface. The force required to produce a reverse fault is perpendicular to the fault surface. Thus, this 90° difference in the direction of the forces can help identify the true nature of the fault in question. Several subsurface cross sections were made across the Washita Valley fault. These structural cross sections indicate that compressive forces were involved, and they strongly support the reverse-fault concept.

Wilkinson, R. P., 2002, Surface and subsurface evidence indicative of possible significant oil and gas accumulations beneath the Arbuckle Mountains, southern Oklahoma, *in* Cardott, B. J. (ed.), Revisiting old and assessing new petroleum plays in the southern Midcontinent, 2001 symposium: Oklahoma Geological Survey Circular 107, p. 183.